Dopaminergic control of astrocytic calcium dynamics *in situ* and its potential effect on local synaptic activity

Alistair Edward Jennings

Dissertation submitted for the degree of Doctor of Philosophy

University College London

Department of Clinical and Experimental Epilepsy, Institute of Neurology

Declaration

I, Alistair Jennings, confirm that the work presented in this thesis is my own. Where information has been derived from other sources, I confirm that this has been indicated in the thesis.

14th May 2014.

Abstract

Astrocytes in culture display large cytosolic calcium increases upon stimulation with dopamine, however the mechanism and physiological significance of this calcium response is still unknown. In this thesis, I demonstrate that hippocampal astrocytes *in situ* respond to dopamine with similar large calcium transients. I also describe a novel astrocyte calcium decrease, which appears specific to dopaminergic stimulation. Dopamine is a potent neuromodulator of hippocampal synaptic activity, as are astrocytes. However, I found no evidence to suggest that dopamine-induced calcium transients in astrocytes affect excitatory synaptic transmission and its short-term plasticity in the hippocampal stratum radiatum. In perforant path - CA1 pyramidal synapses of stratum lacunosum-moleculare, astrocytes were found to lessen the inhibitory effect of dopamine on evoked PTP. This work shows for the first time that astrocytes *in situ* can robustly respond to dopamine with a complex Ca^{2+} signal thus may participate in dopaminergic signalling in the brain.

Acknowledgements

Thank you to everyone from the department that I have known during my time here. Every single one has contributed in some way to this thesis.

Foremost I would like to thank my primary supervisor, Professor Rusakov, for believing in me from the start until the end; for providing me with limitless opportunity and for opening up the world of science to me.

Christian Henneberger taught me almost all I now claim to know. Without Christian I could not have accomplished the experiments in this thesis, much less understood them. I am greatly indebted to him for always helping me to learn more and for having patience when I persistently broke everything.

I also wish to thank Alexander Gourine for his expert help and support and similarly Alexey Semyanov – they were both generous with their space and their time. Thank you Isabel, Lucie, Tom, Piotr, Sergey and Ivan for all of your expertise and guidance; thank you Umesh, Nicola and Yamina for listening to my rubbish.

There are too many to thank from my private life for helping me see this whole PhD through, but I will single out three: thank you Lawrence for keeping me sane; thank you Adrien for keeping me hairy and thank you Liz for keeping me happy.

Finally, my family have always supported me and it is to them that my greatest thanks must go, for getting me here and getting me through.

Table of Contents

List of Figures

Chapter 1

Chapter 2

Chapter 3

Chapter 4

Chapter 5

Chapter 7

Chapter 8

Chapter 9

Chapter 1: Introduction

1.1 Astrocytes: structure, function and calcium dynamics

Virchow (1856) is commonly credited with first describing glial tissue as separate from the neuronal cells of the brain. Until recently, their function was considered limited to metabolic support of neurons and homeostatic control of the extracellular milieu. The difficulty of studying them has often been prohibitive (Somjen 1988), but in the last 20 years, we have begun to uncover wide-ranging exciting new glial functions (thanks largely to advances in live cell fluorescence imaging technology). Glia fall into two main groups: microglia and macroglia – of different developmental origin, morphology and function. Macroglia includes astrocytes, oligodendrocyts and NG2 cells , of which astrocytes are the subject of this thesis. Astrocytes play a crucial role in neurodevelopment, during which time they are pluripotent and can differentiate into neurons, mature astrocytes or NG2 cells, as well as providing scaffolding for neuronal migration and regulating synaptogenesis (Molofsky et al. 2012). In the adult brain astrocytes regulate uptake of essential chemicals and ions from the blood at the glial-vascular interface, forming a part of the blood-brain barrier, as well as controlling the volume of blood circulation through capillary constriction(Cavelier and Attwell 2005). They create the microarchitecture of the brain tissue through their characterstic shape, separating individual synapses (Clarke and Barres 2013) and have recently been suggested to influence synaptic transmission through the release of various neuroactive compounds (Perea et al. 2009). Very importantly, they provide metabolic support for energy-intensive neurons (Pellerin 2005) – supplying them with lactate. They remove glutamate from the synaptic cleft after presynaptic release(Danbolt 2001) and buffer extracellular potassium, keeping it at low enough

concentrations to avoid local neuronal depolarization (Butt and Kalsi 2006). They are widely implicated in the pathogenesis of mental diseases including epilepsy, Parkinson's disease and Alzheimer's disease (Verkhratsky and Parpura 2010). In this thesis I am interested in the role of astrocytes in the modulation of synaptic transmission – I investigate the possible involvement of astrocytes in the dopaminergic modulation of synaptic transmission.

1.1.1 Astrocytic morphology

Astrocytes are found throughout brain tissue and are highly heterogenous in their morphology (Miller and Raff 1984) – this thesis deals solely with protoplasmic astrocytes, so called because the fine branching of their processes forms a cloud under light microscopy, although many other kinds exist and differ between species (Verkhratsky and Butt 2007). Hereafter protoplasmic astrocytes are referred to simply as astrocytes. In the forebrain, astrocytes have relatively small somata (8-10µm diameter) and multiple large processes that are visible under light microscopy (figure 1.1a). But imaged with fluorescence microscopy, their processes are highly ramified, closely covering the membranes throughout their entire territories, around 23,000µm^3, which can contain up to 600 synapses (Bushong et al. 2002; Halassa et al. 2007) – see figure 1.1b. Their processes enwrap blood-vessels and individual synapses, and these astrocytic process territories overlap very little with each other (figure 1.1c). Astrocytes are not completely mobile (unlike microglia), but they can change the extent to which they enwrap neighbouring synapses throughout the brain (Oliet et al. 2001; Theodosis et al. 2008). Their processes are also mobile and can form lamellipodia and filopodia-like structures (Hirrlinger et al. 2004). These morphological changes can influence synaptic physiology: in the hypothalamus, the astrocytic morphological changes induced by changes oxytocin release during lactation

Figure 1.1 Protoplasmic astrocyte morphology.

a) Human hippocampal astrocytes stained with ammoniacal silver oxide method from Ramon y Cajal's original slides; **b**) Rat CA1 hippocampal astrocyte filled with fluorescent dye Alexa 488 and imaged with confocal laser microscopy; **c**) Two rat CA1 hippocampal astrocytes filled with fluorescent dyes – Alexa 488 (green), Alexa 568 (red) – from a patch pipette, do not occupy overlapping territories. **a**) adapated from Garcia-Marin et al. 2007 (Fig.3b); **b**) adapted from Bushong et al. 2002 (Fig.1b); **c**) adapted from Bushong et al. 2002 (Fig.3c).

---

have been shown to decrease presynaptic transmitter release (Oliet et al. 2001) and modulate induction of long-term potentiation (LTP) and depression (LTD) (Panatier et al. 2006). In striatal tissue from parkinsonian sufferers, the astroglial coverage of the synapse is increased (Villalba and Smith 2011). Protoplasmic astrocytes change their morphology upon pathological stimulation, increasing GFAP expression and the thickness and length of their processes (Sun and Jakobs 2012) – astrocytes that have undergone this change are considered 'reactive'. Healthy astrocytes form a functional syncytium, their cytoplasmata are connected by gap-junctions and this allows the flow of current, ions, metabolites and other small molecules between cells (Sohl and Willecke 2004; Giaume et al. 2013).

1.1.2 Astrocytic role in homeostasis

Astrocytes buffer extracellular K^+ through inwardly rectifying K^+ channels (Hertz 1965; Higashi et al. 2001) and through the $Na^+/K^+/2Cl^-$ cotransporter. Astrocytic membranes are highly polarized, K^+ with their resting potential lower than the K^+ reversal potential. Hence K^+ flows down it's electrochemical gradient, through these membrane channels, into the astrocyte – here it is redistributed throughout the reservoir of the astrocytic syncytium along its concentration gradient, eventually to be excreted into the blood through inwardly rectifying K^+ channels (Verkhratsky and Butt 2007). They take up glutamate released into the extracellular space through perisynaptically concentrated glutamate transporters, using the Na^+ and K^+ electrochemical gradients across the cell membrane (Bergles and Jahr 1997). Once in the intracellular milieu, glutamate is broken down into glutamine which is not physiologically active at the synapse and can be released into the extracellular space and taken up by the presynaptic terminal to be converted back into glutamate and released again (Parpura and Haydon, 2009). They play a very important role in metabolic support of neurons (that are far more energy intensive) through provision of lactate: astrocytes convert glucose to lactacte and then release it to be taken up by presynaptic neuronal terminals and converted into pyruvate and then ATP, to fuel neurotransmitter release.Although astrocytes play a key role in brain metabolism, I go into no further detail here (please see Parpura and Haydon (2009) for further information), as the focus of this thesis is astrocytic Ca^{2+} signalling and its potential effects on synaptic transmission.

1.1.3 Studying astrocytic calcium dynamics

A major turning point in the understanding of astrocyte function was the discovery that they exhibit both spontaneous (Cornell-Bell et al. 1990) and evoked (Porter and McCarthy 1996) changes in intracellular free Ca^{2+} (figure 1.2). Our first inklings as to

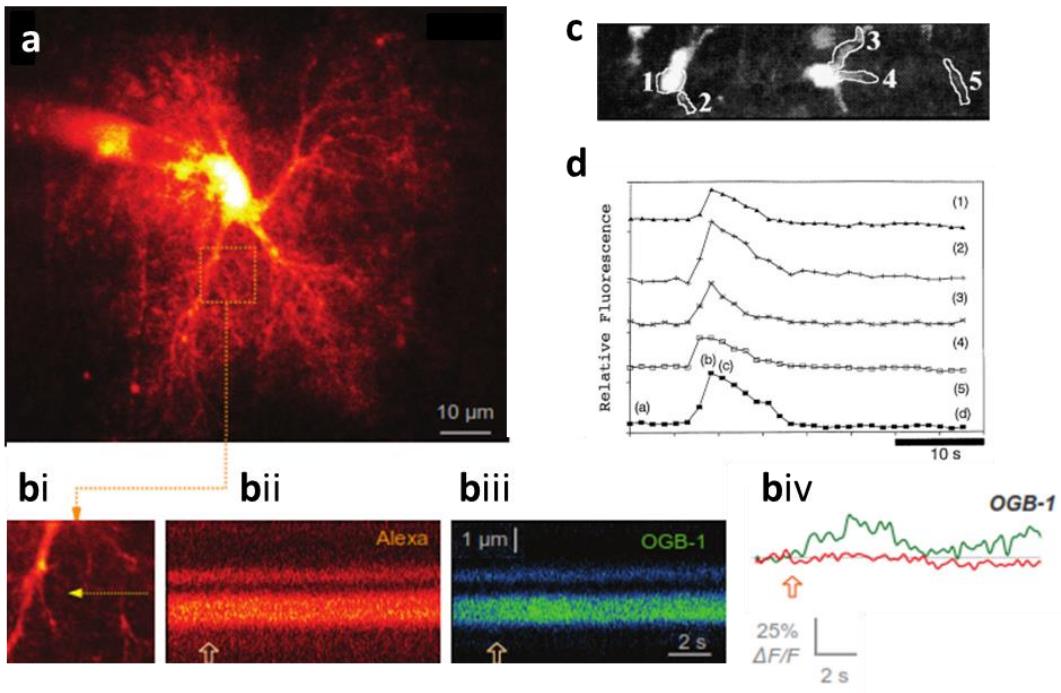

Figure 1.2 Astrocyte calcium signals.

a) CA1 hippocampal astrocyte filled with cell-impermeable Alexa 594 (morphological tracer) and OGB-1 (calcium indicator) imaged through the Alexa 594 channel; **b**) Calcium-dependent fluorescence transients in response to HFS; i) enlarged dotted square region of **a**) ii) line scan of region indicated by dotted arrow in **b**i – Alexa 594 fluorescence after HFS (hollow arrow); iii) as in **b**ii) but calcium indicator (OGB-1) channel; iv) normalized change in fluorescence of Alexa 594 (red) and OGB-1 (green) in **b**ii) and **b**iii) respectively. **c**) CA1 hippocampal astrocytes filled with AM-dye Calcium Green-1 AM. **d**) Calcium-dependent fluorescence transients in response to HFS in astrocyte regions indicated in **c**). **a**), **b**) adapted from Henneberger et al. (2010), Supp. Fig. 2a, b. **c**), **d**) adapted from Porter and McCarthy (1996) fig. 3a, b.

---

the nature of cytoplasmic Ca^{2+} dynamics and the potential role of intracellular Ca^{2+} in astrocytes came from electrophysiology. In 1989, Barres et al. recorded inducible, voltage-sensitive Ca^{2+} currents in whole-cell patch-clamped cultured astroglia. Before them, Quandt and MacVicar (1986) had found that Ca^{2+} concentration at the internal surface of excised astrocytic membrane could control its permeability to potassium (K^{+}) ions. However, it was

the use of Ca^{2+}-sensitive fluorescent dyes that first allowed the visualization of their complex intracellular Ca^{2+} activity. The first dyes to be used were based on acetoxymethyl (AM) esters (Cornell-Bell et al. 1990). These dyes are initially liphophilic and capable of crossing cell plasma membranes, but they are cleaved in a reducing environment (such as inside the cytosol) to become hydrophilic, preventing them from diffusing back out of the cell. Membrane-impermeable Ca^{2+} indicators can also be loaded into cells through patch pipettes (Perea and Araque 2005): both calcium-imaging methods are used in this thesis.

1.1.4 Spontaneous astrocytic calcium activity

Spontaneous changes in cytosolic Ca^{2+} concentrations can be witnessed in culture (Fatatis and Russell 1992; Shigetomi et al. 2011), in slice (Parri et al. 2001) – see figure 1.2 – and *in vivo* (Hirase et al. 2004). This activity is intracellular Ca^{2+} store-mediated – it can be triggered by Ca^{2+} binding to the IP_3 receptor on the smooth endoplasmic reticulum (an intracellular reservoir of Ca^{2+}) (Parri and Crunelli 2003). Similarly inositoltrisphosphate (IP_3) can stimulate the opening of the IP_3R and is also temperature-dependent (Wang et al. 2006; Petravicz et al. 2008; Schipke et al. 2008) and affects neuronal activity in turn (Parri et al. 2001; Aguado et al. 2002; Kanemaru et al. 2007; Bonansco et al. 2011), although this is still controversial (Nett et al. 2002). In this thesis, spontaneous activity is taken to mean any changes in local Ca^{2+} activity visible without prior stimulation of the imaged cell(s).

1.1.5 Astrocytic calcium response to neurotransmitter release

The astrocytic Ca^{2+} transients induced by released neurotransmitter have only been studied in depth in the last 20 years and their mechanism of action and physiological function are still sometimes controversial. Astrocyte Ca^{2+} can be increased through voltage

gated calcium channels (VGCCs), reverse of the Na^{+}/Ca^{2+} exchanger, from mitochondria, from Ca^{2+} permeable ionotropic receptors and from metabotropic receptor-mediated release from the endoplasmic reticulum (ER) (Verkhratsky et al. 2012; Rusakov et al. 2014). This latter form of Ca^{2+} increase is currently considered one of the most important in astrocyte signalling and is strongly potentiated by the presence of IP_3, a 2nd messenger that, along with Ca^{2+} itself, is a ligand for the IP_3 receptor (type 2 in rat adult astrocytes (Holtzclaw et al. 2002))on the ER (Foskett et al. 2007). Knock out of the IP_3R in astrocytes blocks both spontaneous and evoked astrocytic Ca^{2+} events (Petravicz et al. 2008).The effect of dopamine on astrocytic Ca^{2+}, the subject of this thesis, is poorly characterized; however an understanding of the modes of action of other, better characterized, neurotransmitters on astrocyte Ca^{2+} will aid the elucidation of any possible dopaminergic action on Ca^{2+}.

Much of the original work on neurotransmitter-induced astrocyte Ca^{2+} transients was carried out in cell culture systems. Exogenous application of glutamate was found to induce intracellular astrocytic Ca^{2+} transients (Cornell-Bell et al. 1990) mediated by an IP_3 increase (Pearce et al. 1986b; Jensen and Chiu 1990), via intracellular calcium stores (Charles et al. 1993). Similarly, ATP-induced intracellular Ca^{2+} activity was imaged in culture by McCarthy et al. in 1991, with ATP triggering intracellular IP_3 release through purinergic-2-Y receptor (P2YR) activation (Kastritsis et al. 1992; Porter and McCarthy 1995a). ACh application in culture also stimulates intracellular Ca^{2+} increases (Shao and McCarthy 1995), as does GABA (Nilsson et al. 1992; Nilsson et al. 1993), serotonin (Nilsson et al. 1991; Jalonen et al. 1997), adenosine (Marin et al. 1993), endocannabinoids (Navarrete and Araque 2008), TNFα (Koller et al. 1996), glucocorticoids (Simard et al. 1999); Prostaglandins (Bezzi et al. 1998), noradrenaline (norepinephrine) (Salm and McCarthy 1990) and, of course, dopamine (Parpura and Haydon 2000).

However cultured astrocytes may not accurately represent astrocytic Ca^{2+} dynamics *in situ*: astrocytic mGluRs, through which Ca^{2+} transients can be stimulated (Porter and McCarthy 1996), are developmentally regulated – mGluR5 expression decreases and mGluR3 increases (Cai et al. 2000; Sun et al. 2013); as cultured cells are often taken from very young animals their glutamatergic pharmacology may be different from cells *in situ*. Purinergic receptor P2Y has also been reported to be upregulated during development (Zhu and Kimelberg 2001) and GABAR expression changes developmentally as well, with $GABA_BR$ responsiveness peaking at P11-15, then dropping by P33 (Meier et al. 2008). Cultured astrocytes show Ca^{2+} response to serotonin (Nilsson et al. 1991; Jalonen et al. 1997) – that could be modulated by mGluR activation (Haak et al. 1997) – but acutely isolated astrocytes have been reported to show no Ca^{2+} sensitivity to serotonin, developing it only after extended time under culture conditions (Kimelberg et al. 1997). ACh sensitivity is also developmentally mediated, becoming apparent only after p8 (Shelton and McCarthy 2000). Another important factor to consider is the very different morphology that astrocytes assume in culture – flat and solid instead of covering a spherical area with highly ramified processes (Bushong et al. 2002). These morphology of these processes creates compartmentalization throughout the astrocytic territory that form microdomains of Ca^{2+} events (Di Castro et al. 2011) that may well have functional importance (Rusakov et al. 2014). Although culture systems allow for unparalled environmental control over cells, as well as avoiding the physical trauma associated with *in situ* preparations and often clearer conditions for live cell imaging, they suffer from the drawbacks noted above. Given this, it is very important to study neurotransmitter-evoked astrocytic Ca^{2+} dynamics *in situ* as a complementary approach to culture studies; this has been done for many of the transmitters listed above, as I go into below, but not yet for dopamine – the subject of this thesis.

What kinds of astrocyte Ca^{2+} responses have been already reported from *in situ* preparations? Bath application of mGluRI/5 agonists and ATP to hippocampal slices stimulated similar Ca^{2+} transients to those recorded from cultured cells (Porter and McCarthy 1995b; Porter and McCarthy 1995a) – see figure 1.5. High-frequency stimulation of the Schaffer collateral input to CA1, a more physiological stimulation paradigm, also triggered local astrocyte Ca^{2+} increases (Porter and McCarthy 1996; Zhu and Kimelberg 2001; Henneberger et al. 2010). ATP can be endogenously released by both neurons and astrocytes (Fields 2011) but hippocampal astrocytes are thought to be the main source of ATP in the hippocampus (Pascual et al. 2005; Heinrich et al. 2012). It has been demonstrated that inhibition of tonic ATP release from astrocytes in hippocampal slices decreases astrocyte network Ca^{2+} response to glutamate stimulus (Sul et al. 2004); similarly, ATP application enhances glutamate-induced Ca^{2+} transients (Sul et al. 2004). Endogenously released ACh (Araque et al. 2002) and endocannabinoids (Navarrete and Araque 2010) have also been shown to stimulate astrocytic Ca^{2+} increases in the hippocampus.

It is clear that the hippocampal astrocytes, *in situ*, are responsive to challenge from multiple neurotransmitters and many of these Ca^{2+} transient-evoking metabotropic intracellular pathways are common to dopamine receptor pathways. mGluR type I stimulation increases PLC and IP_3, as does D2-type receptor stimulation, mGluR type II stimulation decreases cAMP – an effect also shared with D2-type receptors. Purinergic P2YR activation also activates PLC (Illes et al. 2012) and IP_3 production in astrocytes. Adenosine also raises intracellular IP_3 and also enhances glutamate-induced astrocyte Ca^{2+} signals (Ogata et al. 1994) and acetylcholine-induced Ca^{2+} signals (Ferroni et al. 2002). It can also raises intracellular cAMP (Ogata et al. 1996). Thus astrocytes express common intracellular machinery required for metabotropic dopaminergic signalling – the subject of this thesis – *in situ* and *in vitro*. In section 1.5, I will review in detail the current literature regarding

dopaminergic signalling in astrocytes, but first I will briefly discuss non-neurotransmitter-induced astrocytic Ca^{2+} transients.

1.1.6 Stimulating astrocytic Ca^{2+} signals without neurotransmitters

Astrocyte Ca^{2+} transients can be triggered through other stimuli: mechanical stimulation (Charles et al. 1993); pH change (Gourine et al. 2010) and osmolarity change (Fischer et al. 1997). Transient receptor potential channels (TRPCs) are expressed in astrocytes (Golovina 2005; Malarkey et al. 2008) and their activation triggers calcium influx (Grimaldi et al. 2003; Malarkey et al. 2008) which has been implicated in refilling intracellular calcium stores through regulation extracellular calcium influx. Transient receptor potential A1 (TRPA1) channels have been reported to mediate astrocytic basal Ca^{2+} levels and also give rise to a stereotyped 'spotty' spontaneous calcium signal in cultured astrocytes (Shigetomi et al. 2011; Shigetomi et al. 2013)**.** Similarly TRPV4 channels, expressed in astrocytic endfeet onto blood vessels, mediate Ca^{2+} transients (Dunn et al. 2013). Depletion of intracellular Ca^{2+} stores by release of Ca^{2+} into the cytosol triggers relocation of the SER to the plasma membrane through interaction of the ORAI1 and STIM1 proteins. Calcium then enters from the extracellular space, through ORA1 into the SER to refill it. By expressing an exogenous Gq-coupled receptor specifically on astrocytes – the MRGA1 receptor – it is also possible to artificially induce increases in astrocytic Ca2+ (Fiacco et al. 2007). There is also evidence for VGCC-mediated Ca^{2+} increase, one that is secondary to mGluR activation (Pearce et al. 1986a) and interacts with store-mediated Ca^{2+} signals (Glaum et al. 1990); astrocytes express certain VGCC subtypes (Parpura et al. 2011) and it is possible that the astrocyte plasma membrane may become sufficiently depolarized in certain places (near local hotspots of neuronal activity for example) to allow them to open – their activity can be modified by metabotropic receptor, and specifically by D1-type

receptor activation (Surmeier et al. 1995), making them a potential pathway for dopamine-induced Ca^{2+} transients. However, it is important to note that, were VGCCs an important player in astrocytic calcium signals, one would expect that astrocytic depolarization (through K^+ manipulation for example) would trigger widespread astroytic calcium activity and downstream activity – but this is not the case. That said, it is not possible experimentally to locally depolarize small astrocyte subregions in a physiological manner, which may be necessary for VGCC opening to trigger downstream cascades.

1.2 Physiological relevance of astrocyte Ca^{2+} activity

1.2.1 Astrocytic release of neurotransmitter: gliotransmission

As soon as the clear astrocytic Ca^{2+} response to wide-ranging stimuli became apparent, the burning question was whether this triggered astrocytic communication with neighbouring neurons via release of neuroactive compounds – 'gliotransmission'.

Astrocytes have often been shown to contain the necessary cellular machinery for release of transmitter molecules: they express the vesicular docking proteins synaptobrevin II, cellulobrevin, syantaxin and SNAP23 (Parpura et al. 1995; Hepp et al. 1999) necessary for vesicular release. This release machinery is activated by the presence of intracellular Ca^{2+} and is regulated by tonic TNFα (Santello et al. 2011). Cleavage of astrocyte soluble NSF attachment protein receptor (SNARE) proteins with botulinum B toxin inhibits their release of glutamate (Araque et al. 2000) and also their release of d-serine (Henneberger et al. 2010) and they have been shown to exhibit 'kiss-and-run'-style vesicle secretion (Chen et al. 2005). Astrocytic lysosomal exocytosis of ATP, mediated by intracellular Ca^{2+} concentration, has also been reported (Zhang et al. 2007), as has transmitter release from spontaneously opening hemi-channels (Contreras et al. 2002; Kang et al. 2008). Astrocytes can also release

glutamate through reversal of the Glutamate transporter, anion channel opening after cell swelling and action of the cysteine-glutamate antiporter (Malarkey and Parpura 2008).

Arachidonic Acid release from astrocytes in response to ATP (Bruner and Murphy 1990; Murphy and Welk 1990) and glutamate stimulation (Stella et al. 1994) were the first to be shown, and intracellular Ca^{2+}-dependent glutamate release from astrocytes was soon demonstrated in culture (Parpura et al. 1994), using non-physiological agonists. Later it was found that more physiological stimulation of astrocytes (although still in culture) increased intracellular Ca^{2+} in excess of levels that could stimulate glutamate release (Parpura and Haydon 2000), although it is important to bear in mind that any external agonist applied in culture will not have the same spatio-temporal stimulation properties displayed *in situ*. In thalamic slices, spontaneous Ca^{2+} oscillations have been suggested to drive slow NMDAR-mediated currents (Parri et al. 2001) and fast AMPAR-mediated currents in hippocampal slices (Fiacco and McCarthy 2004) – but this is controversial: Fiacco et al. (2007) strongly refute their original work, finding that artificially induced Ca^{2+} increases do not induce neuronal currents – the nature of the induced Ca^{2+} increase, not simply an increase in Ca^{2+} alone, has now been shown to affect whether an astrocyte will release glutamate (Wang et al. 2013b; Rusakov et al. 2014).

Astrocytes control GABAergic inhibition in mouse barrel cortex (Benedetti et al. 2011), glia in the cerebellum have been found to tonically release GABA (Lee et al. 2010) and cultured human astrocytes can also release GABA (Lee et al. 2011). Astrocytes can also release ATP – which is broken down extracellularly to form Adenosine (Cotrina et al. 1998) – which plays a role both in communication with neurons (Pascual et al. 2005) and between astrocytes themselves (Guthrie et al. 1999) – this ATP release can be stimulated by glutamate (Queiroz et al. 1999) and pH-sensitive ATP release from astrocytes has been shown to propagate astrocyte Ca^{2+} transients in acute and organotypic brain stem slices

(Gourine et al. 2010). Astrocytes have also been reported to release d-serine (Panatier et al. 2006; Henneberger et al. 2010) this d-serine release is, SNARE-mediated, and is reported to be regulated by basal Ca2+ concentration mediated by TRPA1 channels (Shigetomi et al. 2013), nitric oxide (NO) (Janigro et al. 1996), NGF and S-100B (Ciccarelli et al. 1999; Chang et al. 2005)

.

1.2.2 Astrocyte Ca^{2+}-mediated control of gliotransmitter release

It is well-accepted that astrocytes can release gliotransmitters, but whether such release is dependent on the Ca^{2+} dynamics reported in the literature is still controversial, as is the possibility of gliotransmission *in vivo*. The first studies to look at astrocyte contribution to neuronal function, were in acute hippocampal slices: Fellin et al. (2004) documented an increase in CA1 pyramidal cell NMDAR response synchrony upon stimulated Ca^{2+} increase in the astrocytic network – from either mGluR stimulation or intracellular Ca^{2+} uncaging; intracellular Ca^{2+} release into the cytosol is considered to be the predominant mechanism for astrocytic glutamate release (Parpura et al. 2011). IP_3 uncaging in astrocytes has been shown to increase glutamate release probability in adjacent CA1 pyramidal cells (Fiacco and McCarthy 2004) and in 2007, Perea and Araque showed that inducing large Ca^{2+} transients in astrocytes (by puffing ATP or uncaging Ca^{2+}) whilst simultaneously depolarizing adjacent neurons, could induce neuronal long-term potentiation (LTP) through mGluR activation – and the same group later showed endocannabinoids could trigger such a Ca^{2+} increase (Navarrete and Araque 2010). Cytosolic Ca^{2+} -mediated astrocytically released glutamate (Jourdain, Bergersen 2007) controls synaptic strength in dentate gyrus and cortical UP states (Poskanzer and Yuste 2011). Henneberger et al. (2010) used a subtle approach: blocking all Ca^{2+} activity in hippocampal CA1 astrocytes – by 'clamping' their intracellular Ca^{2+} – and demonstrating an astrocytic

control of LTP, mediated by D-serine release. Astrocytes have been found to mediate spike timing-dependent LTD via endocannabinoid signalling (Min and Nevian 2012). Astrocyte-derived ATP can excite interneurons, thus inhibiting excitatory transmission, in the hippocampus (Bowser and Khakh 2004; Lalo et al. 2014); astrocytes also control chemosensory neurons through ATP release, via intracellular Ca^{2+} increase, in the brainstem (Gourine et al. 2010). Di Castro et al. (2011) show that local spontaneous astrocyte Ca^{2+} activity is necessary for synaptic transmission reliability. Knock-out of astrocytic SNARE-dependent gliotransmission also effects sleep behaviour in mice (Halassa et al. 2009) and sleep loss-induced deficits via changes in hippocampal synaptic plasticity (Florian et al. 2011). Astrocyte Ca^{2+} also regulates brain blood flow (Zonta et al. 2003).

There are two major lines of argument against the physiological role of certain astrocyte Ca^{2+} activity. The first pioneered a method that artificially creates Ca^{2+} transients within astrocytes: Fiacco et al. (2007) created a transgenic mouse expressing a extracellular membrane receptor to an exogenous ligand – MRGA1; these Gq-linked MRGA1 receptors, when activated, trigger long-lasting astrocytic Ca^{2+} transients via increase in intracellular, IP_3 but this group reported no effect of increasing astrocytic Ca^{2+} in this manner on glutamatergic currents in hippocampal CA1 pyramidal neurons or neuronal LTP induction (Agulhon et al. 2010). This conflict serves to highlight an important limitation in the literature – often 'Ca^{2+} transients' are reported after only having been imaged in specific areas of an astrocyte (in the case of Fiacco et al. (2007) the soma and large processes), whereas the astrocytic Ca^{2+} activity relevant to neuronal function may take place in the finer processes, neighbouring the synapses. This could explain how they report MRGA1-induced Ca2+ transients in astrocytes, but see no change in neuronal activity. It is also important to note that activation of astrocytic Ca^{2+} transients via MRGA1 receptor activation does induce a phenotypic response – the mouse analogue of depression (Cao et al. 2013).

The second major line of evidence comes from the same group, who showed that genetic knock-out of the astrocytic IP_3 receptor 2 displayed no Ca^{2+} response to g-protein receptor activation and showed no difference regarding neuronal baseline activity (as measured by spontaneous neuronal EPSCs in hippocampal CA1 pyramidal cells and tonic NMDAR-mediated currents) (Petravicz et al. 2008) or potentiation (Agulhon et al. 2010). This mouse is a constuitive knock out, and it may be that astrocytes in this mouse have developmentally upregulated other Ca^{2+} sources – VGCCs, TRP channels, hemi-channels for example – and that Ca^{2+} signalling still exists at a low level in astrocytes. Or it may indicate that whilst astrocytic involvement in neuronal activity is important in normal brain tissue, neurons possess the homeostatic machinery to compensate in a developmental environment lacking astrocytic Ca^{2+} signalling. Recently this mouse has been found to show MRGA1-mediated astrocyte Ca^{2+} increases *in vivo* that stimulate ATP release and concomitant behavioural change related to depression (Cao et al. 2013) – further muddying the waters.

Astrocytes can communicate with each other through intracellular Ca^{2+} waves (Venance et al. 1997; Scemes and Giaume 2006) and Ca^{2+}-mediated release of gliotransmitters, specifically ATP. This was first postulated in 1996 (Hassinger et al. 1996) with the observation that astrocytes could propagate Ca2+ waves over an astrocyte-free space of over 100µm, propagation that could be blocked by purinergic receptor blockers (Guthrie et al. 1999). Imaging ATP release from cultured astrocytes confirmed that they can spontaneously release ATP (Arcuino et al. 2002). *In vivo*, Gourine et al. (2010) have shown that this inter-astrocyte ATP-mediated signalling controls chemoreceptor neuron activation in the brainstem. Astrocyte-derived ATP has also been implicated in local astrocytic Ca^{2+} activity synchronization and regulation of cortical UP states (Poskanzer and Yuste 2011).

1.2.3 Astrocytic Ca^{2+} signalling and neurological disease

Abnormalities in astrocyte Ca^{2+} signalling have been correlated with neurological disorders. Astrocytic intracellular resting Ca^{2+} concentration and synchronous activity was found to be higher in mice with the amyloidβ (Aβ) plaques (a symptom of Alzheimer's disease) (Kuchibhotla et al. 2009) – this Ca^{2+} increase has been shown to act through Aβ stimulation of astrocytic α7 nAChRs, which in turn trigger synaptotoxic release of astrocytic glutamate (Talantova et al. 2013) – although a direct link between astrocyte Ca^{2+} dysfunction in Alzeimer's and the disease initiation and progression is still controversial (Lim et al. 2014) Astrocytic glutamate release – triggered by intracellular Ca^{2+} increase – has also been shown to trigger the paroxysmal depolarizing shifts seen in epileptic discharges (Tian et al. 2005) – although this is still controversial (Hubbard et al. 2013); *in vivo*, abnormal astrocytic Ca^{2+} activity induced by the application 4-AP (a drug commonly used to model epileptic activity in tissue), was decreased by systemic administration of the antiepileptic drugs valproate, gabapentin and phenytoin (Tian et al. 2005). This change in Ca^{2+} activity has been suggested to affect gliotransmission (Agulhon et al. 2012) and the increase in astrocytic Ca^{2+} activity in epileptic tissue has been found to promote cell death (Ding et al. 2007). Astrocyte-derived ATP has recently been found to modulate depressive-like behaviours, via P2X receptors, in an adult mouse model of depression (Cao et al. 2013). One must bear in mind, however, that astrocytes have a plethora of other functions and that abnormilties in any of these could be have as great or greater effect on epilepsy pathology (Hubbard et al. 2013).

1.3 The rodent hippocampus: structure and function

1.3.1. Basic anatomy of the hippocampus

The hippocampal formation is a much-studied brain region located in the medial temporal lobe in primates and embedded rostro-dorsal to caudocentrally under the surface of the cortex in rodents (figure 1.3a). Its structure is highly conserved across mammals, forming a trisynaptic circuit (figure 1.3b) between its three major regions: it receives its main input from the entorhinal cortex to the granule cells of the dentate gyrus; the granule cells synapse with the pyramidal cells of CA3 via the mossy fibre pathway, which synapse in turn with the pyramidal cells of CA1 through the Schaffer collaterals. CA1 pyramidal cells project to the subiculum and back into the entorhinal cortex, the main structure to which the hippocampus outputs. This organized structure makes the hippocampus an ideal structure to study synaptic transmission, as stimulation of many innervating axons and recording of large synaptic currents is simply done and highly reproducible *in situ*. This thesis concerns itself with the CA1 region, the 'final synapse' of the hippocampus. CA1 can be divided into four layers (figure 1.3b). Stratum Pyramidale contains the pyramidal cell bodies. Stratum Oriens contains the basal dendrites of the principle CA1 pyramidal cells and cholinergic (Fernandez de Sevilla and Buno 2003) and sparse dopaminergic (Swanson et al. 1987) input (see figure1.3c); Stratum Radiatum contains the primary Schaffer collateral input – axons from the principle pyramidal cells in CA3; Stratum Lacunosum Moleculare contains inputs from the entorhinal cortex and sparse dopaminergic, noradrenergic and serotonergic inputs (Swanson et al. 1987). Each layer of CA1 is populated with various interneurons (Klausberger and Somogyi 2008), glial cells – of which astrocytes form a large proportion – and microglia. The astrocyte population is considered to be homogenous both in morphology and function – occupying distinct, equal and tesselating territories

Figure 1.3 Hippocampal anatomy of the rat.

a) Location of the hippocampus (in pink) in the rat brain, black square indicates transverse plane. **b**) transverse slice through the hippocampus, displaying three major areas: DG – dentate gyrus; CA3 – Cornu Ammonis 3; CA1 – Cornu Ammonis 1; SLM – stratum Lacunosum-Moleculare; SR – Stratum Radiatum; SP – Stratum Pyramidale; SO – Stratum Oriens. **c**) Dopaminergic afferents to the hippocampus and surrounding entorhinal cortex. a) adapted from www.neuroscience.bham.ac.uk/neurophysiology/, 2007; b) adapted from Santiago Ramón y Cajal (1911); c) adapted from Swanson et al. 1987.

---

throughout CA1 (Halassa et al. 2007) – see figure 1.1 – although these territories become slightly smaller in stratum Lacunosum-Moleculare (Ogata and Kosaka 2002).

1.3.2 Basic behavioural functions of the hippocampus

In humans, the hippocampus is necessary for declarative memory formation (Small et al. 2001) (Chun and Phelps 1999) – most famously in the case of patient H.M. (Scoville and Milner 1957) – and memory retrieval (Eldridge et al. 2000). The hippocampus has also been implicated in perception – contributing to the processing of image configuration (Aly et al. 2013). In rats, the hippocampus is responsible for spatial memory formation (Schenk and Morris 1985; Li et al. 2003). Pyramidal cells of the CA1 region form a cognitive map of the environment (O'Keefe and Nadel 1978), with a proportion of CA1 pyramidal cells becoming active only in certain locations (termed 'place cells'). There is also a population of 'head-direction' cells in the subiculum that fire in relation to the position of the rat's head in it's relation to the environment (Taube et al. 1990). There is some evidence from operant conditioning tasks (in which rats must differentiate between rewarding and non-rewarding stimuli) that a small subset of hippocampal neurons are sensitive to positively reinforcing stimuli (Wiener et al. 1989; Otto and Eichenbaum 1992); this is interesting, given dopamine's role in operant conditioning, but the proportion of cells that are reward-valence sensitive (2%) is far smaller than the proportion sensitive to the reward-valence independent location of the stimuli (9%) (Wiener et al. 1989). Recording hippocampal network activity *in vivo* reveals synchronous oscillation of membrane potential at various frequencies – some of which display specific behavioural correlates. Theta oscillations (6-12Hz) occur during an animal's movement through space (Rivas et al. 1996) and during arousal (Sainsbury et al. 1987); gamma oscillations (20Hz) can occur during olfactory sensation (Vanderwolf 2001) – their concrete behavioural function is still unclear but they may be involved, at a network level, in synchronizing activity and biasing information transfer between brain regions (Akam et al. 2012); sharp ripples – short lasting (up to 100ms) high frequency (120-200Hz) oscillations – are observed when an animal is at rest, which may serve to consolidate recently modified synaptic strengths (Buzsaki 1989). In this

thesis I am concerned less with these, broader functions of the hippocampus, but rather with synaptic transmission in smaller populations of synapses in the CA1 region alone.

1.3.3 An overview of CA1 synaptic physiology

Small central synapses (see figure 1.4) consist of a presynaptic axonal bouton juxtaposed with a postsynaptic dendritic spine, forming a synaptic cleft approximately 20nm in width (synapses can also form between pre-synaptic boutons and the post-

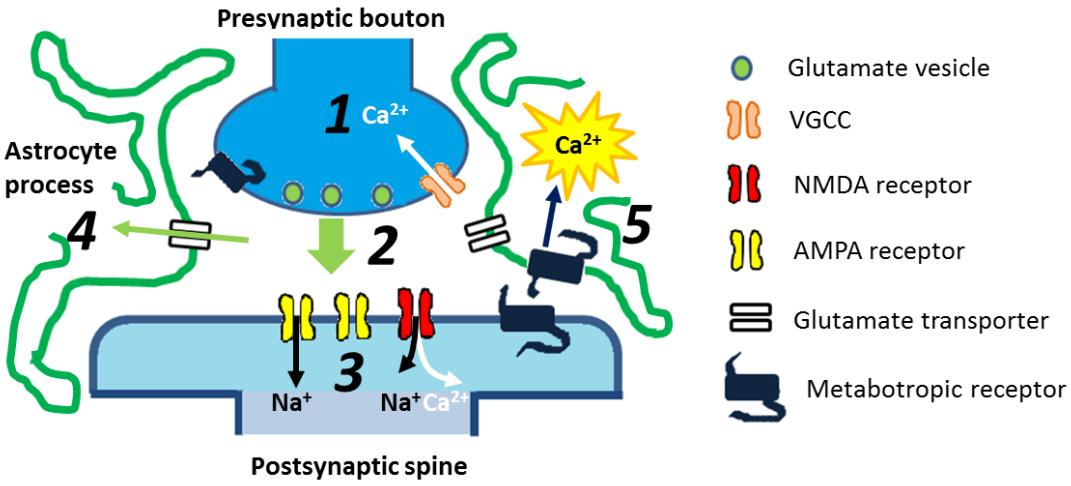

Figure 1.4 Basic physiology of glutamatergic synapses.

Figure shows physical layout of the synapse: presynaptic bouton (blue), postsynaptic spine (light blue) and astrocyte processes (green). **1** – presynaptic depolarization induced Ca^{2+} entry through voltage-gated calcium channels (VGCCs) triggers **2** – release of glutamate from presynaptic vesicles into the synaptic cleft. **3** – glutamate binds to AMPA and NMDA receptors in the postsynaptic membrane, triggering receptor opening and allowing Na^{+} and both Na^{+} and Ca^{2+} entry, respectively, leading to postsynaptic depolarization. **4** – astrocytic glutamate uptake from the synaptic cleft through astrocytic . **5** – metabotropic glutamate receptor activation can alter Ca^{2+} dynamics in both astrocytes and neurons.

synaptic cell soma or axon-initial segment). The presynaptic bouton contains a pool of readily releasable vesicles, docked to the presynaptic plasma membrane (Stevens and Tsujimoto 1995) that are loaded with neurotransmitter. Depolarization of the presynaptic membrane (for example during action potential invasion) opens voltage-gated calcium channels (VGCCs) (primarily P/Q and N-type at excitatory synapses onto CA1 pyramidal cells, (Dunlap et al. 1995)). The resulting Ca^{2+} influx into the presynaptic bouton triggers SNARE-protein dependent (Lin and Scheller 2000) exocytosis of neurotransmitter through the calcium sensor synaptotagmin (Geppert et al. 1994).

After release, neurotransmitter molecules diffuse across, or out of the synaptic cleft. They are then either taken up through plasma-membrane bound transporters into neighbouring astrocytes (or the presynaptic terminal) or can bind to receptors on the post-synaptic cell membrane. Such receptors fall into two categories: ionotropic receptors open upon ligand binding, allowing charged ions to travel down their electrochemical gradient; metabotropic receptors, when ligand bound, trigger an intracellular signalling cascade through dissociation of g-proteins. The main excitatory ionotropic receptors in the hippocampus CA1 region are glutamate receptors – the α-amino-3-hydroxy-5-methyl-4-isoxazolepropionic acid receptor (AMPAR), which allows influx of Na^{+} upon opening, and the N-methyl-D-aspartate receptor (NMDAR) that allows Na^{+} and Ca^{2+} influx (the NMDAR has a voltage-sensitive Mg^{2+} block that requires concurrent postsynaptic depolarization and glutamate binding to open). Gamma-aminobutyric acid type A receptors ($GABA_A$Rs) are the main inhibitory ionotropic receptors in the CNS, that open upon GABA stimulation to allow Cl^{-} influx. Other ionotropic receptors are present, including purinergic P2X receptors, nicotinic acetylcholine receptors (nAChRs) and serotonergic $5HT_3$ receptors, but are fewer in number.

Metabotropic receptors have a slower mode of action and can also be both excitatory and inhibitory. Group I metabotropic glutamate receptors (mGluRs) are generally excitatory: they are positively linked to phospholipase C via G-proteins and their activation leads to an increase in both inositol trisphosphate (IP_3) and diaglycerol (Fagni et al. 2000) – although they may become inhibitory through depletion of IP_3, in turn inhibiting other IP_3 dependent excitatory channels (e.g. purinergic X receptors). Type II/III mGluRs are broadly inhibitory, decreasing intracellular adenylate cyclase concentration via G-proteins, and are localized more presynaptically. Similarly, $GABA_B$ receptors are inhibitory and are found both presynaptically, where their activation has a negative effect on VGCC activity (Mintz and Bean 1993), and postsynaptically – triggering G protein-gated inward rectifying K^+ channels (Andrade et al. 1986). Adenosine receptors, Muscarinic acytlcholine receptors, serotoninergic 5HT receptors, noradrenergic receptors and dopaminergic receptors (see section 1) also have neuromodulatory actions at the synapse.

Leaf-like astrocytic processes enwrap ~60% of hippocampal synapses (although this is disproportionately weighted towards more active – large perforated – synapses, of which ~80% are enwrapped), forming the 'tripartite synapse' (Perea et al. 2009). These astrocytic processes maintain homeostatic stability by rapidly taking up presynaptically released glutamate (Bergles and Jahr 1997), through perisynaptic glutamate/Na^+ co-transporters, before converting it to glutamine and shuttling it back to the presynaptic neuron. Astrocytesas also buffer extracellular K^+ (Hertz 1965) through inwardly rectifying K^+ channels and $Na^+/K^+/2Cl^-$(Verkhratsky and Butt 2007).They can thus affect synaptic transmission through homeostatic mechanisms: glutamatergic excitation and control of membrane depolarization respectively (see section 1.1.2). In the last 20 years, astrocytes have been found to express many kinds of receptors whose activation can trigger intracellular Ca^{2+} increases (see section 1.1.4) and glial release of neuroactive compounds –

but the extent to which these astrocytic actions affect physiological synaptic activity is still unsure (Agulhon et al. 2010; Wang et al. 2013a).

1.3.4 AMPAR and NMDAR-mediated components of the Schaffer collateral and perforant-path synapses with CA1 pyramidal cells

The main excitatory input to CA1 pyramidal cells is the glutamatergic Schaffer collateral-CA1 synapse. Field recordings from the stratum radiatum display a voltage deflection (fPSP) mediated primarily by postsynaptic AMPA receptors after low-frequency stimulation (See chapter 2 for further detail on field recordings), with a much smaller postsynaptic NMDAR component (Herron et al. 1986; Morris et al. 1986; Otmakhova and Lisman 1999) due to the partial, voltage-dependent, Mg^{2+} block of the NMDA receptor pore at the negatively polarized membrane potentials of the CA1 pyramidal neurons. When these cells are voltage clamped to -70mV, this NMDAR blockade by Mg^{2+} is complete (Herron et al. 1986). Perforant path-CA1 synapses display smaller overall fPSPs in response to perforant-path stimulation than Schaffer-collateral-CA1 synapses (Otmakhova and Lisman 1999); and the NMDAR-mediated component is larger (in APV – an NMDAR blocker – pp. synapses display 18% reduction in response, and there is no significant APV effect at the S.C. synapse).

1.3.5 Different kinds of potentiation of the Schaffer collateral CA1 synapses

Potentiation refers to the increase of the synaptic current triggered by an unchanged stimulus. At the Schaffer collateral synapse, this phenomenon can fall roughly into three categories, based on length of persistence:

1.3.5.1 Paired-pulse (short-term) facilitation at Schaffer collateral synapses of the CA1 region of the hippocampus

After an initial electrical stimulation, a second stimulus, with an interstimulus interval up to several hundred milliseconds, gives a larger response. This is due to an increased residual Ca^{2+} in the presynaptic bouton, from the first stimulus, leading to an increased total Ca^{2+} concentration upon Ca^{2+} influx triggered by the second stimulus (Wu and Saggau, 1994). Change in the relative magnitude of this facilitation is evidence of a change in presynaptic release probability (Zucker and Regehr 2002) – important to bear in mind when considering the locus of all kinds of potentiation. Astrocytes can actively modulate facilitation by releasing ATP that, after being broken down to adenosine extracellularly by ectonucleotidases (Zimmermann and Braun 1996), inhibits presynaptic release through A1 receptors (Pascual et al. 2005); they can also modulate action-potential width and hence the magnitude of presynaptic Ca^{2+} influx from a constant axonal stimulus (Sasaki et al. 2011).

1.3.5.2 Post-tetanic potentiation at Schaffer collateral synapses of the CA1 region of the hippocampus

Repeated trains of stimuli can trigger longer lasting potentiation (up to several minutes) that cannot be completely explained by exponential decay of Ca^{2+} concentration in the presynaptic bouton, but is still dependent on presynaptic Ca^{2+}. This post-tetanic potentiation (PTP) is not fully understood, but could be mediated through presynaptic Ca2+ binding proteins (Zucker and Regehr 2002), metabotropic receptors (Miller 1998) and

ionotropic receptors (MacDermott et al. 1999). Although there is no implication in the literature that astrocytic Ca^{2+} activity is necessary for PTP, Sibille et al. (2014) have recently demonstrated that astrocyte K+ clearance from the extracellular space can regulate PTP – K+-channel 4.1 knockout in astrocytes increases PTP at Schaffer collateral synapses – a phenomenon that can be regulated by mGluRI activation (Devaraju et al. 2013).

1.3.5.3 Long-term potentiation at Schaffer collateral synapses of the CA1 region of the hippocampus

A more powerful stimulus – increased frequency, current, or number of stimuli than trigger TBS (e.g. classic high-frequency stimulation (HFS) consisting of 100 stimuli at 100Hz, given three times at 30s intervals) – can induce synaptic potentiation that lasts from hours *in vitro* (Bliss and Lomo 1973) to months *in vivo* (Abraham et al. 2002). This long-term potentiation (LTP) is mediated by the NMDA receptor (Collingridge et al. 1983). And can be divided into e-LTP, dependent on protein synthesis, and l-LTP, dependent on gene expression (Andersen et al. 2007). A huge amount of work has gone into demystifying the locus of LTP – but although it is generally agreed that at the Schaffer collateral it is primarily post-synaptically expressed (Andersen et al. 2007), there are studies that argue for a pre-synaptic component (Emptage et al. 2003). Astrocytes have been shown to be necessary for LTP induction (Henneberger et al. 2010) and also able to trigger LTP induction themselves (Perea and Araque 2007). LTP can be triggered chemically as well as electrically – for example, application of the chemical astrocyte marker sulforhdamine 101 triggers a long term increase in neuronal excitability by enhancing evoked synaptic NMDAR currents (Kang et al. 2010).

1.3.6 Potentiation of the Perforant Path-CA1 pyramidal cell synapses of the hippocampus

The perforant path input to CA1 pyramids in stratum Lacunosum-Moleculare does not display the same characteristic plasticity as the Schaffer collateral in stratum radiatum. LTP can only be induced in the presence of $GABA_AR$ blockers (Colbert and Levy 1993) – with GABA inhibition present, only short term PTP (<1min) is induced by their powerful potentiation protocol (8 pulses at 100Hz, delivered 8 times at 200ms intervals – repeated 3 times at 5 minute intervals). This can be explained by powerful local GABAergic inhibition at the perforant path synapse to CA1 (Ang et al. 2005; Capogna 2011) and, until recently, LTP at perforant path-interneuron synapses had yet to be found. However Leao et al. (2012) published modification of LTP supposedly induced at the SLM synapse – so the literature is controversial. It has been reported that perforant path input has a potentiating effect on Schaffer collateral inputs when temporally paired (Basu et al. 2013) – a phenomenon mediated by endocannabinoids (Xu et al. 2012) – so it may be that long-term potentiation of the perforant path-SLM synapses themselves may not occur *in vivo*.

1.3.7 Neuromodulation of hippocampal CA1 synaptic activity

The activity of CA1 pyramidal cells can be modulated by various neurotransmitters apart from the principle pair of Glutamate and GABA. Given the varied innervation that CA1 receives from amongst others, the septum (Cholinergic), Nucleus Coeruleus (noradrenergic), Raphe Nuclei (Serotonergic) and Ventral Tegmental Area (dopaminergic), this is hardly surprising. In the following section I will focus only on the neuromodulatory effects of dopamine in CA1 – for a review of other neurotransmitter effects please see Andersen et al. (2007).

1.4 Dopaminergic physiology

1.4.1 Dopamine in the mammalian brain

The monoamine dopamine is a major neurotransmitter of the brain. The dopaminergic system is complex and has been the subject of great interest since its discovery in brain tissue, in 1957 (Montagu 1957). Dopamine acts through both synaptic and extrasynaptic D1 and D2-like receptors (see section 1.1.2) – it is necessary for control of movement, reward processing and has been implicated in Parkinson's disease, schizophrenia and addiction (Iversen et al. 2010). Dopaminergic neurons are found in two neighbouring nuclei in the midbrain – the Substantia Nigra (SN) and the Ventral Tegmental Area (VTA) (Hokfelt et al. 1984). Dopaminergic efferents project from these two subcortical nuclei to the striatum, the limbic system and to the frontal cortices. Dopaminergic efferents from the more lateral substantia nigra pars reticulata (SNr) project primarily to the basal ganglia, and receives return projections, forming functionally separate, parallel-processing, loops; this dopaminergic nigro-striatal system is involved in action initiation (Iversen et al. 2010) – consequences of its disruption are vividly demonstrated in those suffering from Parkinson's disease. Dopaminergic efferents from the VTA to the basal ganglia target the shell of only the ventral striatum, but also innervate other brain regions (as do projections from the more medial Substantia Nigra Pars Compacta (SNc)) – the orbitofrontal (OFC) and prefrontal (PFC) cortices – the mesocortical pathway; the amygdala (Everitt et al. 1999) and the hippocampus (Gasbarri et al. 1994a; Gasbarri et al. 1994b) – the mesolimbic pathway. The mesocortical system has been implicated in working memory in the rat (Zahrt et al. 1997), macaque (Williams and Goldman-Rakic 1995) and human (Luciana and Collins 1997) and also encodes a reward signal in rat (Olds and Milner 1954) (and see Schultz et al. (1997) for further review), macaque (Mirenowicz and Schultz 1996) and human (Tobler et al.

2007). Addictive behaviour is caused by the pathological over-stimulation of this reward system; addictive drugs increase dopaminergic activity, assigning artificially high reward values to the environmental cues that conincide with drug action (Iversen et al. 2010). The mesolimbic pathway also controls incentive salience (Berridge 2007) – the strength of a conditioned response to a reward – through the amygdala (Everitt et al. 1999) and memory consolidation through the hippocampus (Li et al. 2003; Bethus et al. 2010; da Silva et al. 2012). It is the role of dopamine in the hippocampus that is central to this thesis and it is discussed in greater detail in section 1.5.3.

Dopamine exerts its cellular effects primarily (but not exclusively – see section 1.7.4) through activation of metabotropic, g-protein coupled receptors. These receptors fall into two categories – D1-type and D2-type receptors; understanding of their two different downstream signalling cascades, and the potential targets for their modulation, is crucial to the understanding of any effect of dopamine on astrocytes.

1.4.2 Dopamine receptor intracellular signalling cascades

The down-stream signalling cascades for D1-type and D2-type dopamine receptors are well described – but it is important to bear in mind that almost all the work so far has been done in neurons or culture expression systems (fibroblasts, HEK cells). Hence putative glial dopamine receptor signalling pathways may differ in some ways.

1.4.2.1 D1-type receptor signalling pathways

D1Rs and D5Rs are both excitatory in neurons (enhancing AMPA and NMDA receptor conductance (Snyder et al. 1998; Flores-Hernandez et al. 2000) and L-type

calcium-channel currents (Surmeier et al. 1995), contributing to neuronal depolarization) and hence they have been classified together, as the 'D1-type receptors' – see figure 1.1. They have 7 transmembrane domains (TMDs) and they interact with Gα and Gβγ proteins at a point between TMD6 and their N-terminus (Mackenzie et al. 1993). D5Rs show a higher affinity for the endogenous ligand dopamine compared to D1Rs and also display constituent activity, unlike D1Rs (Demchyshyn et al. 2000). D1-type receptors can oligomerize with many other proteins, most notably D2Rs – forming a receptor that activates Ca2+ transients via PLC (Lee et al. 2004), NMDARs (Lee et al. 2002) and adenosine receptors (Gines et al. 2000). Binding to these receptors activates αolf/αs subunit containing g-proteins that dissociate to Gβγ and Gαolf/s-GTP. Gαolf/s-GTP activates the enzyme adenylyl cyclase (AC) which synthesises cyclic AMP (cAMP) and in turn, cAMP activates PKA which has many phosphorylation targets (figure 1.5). One of these is DARPP-32 which is crucial in maintaining dopamine induced intracellular effects, by inhibiting dephosphorylation of downstream target proteins. D1-type receptors can potentiate AMPAR currents via cAMP mediated AMPAR phosphorylation (Roche et al. 1996) and NMDAR function through phosphorylation of the GluN1 subunit (Snyder et al. 1998); they can inhibit $GABA_A$Rs through the cAMP signalling pathway (Flores-Hernandez et al. 2000) and also inhibit voltage-dependent Na+ channels (Cantrell et al. 1997). They can enhance L-type Ca2+ channel opening, inhibit N- and P-type Ca2+ channels via cAMP (Surmeier et al. 1995) and regulate many cellular functions, including synaptic plasticity and transcription, through DARPP-32 activated ERK signalling (Thomas and Huganir 2004). Of particular relevance to this thesis is the possible existence of a phosphatidylinositol(PI)-linked D1-like receptor (so called because of its high affinity to the D1R selective ligand SCH23390) which couples to PLC through Gαq and can increase intracellular Ca2+ (Ming et al. 2006; Hasbi et al. 2009). As intracellular Ca^{2+} dynamics are thought to be crucial to astrocytic function

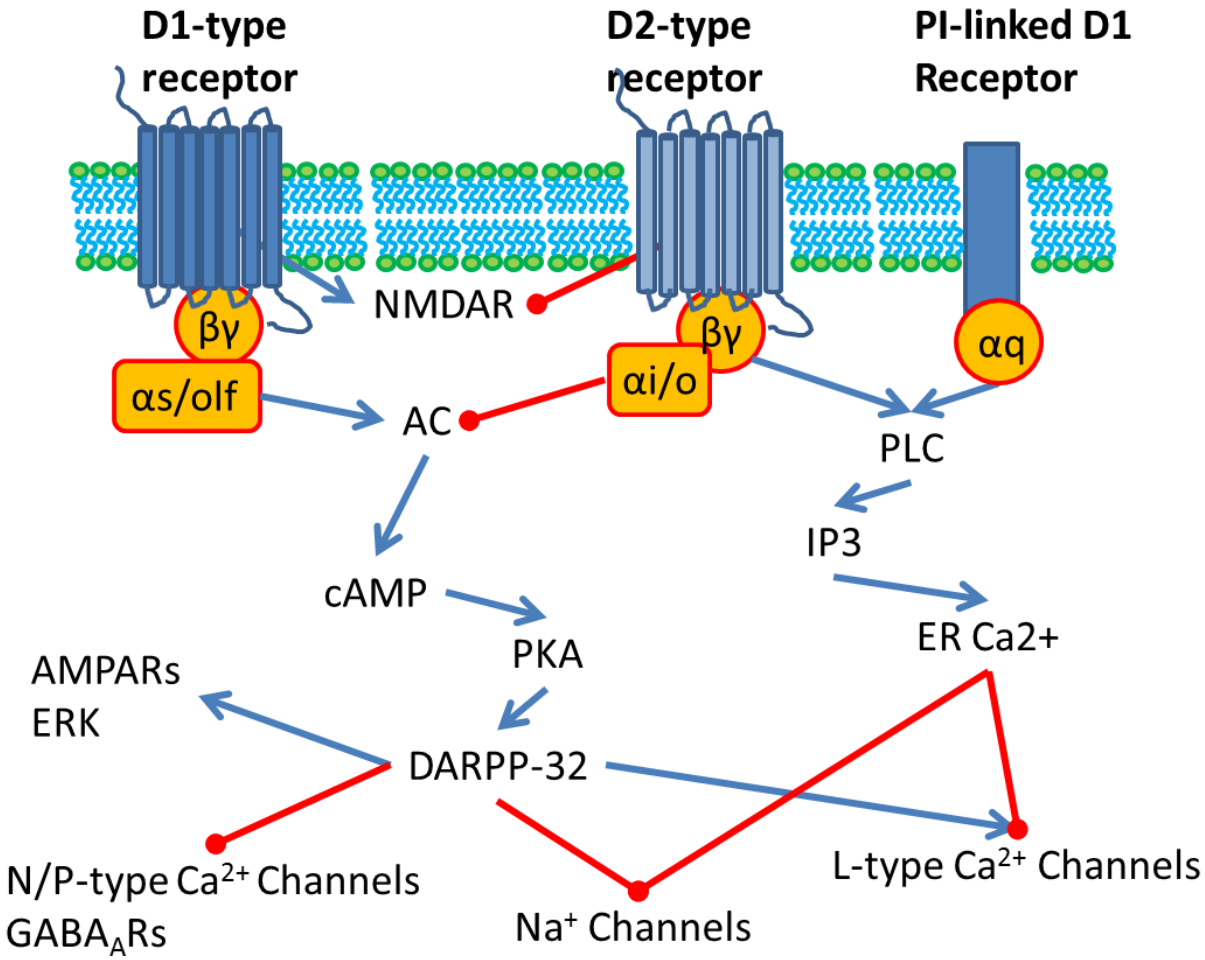

Figure 1.5 Summary of dopamine receptor signalling pathways.

D1-type dopamine receptors couple to Gαs/olf proteins that stimulate the AC/cAMP/PKA cascade. This activates DARPP-32 which can facilitate AMPARs, L-type Ca^{2+} Channels, and stimulates the ERK signalling cascade; it inhibits N/P-type Ca^{2+} Channels, Na+ channels and $GABA_A$Rs. D1-like receptors directly promote NMDAR function through protein-protein interaction. D2-like receptors couple to Gαi/o proteins that inhibit the AC/cAMP/PKA cascade. The Gβγ proteins activate PLC, which increases IP_3 production and hence Ca2+ release from the ER – this inactivates L-type Ca2+ channels and Na+ channels. PI-linked D1 receptors activate PLC through the Gαq protein.

(see sections 1.1, 1.2), this receptor could represent a plausible site of extracellular dopamine signal transduction into astrocytes (see section 1.1.3).

1.4.2.2 D2-type receptor signalling pathways

D2, D3 and D4 receptors are inhibitory in neurons (through AMPAR, NMDAR and L-type Ca^{2+} channel current decrease and subsequent neuronal excitability decrease (Iversen et al. (2010)) and are grouped together as 'D2-type receptors' – see figure 1.1. They have 7 TMDs, with the g-protein interaction occurring at intracellular loop 3. D3 shows slightly higher agonist affinity than D2 and D4, which are similar in this respect (Lachowicz and Sibley 1997). They can oligomerize with D1Rs (Lee et al. 2004) , CB1Rs (Kearn et al. 2005) and A2ARs (Torvinen et al. 2004; Torvinen et al. 2005). D2-like receptors are coupled to αi/o G-proteins that inhibit AC activation and its concomitant downstream pathways – this inhibition is tonically active in medium spiny neurons (MSNs) of the striatum. D2-type receptors activate PLC via Gβγ, increasing IP_3 production – raising the probability of intracellular Ca2+ release from the ER – which can inactivate L-type Ca2+ channels via calcineurin (Hernandez-Lopez et al. 2000). They can also inhibit NMDAR transmission via tyrosine kinase activation (Kotecha et al. 2002). The IP3 signalling cascade is an important excitatory one in astrocytes (Rusakov et al. 2011) – this could amount to a large difference between the role of dopaminergic signalling in neurons and astrocytes. D2-like receptors can also inhibit phosphorylation of the NMDAR directly through formation of the D2R-NR2B complex (Liu et al. 2006).

Hetero-oligomerization of D1 and D2 receptors has been found in cells co-expressing both receptor types in striatal neurons of the rat brain (Hasbi et al. 2011) – activation of this hetero-oligomer increases intracellular Ca^{2+} (in HEK cells) in a PLC-dependent fashion (Lee et al. 2004), via the Gq/11 protein (Rashid et al. 2007). This D1-D2 receptor oligomer activation has been found to modulate neuronal BDNF (Hasbi et al. 2009), GAD67 and VGLUT1/2 (Perreault et al. 2012) expression in the striatum. This could

be a neat way for existing dopamine receptor function to activate known astrocytic intracellular signalling pathways.

Dopamine's actions have been studied in many cell types and in many regions of the brain. It is clear from the literature that different brain regions and different cell populations display heterogenous responses to dopamine. In this thesis, I study the effects of dopamine in the hippocampus: dopamine plays a critical role in overall hippocampal function (Li et al. 2003) and in individual hippocampal cellular activity (Frey et al. 1990; Otmakhova and Lisman 1998; Andersson et al. 2012). Next I will describe the structure and function of the hippocampus, as well as the physiology of the synaptic transmission that is studied in this thesis.

1.5 Dopaminergic innervation and function in the hippocampus

1.5.1 The role of dopamine in hippocampus-dependent behaviour

The hippocampus is now considered an important target for dopaminergic innervation: novelty exposure induces hippocampal dopamine release (Ihalainen et al. 1999); in rats, hippocampal dopaminergic infusion enhances hippocampus-mediated 'win-shift' behaviour – the ability of the animal not to persevere in its response to a previously rewarding task, when the reward is switched to a different behavioural response (Packard and White 1991); lesion of the mesohippocampal afferents hinders performance in the Morris water maze (Gasbarri et al. 1996) – as does blockade of hippocampal dopamine receptor 1/5 (D1/5R), whilst D1/5R agonist infusion increases it (da Silva et al. 2012) – and spatial-novelty induced facilitation of hippocampal CA1 LTP could be blocked by intra-hippocampal infusion of a D1/5R antagonist (Li et al. 2003; Lemon and Manahan-Vaughan 2006) as could LTD (Lemon and Manahan-Vaughan 2006). Similarly VTA inhibition, through

baclofen infusion, decreases place cell stability (Martig and Mizumori 2011). Rossato et al. (2009) found that D1R activation controlled the persistence of hippocampus-dependent long-term memory storage and likewise, Bethus et al. (2010), found that long-term, location-dependent memory formation – but not short term – is mediated by hippocampal D1/5Rs; although a later study, using a more sensitive behavioural test has shown D1R-blockade induced working memory (~30 minute delay) impairment. The literature clearly posits a role for dopamine in hippocampal behavioural function, and specifically in the formation of long-term memory (Shohamy and Adcock 2010) and this is mirrored at a cellular level in the reported effects of dopamine on hippocampal CA1 pyramidal cellular physiology (see below).

1.5.2 Anatomy of the dopaminergic system of the hippocampus

The hippocampus receives dopaminergic innervation from the VTA primarily in the subiculum and S.L.M (Swanson et al. 1987) and stratum oriens (S.O) of CA1 (Beckstead et al. 1979; Verney et al. 1985; Gasbarri et al. 1997; Kwon et al. 2008) – see figure 1.2c – and these dopaminergic afferents form roughly 20% of the total innervation from both the VTA and the SNc (Gasbarri et al. 1994b), the rest of which is both glutamatergic and GABAergic. Dopamine release can be synaptic (Iversen et al. 2010) – or through volume transmission (Fuxe et al. 2010, Iversen et al. 2010), a form of transmission that is able to stimulate high-affinity dopamine receptors up to 8µm away (Rice and Cragg 2008). Given the location of the dopaminergic afferents in the hippocampus, this suggests a role for dopaminergic phasic transmission in the S.L.M and the subiculum, although slower-changing, wider-spreading tonic dopaminergic stimulation could play a role over a greater region. The hippocampus expresses both D1 and D2-like receptors in rat, monkey and humans in DG, CA3 and CA1 areas (Shohamy and Adcock 2010). In rat, D1Rs have been localized

histochemically in dorsal hippocampal CA1 (at higher concentrations in S.L.M) and in DG (Savasta et al. 1986). Likewise D2Rs have been found in dorsal and ventral CA1 (Yokoyama et al. 1995) and have been reported to be localized in S.L.M (Goldsmith and Joyce 1994); D3R mRNA is found in the hippocampus (Richtand et al. 2010); hippocampal D4Rs have been detected with antibody staining (Defagot et al. 1997) and D5Rs are expressed in rat CA1 cell bodies only (although throughout the dendritic tree in humans) (Khan et al. 2000).

It is clear that dopamine can be released and sensed in the hippocampus – and that this plays a role in behaviour – but the physiological mechanisms of its action are controversial: it is not clear which hippocampal subregions and cell populations express the various dopamine receptor subtypes, the extent of their modulation of neuronal activity and what constitutes a physiological release of dopamine. Here I discuss only the effects of dopamine in area CA1 – the region relevant to this thesis.

1.5.3 Dopamine's actions on basal neural activity in Stratum radiatum

Dopamine can have biphasic effects on CA1 pyramidal cell firing rates (recorded extracellularly), that are mediated by different receptors (Smialowski and Bijak 1987). This is indicative of the complex nature of dopaminergic modulation of the CA1 region. Dopamine application has a small, but highly significant inhibitory effect on basal synaptic transmission, mediated through NMDARs (Otmakhova and Lisman 1999) – the authors did not investigate through what dopamine receptors (if any) this effect is mediated in the S.R, although it does appear to act presynaptically. In another paper published the same year the same authors report that addition of the D1/5R agonist 6-Chloro-PB does not inhibit combined AMPAR and NMDAR-mediated synaptic transmission (Otmakhova and Lisman 1998), this is indirect evidence that the inhibitory effect could be D-2 receptor mediated (if it is mediated by a dopamine receptor at all). Interestingly, they appear to see the

maximum inhibition at the lowest tested dopamine concentration (1µM), with inhibition having disappeared by 100µM application: this could be explained either by preferential activation of higher affinity D2-like receptors at lower concentrations (Hsu 1996) or activation of a different, more sensitive, inhibitory cell type: dopamine activates GABAergic signalling in the hippocampus (Gulledge and Jaffe 2001), and in the PFC (Trantham-Davidson et al. 2004) which has a transient inhibitory effect on CA1 pyramidal neurons (Gribkoff and Ashe 1984) – although it has also been reported to decrease GABAergic signalling in the prefrontal cortex via D2Rs and D4Rs (Wang et al. 2002; Trantham-Davidson et al. 2004).

1.5.4 Dopaminergic control of synaptic plasticity in Stratum radiatum

The primary action of hippocampal dopamine has been reported on plasticity, where dopamine has been proposed to mediate informational saliency-induced long term potentiation (LTP) (Hansen and Manahan-Vaughan 2012). Frey et al. (1989), first reported that D2-like receptor blockade with domperidone blocked late hippocampal LTP (l-LTP) (reproduced by O'Carroll and Morris, 2004), and then went on to show that the D1-like receptor was also necessary for hippocampal l-LTP (Frey et al. 1990). This is a confusing result, as D1-like and D2-like receptors have opposing actions on pyramidal neurons (see section 1.3.2), but it could be explained by the mediation of l-LTP through a D1-D2 receptor oligomer, requiring activation of both D1 and D2 subunits to activate downstream pathways – such oligomers have been found in striatum (Rashid et al. 2007). As noted above, the hippocampus has been reported to express both D1 and D2-type receptors – but which is responsible for dopamine's documented effects on synaptic plasticity? Below I discuss the evidence for D1 and D2-type receptor involvement.

1.5.4.1 D1-type receptor-mediated dopaminergic actions in the hippocampus

There is support for both the involvement of both receptor types: pharmacological D1/5R activation alone can induce l-LTP (Huang and Kandel 1995; Yang 2000) – but see Mockett and Brooks and Navakkode et al. (2007). D1R knockout mice do not express l-LTP (Matthies et al. 1997). D1/5R activation can also enhance e-LTP (Otmakhova and Lisman 1996), inhibit LTP depotentiation (Otmakhova and Lisman 1998; Kwon et al. 2008) and have been reported to reverse LTD (Mockett et al. 2007). Swanson-Park et al. (1999) also show D1/5R mediated enhanced LTP maintenance. However, counter-intuitively, they also find that stimulation of the cAMP pathway through which D1/5Rs act, this time by β-adrenergic receptor stimulation, does not enhance LTP maintenance. Rather it enhances LTP induction. They suggest this dissociation could be due different location of dopamine and adrenergic receptors, dopamine receptors synaptically and adrenergic receptors on the cell body. A location-specific function of cAMP coupled receptors could explain the effects of dopamine on intrinsic pyramidal cell excitability: Roggenhofer et al. (2010) found that D1/5R agonists facilitated potentiation of intrinsic excitability in Subicular, but not CA1 pyramidal cells (using alvear, not Schaffer collateral stimulation) and Wei et al. (2013) report that dopamine inhibits potentiation of intrinsic CA1 pyramidal neuron excitability. This could also be explained by cell location – PFC neurons, like subicular neurons, exhibit D1R (via NMDARs)-mediated excitability increases (Wang and O'Donnell 2001; Tseng and O'Donnell 2004). VTA inactivation has recently been shown to block LTP consolidation from a high-frequency stimulation (HFS) in CA1 *in* vivo (Ghanbarian and Motamedi 2013). It has also been found that D1-type receptors can enhance LTD at CA1 pyramidal cells in an NMDAR and GABA-mediated fashion (Chen et al. 1996), and Phosphatidylinositol-linked novel D1R (a recently described dopamine receptor type) stimulation has been reported to facilitate hippocampal LTD (Liu et al. 2009b), increasing the likelihood that dopamine action

in the hippocampus is linked to interneuronal function. Co-incident D1R activation and taurine uptake has been reported to potentiate l-LTP induction in the hippocampus (Suarez et al. 2013) – this is potentially exciting as astrocytes can release taurine (Hogerton and Bowser 2013; Suarez et al. 2013) and, in the NAcc *in vivo*, local infusion of ethanol simultaneously increases concentrations of both dopamine and taurine through astrocyte swelling (Adermark et al. 2011). Dopamine has also been reported to decrease PTP amplitude and enable STP induction in prefrontal cortex (PFC) pyramidal neurons in a layer specific, D1-type receptor-dependent fashion (Young and Yang 2005) as well as increasing short-term depression at recurrent inhibitory synapses in the neostriatum via D1-type receptors (Tecuapetla et al. 2007).

1.5.4.2 D2-type receptor-mediated dopaminergic action in the hippocampus

With regard to D2-type receptors, blockade of dopamine transporters, and the concomitant increase in extracellular dopamine, was found to enhance e-LTP induction in a D3 receptor-dependent manner (Thompson et al. 2005; Swant and Wagner 2006) and D3 activation has been found to disinhibit activity at the Schaffer collateral synapses via $GABA_AR$ endocytosis (Hammad and Wagner 2006; Swant et al. 2008); but D4 receptor activation – following NRG1 induced phasic dopamine release – was found to trigger LTP depotentiation (Kwon et al. 2008). These different findings could be explained by the kinetics of the dopaminergic stimulus – tonic (slower) in the former, phasic (faster) in the latter – as well as the location of the dopamine release and the maximal concentration of dopamine reached: it is reasonable to assume that phasic application would reach higher concentrations than tonic, given the washout of intrinsic dopamine released by the solution perfusion. Interestingly, in the prefrontal cortex (PFC), tonic hyperactivation of D2 receptors

can erode electrically induced long-term potentiation of pyramidal neurons (Xu et al. 2009) – supporting an inhibitory role for D2-type receptors. This could indicate a functional difference between brain areas, or it could be due to the difference in the LTP induction protocols used by Swant and Wagner – High-frequency stimulation (HFS) – and Xu et al. – Theta-burst stimulation (TBS) – as TBS activates less GABAergic inhibition, due to $GABA_B$ autoreceptor activation (Davies et al. 1991), and so will stimulate fewer downstream signalling pathways and less interneuron activation. Stratum radiatum interneurons also respond to dopamine, which has been suggested to inhibit GABAergic transmission via D3Rs (Swant et al. 2008) (although see Xing et al. 2010) and to regulate gamma-oscillations via D4Rs (Andersson et al. 2012).

It is worth considering that some of this controversy around dopamine function may be due to the *in vitro* nature of the recordings in many of the studies, *in vivo* work points more consistently towards D1-like receptor mediated potentiation in hippocampal CA1 excitatory transmission (Li et al. 2003; Ortiz et al. 2010).

1.5.5 Dopaminergic physiology in Stratum Oriens of the hippocampus

Recording from the basal dendrites of CA1 pyramidal cells In the stratum oriens, there is no reported effect of dopamine on baseline glutamatergic transmission (from alvear stimulation), but both blockade of the dopamine transporter and activation of D1/5Rs with specific agonists have been reported to potentiate LTP (Stramiello and Wagner 2010); conversely, activation of the D4 receptor reduces e-LTP, through inactivation of the NMDAR (Herwerth et al. 2012).

1.5.6 Dopaminergic physiology in Stratum Lacunosum-Moleculare of the hippocampus

In the stratum Lacunosum-Moleculare, basal glutamatergic transmission at the perforant path-CA1 pyramidal cell synapse is strongly inhibited (~40% decrease) by dopamine application (Otmakhova and Lisman 1999; Otmakhova and Lisman 2000) – although this was at high concentrations (20μM) of dopamine and the effect may not be this marked in more physiological situations. This inhibition affects NMDAR current (~60% drop) disproportionately compared to AMPAR current (~40% drop) and which can be partially blocked by either D1/5 or D2/3 receptors, mostly blocked by concurrent blockade of both and completely blocked by the atypical dopamine receptor antagonist clozapine – although clozapine is not specific to dopamine receptor subtype, and can also antagonize serotonergic 5HT receptors, so it is uncertain whether clozapine acts here only as a dopaminergic antagonist. No other action of dopamine in the SLM has been reported.

The above studies have focussed on neuronal activity in the hippocampus and dopaminergic modulation of such activity. However the hippocampus contains a large population of glial cells, cells that have over the last 20 years been considered increasingly important to our understanding of brain function. To date, surprisingly, nothing has been published on hippocampal glial interaction with dopamine throughout CA1. Astrocytes are the glial cells I investigate in this thesis and in the next section I will describe their structure and functions.

1.6 Dopaminergic signalling in astrocytes

Throughout this thesis, I am concerned with the putative interaction between astrocytes and dopamine *in situ* – specifically in the hippocampus. In this section I will examine, in detail, the previous work that has been done trying to establish whether dopamine can stimulate astrocytes and whether this is physiologically relevant (figure 1.7). Based on the literature below, I look to test two broad hypotheses in this thesis: firstly, do astrocytes *in situ* respond to dopamine with Ca^{2+} transients and if so, through what mechanism? Secondly, do such Ca^{2+} transients play a role in synaptic communication? I will now discuss the current position of the field with regards astrocytic response to dopamine; in the next section I will discuss the possible physiological relevance of previously reported astrocytic Ca^{2+} signals.

1.6.1 First reports of an astrocytic response to dopamine

In 1999, cultured astrocytes were found to respond with increases in intracellular cAMP to application of dopamine, as well as the D1 receptor agonist SKF 38393 and the mixed D1/2 receptor agonist apomorphine (Zanassi et al. 1999). This cAMP accumulation was region-dependent, being highest in striatally-derived astrocytes, lower in cortical astrocytes and not present in cerebellar Bergmann glia. They also showed that striatal astrocytes exclusively express D1R mRNA which is translated into the D1R protein. This is an important result for a number of reasons – not only does it show that astrocytes can express functional dopamine receptors, that can activate similar pathways to those in neurons, but also that their expression of these receptors is heterogeneous throughout the brain. Heterogeneous expression could indicate situational control of the receptor expression *in situ*, arguing for a physiological role for the D1R in astrocytes. A major caveat when considering culture studies is the extreme responsiveness of astrocytes to their

surroundings and their ability to change their receptor expression patterns when shifted into a culture environment for more than a few hours (Shao and McCarthy 1993; Kimelberg et al. 1997) – and the cells studied by Zanassi et al. had most likely been cultured for over 2 weeks – not to mention the fact that the cells for culture are harvested at a very different developmental stage to adult astrocytes. However the fact that tissue-related differences can be seen between populations of astrocytes in this study is a reassuring sign – if dopamine receptor expression were a methodological artefact, one would expect all cultured cells to respond similarly. Striatal astrocytes have since been found to respond to dopamine, over a 12h exposure, with a decrease in FGF-2 expression (Reuss and Unsicker 2000) but an increase NGF and GDNF upon 24h stimulation with non-selective dopamine receptor agonist apomorphine (Mizuta et al. 2000).

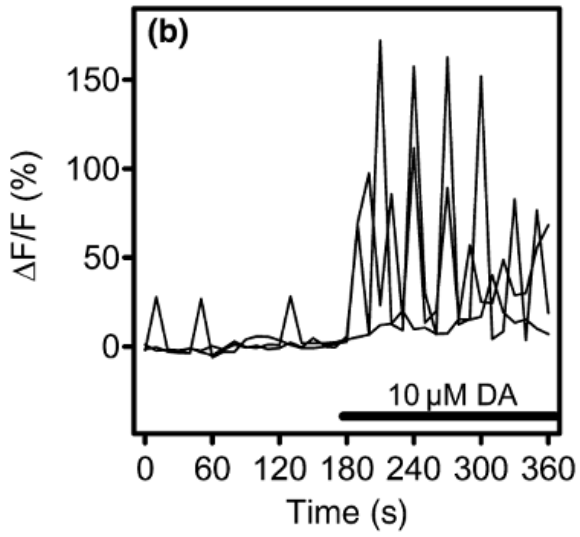

Figure 1.6 Change in calcium-dependent dye fluorescence in cultured astrocytes in response to dopamine.

10µM dopamine application to cultured astrocytes triggers an increase in amplitude and frequency of somatic calcium transients. Adapted from Requardt et al. 2012, Fig 1b.

Dopamine application (a high concentration – 50µM) was then shown to trigger massive intracellular Ca2+ increase in cultured hippocampal astrocytes (Parpura and Haydon 2000) – an increase they argued crossed the threshold for astrocytic activation of a slow inward current (SIC) in neurons, thus displaying a possible physiological role for astrocytes in dopaminergic transmission. In fact it comprehensively smashes the threshold Ca^{2+} concentration increase required for SIC stimulation – an increase to 200nM from ~90nM is sufficient for SIC generation and dopamine triggers an estimated (transient) concentration increase to 2.5mM. However the almost qualitative difference between the Ca^{2+} responses to uncaging and dopamine may indicate that they do not necessarily trigger the same downstream pathways (in this case neuronal SICs), and the authors fo not directly test the application of dopamine on SIC induction. An example of dopamine-induced (10µM) astrocytic Ca^{2+} increases is given in figure 1.6. Khan et al. (2001) identified a population of cortical astrocytes in monkey that expressed D2 receptors: this precise localization in fixed brain tissue was only possible with electron microscopy, given the extreme proximity of the D2- expressing astrocytic processes to the neighbouring interneurons. They went on to show D2R expression and agonist (quinpirole) induced astrocytic Ca2+ transients in freshly isolated rat and mouse cortical astrocytes – this is the only study reporting a D2 receptor agonists induced Ca^{2+} increase, but it is important to note that their Ca^{2+} fluorescence measurements are taken at low temporal resolution (every 3s) and their cells show heterogenous dye loading across the cytoplasm (indicating possible unequal loading of intracellular compartments). The small response amplitudes are also very small (peaking at 1.2 F/F_0) and no clear link between the time-course of drug application and the observed Ca^{2+} signal.

1.6.2 Astrocyte dopamine physiology mediated by D2-like receptor signalling

As mentioned above, the only study to report a D2R-mediated astrocyte Ca^{2+} increase does not provide strong evidence for a D2R-linked Ca^{2+} signalling mechanism. However, there is now considerable evidence for astrocytic expression of D2-like receptors in rat brain – cultured glioma cells are sensitive to D2R stimulation (Luo et al. 1999) as are normal cultured astrocytes taken from the whole brain (Ohta et al. 2010) and from the striatum specifically (Hosli and Hosli 1986; Bal et al. 1994; Miyazaki et al. 2004) – which also express D2R mRNA (Bal et al. 1994). Human astrocytes express D2Rs in the PFC, as assayed immunohistochemically and under electron microscopy (Khan et al. 2001). Rodent astrocytes also display D2Rs labelling under electron microscopy (Duffy et al. 2011) and astrocytic αβ-crystallin production is disrupted in astrocyte-specific D2R knockout mice (Shao et al. 2013). Astrocytic D2R activation has been linked to various downstream effects: increase in BDNF, GDNF and NGF mRNA expression and protein synthesis (Ohta et al. 2010); increased protein tyrosine phosphorylation (Luo et al. 1999); FGF-2 secretion (Li et al. 2006); reduction of S100β secretion (Nardin et al. 2011); suppression of αβcrystallin mediated neuroinflammation (Shao et al. 2013) and increases in intracellular free Ca^{2+} (Khan et al. 2001; Reuss and Unsicker 2001). With the notable exception of Shao et al. (2013) and Nardin et al. (2011), the above studies have all been done in culture. Although evidence is accumulating for a physiological role of astrocytic D2Rs a convincing demonstration of their ability to induce astrocytic Ca^{2+} transients (if at all) is still lacking.

1.6.3 Astrocyte dopamine physiology mediated by D1-like receptor signalling

Classical D1-likeRs are expressed on rat striatal astrocytes (Hosli and Hosli 1986; Vermeulen et al. 1994; Zanassi et al. 1999; Miyazaki et al. 2004; Li et al. 2006) and may be expressed in cortical astrocytes (Zanassi et al. 1999; Requardt et al. 2012). Astrocytic

classical D1-likeRs have been reported to stimulate cAMP production and PKA activation (Zanassi et al. 1999), increase astrocytic GDNF and NGF expression (Ohta et al. 2010); increase FGF-2 expression (Li et al. 2006) and modulate NADH expression (Requardt et al. 2012 – see below).

Reports of astrocytic expression of novel PI-linked D1-likeRs is of great interest – given their interaction with IP3-mediated Ca^{2+} release, the major astrocytic intracellular signalling pathway. Increases in intracellular free Ca^{2+} in cultured cortical astrocytes can be stimulated by a specific PI-linked D1-likeR agonist (SKF83959) in a D1R and IP3 dependent manner (Liu et al. 2009b), this Ca^{2+} signal promotes ERK activation (Huang et al. 2012); in the striatum, this Ca^{2+} signal modulates astrocytic FGF-2 expression (Zhang et al. 2009).

1.6.4 Astrocyte metabolic interaction with dopamine

Recently, the DA-induced astrocytic Ca^{2+} signal was proposed to have a metabolic route (figure 1.7). Astrocytes can express the dopamine transporter (DAT) in glioma cells (Russ et al. 1996), cultured cortical astrocytes (Inazu et al. 1999) and in striatal tissue – although Kittel-Schneider et al. (2012) found no DAT expression in cultured astrocytes. The norepinephrin transporter (NET) has also been found in cultured cortical astrocytes (Inazu et al. 2003) – Takeda et al. (2002) reported that dopamine uptake was mediated by the NET, not the DAT. Regardless of the transporter type, it is possible for astrocytes to move dopamine from the extracellular space into their cytosol. Vaarmann et al. 2010 propose that intracellular DA catabolism triggers astrocytic Ca^{2+} transients. DA is one of several monoamines catabolized by monoamine oxidase (MAO), which is expressed in astrocytes, and the H2O2 produced was proposed to activate PLC and IP3 Ca signalling via lipid peroxidation, in a DAR-independent manner. Requardt et al. (2012) could not reproduce this, however, and suggest it may be an artefact from H2O2 build up from DA auto-

oxidation. Takano et al. (2013) reported a slight increase in extracellular superoxide dismutase production upon stimulation of cultured cortical astrocytes with DA – so

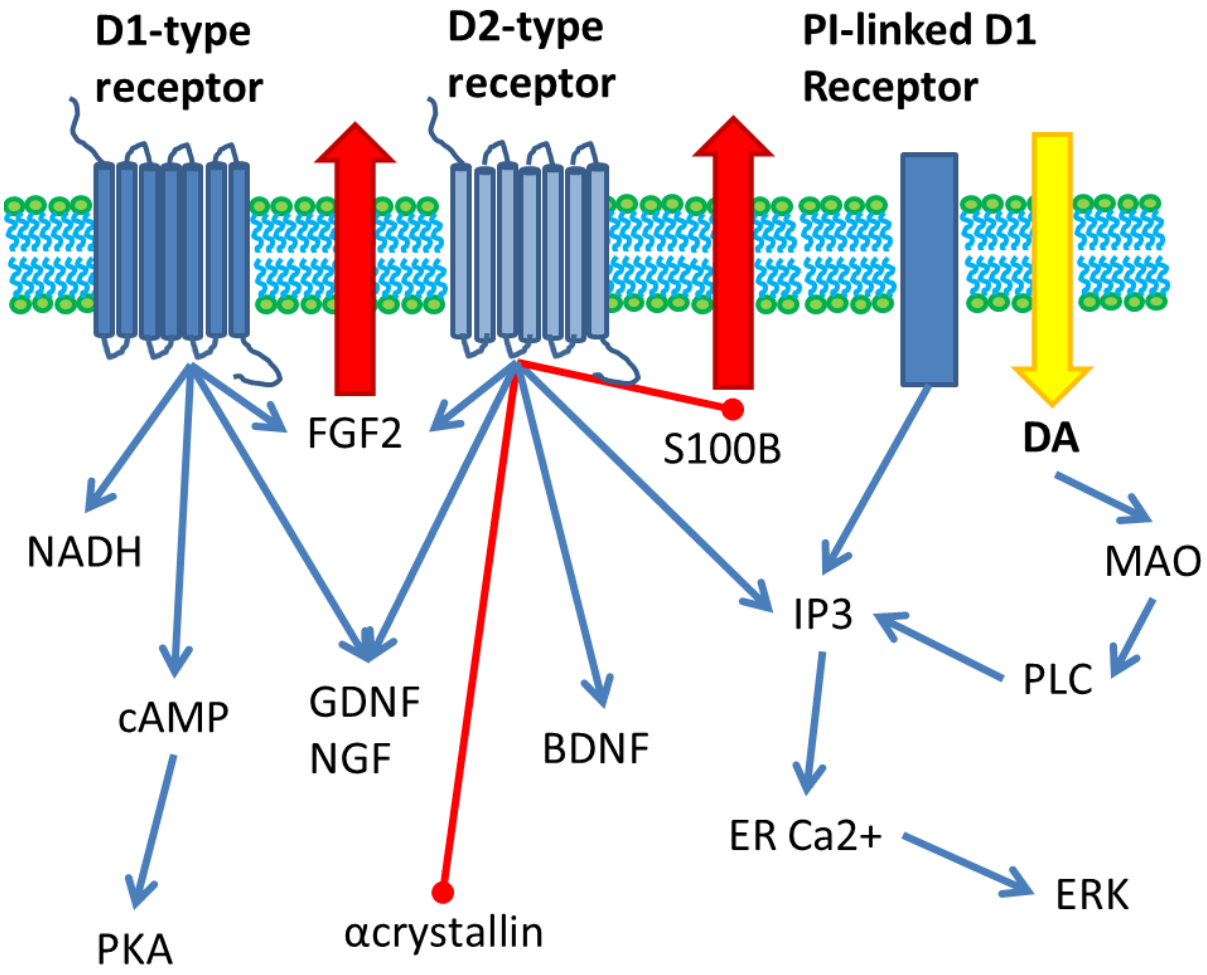

Figure 1.7 Summary of reported dopamine signalling pathways in Astrocytes.

D1-type dopamine receptors can trigger NADH increase, cAMP and concomitant PKA increases, and it can trigger increased expression of NGF, GDNF and FGF2. D2-type dopamine receptors can increase NGF, GDNF, BDNF and αcrystallin expression as well as inhibiting S100B and FGF2 secretion. They also trigger ER Ca2+ increase through IP3, which itself can enhance ERK signalling. Dopamine entry into the cytoplasm, upon breakdown by MAO can stimulate IP3 production through PLC activation.

astrocytes may be involved in extracellular free radical removal. Requardt et al. (2010) found that DA triggers an increase in intracellular NADH, both in cortical cultures and slices; they later showed (Requardt et al. 2012) that DA can act synergistically with NADH (via D1Rs) to stimulate cultured cortical astrocyte Ca^{2+} activity.

1.6.5 Effect of antipsychotics on astrocyte cellular physiology

The atypical neuroleptic (a class of antipsychotic medicinal drugs) clozapine is a non-specific dopamine receptor antagonist (as well as a serotonergic, adrenergic and muscarinic receptors) that has been reported to stimulate astrocytes directly and hence is a source of separate interest. They have been shown to downregulate astrocytic dopaminergic sensitivity after a 12h exposure (Reuss and Unsicker 2001); enhance D-Serine and glutamate release after a 1h clozapine incubation (Tanahashi et al. 2012) and enhance S100β secretion in cultured astrocytic C6 glioma cells – the same is true for Haloperidol, another antipsychotic that also blocks dopamine receptors. However, it is important to note that these antipsychotics are dirty drugs, acting on all kinds of dopamine receptors to a degree as well as 5-HT receptors.

Overall, the literature is clear that astrocytes can express DARs and that DA itself can induce astrocytic Ca^{2+} transients (at least in culture) – but there is still uncertainty as to the mechanism by which it does so. However the physiological relevance of the Ca^{2+} dynamics, from various kinds of astrocytic stimulation, is still hotly debated. I will next detail the one outstanding area of research regarding the role of astrocytic Ca^{2+} transients – gliotransmission – and the controversy over their physiological importance.

1.7 Thesis aims

Dopamine is a hugely powerful neurotransmitter in the brain and likewise astrocytes are becoming recognized as highly functional targets for neurotransmitter signalling – both are intimately involved with fundamental neurophysiological function and in pathogenesis of the brain. Hence elucidating the physiological connection between astrocytes and dopamine is of the great importance, with potential benefits for our understanding of the brain and in tackling health and disease. However, our understanding of astrocyte-dopamine physiology is still rudimentary – most of our knowledge comes from studies in culture and the literature has yet to agree on an astrocytic signalling mechanism for dopaminergic stimulation. Our knowledge of astrocytic Ca^{2+} activity and dopaminergic function is wide-ranging and detailed enough to allow clearer characterization of their possible interactions *in situ* – and this is the aim of this thesis.

To complete this aim I have split this thesis into four main objectives:

1.7.1 Thesis objective 1: characterize the astrocytic Ca^{2+} response to dopamine in hippocampal slice

. Dopamine-induced astrocytic Ca^{2+} activity has only previously been recorded in culture conditions (see section 1.6), so the nature of the Ca^{2+} response recorded *in situ* will be novel because of the morphological, developmental and possibly biochemical differences of astrocytes *in situ*. This objective is split over two results chapters, organized by the method used to image intracellular Ca^{2+}: chapter 3 uses AM-dye bulk-loading, chapter 4 uses membrane-impermeable dye loading via whole-cell patch clamp. These methods are complimentary, given that bulk-loading will not affect the intracellular milieu, whereas whole-cell patch-clamp will offer greater sensitivity and spatial resolution.I will

first address the simple question: Can astrocytes respond to topically applied dopamine with Ca^{2+} transients *in situ*? Secondly, I will investigate the intracellular signalling pathways that underlie the dopaminergic Ca^{2+} transients – this will be done primarily through pharmacological blockade of putative elements of the signalling cascades, but also with some genetic tools.

1.7.2 Thesis objective 2: test for an astrocytic role in dopaminergic modulation of neuronal activity in the hippocampus.

Dopamine has various effects on the activity of neurons in the CA1 region of the hippocampus (see section 1.5). It has a clearly defined inhibitory effect on basal synaptic transmission at the perforant path synapse in Stratum Lacunosum-Moleculare – in chapter 5, I test whether interfering with local astrocytic Ca^{2+} dynamics (using both fluoracetate and astrocytic internal calcium clamp) changes the dopaminergic inhibition of these synapses' response to perforant path stimulus.

In Stratum Radiatum, at the Schaffer Collateral synapse, dopamine's actions on neuronal activity are more controversial; but the prevailing opinion is that it positively modulates synaptic potentiation (as well as a slight, but significant depression of baseline transmission). In chapter 6, I use fluoroacetate to interfere with astrocytic metabolism and then probe dopamine's ability to affect short-term potentiation and baseline synaptic transmission in response to Schaffer Collateral stimulation. 3

1.7.3 Thesis objective 3: creation of a model system to study physiologically released dopamine in hippocampal slice

A major shortcoming of work on dopamine's action in the hippocampus is the inability to stimulate dopamine release from hippocampal dopaminergic terminals in a physiological manner (see section 5). Chapter 7 details the attempted development of channelrhodopsin-expressing projections from dopaminergic neurons of the ventral tegmental area that would innervate the hippocampus and be under light-control.

Chapter 2: Methods

2.1 Hippocampal slice work: methods for preparation, electrophysiology and imaging *in situ*

2.1.1 Hippocampal slice preparation

2.1.1.1 Animals sacrificed

Unless otherwise stated, all experiments were carried out on tissue taken from 3-4-week-old male Sprague–Dawley rats. A series of calcium imaging experiments were carried out on 'IP_3-sponge' mice: these mice express an IP_3 buffer specifically in astrocytes. *GST-IP_3 sponge-TetO-nls-LacZ* mice, expressing doxycycline-gated glutothione-linked IP_3 receptor fragments that are capable of buffering IP_3 signalling, (Uchiyama et al. 2002), were crossed with *GLT-1-tTA* mice for specific astrocytic expression of the IP_3 sponge. For details of the generation of this mouse line see (Tanaka et al. 2013). Control animals came from C57BL/6 lineage. 3-4-week-old male mice were used in all experiments. All experiments were performed blind to genotype. All experimental protocols were carried out in full compliance with UK guidelines on animal experimentation or were approved by the RIKEN Institutional Animal Care and Use Committee.

2.1.1.2 Acute excision and slicing of hippocampal tissue

Acute hippocampal slices, 350µm thick, were obtained from 3-4-week-old male Sprague–Dawley rats or 3-4 week old 'IP_3-sponge' mice. Animals were anaesthetized to death with a lethal intraperitoneal injection of Sodium Pentobarbitol. The skull was opened up and the brain excised into an ice-cold slicing solution containing (in mM): NaCl 50,

sucrose 105, KCl 2.5, $MgCl_2$ 7, NaH_2PO_4 1.25, $CaCl_2$0.5, Ascorbic acid 1.3, Sodium Pyruvate 3, and glucose 6 (osmolarity 304–312 mOsM), continuously bubbled with 95% O_2/5% CO_2. The whole hippocampus was dissected, placed in an agar block and transverse slices were prepared using a Leica VT 1200S slicer**.** Slices were then transferred to slicing solution kept at 34 °C for 15 min before being transferred to an interface or an immersion chamber containing Ringer solution (see below for solution recipe). For recording in the Stratum Lacunsom-Moleculare (SLM) and for recording NMDA receptor-mediated currents, CA3 was cut off from the slice.

2.1.1.3 Post-slicing tissue incubation

Slices were allowed to rest for at least 1h before recordings, in Ringer solution containing (in mM) NaCl 119, KCl 2.5, $MgSO_4$ 1.3, NaH_2PO_4 1, $NaHCO_3$ 26, $CaCl_2$ 2, glucose 10 (osmolarity adjusted to 298–302 mOsM with glucose). All solutions were continuously bubbled with 95% O_2/5% CO_2.

For bulk-loading slices with the astrocyte-specific morphological dye Sulforhodamine 101 (SR101) and Fluo-4-AM (chapter 3)**,** the following protocol was used:

1) Rest for 30 minutes in Ringer
2) Incubate in 10µM SR101 for 10 minutes at 35°C
3) Wash in Ringer
4) Incubate in 5µM SR101 + 5µM Fluo-4-AM + 0.04% Pluronic Acid for 40 minutes at 35°C
5) Wash in Ringer
6) Rest in Ringer for 30 minutes.
7) Slices ready for recording

Slices were stored for up to 1h after completing this protocol before recording.

2.1.2 Recording equipment preparation

2.1.2.1 Patch pipettes and intracellular pipette solutions

Micropipettes, pulled from borosilicate, filamented glass, were used for all electrophysiological recordings. For astrocyte whole-cell patching, pipette resistances were 3-5MΩ. For field recordings, extracellular pipette resistance was reduced to 1-2MΩ, except for when recording fEPSPs in proximity to a patched astrocyte – here pipettes with higher resistance tips (3-5MΩ) were used in order to disturb the tissue less. Extracellular fEPSP recording electrodes are filled with the same Ringer solution as in the recording bath, including any additional drugs used. Pipette tips were not polished. Upon filling with solution, pipettes with visible blockage were discarded.

Whole cell recording electrodes were filled with intracellular Potassium methyl-sulphonate (KMS) solution containing (in mM): KCH_3O_3S 135, HEPES 10, disodium phosphocreatine 10, $MgCl_2$ 4, Na_2ATP 4, NaGTP 0.4 (pH adjusted to 7.2 with KOH, osmolarity 290–295 mOsM). For imaging Ca^{2+}, two fluorescent dyes are added to the KMS solution – Alexa 594 (50µM) as a morphological marker and Fluo-4 (200µM) as a calcium indicator. For performing 'Ca^{2+} clamp' experiments, where specified, 0.45mM EGTA and 0.14mM $CaCl_2$ were added to the control intracellular solution, to clamp intracellular free Ca_2 at a steady-state concentration of 50–80nM (Henneberger et al. 2010).

2.1.2.2. Recording bath solution and drugs used

For recordings, slices were transferred to a submersion-type recording chamber and perfused with Ringer solution saturated with 95%O_2/5%CO_2. For measuring NMDAR

Chemical	**Chemical abbreviation**	**Concentration**	**Blocker target**
Tetrodotoxin	TTX	1 µM	Na+ channel
(s) MCPG	MCPG	200 µM	mGluR group I/II
MPEP	MPEP	1 µM	mGluR5
LY 367385	LY 367385	100 µM	mGluR1a
LY 341495	LY 341495	500nM	mGluR group II
CGP 55845	CGP	1 µM	GABAbR
Picrotoxin	PTX	50 µM	GABAaR
SCH23390	SCH	20 µM	D1/5R
Sulpiride	Sul	20 µM	D2/3R
Selegiline	Sg	20 µM	MAOb
D-AP5	AP5	50 µM	NMDAR
NBQX	NBQX	100 µM	AMPAR
PPADS	PPADS	100 µM	P2XR
2-APB	APB	100 µM	IP3R

Table 2.1 Summary of pharmacological agents used throughout thesis.

This table shows the full name of the drugs used in this thesis, their common abbreviations, the concentration they were used in (unless otherwise stated) and the primary locus of their effect.

currents, the Mg^{2+} concentration was decreased to 0.1mM and the $GABA_A$ antagonist picrotoxin (50µM) was added. This solution was either kept at room temperature (18-21°C) or at 33°C, as stated. Ringer pH was confirmed at 7.4. Where stated, pharmacological agents were added to the bath at the below listed concentrations – see table 2.1 (unless otherwise indicated):

2.1.3 Electrophysiology: equipment, recording and stimulation technique

2.1.3.1 Recording hardware used for electrophysiological recordings

Electrical signals were acquired through an Axon instruments CV-7B headstage, connected to the pipette solution by a chlorided silver wire, and a multiclamp 700B amplifier. Each primary output is connected to a Humbug to reduce 50Hz background noise. Signals are filtered at 3–6 kHz, digitized and sampled through an analogue-to-digital converter, either an Axon CNS 1440A, or National Instruments BNC 2090, at 10KHz. Software used for acquisition was either WinCP 4.2.1 or Clampex 10.2.

2.1.3.2 Extracellular electrical field recording: theory and technique

Field excitatory post-synaptic potentials (fEPSPs) are the measurement of synaptic activity used in this thesis. For these measurements the recording electrode is placed in the extracellular space in the vicinity of the synapses of interest; it is then set to maintain a net flow of no current from the electrode into the extracellular space – any current flowing from the surrounding extracellular medium into neighbouring synapses, or cells will register as a change in the voltage between the extracellular medium and the recording electrode. The formation of voltage sources and sinks from layer specific or input specific neuronal

activity in the slice will also affect the local voltage change at the recording pipette. Stimulation of the axonal afferents in hippocampal slices leads to release of neurotransmitter (primarily glutamate), triggering opening of postsynaptic ionotropic receptors and a net influx of positive charge (in the form of Ca2+ and Na+ ions) into both pyramidal cells and interneurons. The voltage recorded is mostly from current flowing through the post-synaptic membrane – the initial gradient of the voltage recorded over time gives the best measure of this current.

A stereotypical Schaffer collateral (SC) fEPSP (figure 2.1) displays a stimulation artefact (from the current passed into/across the stimulation electrode), a fibre volley (axonal sodium influx from action potentials), an initial fast, downwards voltage deflection and a slow decay of the initial voltage change back to baseline. All voltage deflections are negative, as the current flows overwhelmingly from the extracellular space into the

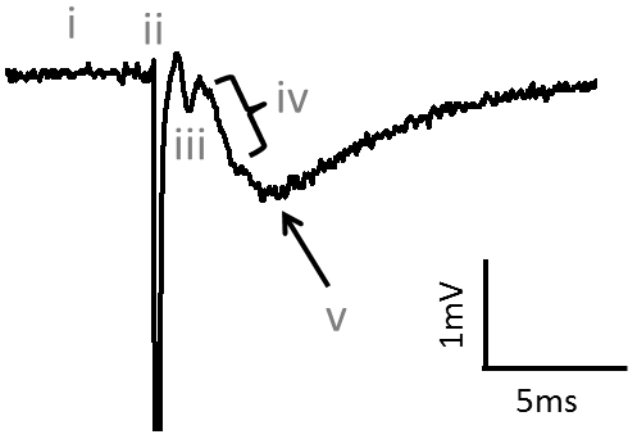

Figure 2.1 Typical field Excitatory Post-Synaptic Potential (fEPSP)

i) baseline. ii) stimulus artefact. iii) fibre volley. iv) slope. v) peak amplitude.

surrounding cells. This is only reversed if the stimulus is strong enough to cause the pyramidal cells to spike (population spike) – when recording fEPSPs in this thesis, baseline stimulation strength was adjusted. The baseline SC fEPSPs recorded in this thesis had an average slope of 0.79 ± 0.06 mV/ms (± standard error), which is similar to the published reported value (Otmakhova and Lisman 1999; Henneberger et al. 2010). The synaptic fEPSP responses recorded at the perforant path-CA1 (PP-CA1) synapse were too small (0.27 ± 0.01 mV average amplitude) to reliably record the value of the fEPSP slopes. Hence, for PP-CA1 recordings, amplitudes, not slopes, are reported in this thesis (chapter 5).

2.1.3.3 Extracellular axonal pathway electrical stimulation

For SR stimulation, axonal fibres were stimulated with either a monopolar electrode or a bipolar electrode (as stated) from a Digitimer DS3 constant current stimulator box. The stimulating electrode was placed in the S.R. 100-200µM closer to CA3 then the recording electrode. The configuration was allowed to settle for up to 10 mins and then the stimulus intensity was gradually increased until no further increase in the fEPSP slope was seen. The stimulus power was then adjust to give 50-60% of the maximal fEPSP slope – stimulus power did not exceed 70µA and lasted 100µs.

For SLM stimulation, the stimulating electrode was placed in the perforant path (pp) in SLM, 100-200µm from the recording electrode, at the CA1/Subiculum border, to selectively stimulate incoming perforant path afferents. Stimulation intensity was set to induce a fEPSP peak of 50-60% of the maximum amplitude obtainable. This required relatively high stimulation currents (200-500µA), consistent whith stimulation intensities in the literature: Otmakhova and Lisman (1998) find that, in perforant path, stimulation strengths of 2-5 times that needed in Schaffer collateral were required for the same fEPSP size and others (Judge and Hasselmo 2004) stimulated at 200µA.

For generating recording fEPSPs in both SR and SLM, a paired-pulse stimulation protocol was used, with 50ms between the two equal electrical stimulation pulses, with at least 200ms baseline preceding the first stimulus. For recording NMDAR-mediated fEPSPs in the stratum oriens (SO), the inter-stimulus interval was increased to 100ms to allow for the slower decay kinetics of this current. Unless otherwise stated, there was a 15s interval between each paired-pulse recording.

For generating post-tetanic potentiation in both SLM and SR, a weak theta-burst stimulation (TBS) paradigm was used. This consisted of 100ms baseline followed by 8 pulses at 100Hz, given twice with a 200ms interval between the first pulse of each 100Hz train.

2.1.3.4 Rejection criteria for fEPSP recordings

For SLM fEPSP recordings, fibre volley amplitudes similar or greater than maximum fEPSP amplitudes are expected (Otmakhova and Lisman, 1998). Therefore, unlike at the Schaffer collaterals, a large fibre volley was *not* a rejection criterion. However, due to the need to measure a decrease in fEPSP amplitude and slope, recordings were rejected if the baseline fEPSP maximum amplitude was <0.2mV. As voltages were generally small (see above) recordings with a high baseline noise level were also excluded. In SR, recordings that required over 70μA stimulation to reach 50% slope maximum were discarded.

For post-tetanic potentiation experiments, recordings were discarded if the fEPSP amplitude had not returned to baseline after 10 minutes in SR or 5 minutes in SLM. Due to the run-up witnessed at the SLM pp synapse (Otmakhova and Lisman 1999) some leeway was allowed here (up to ~5% increase).

2.1.3.5 Astrocyte whole-cell patch-clamp electrophysiology

For every patched astrocyte, the membrane current-voltage (IV) relationship was plotted by stepped injection of current through the patch pipette, generally at 200pA intervals, (figure 2.2). Positive electrophysiological identification of a protoplasmic astrocyte required a linear IV relationship and a low input resistance (<10MΩ) as well as a membrane holding voltage of -80mV, or more negative – consistent with their highly K^+ permeable membrane.

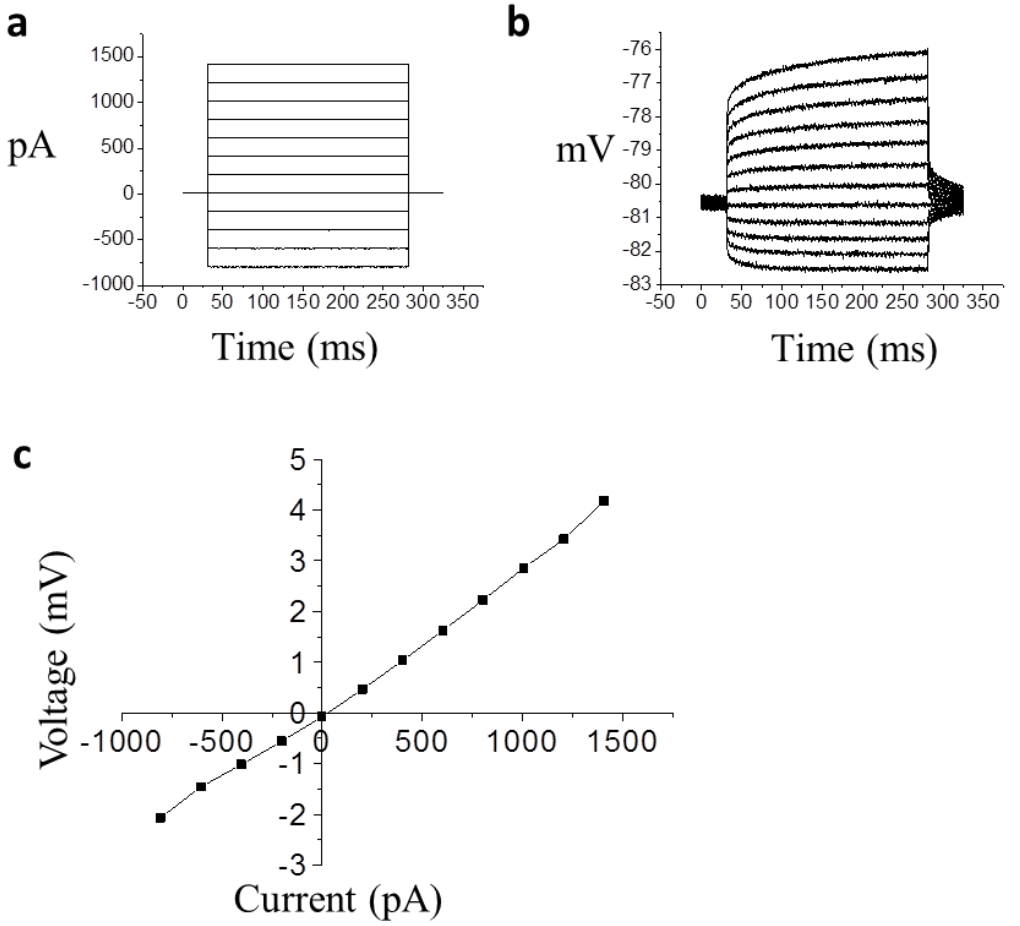

Figure 2.2 Typical astrocytic electrophysiology

a) Example current injection protocol. **b**) corresponding membrane voltage change for current injection in **a**). **c**) plotted IV curve.

2.1.3.6 Recording fEPSP through the membranes of patched astrocytes

Given the low input resistance of patched astrocytes, fEPSPs can be recorded through their cell membranes by the patch pipette (Henneberger and Rusakov 2012). For these astrocyte fEPSP (afEPSP) recordings, the amplitude of the downward voltage deflection is subtracted from the eventual stable holding current 30-50ms post stimulus. The downward peak was sometimes masked by the upward deflection, but the fEPSP can be calculated post-hoc in this case, so this was not considered a rejection criteria. Stable access resistance is vital for these recordings: upon entering whole-cell mode the bridge balance was set automatically through the Multiclamp software and regularly and frequently reset throughout the experiment to correct for possible pipette resistance shifts.

2.1.4 Two-photon excitation imaging of fluorescent dyes *in situ*

2.1.4.1 Fluorescence excitation and recording hardware

Two setups were used to record fluorescent images; either a modified Bio-Rad Radiance 2000 on an Olympus BW50 microscope with a 40x objective, or a Fluoview FV1000 MPE microscope with a 25x objective. Both were optically linked to a femtosecond pulse TiSapphire MaiTai laser (SpectraPhysics) emitting at 800nm. Laser power was kept between 5-8mW for bulk-loaded Fluo-4-AM imaging, 2-5mW for patch-pipette-loaded fluo-4 imaging (as measured at the objective at 800nM).

2.1.4.2 Visual identification and patch-clamp of astrocytes under DIC light microscopy

Astrocytes were identified for patching using the differential interference contrast (DIC) light image. Astrocytes are found scattered regularly throughout the CA1 region (Halassa et al. 2007) and cell location (regarding hippocampal subfields) was defined by the position of the cell soma. Subfield boundaries were defined visually as follows: astrocyte cell bodies on the basal dendritic side of the pyramidal cell layer were defined as being stratum oriens, cell bodies on the apical dendritic side, in the proximal region - appearing lighter under DIC image - were defined as stratum radiatum and cells in the furthest, darker, distil apical dendritic section were defined as being in the stratum Lacunosum-Moleculare. Generally only astrocytic cell bodies are visible, although sometimes large proximal processes can also be distinguished. Astrocyte somata are characteristically round (although not perfectly circular), and generally around 8-10µm in diameter.

Astrocytes were approached with a patch-pipette tip under visual control. Upon contact with the soma, a giga-seal (a pipette tip resistance of >1GΩ) was formed. Gigaseals were then broken with light suction (or occasionally the 'zap' function from the Multiclamp command window) to attain whole-cell mode. Astrocyte resting membrane potential is highly hyperpolarized, and cells were discarded if the membrane dropped beneath -80mV during an experiment; the average astrocyte resting membrane potential was -84.3 ± 0.6mV. The pipette solution was then allowed to equilibrate with the intra-cellular milieu for at least 20 mins. If, after this time, no gap-junction coupled cells (GJCs) have become visible, the cell was discarded. For 'calcium-clamp' experiments, the cell was held in cell-attach mode (seal unbroken) for a set baseline time before entering whole-cell mode. NG2 cells and oligodendrocytes look similar under DIC and are often patched in error – however they can be distinguished from protoplasmic astrocytes through their electrophysiological (higher input resistance of >20MΩ) and morphological properties (thinner, sparser processes - visible under fluorescent 2P imaging). Upon identification they are discarded.

2.1.4.3 Fluorescence-excitation imaging of dye-loaded astrocytes

Alexa594 normally equilibrated across the astrocyte tree within 10–15 min. The morphology of astrocytes loaded with fluorescence indicators (see above) was imaged in the Alexa emission channel (red) (540LP/700SP filter) at the end of every experiment, either as Kalman-averaged 512x512 pixel image or as a stack of 150-250 Kalman averaged, 256x256 pixel, images, stacked in the z-plane with an inter-image distance of 0.5µm.

During recordings, images were acquired simultaneously as frame scans in the Alexa emission channel and the fluo-4 emission channel (green) (515LP/530SP filter), at various pixel resolutions, depending on the sensitivity of the setup and the spatial resolution required for the recording. When recording from bulk-loaded astrocytes unreliable dye loading of processes, and relatively poor signal to noise ratio (in comparison to whole-cell patch-clamp loaded astrocytes), necessitated data acquisition from somata alone. Hence a low pixel resolution, 64x64 pixels, could be used in conjunction with a high image magnification, without losing useful signal. For patch-clamped astrocytes, signal to noise ratio is far better and simultaneous recordings from GJCs, as well as patched-cell distil processes in the same image frame required a higher resolution –generally around 256x256 pixels, although the exact height and width was adjusted to best fit the features of the recorded cells at the zoom chosen (see below).

Image zoom was adjusted to best capture the salient features of the imaged cells – somata of GJCs and visible (within resolution) patched astrocyte processes. Unless otherwise stated, image gain for both channels was kept the same and constant within a particular 2-P setup. Pixel dwell time was kept constant (4µs), as was the movement of the detector – recording unidirectionally.

Unless otherwise stated, images were acquired at 1Hz frequency.

If cells failed to show protoplasmic astrocytic morphology after 10-15 minutes dye equilibration and GJCs they were discarded. If they showed abnormally high resting fluo-4 fluorescence signal compared to the morphological marker, they were likewise discarded.

2.1.4.4 Astrocyte 'perforated patch': imaging fluorescent dyes in neighbouring astrocytes that have diffused in through gap junctions

As detailed in chapter 4, this thesis incorporates a novel ‘astrocyte perforated patch’ method. This entails whole cell patch clamp of an astrocyte and the subsequent imaging of nearby gap-junction coupled astrocytes. This requires low input resistance, a healthy astrocyte population and some time for dye perfusion through the syncytium – all of which are standard for astrocyte patch clamp. Hence the success rate for ‘astrocyte perforated-patch’ recordings is the same as for normal astrocyte patch recordings, as all the criteria for a viable recording are the same. For these recordings a recording configuration was chosen to allow simultaneous recording from both the patched cell processes and the GJC somata. On some occasions, where it was impossible to achieve this, GJC somata, only were recorded. Recordings were only made when the diffusion of the dye from the pipette into the syncytium had reached a constant rate, as measured by the intensity of the reference dye, Alexa 594. If large fluctuations in Alexa 594 intensity in GJCs were witnessed, the recording was discarded.

2.1.4.5 Clamping intracellular astrocytic calcium through the patch pipette

For Ca^{2+}-clamp experiments in chapter 5, 0.45mM EGTA and 0.14mM $CaCl_2$ were added to the pipette solution. Alexa 594 was also included in the intracellular pipette solution as a morphological marker, if astrocyte-type morphology and gap-junction coupling was not observed, recordings were discarded.

2.1.5 Post-Hoc analysis of electrophysiological recordings and fluorescence images

2.1.5.1 Electrophysiology: analysis of fEPSP voltage traces

Raw wincp and pClamp data files were exported in ABF format, and analysed using clampfit 10.2. To analyse fEPSPs, baseline regions in a trace were set manually over at least 50ms before any external stimuli given; regions of interest (ROIs) were also delineated manually and analysed automatically. ROIs were fibre-volley, fEPSP slope (20-60%) and fEPSP amplitude (as shown in figure 2.1), analysed for both stimuli in a paired-pulse protocol. All fEPSP data presented is baseline subtracted. To analyse afEPSPs the average membrane potential 30-50ms post stimulus was subtracted from the amplitude at the time of maximal fEPSP response amplitude – a measurement linearly correlated with the nearby fEPSP slope (Henneberger and Rusakov, 2012).

2.1.5.2 Fluorescence imaging: raw image intensity analysis, normalization to dye concentration, normalization to tissue movement and normalization to baseline calcium indicator fluorescence

Raw .pic image files (Biorad imaging software) and .oib image files (Olympus imaging software) were analysed in ImageJ. ROIs were divided into four categories: Patched cell (PC) soma; PC process; PC arbour and GJC soma. Each ROI was manually outlined in the morphological dye channel image and saved in the ROI manager, to allow analysis of exactly the same area in any other channel. Only visible structures with clear astrocyte morphology were chosen as ROIs. An area of each image showing no fluorescence from the morphological marker was chosen to give a measure of average background fluorescence. For each ROI the average pixel fluorescence was taken for each frame and the average background pixel fluorescence for that frame was subtracted (to correct for instrumental noise). Fluo-4 signal was normalized to the morphological marker signal to correct for fluorescence changes due to tissue movement (giving G/R) and laser power fluctuation. Fluo-4 signals presented here have been normalized to the average fluorescence from each ROI in the baseline phase of each recording, to give $\Delta F/F_0$. The normalizing value includes fluorescence increases from spontaneous calcium dynamics and may therefore be higher than the fluorescence value at 'resting' calcium state.

I consider there to be an important semantic difference between 'resting' and 'baseline' Ca^{2+} states as recorded from the astrocytes in this thesis: the 'resting' state refers to the intracellular Ca^{2+} level (as measured by dye fluorescence) to which the cytoplasm returns to when not undergoing spontaneous activity, during a defined pre-stimulation period. This can also be thought of as the modal fluorescence value recorded from pre-stimulation astrocytes, the one at which it can be most often found. By binning continuous G/R values, one can determine the modal value of a fluorescence data set. The 'baseline' Ca^{2+} state includes spontaneous activity – it simply takes the mean of all G/R values. Hence normalization of G/R to the 'baseline' value reports all effects relative to the amount of pre-existing Ca^{2+} activity in the recorded area, whereas normalization to 'resting' shows change in Ca^{2+} dynamics relative to the recorded area's preferred Ca^{2+} concentration.

It is only possible to use a modal analysis in cells with a clear 'resting' Ca^{2+} concentration. This is only practically possible in whole-cell recordings, when the resolution of spontaneous events is clear – here, the relative increase in F/F_0 during a spontaneous event at baseline can be so great that it raises the mean baseline fluorescence noticeably above the 'resting' baseline fluorescence. If it is impossible to reliably resolve individual Ca^{2+} transients (as in many bulk-loaded slice recordings) then one cannot define the 'resting' calcium level. For consistency across my experimental methods, the baseline fluorescence (mean G/R over 10 minutes pre-stimulation) is always used for normalization purposes. For all experiments involving a single dopamine application, the aim was to record average calcium dynamics over separate conditions; therefore all cells were included in the analysis regardless of the size of their calcium response. For double dopamine application protocols, the aim was to compare the effect of a modulator on a pre-established dopamine response in one slice – in this case cells that did not respond to the first dopamine stimulus were excluded from analysis. Averages obtained for bar charts were taken from the average of t=13-17 minutes for each trace (unless otherwise stated) and error bars indicate standard error.

Dopamine induced astrocytic calcium signals stop when the dopamine is removed from the environment (Otmakhova and Lisman 1999; Parpura and Haydon 2000); therefore, if no washout of the effect was seen (in experimental protocols featuring washout stage) the cells were judged to have become unhealthy (through over-stimulation or poor slice health), their homeostatic mechanisms failed, and the data were discarded. If the resting calcium dynamics was unstable during the baseline phase of an experiment, cells were also discarded.

2.1.5.3 Novel spontaneous astrocyte calcium-oscillation analysis

In order to analyse the relative spontaneous fluorescence activity between different regions of $\Delta F/F_0$ traces a modified coastline analysis was designed to give a quantitative readout of relative astrocyte calcium signalling. Oscillatory activity is characterized by large, rapid changes in F/F_0 – this is quantified by finding the range of $\Delta F/F_0$ for each recording minute (*max-min*). This readout is highly noise sensitive – large noise would give equal *max-min* values to those recorded from spontaneous oscillations – and the coastline [the cumulative absolute difference in fluorescence between consecutive data points] takes the noise over each minute into account, in effect normalizing the *max-min* values to the noise of the recording. So, oscillatory values were obtained by taking the coastline, the minimum and the maximum value for each minute and then entered into the following equation:

$$Oscillatory\ activity = \frac{max - min}{coastline}$$

Averages obtained for bar charts were taken from the average of t=13-17 minutes for each trace (unless otherwise stated) and error bars indicate standard error. This analysis is further detailed in chapter 3.

2.1.5.4 Novel relative frequency distribution analysis of normalized fluorescence change ($\Delta F/F_0$) over baseline and test epochs

For analysing dopamine induced $\Delta F/F_0$ decreases, averaging $\Delta F/F_0$ over time is not possible. This is because the increase in $\Delta F/F_0$, when averaged over the whole population of recorded cells, is of much greater amplitude than any decrease in $\Delta F/F_0$ during any given minute. Therefore, as detailed in chapter 4, I plotted the $\Delta F/F_0$ relative frequency distribution in both baseline and dopamine conditions. These can be compared by eye in the main figures, but I also modelled each distribution, based on the assumption that each

one could be modelled as the sum of 1, 2 or 3 Guassian distributions. These are plotted in the supplementary figures. For each Guassian fit the following was given: the x-coordinate of the peak, the standard deviation, the full width at half maximum and the R^2 measurement of how well the distribution correlates with the observed data. Histograms are binned in divisions of 0.05, each $\Delta F/F_0$ recording, at 1Hz, is plotted on these histograms. 'Baseline' distribution data is sampled from t=1-720s and 'dopamine' distribution data is sampled from t=721-1200s.

2.2 Ventral tegmental area transfection with channelrhodopsin in a viral vector

2.2.1 Virus injection: surgery and injection parameters

50-60g juvenile male Sprague-Dawley rats were anaesthetised with a mixture of ketamine (60 mg/kg) and medetomidine (250 mg/kg) intra-muscular. Additional anaesthesia was administered depending on the duration of the surgery. The head was shaved and cleaned with chlorohexidine. The head was positioned in a stereotaxic frame and protective ophthalmic gel was applied. A midline incision was made and the skull was cleaned and dried. A small craniotomy was performed within the right parietal bone. The surface of the brain was flushed with Ringer to remove any blood products. The virus (AAVsCaMKII-ChR2(H134R)-Venus YFP suspended in filtered saline (1:10) was injected into two sites in the Ventral Tegmental Area (VTA) (2µl per injection). The distance between Bregma and Lamda for these juvenile rats was measured and used to calculate the relative position of the VTA compared to that in adults – the recorded distance between bregma and lamda was divided by the value in the Rat brain atlas and the resulting ratio multiplied by the co-ordinates of the VTA in the atlas (x=2, y=8, z=6,7) to give approximate co-ordinates of VTA for each juvenile rat. The injection pipette was slowly inserted and injections were made at two depths at 0.5mm intervals, injecting 1µl at each depth

followed by a 5 minute pause, then the pipette slowly removed. The skin was sutured. Buprenorphonine was administered (0.05 mg/kg s.c.) and the anaesthesia was reversed with atipemazole (1mg/kg i.m.). Post-operative care was given. The animals were allowed to recover for 14/21 days to allow transgene expression.

2.2.2 Transfected brain fixation, VTA and hippocampal slice preparation and tyrosine hydroxylase immunohistochemistry

Rats were terminally anesthatised (urethane, 1.5 g/kg i.p.) and intracardially perfused with saline followed by ice cold 4% paraformaldehyde. The brains were removed and post-fixed overnight at 4°C. The brains were soaked in sucrose (30%, 4°C) for a further 24 hours. The brains were sliced into 60µm thick sections and serially mounted. Mounting medium containing DAPI (Vectashield) was applied and the coverslips secured. For immunohistochemical identification of dopaminergic neurons and axons, tissue was incubated in sheep anti-Tyrosine Hydroxylase antibody (1:250, Abcam) overnight at 4°C, then again in secondary donkey anti-sheep Alexa 568 (1:500, Molecular probes). Fluorescence of YFP and Alexa 568 were imaged on a Zeiss AX10 bright-field microscope.

Chapter 3: Results 1

Dopamine triggers an increase in cytosolic calcium of hippocampal astrocytes in a dopamine receptor and monoamine oxidase-modulated manner.

3.1 Introduction

Astrocytes are known to respond to application of various endogenous ligands with increases in cytosolic Ca^{2+}, most notably glutamate (Cornell-Bell et al. 1990; Porter and McCarthy 1995b) and ATP (McCarthy and Salm 1991; Porter and McCarthy 1995a), both in culture conditions and in hippocampal slice preparation. These Ca^{2+} transients can be mediated by metabotropic receptors (Kastritsis et al. 1992; Porter and McCarthy 1995a), dependent on release of Ca^{2+} from the smooth endoplasmic reticulum via inositol trisphosphate (IP_3) production (Pearce et al. 1986a; Glaum et al. 1990; Foskett et al. 2007; Verkhratsky et al. 2012), and also potentially by Ca^{2+} entry through VGCCs and the sodium/calcium exchanger (Rusakov et al. 2014), as well as through extracellular concentration of Ca^{2+} itself (Torres et al. 2012). Unlike neurons, individual astrocytes do not exhibit stereotyped Ca^{2+} responses to identical stimuli (Cornell-Bell et al. 1990; Bernardinelli et al. 2011). Ca^{2+} responses can be broadly divided into increases in resting Ca^{2+} level from baseline (Parpura and Haydon 2000) or changes in the frequency or nature of spontaneous Ca^{2+} oscillations (Parri et al. 2001; Shigetomi et al. 2011; Tanaka et al. 2013). Exogenous application of the endogenous ligand dopamine has been shown to trigger increases in intracellular calcium (Parpura and Haydon 2000; Requardt et al. 2012) in cultured astrocytes, through D1, D2 and novel D1-type dopamine receptors, as well as through ROS creation from dopamine metabolism (Khan et al. 2001; Liu et al. 2009a; Vaarmann et al.

2010; Requardt et al. 2012). In this chapter I provide evidence that exogenous application of dopamine can trigger calcium transients *in situ* in intact rodent hippocampal tissue.

3.2 Methods

Briefly, transverse hippocampal slices were taken from p21-25 male Sprague-Dawley rats, or C57/BL6 wild-type and transgenic mice where stated, and bulk loaded with the specific astrocyte marker SR101 (NimmerJahn et al. 2004) and the calcium indicator Fluo-4-AM. All experiments were conducted at room temperature (19-21°C). Astrocyte somata (up to three at a time) were imaged from the Schaffer collateral region of CA1 with a 2P-setup at an excitation laser power of 5-8mW, at a frame rate of 1Hz. Emitted light was collected in two channels, 515-530nm (peak Fluo-4-AM emission wavelength = 515nm) and 540-700nm (peak SR101 emission wavelength = 592nm) using a modified Bio-Rad Radiance 2000 two-photon imaging system. Fluorescence intensity for each cell, per frame, is calculated as the average fluorescence of all pixels in the area manually defined as the cell soma. Fluo-4-AM fluorescence intensity is normalized to SR101 fluorescence intensity (G/R) to correct for tissue movement. This normalized value (G/R) is then itself normalized to its baseline average value, to give a baseline-normalized time course of cytosolic calcium dynamics ($\Delta F/F_0$) from astrocyte somata. Cells with unstable resting calcium in the baseline condition (i.e. fluctuations unlike normally observed calcium transients or a constantly rising baseline) were discarded. Unless otherwise stated, dopamine (DA) was applied at 100µM. Cells with no DA washout were also discarded. For single DA applications, all recorded cells were used in the analysis; for double DA applications only cells showing a clear calcium change in response to the first DA application were used. For single DA application, the peak response to DA was found to be between 3-7 minutes post application (likely due to the perfusion time of the DA through the system) and so it was

from t=13-17 that the average fluorescence intensity was taken for statistics. Baseline average fluorescence intensity was taken from the 5 minutes preceding DA application. The data presented in this chapter are averaged over the total number of cells and for each experimental minute, error bars show the SEM. For the purposes of statistical analysis, *n* was taken to be the total number of cells sampled, although total number of slices and animals are also given. Baseline ΔF/F was assumed to be 1 and the population of ΔF/F averages during dopamine application was tested for normality using the Shapiro-Wilk test, before using a single sample t-test; unless otherwise stated, data was normally distributed**.** Where the normality test failed the Wilcolxon signed rank test was used. To compare two normally distributed populations, a two-sample t-test was used. If either population was not normally distributed the Mann-Whitney test was used to compare both.

3.3 Results

3.3.1 Bulk-loaded astrocytes respond to dopamine with an average increase in cytosolic calcium concentration, in a concentration dependent manner.

First, I tested whether astrocytes *in situ* could respond at all to dopamine (DA) application, as has been reported in culture. Hippocampal CA1 astrocytes loaded with SR101 and Fluo-4-AM show a clear increase in Fluo-4 fluorescence in response to a bath application of 100μM DA from t = 11-20 (figure 3.1a, b) – the average $\Delta F/F_0$ during DA application (t=13-17) is significantly increased to 1.93 ± 0.12 of baseline (figure 3.1c, d) ($p<0.001$, 1-sample t-test, n=16; data from 16 cells, 6 slices, 4 animals).

I then went on to test the sensitivity of astrocytes to dopamine. 10μM DA application also elicited a significant fluorescence increase (figure 3.1d) ($p=0.026$, 1-sample t-test, n=11; data from 11 cells, 4 slices, 4 animals), but to a smaller degree – 1.46 ± 0.18.

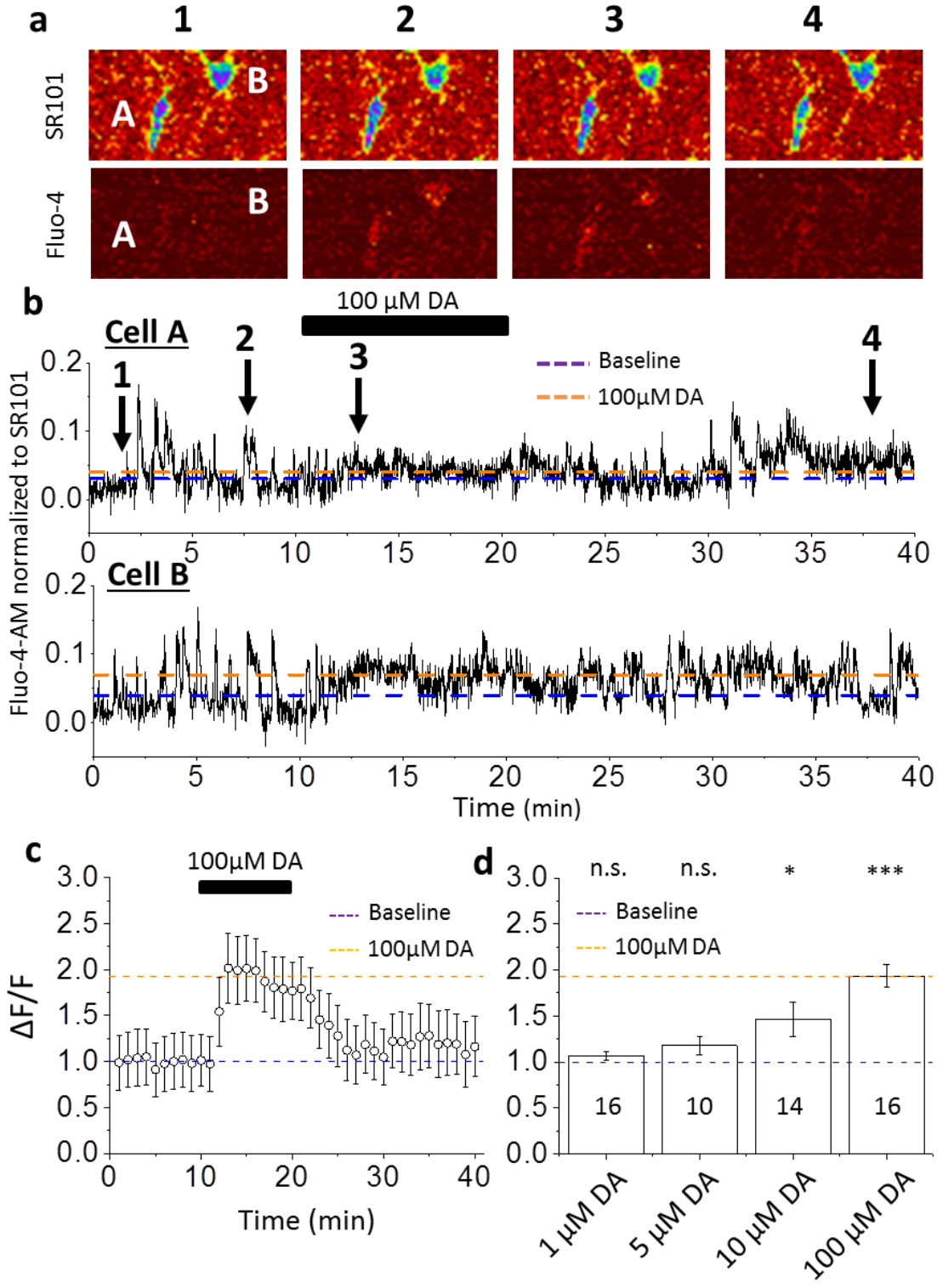

Figure 3.1 **Bulk loaded astrocytes respond to Dopamine with an increase in cytosolic calcium concentration.**

a) Representative images of SR101 channel (top row) and Fluo-4 channel (bottom row) for time points marked in traces in **b**) time course of Fluo-4/SR101 for cell A (top) and cell B (bottom) during 100µM dopamine application. **c**) Average $\Delta F/F_0$ for 100µM dopamine application. **d**) Summary bar

chart of $\Delta F/F_0$ in response to different DA concentrations; cell n-numbers shown inside bars, n.s. = non-significant, * = p<0.05, *** = p<0.001 – t-test (1).

The population of averages during 5µM DA application is not normally distributed (p=0.001, Shapiro-Wilk test), and is not significant significantly different from baseline when tested non-parametrically (p=0.147, 1-sample Wilcolxon signed rank test, n=14). Application of 1µM DA also shows no significant F/F_0 change from baseline (p=0.14, 1-sample t-test, n=14; data from 16 cells, 7 slices, 4 animals).

3.3.2 A modified coastline analysis of spontaneous calcium dynamics.

Astrocytes exhibit spontaneous Ca^{2+} transients, visible as short, sharp increases in Fluo-4-AM intensity (figure 3.1b). Application of DA can decrease the frequency of these spontaneous oscillations recorded at baseline, but increase the average recorded fluorescence by increasing the resting Fluo-4 fluorescence visible at the soma. A change in the oscillatory activity could indicate a change in the information carried by the Ca^{2+} signal – hence it is an important feature to analyse.

I have created a simple measure of oscillatory activity for any fluorescence signal over a given time interval (see chapter 2) – the interval chosen here is always 1 minute. The range of fluorescence intensity (*min-max*) is normalized to the coastline [the cumulative absolute difference in fluorescence between consecutive data points] (figure 3.2a). This can be expressed as:

$$\textit{Oscillatory activity} = \frac{max - min}{coastline}$$

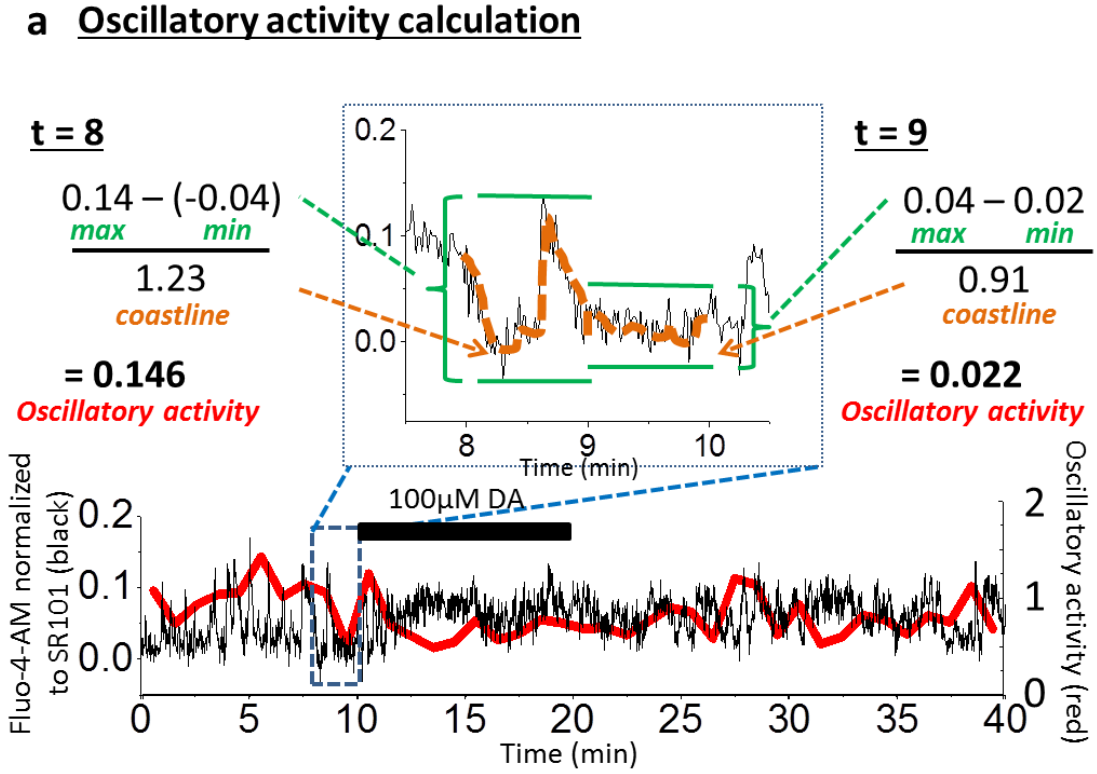

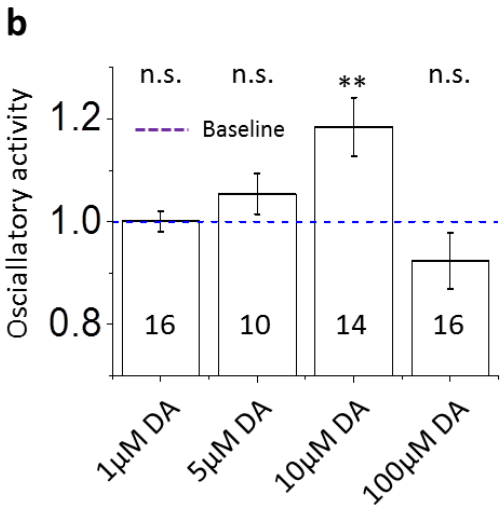

Figure 3.2 Dopamine increases oscillatory calcium activity in a concentration dependent manner.

a) Representative Fluo-4/SR101 time course during 100uM DA application, superimposed red trace displays oscillatory activity: calculated by $\frac{\max - \min}{\text{coastline}}$ for a given minute. Enlarged section shows worked example for calculating oscillatory activity of neighbouring time-points. **b**) Summary bar chart of oscillatory activity in response to different DA concentrations (at t=13-17), data pool same as from figure 1; cell n-numbers shown inside bars, n.s. = non-significant – t-test (1), ** = p≤0.001).

An *oscillatory activity* value is computed for each minute of a given $\Delta F/F_0$ trace. Unlike manual selection of putative astrocytic calcium transients, which is open to bias, this is a

truly independent measure of oscillatory activity. A high output value indicates the presence of a large range of fluorescence (a hallmark of astrocyte Ca^{2+} transients) that cannot be attributed to high noise (as this would increase the coastline value, bringing down the output value), whereas a low output value indicates a low range, and therefore no oscillatory activity, or high background noise – conditions where identification of Ca^{2+} transients is not possible. As the output value is highly sensitive to signal variability, this formula should only be used to compare baseline and test conditions in the same experimental setup where the background noise is similar.

3.3.3 Dopamine at lower, but not higher concentrations, increases oscillatory calcium dynamics.

The same cells as were analysed for average change in fluorescence intensity in section 3.3.1 were now analysed for changes in oscillatory activity, comparing baseline conditions to during dopamine application. Oscillatory activity values were calculated for each minute. 1µM dopamine does not change average oscillatory activity (p=0.967, 1-sample t-test, n=14) and neither does 5µM dopamine (p=0.202, 1-sample t-test, n=14). The oscillatory activity data from the application of 10µM dopamine are not normally distributed (p=0.025, Shapiro-Wilk test) but their median is significantly increased – 1.11 of baseline (p=0.001, 1-sample Wilcolxon signed rank test, n=11). However 100µM dopamine does not significantly increase oscillatory activity (p=0.3, 1-sample t-test, n=16).

3.3.4 Dopamine can act directly on astrocytes.

The next task was to check whether this dopamine-induced fluorescence increase was an indirect result of a dopaminergic effect on neurons. This was done first by blocking

neuronal firing: blockade of voltage-gated sodium channels with tetrodotoxin (TTX) (1µM) during dopamine (100µM) application had no effect on the dopamine-induced increase in Fluo-4 (figure 3.3a): $\Delta F/F_0$ during dopamine application is 2.06, significantly increased from baseline ($p<0.001$, 1-sample t-test, n=18) and not significantly different from the response to 100µM dopamine in control conditions ($p=0.567$, 2-sample t-test). There is however a change in the oscillatory activity, an increase to 1.07 ± 0.03 compared to baseline ($p=0.044$, 1-sample t-test, n=18) and a significant increase of 0.12 from the oscillatory activity of 100µM dopamine control ($p=0.035$, 2-sample t-test) – data not shown. There is no significant effect of TTX alone on the resting fluorescence, measured at t=16-20 ($p=0.078$,1-sample t-test, n=18) or oscillatory activity ($p=0.13$, 1-sample t-test, n=18); data from 18 cells, 8 slices, 3 animals.

Direct dopaminergic activation of neurons could lead to TTX-insensitive glutamate release, which could trigger mGluR-dependent Ca^{2+} increases. Hence, dopamine stimulation was conducted the presence of MCPG, a group I/II metabotropic glutamate receptor (mGluR) antagonist, (200µM). 100µM did not affect the dopamine response (figure 3a): $\Delta F/F_0$ in MCPG and dopamine is 2.3 ± 0.21 of baseline ($p<0.001$, paired t-test, n=11) – not significantly different from the fluorescence increase in 100µM dopamine control conditions ($p=0.131$, 2-sample t-test) – and does not change oscillatory activity ($p=0.612$, 1-sample t-test, n=11); MCPG alone has no effect on baseline fluorescence ($p=0.607$, 1-sample t-test, n=11) or oscillatory activity ($p=0.793$, 1-sample t-test, n=11); data from 11 cells, 5 slices, 3 animals. There is no significant difference in fluorescence increase between 100µM DA alone and in TTX ($p=0.9$, two-sample t-test) or in MCPG ($p=0.335$, two-sample t-test).

3.3.5 Dopamine acts through dopamine receptors.

Is this fluorescence increase mediated by dopamine receptors? When D1/5Rs and D2/3Rs are blocked simultaneously with SCH23390 (20µM) and Sulpiride (50µM) respectively, dopamine ceases to have any effect on Fluo-4 fluorescence (figure 3.3a): the distribution of averages is not normal (p=0.018, Shapiro-Wilk test) and there is no

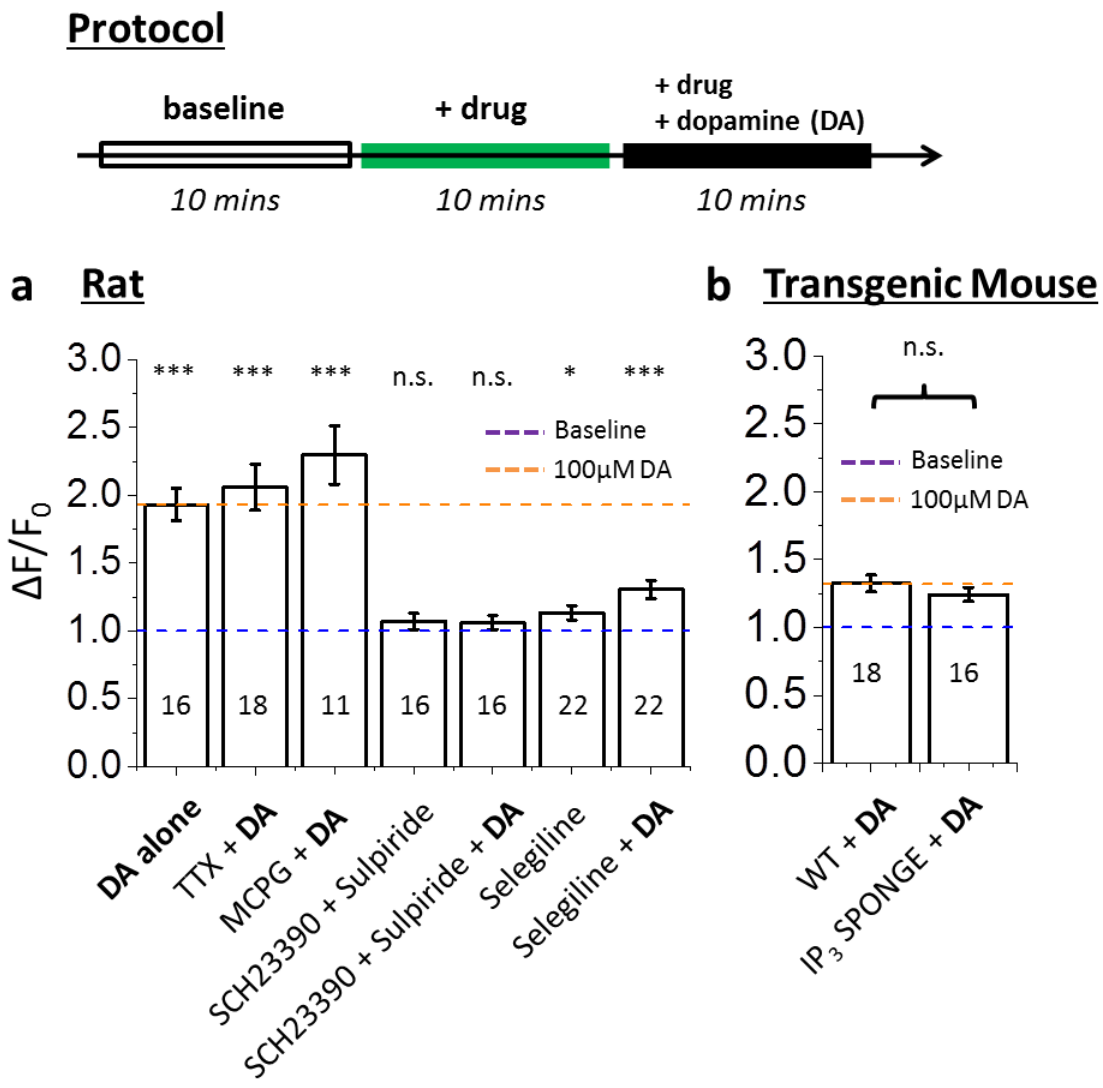

Figure 3.3 Pharmacology of the astrocytic calcium response to dopamine.

a) Summary bar chart of fluorescence responses to 100µM dopamine in presence of various receptor blockers: 1µM TTX, 200µM MCPG, 25µM SCH23390 + 50µM Sulpiride, 20µM Selegiline; **b**) Summary bar chart of wild type (WT) and IP_3 Sponge response to 100µM dopamine. Cell n-numbers shown

inside bars, * = p<0.05, *** = p<0.001 – t-test (1); n.s. = non-significant – 1-sample Wilcoxon-signed rank test, or Mann-Whitney test for WT/IP_3 Sponge comparison.

---

fluorescence (p=0.348, 1-sample Wilcolxon signed rank test, n=16); data from 16 cells, 13 slices, 9 animals. significant difference between the median fluorescence response to dopamine in the presence of dopamine-receptor (DR) blockers – and baseline (p=0.274, 1-sample Wilcolxon signed rank test, n=16); likewise in the presence of only DR blockers the data are not normally distributed (p=0.017, Shapiro-Wilk test) and there is no significant difference in

Using a repetead DA application protocol (see section 3.3.7), blockade of DRs with SCH23390 (20µM) and Sulpiride (50µM) reduced $\Delta F/F_0$ in response to the 2^{nd} dopamine application to a level not significantly different (but approaching significance) from baseline (p=0.065, 1-sample Wilcolxon signed rank test, n=16; data not normally distributed, p=0.044, Shapiro-Wilk test) and significantly smaller than the response to the 1^{st} dopamine application (0.2 difference in medians, p<0.001, Wilcoxon signed ranks test); data from 16 cells, 12 slices, 6 animals. The ratio of $2^{nd}/1^{st}$ $\Delta F/F_0$ means was significantly different from 1 (p<0.001, 1-sample t-test, n=16) and significantly different from the control $2^{nd}/1^{st}$ $\Delta F/F_0$ ratio (p=0.009, Mann-Whitney test). However, when the 2^{nd} dopamine applications are compared between conditions (unpaired data), there is no significant difference between control and dopamine application and that in SCH23390 and Sulpiride (p=0.062, 2-sample t-test).

3.3.6 There is no clear evidence that dopamine acts through the IP_3 receptor signalling cascade

Blockade of intracellular IP_3Rs with 2-APB (100µM) in the double dopamine-application paradigm decreased the dopamine-induced fluorescence response upon 2nd application (figure 3.4d) to a level statistically indistinguishable from baseline (p=0.251, 1-sample t-test, n=20) and significantly lower than that evoked by the 1st dopamine application (0.38 median difference, p<0.001, Wilcoxon signed ranks test). 2-APB alone, prior to 2nd dopamine, did not reach a significant increase (p=0.177, 1-sample Wilcolxon signed rank test, n=20; not normally distributed, p=0.016, Shapiro-Wilk test); data from 20 cells, 7 slices, 5 animals. The ratio of 2nd/1st dopamine-induced fluorescence increases is less than 1 (p<0.001, 1-sample t-test, n=20), but is not significantly different from the control ratio (p=0.137, Mann-Whitney test). However, when the 2nd dopamine applications are compared between conditions (unpaired data), there is no significant difference between control and dopamine application and that in 2-APB (p=0.072, 2-sample t-test).

IP_3 involvement was also investigated using a transgenic mouse line expressing a genetically encoded IP_3-buffering sponge protein – but this did not show an effect of the transgene (figure 3.3b). Single application of 100µM dopamine raised Fluo-4 fluorescence in both wild-type (WT) and IP_3-sponge animals: neither averages from WT or sponge have a normal distribution (p=0.015 and p=0.033 respectively, Shapiro-Wilk test), both medians are significantly greater than baseline, 1.25 and 1.20 (p<0.001 for both, 1-sample Wilcolxon signed rank test, n=18 and n=16) but they are not significantly different from each other (p=0.283, Mann-Whitney); WT data from 18 cells, 10 slices, 8 animals; Sponge data from 16 cells, 8 slices, 5 animals.

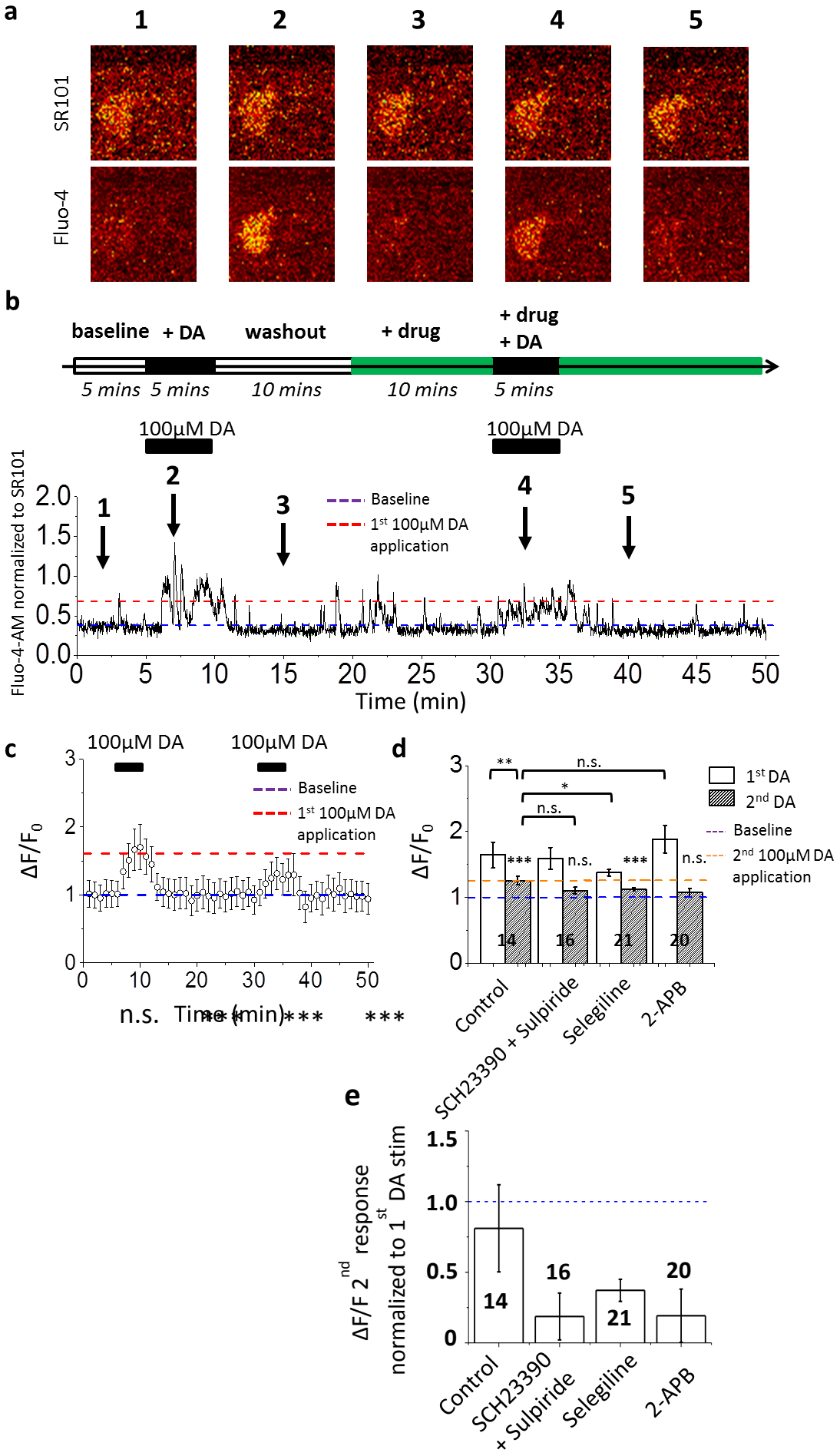
a
1
2
3
4
5
SR101
Fluo-4
b
baseline
+ DA
washout
+ drug
+ drug
+ DA
5 mins
5 mins
10 mins
10 mins
5 mins
100μM DA
100μM DA
Fluo-4-AM normalized to SR101
Baseline
1st 100μM DA application
Time (min)
c
100μM DA
100μM DA
Baseline
1st 100μM DA application
ΔF/F0
Time (min)
n.s.
***
***
***
d
1st DA
2nd DA
Baseline
2nd 100μM DA application
ΔF/F0
**
n.s.
*
n.s.
***
n.s.
***
n.s.
14
16
21
20
Control
SCH23390 + Sulpiride
Selegiline
2-APB
e
ΔF/F 2nd response normalized to 1st DA stim
14
16
21
20
Control
SCH23390 + Sulpiride
Selegiline
2-APB

Figure 3.4 Astrocytic calcium response to a repeated dopamine application.

a) Representative images of SR101 channel (top row) and Fluo-4 channel (bottom row) for time points marked in traces in **b**) representitive time course of Fluo-4/SR101 during 100μM dopamine application. **c**) Average $\Delta F/F_0$ for double 100μM dopamine application. **d**) Summary bar chart of $\Delta F/F_0$ for 1st (hollow bars) and 2nd (hatched bars) dopamine applications, with the 2nd dopamine stimulus in presence of various receptor blockers: 25μM SCH23390 + 50μM Sulpiride, 20μM Selegiline, 100μM 2-APB. **e**) 1st: 2nd dopamine response ratio of $\Delta F/F_0$ means for conditions shown in **d**). cell n-numbers shown inside bars, n.s. = non-significant, ** = $p<0.01$, * = $p<0.05$ – t-test (1), 1-sample signed wilcoxon rank test, Mann-Whitney test (see text).

3.3.7 A repeated dopamine application triggers comparable calcium increases.

I also used a different dopamine double stimulation paradigm for some recordings (two five-minute 100μM applications – the second in the presence of blockers – see figure 3.4) in order to be sure that each astrocyte which was pharmacologically interrogated did originally have the ability to respond to dopamine. For each pharmacological assay using this protocol, I have shown the mean $\Delta F/F_0$ recorded from both dopamine applications (figure 3.3d) as well as the ratio of the 2nd/1st $\Delta F/F_0$ means (figure 3.3.e).

A repeated application of dopamine (100μM) from t=6-10 and t=31-35 (figure 3.4a, b), with a 20 minute inter-stimulus washout period with and no pharmacological blockade during the second application, triggers a significant increase in $\Delta F/F_0$ from baseline during both the first dopamine application (figure 3.4c) – measured from t=8-10 – to a median of 1.39 ($p=0.017$, 1-sample Wilcolxon signed rank test, n=14; not normally distributed, $p<0.001$, Shapiro-Wilk test) and the second dopamine application – measured from t=33-35 – to a mean of 1.28 ± 0.06 ($p<0.001$, 1-sample t-test, normally distributed). The second of these two dopamine-induced fluorescence increases is significantly smaller than the first

(medians differ by 0.2, p=0.009, Mann-Whitney test). The mean ratios of the $2^{nd}/1^{st}$ $\Delta F/F_0$ (not normally distributed, p<0.001, Shapiro-Wilk test) is significantly different from 1 (p=0.016, Wilcoxon signed ranks test, n=14), with a median of 0.55.

3.3.8 Blockade of mono-amine oxidase both increases baseline calcium concentration and blocks dopamine-induced calcium increase.

Astrocytic dopamine-dependent signalling has been reported to act through DA break down by monoamine-oxidase B (MAOb) (Vaarmann et al. 2010). Addition of the MAOb inhibitor selegiline (20μM) to the bath alone significantly increases the baseline astrocytic fluo-4 fluorescence in a single dopamine application paradigm (figure 3.3a) (p=0.025, 1-sample Wilcolxon signed rank test, n=22; data not normally distributed, p=0.016, Shapiro-Wilk test) but not with a repeated dopamine application (p=0.176, 1-sample t-test, n=21). Subsequent addition of dopamine, following 10 minute pre-incubation with selegiline, caused a significant increase in $\Delta F/F_0$ to a median of 1.19 in a single dopamine application paradigm (p<0.001, 1-sample Wilcolxon signed rank test, n=22; data not normally distributed, p=0.015, Shapiro-Wilk test) and also in a repeated dopamine application paradigm to a mean of 1.12 (p<0.001, 1-sample t-test, n=21). For single application, the dopamine-induced increase was higher than that caused by selegiline alone (0.06 difference in medians, p=0.03, Wilcoxon signed ranks test), but far lower than that recorded in control conditions (difference in medians 0.66, p<0.001, Mann-Whitney test). For repeated application, the increase in fluorescence from 1^{st} dopamine application was larger than the 2^{nd} (in selegiline) (median difference 0.19, p<0.001, Wilcoxon signed ranks test). The ratio of $2^{nd}/1^{st}$ mean fluorescence responses was significantly less than 1 (p<0.001, 1-sample t-test), but not significantly different to the control ratio (p=0.134, Mann-Whitney test). When the 2^{nd} dopamine applications are compared between

conditions (unpaired data), the dopamine application in selegiline is significantly smaller (p=0.039, 2-sample t-test).

3.4 Discussion

3.4.1 How does the average dopamine-induced astrocytic calcium increase in slice compare to that in the culture literature?

3.4.1.1 Peak amplitude of dopamine-induced astrocytic calcium increases

The most striking result from this chapter is dopamine's clear and consistent ability to increase the cytosolic calcium levels in astrocytes *in situ* at concentrations from 10-100µM (figure 3.1) and for application lengths of 5-10 minutes and after repeated application (figure 3.2) – as measured by an increase in fluo-4-AM fluorescence. Dopamine itself, or agonists of the various dopamine receptors, has previously been shown to trigger calcium increases in cultured astrocytes (Parpura and Haydon 2000; Khan et al. 2001; Liu et al. 2009a; Vaarmann et al. 2010; Requardt et al. 2012). up to a wide range of reported values. Parpura and Haydon (2000) show a 100-fold increase in free calcium concentration directly following dopamine application, although they do not give the relative fluorescence. In contrast, Khan et al. (2002) show only a 1.2-fold increase in fluorescence upon addition of the D2R agonist quinpirole. The more recent reports from Vaarmann et al. (2010) and Requardt et al. (2012) reliably find 2 to 3-fold calcium increases upon application of dopamine itself and likewise Liu et al. (2009) show a similar range of fluorescence increases upon astrocyte stimulation with a D1-like receptor agonist. My data show a two-fold average increase in cytosolic calcium upon maximal stimulation with 100µM dopamine (see below in this section for a discussion of 'maximal') – in agreement with the more recent reports. An earlier study by Parpura and Haydon (2000) reports a

much shorter (~10s) and very large (~30 fold increase) Ca^{2+} transient upon DA stimulation – but this may be due to the extended length of time they cultured their cells for (up to 40 days) before recording, allowing the cells to modify their intracellular pathways, change their response to DA. Conversely, the tiny increase seen by Khan et al. (2001) the result of stimulation of only a small proportion of the dopamine-responsive machinery in astrocytes.

3.4.1.2 How do dopamine-induced astrocytic calcium increases change over time?

The response of cultured astrocytes to dopamine, or dopamine receptor agonists, is not uniform over time – often a large initial transient is seen, followed by further smaller transients or a return to baseline (Parpura and Haydon, 2000; Khan et al. 2001; Liu et al. 2009; Vaarmann et al. 2010; Requardt et al. 2012). This is different from the continued increase in baseline calcium concentration, throughout the presence of dopamine, that I report here. The difference can be explained in three ways: firstly, a fundamental difference in the nature of the astrocytic calcium response to dopamine between cultured astrocytes and those *in situ*, support for which is provided by Vaarmann et al. (2010) who show that explant cultures respond differently and more vigorously than normally cultured astrocytes; secondly, a change in the nature of stimulation attributed to adding dopamine to the perfusion solution that is unique to the *in situ* environment; thirdly, a switch between increased calcium transient frequency and sustained baseline calcium increase, dependent upon dopamine concentration. Support for the latter comes from the oscillation analysis I have performed (figure 3.2), see discussion section 3.4.2 – which shows an increase in dopamine-induced calcium transients at 10µM, but not 100µM dopamine. Liu et al. (2009) find that increasing the concentration of their D1-like agonist from 25µM to 100µM (a proportional similar increase) changes their calcium response from a single transient to a

sustained increase, but Requardt et al. (2012) show that 100µM dopamine triggers a qualitatively similar increase in calcium transient frequency to 20µM dopamine. The key difference lies in the specific stimulation of the D1-like receptor by Liu et al; Vaarmann et al. have shown that catabolism of the dopamine molecule (as used by Requardt et al.) can influence astrocytic calcium signalling – and the cortical astrocytes used by Requardt et al. have been shown to express functional D2-like receptors (Khan et al. 2001; Duffy et al. 2011; Shao et al. 2013), which they did not block. Co-activation of D2-like receptors could modulate the intracellular calcium response to dopamine.

3.4.1.3 Active dopamine concentration required to trigger a calcium increase

A dopamine-induced increase in astrocytic Ca^{2+} transients has been reported at 10-20µM dopamine (Liu et al. 2009a; Vaarmann et al. 2010; Requardt et al. 2012) – I examine this further in discussion section 3.4.2 – as well as the sustained increase in resting Ca^{2+} reported above. Regarding the sustained increases reported by Liu et al, Vaarmann et al. (explant work) and myself at 100µM dopamine – it is possible that such high levels of dopamine are cytotoxic (see Vaarmann et al. 2010). However, the fact that the cessation of the effect coincides temporally with the washout of dopamine (only reported in this thesis) suggests that this is not a pathological effect of high dopamine concentrations, but rather the product of a very strong dopaminergic stimulation of astrocytes. Throughout this thesis I treat this exogenous application of 100µM dopamine as 'maximal' stimulation, as it is regarded throughout the dopamine literature, because it is highly unlikely that the concentration of dopamine would ever exceed this under physiological conditions. It is important to note that the concentration of dopamine added to the bath is greater than the concentration that eventually reaches the imaged cells in the slice, for two main

reasons: firstly, dopamine autoxidates in oxygenated, pH 7.4, solution (Herlinger et al. 1995) – producing free-radicals and eventually melanin; secondly, dopamine in the hippocampus is taken up by the norepinephrine transporter (NET) on noradrenergic axon terminals (Carboni et al. 1990; Borgkvist et al. 2012) and astrocytes (Takeda et al. 2002). Hence a portion of any bath applied dopamine may be cleared or may degrade before it reaches the imaged cells, more so than in culture – making direct comparisons of dopamine concentration effects difficult.

3.4.2 What could be the relevance for the increase in oscillatory activity compared to a baseline increase?

Spontaneous calcium oscillations in astrocytes are of great interest as they can occur stochastically (Parri et al. 2001) or can correlate with and display properties dependent on the surrounding spontaneous neuronal activity (Aguado et al. 2002; Di Castro et al. 2011). Evoked transients do not necessarily correspond to those seen under physiological conditions and, when triggered, do not necessarily affect the overall astrocyte action (Fiacco et al. 2007; Agulhon et al. 2010). Indeed, the MRGA1-induced calcium increases described by Fiacco et al. are similar in amplitude and kinetics to those I have recorded in response to 100µM dopamine (although unlike after dopamine stimulation, they record no washout). Hence, identification of a dopamine-induced change in spontaneous activity would provide clearer evidence of a physiological role for dopamine in astrocyte calcium dynamics – a change that was demonstrated in this chapter (figure 3.2).

The novel method I describe for measuring spontaneous oscillatory activity is designed to be entirely objective. To this end it sacrifices the manual identification of individual spontaneous events (for which there is, as yet, no universal classification) and all the potential detail that could be gained from analysis of individual events, for an overall

value per minute. The results, when averaged over the many recorded traces, still show a striking pattern – dopamine increases the relative spontaneous calcium dynamics at 10µM but does not at 100µM. Indeed, there are examples of cells in this chapter (figure 3.1b) that display decreased spontaneous activity, but increased average fluorescence, upon application of 100µM dopamine. This suggests either that increasing the stimulation strength increases the frequency of calcium transients to a point where they elide, appearing as a higher resting calcium level, or that an increase in resting calcium concentration in astrocytes (caused by high dopamine concentrations) negates dopamine's previous capacity to trigger spontaneous calcium oscillations. Given that spontaneous events are often greater in amplitude than the 100µM dopamine-induced calcium increase, the latter seems more likely. This would indicate that spontaneous calcium oscillations and resting calcium concentration are separate, but dependent aspects of astrocytic calcium dynamics, both of which can be controlled by dopamine.

3.4.3 A putative molecular pathway for the actions of dopamine on astrocytic calcium.

3.4.3.1 Dopamine's effects are independent of resting spontaneous neuronal activity in the hippocampal slice

Dopamine has been reported to stimulate glutamate release (Cameron and Williams 1993; Bouron and Reuter 1999) from presynaptic neurons – and glutamate can elicit astrocytic calcium dynamics via mGluRs (Porter and McCarthy 1995b; Porter and McCarthy 1996; Fiacco et al. 2007). However, I found that neither inhibition of neuronal firing, nor inhibition of mGluR signalling could block the dopaminergic initiation of astrocyte calcium transients (figure 3.3). Dopamine has been shown to act on interneurons in the pre-frontal cortex and hippocampus (Gonzalez-Islas and Hablitz 2003; Tseng and O'Donnell

2007; Andersson et al. 2012; Gangarossa et al. 2012), but this is largely in an inhibitory fashion, decreasing GABA release, thus unlikely to affect astrocytic calcium dynamics, which are increased by GABA stimulation (Kang et al. 1998). A decrease in GABAergic activity could lead to an increase in spontaneous glutamate release from neurons, due to decreased inhibition in the slice – however it is unlikely that this contributes to the astrocytic Ca^{2+} increase as MCPG blockade of mGluRs did not affect the nature of the Ca^{2+} increase (figure 3.3). That said, it is possible that increased astrocytic glutamate uptake (from increased glutamate release from neurons) could, through importing Na^{+} and reversing the activity of the Na^{+}/Ca^{2+} exchanger, increase cytosolic Ca^{2+} (Rojas et al. 2007). Intriguingly, there is a small, but significant, increase in oscillatory activity when 100µM dopamine is applied in the presence of TTX, unlike in response to 100µM alone (which tends, non-significantly, downwards – figure 3.2). This could indicate that, in 100µM alone, dopamine stimulates neuronal activity which, in turn, interferes with the generation of spontaneous astrocytic calcium events normally facilitated by dopamine through one or several of the following: release of neurotransmitter and subsequent receptor activation; change in the concentration of extracellular K^{+}, causing local depolarization and VGCC activation (Duffy and MacVicar 1994); change in extracellular Ca^{2+} concentration, triggering ATP mediated Ca^{2+} signalling (Torres et al. 2012) or change in intracellular Na^{+} (Rojas et al. 2007; Reyes et al. 2012).

3.4.3.2 Dopaminergic astrocytic calcium increases are mediated through dopamine receptors

Simultaneous blockade of both D1 and D2-type receptors effectively eradicates the astrocytic dopamine response (figure 3.3), strong evidence that it is through dopamine receptor activation that dopamine increases astrocytic intracellular calcium. This

observation is in line with both Liu et al. (2009) and Requardt et al. (2012) who both report D1-type receptor mediation of intracellular calcium increases as well as the D2-receptor mediated calcium signals reported by Khan et al. (2001), but at odds with Vaarmann et al. (2010) whose calcium signals persist in the presence of both D1-type and D2-type receptor blockers (although they did not try simultaneous blockade). It is difficult to reconcile these data – the concentrations of antagonists used by Vaarmann et al. are sufficient to effectively block any dopamine receptors. Apart from the many-fold differences between culture and slice data, and the fact that these cultured astrocytes had been cultured without the presence of neurons (or endogenous dopamine), the most obvious difference is in the fluorescent calcium indicator used – fluo-4-AM for the results in this chapter, fura-2 by Vaarmann et al. Fura-2 has a lower Kd (~224nM) than fluo-4 (~340nM). Hence it may be that a more sensitive measure of calcium concentration increase can pick up residual calcium dynamics (the responses amplitudes are halved) during dopamine receptor blockade in culture conditions that are far less noisy than those in slice.

3.4.3.3 There is no clear evidence for the involvement of IP_3 receptors in the dopaminergic astrocytic calcium signal

Many astrocyte calcium transients are thought to be primarily mediated by IP_3-mediated release of intracellular calcium from the smooth endoplasmic reticulum (Rusakov et al. 2011; Verkhratsky et al. 2012) – but see (Rusakov et al. 2014) – as has calcium-mediated astrocytic glutamate release (Parpura et al. 2011). Blockade of IP_3Rs produces a non-significant decrease in dopamine-induced Ca^{2+} increase (figure 3.4), suggesting IP_3 is not involved in the signalling pathway – although this may not reach significance due to incomplete blockade of the IP_3R with 2-APB at high IP_3 concentrations (Bilmen and Michelangeli 2002), such as those potentially caused by my powerful (100µM) dopamine

stimulus. Both D1-type and D2-type receptors have been reported to trigger release of IP_3 (Hernandez-Lopez et al. 2000; Hasbi et al. 2009) – but I could find no strong evidence to support this. In astrocytes, both the D1-type receptor-mediated activation of the PLC/IP_3 pathway reported by Liu et al. (2009) and the direct effect of NADH increase on IP_3Rs, also mediated by D1Rs, reported by Requardt et al. (2012) could be responsible for this IP_3R-dependent calcium increase. It is important to note that 2-APB is non-specific in its effects and can act on TRP channels and connexions as well – it has also been reported to inconsistently block IP_3R and block instead store-operated calcium entry (Bootman et al. 2002).

I also tested for the involvement of IP_3 using a transgenic mouse model that over-expresses an IP_3 buffering protein specifically in astrocytes – that found no inhibitory effect on the dopamine-induced calcium increase. These data are difficult to interpret for two reasons: firstly, the calcium increase resulting from a 100µM dopamine application in wild-type mouse astrocytes is less than half that evoked in rat astrocytes, hence the scale of any inhibitory effect would have been far smaller; secondly, to date, the IP_3-Sponge mouse has only been reported to show very slight effects on the properties of spontaneous astrocytic calcium transients, not differences that would be picked up by the oscillation analysis described above. These differences (in duration and event area) rely on prior identification of Ca^{2+} events, a technique I have chosen not to employ in this thesis (see chapter 8). There are other differences between our two studies: their recorded spontaneous calcium transients are in response to a strong glutamate receptor agonist concentration – and these only in astrocytic processes from which I could not record with this method (Tanaka et al. 2013). As with 2-APB, a possible explanation for the lack of a significant effect could lie in the powerful dopaminergic stimulus – such a large IP_3 increase could overwhelm the astrocytic IP_3 buffer, resulting in only a non-significant trend towards a smaller dopamine mediated increase in the IP_3-Sponge animals (figure 3.3).

Given the inconclusive nature of the above data, a crucial next experiment would be to drain the intracellular calcium stores (through which IP_3 stimulates intracellular calcium release) – with heparin, for example – and challenge with dopamine to see if a calcium increase was still visible. Another possible experiment would be to test for a dopamine-induced calcium response in astrocyte-specific IP_3R2 knock-out mice.

3.4.4 What role does monoamine oxidase play in the dopamine-induced calcium increase?

Astrocytes express monoamine-oxidase B (MAOb) throughout the brain (Ekblom et al. 1993) and blockade of MAOb with selegiline has been reported to block dopamine-induced calcium rises in astrocytes (Vaarmann et al. 2010). I tested this property of selegiline in both the single and double dopamine application paradigms and in both cases there was only a partial blockade of the astrocytic dopamine response (figures 3.3, 3.4) – unlike the total blockade reported by Vaarmann et al. This is perhaps unsurprising, given the very different nature of the slice conditions compared to culture and not necessarily at odds with Varmann et al. – blockade of dopamine catalysis will raise dopaminergic tonus in slice conditions (Heinonen and Lammintausta 1991; Huang et al. 1997) and this will affect neuronal activity (Hsu 1996; Huang et al. 1997) which could activate astrocytes through non-dopaminergic pathways. If the blockade of MAOb were incomplete (this is the same selegiline concentration used in culture), the concentration of dopamine could well be high enough to activate residual, unblocked MAOb.

The partial blockade of the dopamine response suggests that lipid peroxidation by dopamine catabolytes may be involved, at least in part, in amplification of the dopamine-

induced fluorescence signal – possibly by increasing the probability of calcium-induced calcium release from intracellular stores by increasing IP_3 concentration through lipid peroxidation. Increased ROS levels (from DA breakdown) can activate transient receptor potential (TRP) channels (Naziroglu 2012), channels that are expressed on astrocytes (Shigetomi et al. 2011; Dunn et al. 2013; Reyes et al. 2013). TRPV4 channels in particular have recently been shown to play a role in astrocyte endfeet Ca^{2+} signals, mediating a small calcium increase that triggers calcium-induced calcium release (Dunn et al. 2013), and these channels are sensitive to an increase in ROS (Bai and Lipski 2010) – this is another possible mechanism for MAOb-mediated Ca^{2+}-signal amplification. Another source of interest is a study that has suggested ROS as a means of communication between astrocytes and neurons (Safiulina et al. 2006) – this would imply that dopaminergic breakdown itself could trigger astrocyte-neuron communication.

However, selegiline has been reported to affect astrocytes directly – stimulating production of FGF-2 (Riva et al. 1997) and NGF, BDNF and GDNF (Mizuta et al. 2000) – and hippocampal neurons (Dimpfel and Hoffmann 2011). Indeed, adding selegiline to the bath before dopamine stimulation induces an increase in resting calcium concentration (figure 3.3) – one not seen upon addition of dopamine receptor blockers. This increase could be result of the off-target effects of selegiline mentioned above, or could be more simply explained by an increase dopaminergic tone (Neusch et al. 1997) stimulating astrocyte calcium rises through a MAOb-independent mechanism. Another possibility is that this slight fluorescence increase is an artefact: H_20_2 produced by MAO activity is acidic – blockade of MAO could, in theory, increase cell alkalinity – fluo4 is pH sensitive, an increase an alkalinity of the environment would lead to greater baseline fluo-4 fluorescence. Additionally, if local spontaneous activity triggers local, compartmentalized astrocytic depolarization, voltage-gated calcium channels could be involved in generating a calcium signal; increased levels of reactive oxygen species (ROS) have been reported to inhibit

voltage-gated calcium channels (VGCCs) – selegiline would block this inhibition by decreasing ROS, therefore increasing VGCC activity and cytosolic calcium (Steullet et al. 2008). However this would imply that VGCCs set astrocytic resting Ca^{2+} levels and there is no evidence yet for this. Conversely, ROS-mediated TRP channel activation (see above) would predict a resting Ca^{2+} decrease (assuming TRP channels spontaneously open at rest).

In contrast to the data just discussed, adding selegiline in between two dopaminergic challenges does not increase the baseline calcium, but this could be due to an interaction with the residual effects of the first dopamine application and hence is a less reliable measure than addition of selegiline alone.

Selegiline's lack of selectivity of action makes concrete conclusions as to MAOb's role in the dopaminergic signalling pathway in astrocytes hard to draw, but it seems clear that it plays an amplifying, if not a necessary role in the dopamine-induced Ca^{2+} increase, possibly via lipid peroxidation multiplying an existing calcium signal initiated by dopamine receptors, as discussed earlier.

3.4.5 Is there a physiological relevance of a dopaminergic astrocytic calcium increase?

One of the most controversial debates in the astrocyte literature is whether astrocyte calcium increases trigger physiologically relevant astrocyte dynamics (Fellin et al. 2004; Ding et al. 2007; Fiacco et al. 2007; Perea and Araque 2007; Agulhon et al. 2010) and to what extent the nature of the calcium increase controls its function (Wang et al. 2013a). Astrocyte calcium increases have been found to play a necessary (Henneberger et al. 2010) and sufficient (Perea and Araque 2007) role in LTP induction in the hippocampus – dopamine is implicated in the generation of hippocampal LTP (Frey et al. 1991; Swanson-

Park et al. 1999), so dopaminergic stimulation of astrocytic calcium increases could form a necessary part of the conditions required for LTP induction.

3.4.6 Methodological caveats to bulk-loading recordings.

3.4.6.1 Sulforhodamine 101 loading causes long-term excitability increases in hippocampal slices

In order both to identify astrocytes and image their morphology, slices were loaded with the morphological dye Sulforhodamine 101 (NimmerJahn et al. 2004) – a commonly used technique. However, SR101 has recently been reported to induce long-term increases intrinsic excitability in CA1 pyramidal cells of the hippocampus and enhanced excitatory input (Kang et al. 2010). Such in an increase in synaptic strength would increase the strength of spontaneous activity and possibly the excitability of the slice (although slice preparations should be relatively quiescent, given their lack of input). I have presented data in this chapter in strong support of dopamine's effect on astrocytic Ca^{2+}, but my argument would be more convincing if I were to replicate the data in non-SR101 loaded slices – methodology that I have employed in chapter 4.

3.4.6.2 Somatic recordings of astrocytic calcium dynamics may not be representative of the calcium activity across the whole cell

In my recordings I have found that it is rarely possible to accurately record from astrocyte processes, given the low signal-to-noise ratio of recordings from bulk-loaded cells, hence all my recordings come from astrocyte somata. There are examples in the literature of recording from the large processes of bulk-loaded astrocytes (Porter and McCarthy 1996)

but here calcium dyes with a higher Ca^{2+} affinity and lower range have been used. As a wealth of calcium dynamics are visible in the processes that are not in the soma (Henneberger et al. 2010; Di Castro et al. 2011) it is desirable to image calcium dynamics in both in response to dopamine stimulation – this has been done in chapter 4.

3.4.6.3 Spontaneous baseline calcium dynamics artificially increase the 'baseline' calcium value used for normalization

It is also important to note that the baseline value to which each recording is normalized is the average fluo-4 fluorescence value. Therefore, where there is spontaneous activity pre-pharmacological manipulation, the normalization value will not correspond to what could be termed the 'resting' calcium indicator fluorescence – the fluorescence value taken between spontaneous oscillations. The advantage of this method is that it allows all data to be grouped and compared to a baseline of 1, a baseline that takes into account any spontaneous Ca^{2+} activity, the disadvantage is that it allows no measure of spontaneous calcium dynamics at baseline. As detailed in the chapter 2, it is possible to analyse G/R fluorescence traces with a modal analysis – this provides an average of the activity at baseline over a population of cells, but it may not be possible to identify the mode in traces with a lower signal/noise ratio.

3.5 Conclusion

Recording astrocytic intracellular calcium changes from hippocampal astrocytes bulk-loaded with Fluo-4-AM reveals that astrocytes respond to dopamine with an overall increase in intracellular somatic calcium, in a concentration, time and repetition-dependent fashion. This phenomenon is independent of the resting neuronal activity in the slice, but is

mediated through dopamine receptors – although the intracellular signalling pathways remain unclear. It is apparent that the response is also amplified by the action of MAOb in the slice.

Chapter 4:

In addition to the reported dopamine-dependent increase in astrocytic cytosolic calcium, whole cell patch-clamping of astrocytes reveals a concurrent dopamine receptor-dependent calcium concentration decrease.

4.1 Introduction

As described previously (Chapters 1 and 3), astrocytes can respond to neurochemical stimulation with changes in internal calcium (Cornell-Bell et al. 1990; Porter and McCarthy 1995b; Kang et al. 1998; Shelton and McCarthy 2000). Bulk-loading of dyes into the slice (Porter and McCarthy 1996), as was done in chapter 3, cannot achieve the level of image resolution possible with whole-cell patch-clamp and loading of the astrocyte syncytium with a cell-impermeant fluorescent indicator. Individual cell loading greatly improves signal-to-noise ratio, allowing for resolution of fine individual processes both morphologically (Bushong et al. 2002) and functionally (Henneberger et al. 2010; Di Castro et al. 2011), processes which display markedly more complex activity than that recorded at the soma: Bergmann glia display hundreds of independent Ca^{2+} signalling microdomains (Grosche et al. 1999); hippocampal astrocytes display Ca^{2+} transients of varying length and amplitude generated in their processes that may never propagate to the soma (Di Castro et al. 2011). It is therefore of interest to better investigate the calcium response to dopamine in astrocytes with both a better signal-to-noise ratio and in the astrocytic processes. Using whole-cell astrocyte patch, I further investigate the pharmacology of the previously reported astrocyte response to dopamine: astrocytes have been reported to express both D1-like (Liu et al. 2009a; Huang et al. 2012) and D2-like receptors (Khan et al. 2001; Duffy et al. 2011; Shao et al. 2013), In the following chapter, I aim to identify which receptor type is

responsible for the reported calcium increase and uncover a previously unreported dopamine-induced astrocyte calcium decrease.

4.2 Methods

In short, transverse hippocampal slices were taken from p21-25 male Sprague-Dawley rats, allowed to rest for 1 hour and then placed in an immersion recording chamber. Whole cell astrocyte recordings were made with electrodes and filled with intracellular Potassium methyl-sulphonate (KMS) solution containing (in mM): KCH_3O_3S 135, HEPES 10, disodium phosphocreatine 10, $MgCl_2$ 4, Na_2ATP 4, NaGTP 0.4 (pH adjusted to 7.2 with KOH, osmolarity 290–295 mOsM); 200µM Fluo-4 and 50µM Alexa were added. After 20 mins dialysis time, the astrocyte syncytium was sufficiently filled with dye to allow imaging of both patched and gap-junction coupled cells. All experiments were conducted at room temperature (19-21°C) unless otherwise stated. Astrocyte somata (up to five at a time) were imaged from the Schaffer collateral region of CA1 with a 2P-setup at an excitation laser power of 2-5mW, at a frame rate of 1Hz. Emitted light was collected in two channels, 515-530nm and 540-700nm using an Olympus BW50 microscope two-photon imaging system. Recording configuration was chosen to best concurrently image patched cell (AC) processes and gap-junction couple cell (GJC) somata. Fluorescence intensity for each cell, per frame, is calculated as the average fluorescence of all pixels in the area manually defined as the cell soma or process. G/R intensity is normalized to the baseline average to give a time course of cytosolic calcium dynamics ($\Delta F/F_0$) from astrocyte somata. Cells with unstable resting calcium in the baseline condition (i.e. fluctuations unlike normally observed calcium transients or a constantly rising or falling baseline) were discarded. Unless otherwise stated, DA was applied at 100µM. Cells with no DA washout were also discarded (in protocols including a washout step). After DA application the peak

response was found to be between 3-7 minutes post application (likely due to the perfusion time of the DA through the system) and so it was from t=13-17 that the average fluorescence intensity was taken for statistics. Baseline average fluorescence intensity was taken from the first 10 minutes of the recording, bar charts values are averaged over the total number of cells for a stated time frame, error bars show the standard error. For the purposes of statistical analysis, *n* was taken to be the total number of cells sampled, although total number of slices and animals are also given. Baseline $\Delta F/F_0$ was assumed to be 1 and the population of $\Delta F/F_0$ averages during dopamine application was tested for normality using the Shapiro-Wilk test, before using a single sample t-test; unless otherwise stated, data was normally distributed**.** Where the normality test failed the Wilcolxon signed rank test was used. Two compare two normal populations a two sample t-test was used. If either population was not normally distributed the Mann-Whitney test was used to compare both. $\Delta F/F_0$ data in this chapter is often presented as proportional frequency histograms; generally, in these graphs, bars represent baseline distribution and the superimposed black line represents distribution in dopamine. These two groups were sampled from 1-12 minutes (baseline epoch) and 3-10 minutes post-dopamine application (dopamine epoch). For analysis, each distribution plotted in a histogram is fitted with either a single or multiple Gaussian distribution: for these curves the peak x (location of Gaussian peak on x-axis), the standard deviation (σ), Full Width Half Max (FWHM) and R^2 value is given, all to 2 decimal places. The fitted curves are plotted in the supplementary data, presented at the end of this chapter.

4.3 Results

4.3.1 The relative dopamine-induced astrocytic calcium increase is greater in gap-junction coupled cells than in patched astrocytes.

Whole-cell patch clamping of astrocytes allowed diffusion of morphological dye (Alexa 594) and calcium indicator (Fluo-4) into neighbouring gap-junction coupled astrocytes (GJCs) from the patched astrocyte (AC). Both AC processes and GJC somata could therefore be simultaneously imaged. A typical example of concurrent Alexa594 and Fluo-4 imaging is shown in figure 4.1ai and figure 4.1aiii respectively. Given the previously reported differences in process and somatic signalling (see section 4.1), I first investigated any possible differences in response to dopamine between astrocyte somata and processes. As physical stimulation from the pipette could also trigger Ca^{2+} transients (Charles et al. 1993), I also recorded from GJC somata. Bath application of 100µM dopamine triggers large calcium increases in all the astrocyte syncytium, with the exception of the AC soma – figure 4.1aii shows this effect in the example cells. During dopamine stimulation (t=11-20), AC somata show no significant change in fluorescence from baseline ($p=0.287$, 1-sample t-test, n=3; data taken from 3 cells, 3 slices, 3 animals). The population of fluorescence averages from AC processes, in the presence of dopamine, is not normally distributed ($p=0.002$, Shapiro-Wilk test, n=15) and is significantly increased to a median of 1.17 of baseline ($p=0.018$, 1-sample Wilcoxon signed ranks test, n=15; data taken from 15 processes, 7 slices, 7 animals). GJC somata showed a significant increase in mean $\Delta F/F_0$ to 3.1 ± 0.67 ($p=0.021$, 1-sample t-test, n=7; data taken from 7 cells, 7 slices, 7 animals), as did GJC processes, to a mean of 2.15 ± 0.15 of baseline ($p<0.001$, 1-sample t-test, n=8; 8 processes, 7 slices, 7 animals). This data is summarized in figure 4.1c: GJC somata show a significantly greater relative increase in Fluo-4/Alexa594 fluorescence from baseline than AC processes ($p=0.009$, Mann-Whitney test), as do GJC processes from AC processes ($p=0.031$, Mann-Whitney test); GJC process responses were not significantly different to those from GJC somata ($p=0.166$, 2-sample t-test). Average time course of dopamine application for AC processes and GJC somata is shown in figure 4.1b.

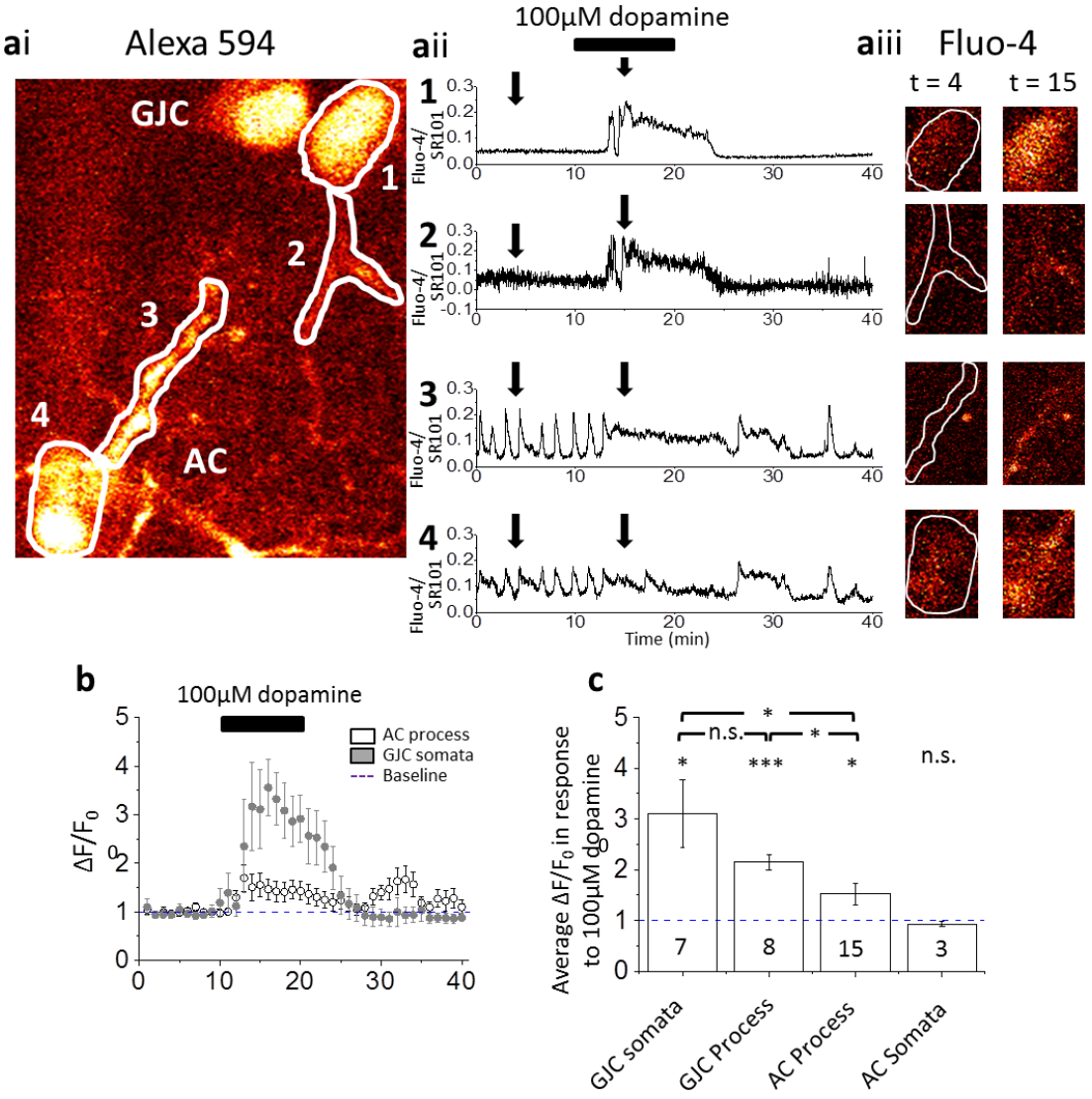

Figure 4.1 Astrocyte 'perforated-patch' and regional calcium responses to dopamine.

ai) Example image of Alexa594 fluorescence showing diffusion of dye into gap junction-coupled cells (GJC) as well as the patched cell (AC) somata and PC processes. Outlined areas indicate regions analysed in **a**ii). **a**ii) Fluo-4/Alexa594 (G/R) signal for regions indicated in **a**i) during application of 100µM dopamine. **a**iii) Left: images from Fluo-4 channel at time point indicated with first arrow on G/R traces before dopamine application for regions in **a**i). Right: as left but during dopamine application (**a**ii second arrow). **b)** summary time-course of GJC somatic calcium responses to dopamine (100µM, black bar). **c**) Summary bar chart of fluo-4 fluorescence changes in response to 100µM dopamine in AC somata, processes and GJC processes and somata respectively (t=13-17); somata/process n-numbers shown inside bars, n.s. = non-significant, * = $p<0.05$, *** = $p<0.001$ – t-test (1), 1-sample wilcoxon signed rank test or Mann-Whitney test (see text).

Given the results from this section, I decided to record only from GJC somata and AC processes – therefore results for the following sections are reported from only AC processes and GJC somata.

4.3.2 Dopamine can have a biphasic effect on astrocytic calcium concentration – both increasing and decreasing cytosolic calcium.

As shown in the example GJCs in figure 4.2a, astrocytes can, counterintuitively, respond to dopamine application with both an increase and a decrease in Fluo-4 fluorescence. As any fluorescence increase reaches far higher amplitudes than a fluorescence decrease, averaging $\Delta F/F_0$ over time obscures any recorded decrease. Hence, in order to identify fluorescence decrease in data from my previous experiments, I have pooled the $\Delta F/F_0$ fluorescence intensity data points from all recorded GJC somata in section 4.3.1, shown in Figure 4.1, and from all AC processes in section 4.3.1, separately, into two time epochs – 'baseline' (t=1-12) and 'dopamine' (t=13-20). These were then normalized to the total number of data points sampled in each condition respectively and plotted as two proportional frequency histograms (figure 4.2b) In the single cell examples in figure 4.2a there is a striking difference in the distribution of fluorescence data in dopamine compared to baseline conditions – two peaks are often visible in the dopamine distribution, one below, one above 1 (baseline average), whereas the baseline distribution peaks stay distributed around 1. The 'dopamine' population from the histograms presented in figure 4.2a is sampled from roughly the time dopamine reaches the cells to 10 minutes post-dopamine washout (t=13-30). These examples are taken from t=13-30 to illustrate the full possible decrease in fluorescence caused by dopamine application.

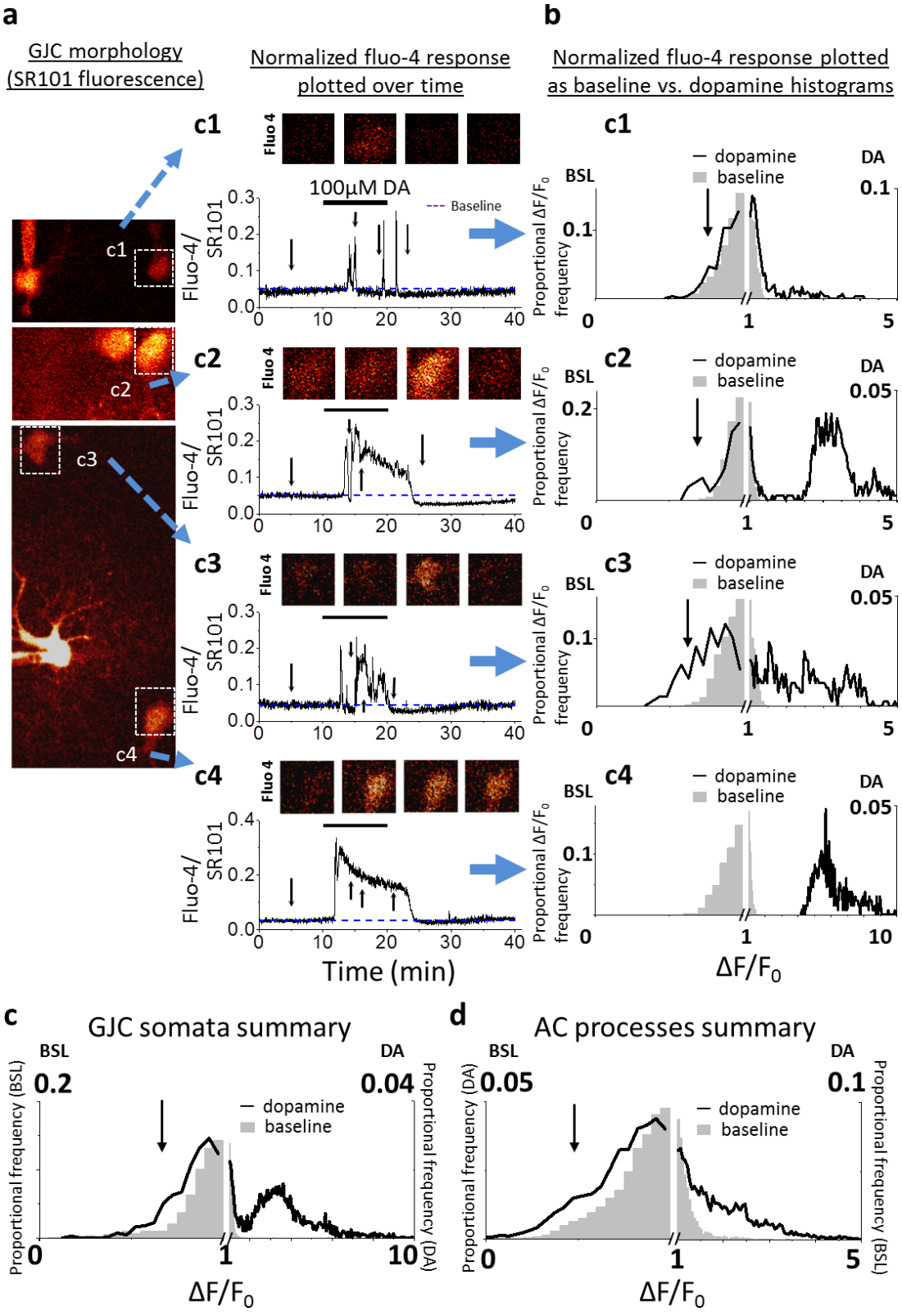

Figure 4.2 **Dopamine triggers both an increase and a decrease in astrocytic calcium levels as revealed with histogrammatical analysis.**

a) Four example GJC's responses to dopamine (100µM). Left – Alexa 594 image of each cell; right Fluo-4/Alexa 594 fluorescence traces for each GJC with example Fluo-4 channel images, arranged chronologically for time-points marked with arrows; black bars indicate dopamine application, grey bracket indicates time-frame sampled for 'baseline' population in **b**), black bracket shows 'dopamine' population for **b**), black arrows indicate putative $\Delta F/F_0$ decrease shoulder. **b**) frequency distributions (normalized to total frequency) of $\Delta F/F_0$ for each cell in **a**) for baseline epoch (t=1-12, grey bars) and 'dopamine epoch (t=13-20, black line); black arrows indicate putative $\Delta F/F_0$ decrease shoulder. **c**) normalized frequency distribution of $\Delta F/F_0$ for all GJCs in presence of 100µM dopamine (t = 13-20) compared to baseline (t = 1-12), black arrows indicate putative $\Delta F/F_0$ decrease shoulder, grey bars – in dopamine, black line – baseline. **d**) as in **c**) for AC processes.

In GJC somata, the proportional $\Delta F/F_0$ distribution at baseline is well fitted with a single Gaussian distribution (x peak=0.98, σ=0.13, FWHM=0.3, R^2=0.99), but poorly during dopamine application (x peak=2.55, σ=2.03, FWHM=4.78, R^2=0.52) – however, double Gaussian fitting is much closer to the observed data (x peaks=0.95/3.28, σ=0.18/1.1, FWHM=0.43/2.58, R^2=0.93). In AC processes baseline fit with a single Gaussian is good (x=0.97, σ=0.21, FWHM=0.49, R^2=0.98), but again, in dopamine, a single Gaussian distribution is a far worse fit (x=1.07, σ=0.51, FWHM=1.21, R^2=0.80) than a double Gaussian fitting (x peaks=0.9/1.75, σ=0.25/0.87, FWHM=0.6/2.05, R^2=0.98) – see supplementary figure S1. One feature of both distributions, that Gaussian fitting fails to capture, is the presence, in dopamine, of the negative going shoulder from the baseline $\Delta F/F_0$ – as marked by arrows in figures 4.2c, d. In both cases in dopamine, the peaks of the two Gaussians are either side of the baseline.

4.3.3 The appearance of an intracellular astrocytic calcium decrease is dependent on the concentration of dopamine used.

4.3.3.1 10µM dopamine triggers no significant change in Ca^{2+} in either AC processes or GJC somata.

Next I tested whether stimulation with lower concentrations of dopamine could replicate the astrocytic sensitive seen in bulk-loaded astrocytes (chapter 3), or separate the two dopamine-induced effects. Application of 10µM dopamine does not significantly change $\Delta F/F_0$ in either AC processes or GJC somata (Figure 4.3a). For AC processes, the population of means of $\Delta F/F_0$ in dopamine (t=13-17), is not normally distributed ($p<0.001$, Shapiro-Wilk test) and is not significantly different from baseline ($p=0.255$, 1-sample Wilcoxon signed rank test, n=12; data from 12 processes, 4 slices, 4 animals). Regarding the proportional frequency distributions, both baseline (x peak=1, σ=0.13, FWHM=0.3, $R^2=0.98$) and dopamine (x peak=1, σ=0.17, FWHM=0.41, $R^2=0.99$) epochs can be well fitted by single Gaussians. In GJC somata the mean $\Delta F/F_0$ is not significantly different from baseline ($p=0.39$, 1-sample t-test, n=13; data from 13 cells, 7 slices, 4 animals) and both baseline (peak x=0.98, σ=0.15, FWHM=0.35, $R^2=0.98$) and dopamine (peak x=1, σ=0.18, FWHM=0.42, $R^2=0.96$) $\Delta F/F_0$ proportional frequency distributions can be tolerably well fitted with single Gaussians– see supplementary figure S2.

4.3.3.2 20µM dopamine triggers a Ca^{2+} increase in both AC processes and GJC somata, but no Ca^{2+} decrease.

20µM dopamine (figure 4.3b) significantly increases fluo-4 fluorescence intensity in both AC processes – to 1.35 ± 0.07 of mean – ($p<0.001$, 1-sample t-test, n=24; data taken from 24 processes; 6 slices and 5 animals) and GJC somata – to 1.37 ± 0.12 of mean – ($p<0.001$, 1-sample t-test, n=12; data taken from 12 cells, 6 slices, 5 animals). The distribution of $\Delta F/F_0$ in AC processes in baseline conditions can be modelled by a single Gaussian distribution (peak x=0.99, σ=0.21, FWHM=0.49, $R^2=0.99$) as can the distribution

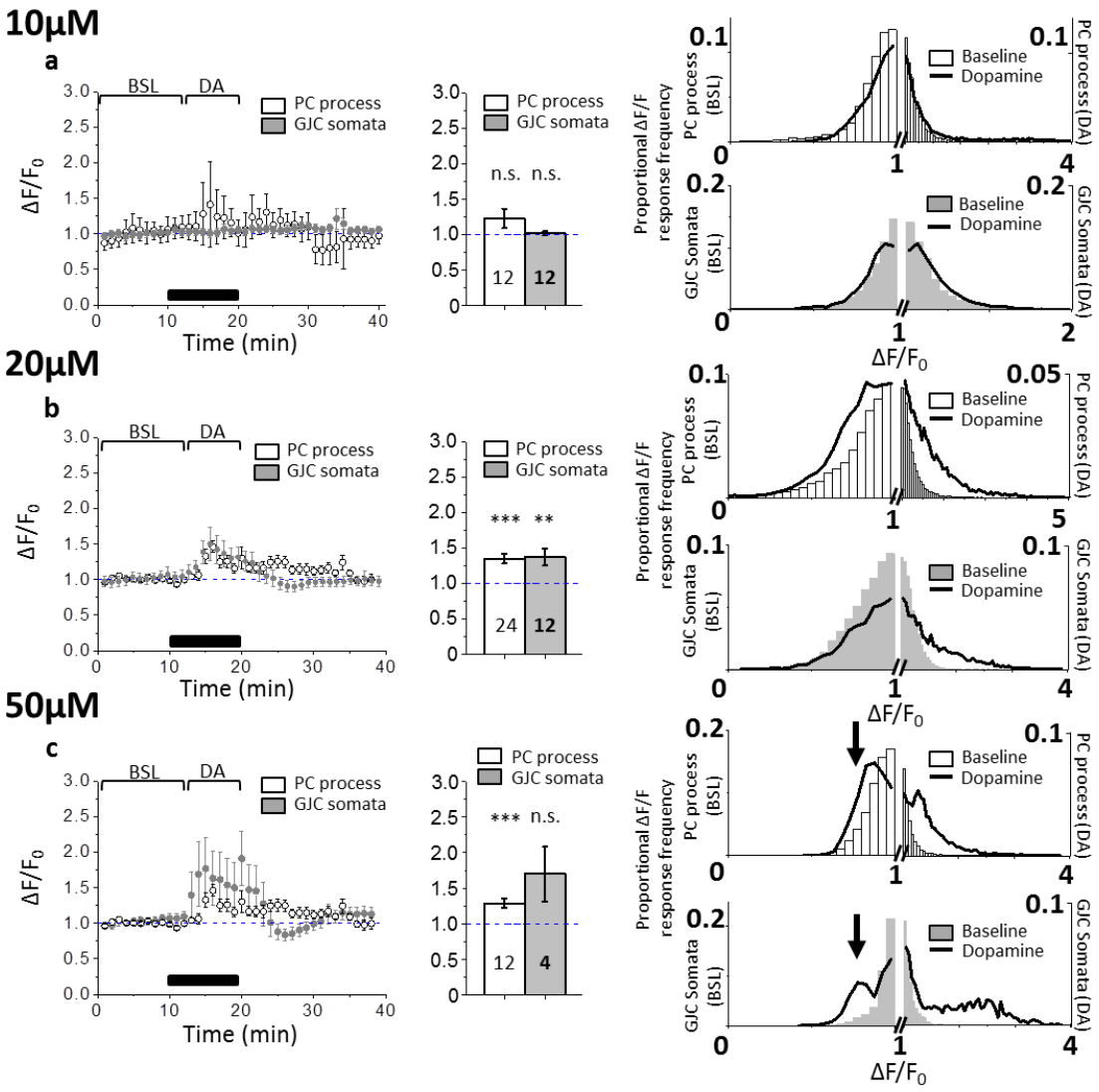

Figure 4.3 Concentration dependent dopamine-induced fluorescence increase and decrease.

a) 10µM dopamine does not affect fluo-4 fluorescence. Left: time course of dopamine application (black bar – dopamine application), brackets indicate time frames sampled for histograms; middle: fluorescence change average over t = 13-17; right: histogram of $\Delta F/F_0$ data points recorded from patched cell (AC) processes (above) and Gap-junction coupled (GJC) somata (below) – bars indicate baseline distribution (t = 1-12), line indicates distribution in presence of dopamine (t = 13-20). **b**) 20µM dopamine increases fluorescence in both AC processes and GJC somata. Layout: as in **a**). **c**) 50µM dopamine triggers both fluorescence increases and decreases in AC processes and GJC somata. Layout: as in **a**), black arrows in histogram indicate negative $\Delta F/F_0$ shoulder in the presence of dopamine. Hollow circles/bars – data from pc processes, grey circles/bars – data from GJC somata, numbers in bars indicate processes/soma n-numbers ,n.s. – not significant, ** - p<0.01, *** p<0.001, t-test (1).

upon dopamine application, although less well (peak x=1.1, σ=0.43, FWHM=1.01, R^2=0.92); a double Gaussian distribution better captures the population shape in dopamine (x peaks=0.92/1.43, σ=0.23/0.53, FWHM=0.53/1.25, R^2=0.99), perhaps unsurprisingly. GJC somata exhibit a similar proportional frequency distribution of $\Delta F/F_0$ to that shown by AC processes: baseline is well modelled by a Gaussian centred on 1 (peak x=1, σ=0.22, FWHM=0.51, R^2=1) but dopamine less so (peak x=1.09, σ=0.35, FWHM=0.83, R^2=0.89); the dopamine distribution is better modelled by a double gaussian (x peaks =0.99/1.58, σ=0.23/0.55, FWHM=0.54/1.3, R^2=0.99) – see supplementary figure S3.

4.3.3.3 50µM dopamine triggers a Ca^{2+} increase and decrease in both AC processes and GJC somata.

In 50µM dopamine $\Delta F/F_0$ significantly increases in AC processes (figure 4.3c) to 1.29 ± 0.06 ($p<0.001$, 1-sample t-test, n=12; data from 12 processes, 2 slices, 2 animals), but not in GJC somata (p=0.17, 1-sample t-test, n=4; data from 4 cells, 3 slices, 2 animals). A single Gaussian models the baseline well for AC processes (peak x=0.96, σ=0.11, FWHM=0.27, R^2=0.99) but not during the dopamine application (peak x=1.07, σ=0.35, FWHM=0.81, R^2=0.85) – this requires a double distribution (peak x's=0.86/1.24, σ=0.09/0.31, FWHM=0.21/0.72, R^2=0.98) the first peak of which falls near the negative-going shoulder indicated by the black arrow. In GJC somata, baseline proportional distribution frequency is fairly well modelled by a single Gaussian (peak x=1.01, σ=0.08, FWHM=0.19, R^2=0.97), but dopamine distribution cannot be modelled be a single Gaussian (x=1.29, σ=0.97, FWHM=2.28, R^2=0.44); a double Gaussian models the dopamine far better (x peaks=1/2.16, σ=0.18/0.62, FWHM=0.42/1.47, R^2=0.92), but still does not describe the negative going shoulder, indicated with the black arrow in figure 4.3c, which is even better modelled by a

triple Guassian (x peaks=0.77/1.03/2.07, σ=0.05/0.12/0.7, FWHM=0.12/0.28/1.66, R^2=0.96) – see supplementary figure S4.

4.3.4 The biphasic dopaminergic effect is independent of neuronal activity and persists when purinergic receptors are blocked.

4.3.4.1 Blocking mGluRs, Na^+ channels and $GABA_B$Rs does not inhibit the dopamine induced Ca^{2+} increase or decrease.

To control for possible indirect actions of dopamine that could trigger astrocyte calcium dynamics through glutamate or GABA release or increase in neuronal firing, I blocked voltage-gated Na^+ channels, mGluRs and $GABA_B$Rs. First, 100μM dopamine was applied in a cocktail of neuronal activity blockers (figure 4.4a). This cocktail consisted of the mGluR5 inhibitor MPEP (1μM), the mGluR1 inhibitor LY367385 (100μM), the mGluR2/3 antagonist LY341495 (500nM), the $GABA_b$ inhibitor CGP 55845 (1μM) and the voltage dependent Na^+-channel blocker TTX (1μM). In this presence of this cocktail neuron action potential firing will be inhibited, as will metabotropic glutamatergic and GABAergic signalling. Under these conditions dopamine still significantly increases the astrocytic calcium in both GJC somata – to 3.64 ± 0.66 of baseline (p=0.016, 1-sample t-test, n=5; data from 5 cells, 3 slices, 3 animals) – and AC processes (data is not normally distributed, p<0.001, Shapiro-Wilk test) to a median of 1.3 of mean (p<0.001, 1-sample Wilcoxon signed rank test, n=17; data from 17 processes, 3 slices, 3 animals). These data are not significantly different from those recorded under control conditions (i.e. application of 100μM dopamine alone) in either GJC somata (p=0.594, 2-sample t-test), or AC processes (p=0.45, Mann-Whitney test). The proportional distribution of GJC somata data from baseline conditions is very well modelled by a single Gaussian distribution (x peak=1, σ=0.12, FWHM=0.27, R^2=1), but in dopamine cannot be modelled with a single Gaussian – instead a

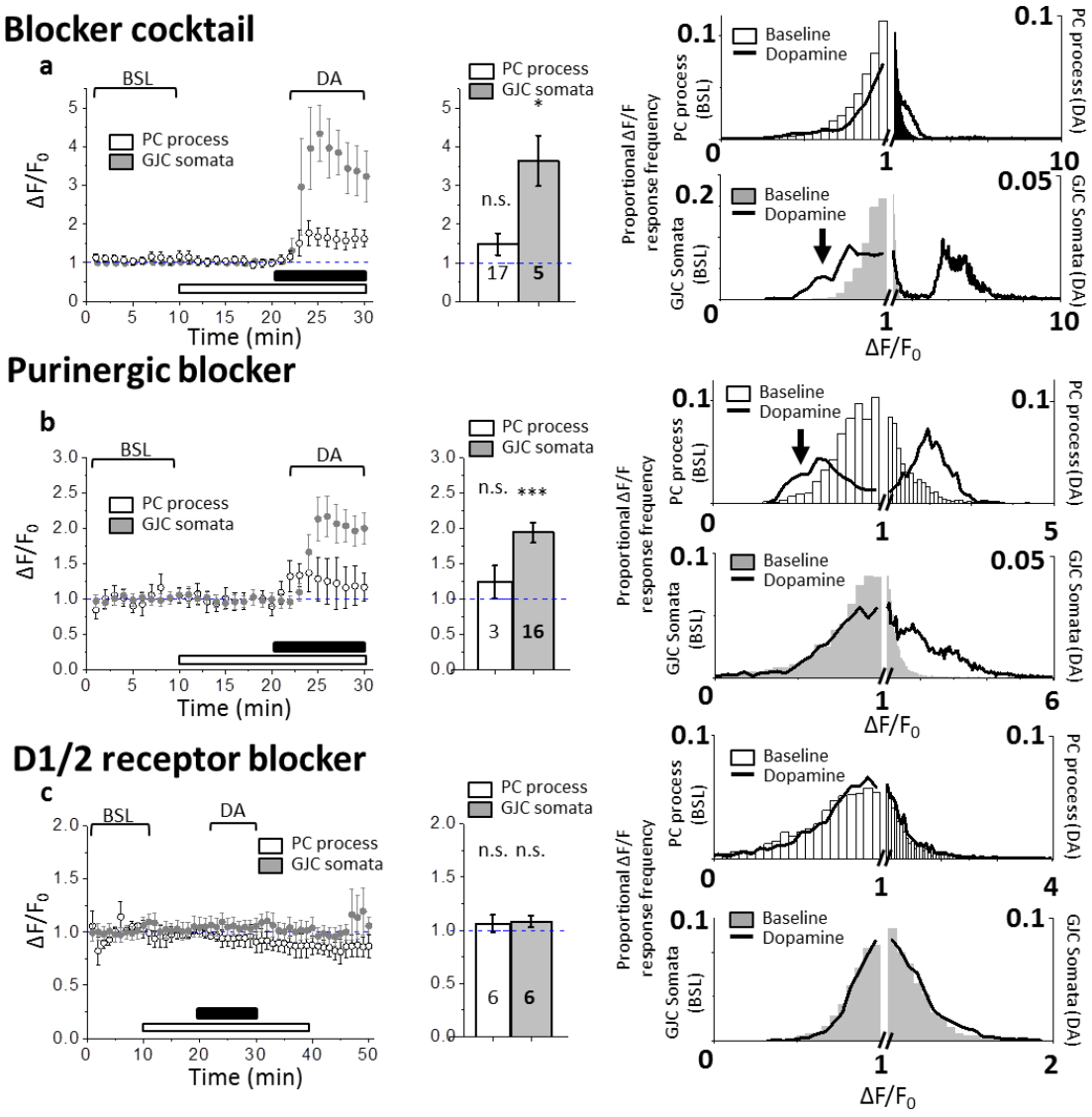

Figure 4.4 The dopamine acts directly on astrocytes and the induced fluorescence change is mediated through dopamine receptors.

a) Dopamine (100µM) fluorescence increase and decrease persists in the presence of a cocktail of neuronal receptor/channel blockers – TTX (1 µM), MPEP (1 µM), LY367385 (100 µM), LY341495 (500nM) and CGP (1 µM). Left: time course of dopamine application (black bar – dopamine application, hollow bar – blocker application), brackets indicate time frames sampled for histograms; middle: fluorescence change average over t = 13-17; right: histogram of $\Delta F/F_0$ data points recorded from patched cell (AC) processes (above) and Gap-junction coupled (GJC) somata (below) – bars indicate baseline distribution (t = 1-12), line indicates distribution in presence of dopamine (t = 13-20). **b**) Purinergic receptor blocker PPADS (100 µM) does not block dopamine induced fluorescence change. Layout: as in **a**). **c**) dopamine receptor blockers – SCH23390 (20 µM) and Sulpiride (50 µM) – block all dopamine-induced fluroescence change. Layout: as in **a**). Hollow circles/bars – data from pc processes, grey circles/bars – data from GJC somata, numbers in bars indicate processes/soma n-

numbers, black arrows in histogram indicate negative $\Delta F/F_0$ shoulder in the presence of dopamine, n.s. – not significant, ** - p<0.01, *** p<0.001, t-test (1) or Wilcoxon signed rank test (see text).

---

double Gaussian models the effect better – displaying peaks either side of the baseline (x peaks=0.92/4.32, σ=0.24/0.84, FWHM=0.57/1.99, R^2=0.9). In AC processes baseline is well modelled by a single Gaussian (x peak=1.02, σ=0.18, FWHM=0.42, R^2=0.96) but dopamine application is not (x peak=1.25, σ=0.44, FWHM=1.04, R^2=0.87) – modelling with a double Gaussian greatly improves the fit (peak x's=1.02/1.45, σ=0.1/0.49, FWHM=0.24/1.15, R^2=0.99) – see supplementary figure S5.

4.3.4.2 Purinergic receptor blockade does not affect the dopamine-induced Ca^{2+} increase in either AC processes or GJC somata, but does inhibit the Ca^{2+} in GJC somata only.

Astrocytes can release ATP upon stimulation to propagate intracellular calcium dynamics between astrocytes themselves and neurons (Fields and Burnstock, 2006). To ascertain if purinergic signalling played a role in the dopamine-induced calcium dynamics, I blocked $P2X_{1,2,3,5}$ and $P2Y_{2,4}$ receptors (using 100µM PPADS) in order to ascertain how much of this inter-astrocyte purinergic signalling made up the total dopamine-induced calcium signal (figure 4.4b). In AC processes, there is no significant increase in average fluorescence from baseline upon 100µM dopamine application in the presence of PPADS (p=0.4, 1-sample t-test, n=3; data from 3 processes, 2 slices, 2 animals) but there is in GJC somata – to 1.94 ± 0.14 of baseline – (p<0.001, 1-sample t-test, n=16; data from 16 cells, 5 slices, 4 animals). Comparing PPADS to control conditions, there is no significant difference between

the two sets of AC process responses (p=0.636, Mann-Whitney test), but GJC somata $\Delta F/F_0$ is significantly greater in control conditions than in PPADS (difference in means=1.16, p=0.026, 2-sample t-test). Fitting Gaussian distributions to AC process responses shows a reasonable single Gaussian fit for baseline (x peak=0.95, σ=0.2, FWHM=0.46, R^2=0.96) but poor for dopamine application (x peak=1.35, σ=0.47, FWHM=1.11, R^2=0.42), which is well fitted with a double Gaussian distribution whose peaks fall either of the modelled baseline x peak of 0.95 (x peaks=0.65/1.49, σ=0.15/0.23, FWHM=0.04/0.54, R^2=0.96) – explaining the lack of significance seen when averaging the data. Considering GJC somata, baseline is again well described by a single Gaussian (x peak=0.98, σ=0.23, FWHM=0.54, R^2=0.98), but the dopamine response is not (x peak=1.58, σ=0.9, FWHM=2.11, R^2=0.82). This requires either two, or even three gaussians to fit well: x peaks=0.97/1.93 (σ=0.22/0.93, FWHM=0.52/2.19, R^2=0.95) and x peaks=0.96/1.71/2.56 (σ=0.25/0.31/0.9, FWHM=0.57/0.72/2.1, R^2=0.98) respectively, but in neither does the first peak move far negative of the fitted baseline x peak of 0.98– see supplementary figure S6.

4.3.5 Both increase and decrease in calcium concentrations in response to dopamine are blocked by simultaneous blockade of D1- and D2-type receptors.

Next I sought to replicate the dopamine-receptor dependency of the dopamine-induced Ca^{2+} increase recorded in bulk-loaded slices and test whether the Ca^{2+} decrease is similarly dopamine receptor-dependent. Simultaneous blockade of D1 and D2-type receptors with SCH23390 (20µM) and Sulpiride (50µM) blocks dopamine-induced astrocytic F_i and F_d (figure 4.4c). AC process $\Delta F/F_0$ data is not normally distributed (p=0.005, Shapiro-wilk test) and in dopamine (100µM) is not significantly different from baseline (p=1, 1-sample Wilcoxon signed rank test, n=6; data from 6 process, 3 slices, 3 animals). $\Delta F/F_0$ data

from GJC somata is not significantly different from baseline in dopamine (p=0.126, 1-sample t-test, n=5; data from 5 cells, 3 slice, 3 animals). Similar single Gaussian curves fit AC process baseline (x peak=0.93, σ=0.32, FWHM=0.75, R^2=0.98) and dopamine (x peak=0.97, σ=0.31, FWHM=0.73, R^2=0.97) distributions well. As is the case with GJC somata baseline (x peak=1, σ=0.17, FWHM=0.38, R^2=0.99) and dopamine (x peak=1.02, σ=0.17, FWHM=0.41, R^2=0.98) distributions– see supplementary figure S7.

4.3.6 Blockade of D1-type receptors alone can partially inhibit the Ca^{2+} increase in response to dopamine but spares the Ca^{2+} decrease.

Is the effect of dopamine on astrocytes mediated by a specific dopamine receptor type? I investigated this through blockade of type-1 dopamine receptors alone first. Application of 100µM dopamine in the presence of 10µM of the D1/5R blocker SCH23390 (figure 4.5a) stimulates only a couple of large responses in the population of AC processes – visible as grey traces in the left panel of figure 5a – and the median $\Delta F/F_0$ for the non-normally distributed means (p=0.004, Shapiro-Wilk test) is not different from baseline (p=0.97, 1-sample Wicoxon signed ranks test, n=12; data from 12 processes, 4 slices, 4 animals). However, the proportional distribution of the $\Delta F/F_0$ data clearly shows a negative skew from baseline (black arrow in right, upper panel of figure 4.5a). Both the baseline and the dopamine distributions can be very well modelled with a single Guassian distribution, but the fitted x peak for baseline (x peak=0.98, σ=0.13, FWHM=0.3, R^2=1) is greater than that for dopamine (x peak=0.88, σ=0.16, FWHM=0.38, R^2=0.98). GJC somata show a similar negative shift in $\Delta F/F_0$ in dopamine, but this is significant – to a mean of 0.93 ± 0.02 (p=0.003, 1-sample t-test, n=8; data from 8 cells, 4 slices, 4 animals). This is reflected in the peak x of the fitted single Gaussians which show decrease in dopamine (x peak=0.94,

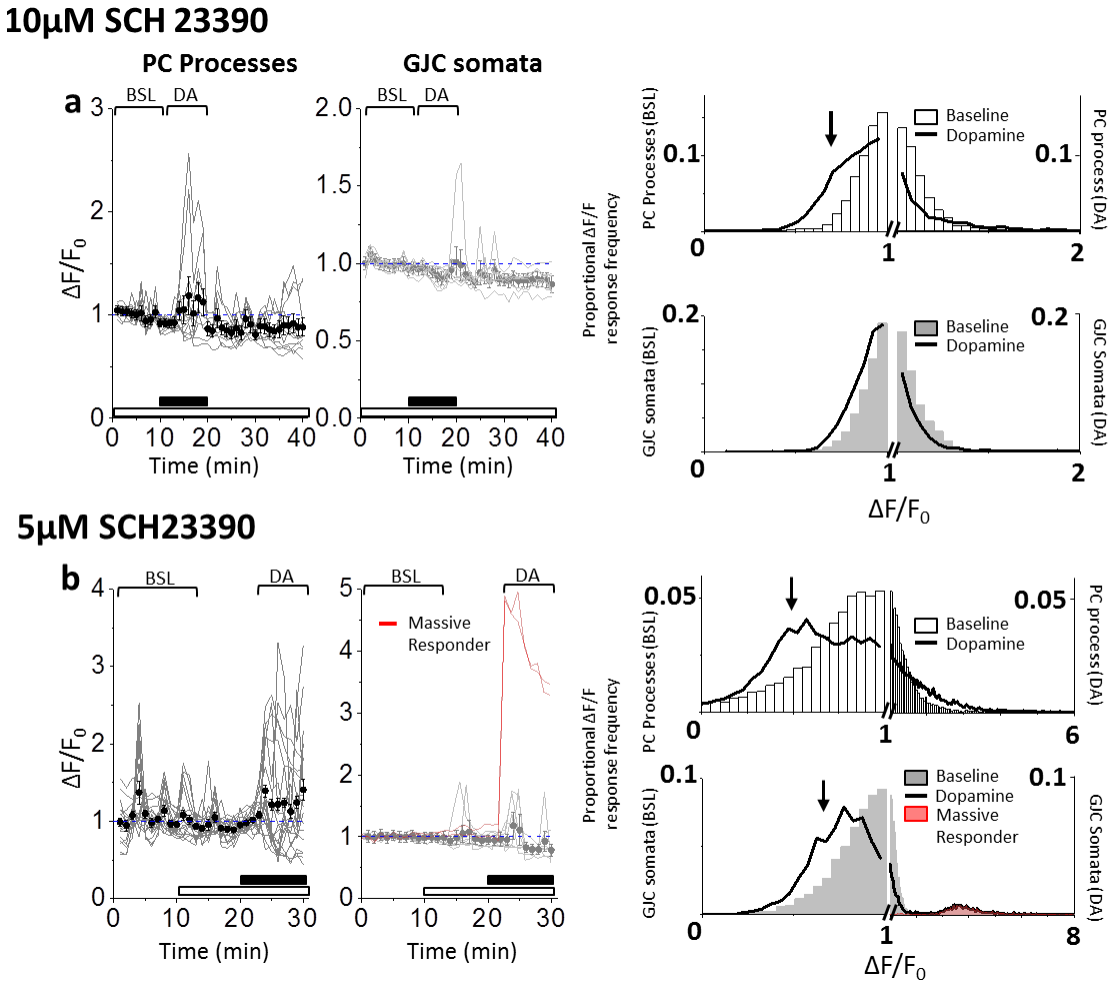

Figure 4.5 D1-type receptor blocker SCH23390 has concentration-dependent effects on dopamine-induced astrocytic calcium dynamics.

a) Dopamine application (100µM) in the presence of 10µM SCH223390 primarily triggers a decrease in $\Delta F/F_0$. Left: time course of dopamine application (hollow bar – SCH23390 application, black bar – dopamine) for AC processes, black points indicate average, grey lines indicate each individual cell response. Middle: time course for GJC somata, grey points indicate average, light grey lines indicate each individual cell response. Right: histogram of $\Delta F/F_0$ data points recorded from patched cell (AC) processes (above) and Gap-junction coupled (GJC) somata (below). Bars indicate baseline distribution (t = 1-12), line indicates distribution in presence of dopamine (t = 13-20), brackets in time courses (left, middle) indicate time frames sampled for histograms. **b**) Dopamine application (100µM) in the presence of 5µM SCH223390 triggers a decrease in baseline $\Delta F/F_0$ but an increase in spontaneous events. Layout: as above. Red lines in GJC somata time course and shading in histogram indicate separate 'massive responder' two cell population. Black arrows in histogram indicate negative $\Delta F/F_0$ shoulder in the presence of dopamine, hollow circles/bars – data from AC processes, grey circles/bars – data from GJC somata.

σ=0.11, FWHM=0.26, R^2=0.98), compared to baseline (x peak=0.99, σ=0.11, FWHM=0.25, R^2=0.99) – see supplementary figure S8.

4.3.7 Decreased blockade of the D1-type receptor results in a decrease in baseline calcium and an increase in spontaneous calcium events.

Is it possible to change the ratio of Ca^{2+} increase to decrease without completely blocking either? In 5µM SCH23390, 100µM dopamine stimulation appears to have paradoxically opposite effects on astrocytic calcium: a decrease in baseline, upon which ride an increased frequency of transient high-amplitude calcium concentration increases (Figure 4.5b**,** left and middle panels). This increased variability translates to a lack of significant difference from baseline when examining the population of $\Delta F/F_0$ means in dopamine: neither AC processes (p=0.01, Shapiro-Wilk) nor GJC somata (p<0.001, Shapiro-Wilk) are normally distributed and neither are significantly different from baseline as p=0.177 (1-sample Wilcoxon signed rank test, n=20; data from 20 processes, 5 slices, 3 animals) and p=0.7 (1-sample Wilcoxon signed rank test, n=10; data from 10 cells, 5 slices, 3 animals) respectively.

However, examining the proportional frequency distribution of $\Delta F/F_0$ in baseline and dopamine conditions reveals the strikingly different possible actions of dopamine on astrocytic calcium in this lower concentration of SCH23390 – the negatively shifted baseline is clearly visible in both AC processes and GJC somata (figure 4.5b, right panel, marked with black arrows). For AC processes, baseline fluorescence data distribution is well fitted with a single Gaussian (peak x=0.99, σ=0.36, FWHM=0.86, R^2=0.98), but dopamine fluorescence data is less so (peak x=0.89, σ=0.57, FWHM=1.34, R^2=0.88) – but is well fitted with a double Gaussian (x peaks=0.65/1.41, σ=0.29/0.72, FWHM=0.69/1.68, R^2=0.97). For GJC somata, 2/10 recorded cells respond to dopamine with very characteristic ‘massive’ sustained

increases (Figure 4.5b**,** middle panel) hence, whilst the baseline is very well fitted by a single Gaussian (peak x=0.99, σ=0.22, FWHM=0.52, R^2=1), the $\Delta F/F_0$ distribution in dopamine needs two gaussians to accommodate these two 'massive responder' cells (x peaks=0.8/3.72, σ=0.21/0.64, FWHM=0.5/1.51, R^2=0.98); the peak x of the lower Gaussian (which accounts for most of the proportional distribution) is lower than the baseline peak by 0.19 – see supplementary figure S9.

4.3.8 Blockade of D2-type receptors alone results in blockade of all dopamine-induced astrocytic calcium dynamics.

What role do D2-type receptors play? Sulpiride is a selective D2/3R blocker used previously in conjunction with SCH23390. Here I tested its inhibitory induced effects on dopamine-induced astrocytic calcium changes. 50μM sulpiride samples are small (figure 4.6a), and the fluorescence means in dopamine show no significant difference to those at baseline for AC processes (p=0.332, 1-sample t-test, n=3; data from 3 processes, 3 slices, 3 animals) or GJC somata (p=0.316, 1-sample t-test; n=3; data from 3 cells, 3 slices, 3 animals). Fitting Gaussian distributions to AC process $\Delta F/F_0$ proportional frequency distributions is feasible: baseline can be well modelled by a single Gaussian (peak x=0.99, σ=0.11, FWHM=0.26, R^2=0.98), dopamine cannot (peak x=0.99, σ=0.13, FWHM=0.31, R^2=0.76) – but can with a double Gaussian (x peaks=0.95/1.2, σ=0.07/0.22, FWHM=0.16/0.52, R^2=0.99), whose peaks fall either side of baseline. Modelling GJC somata $\Delta F/F_0$ proportional frequency distributions is possible with a single Gaussian at baseline (peak x=0.93, σ=0.19, FWHM=0.46, R^2=0.99) and in dopamine (peak x=1.07, σ=0.19, FWHM=0.45, R^2=0.99) – see supplementary figure S10.

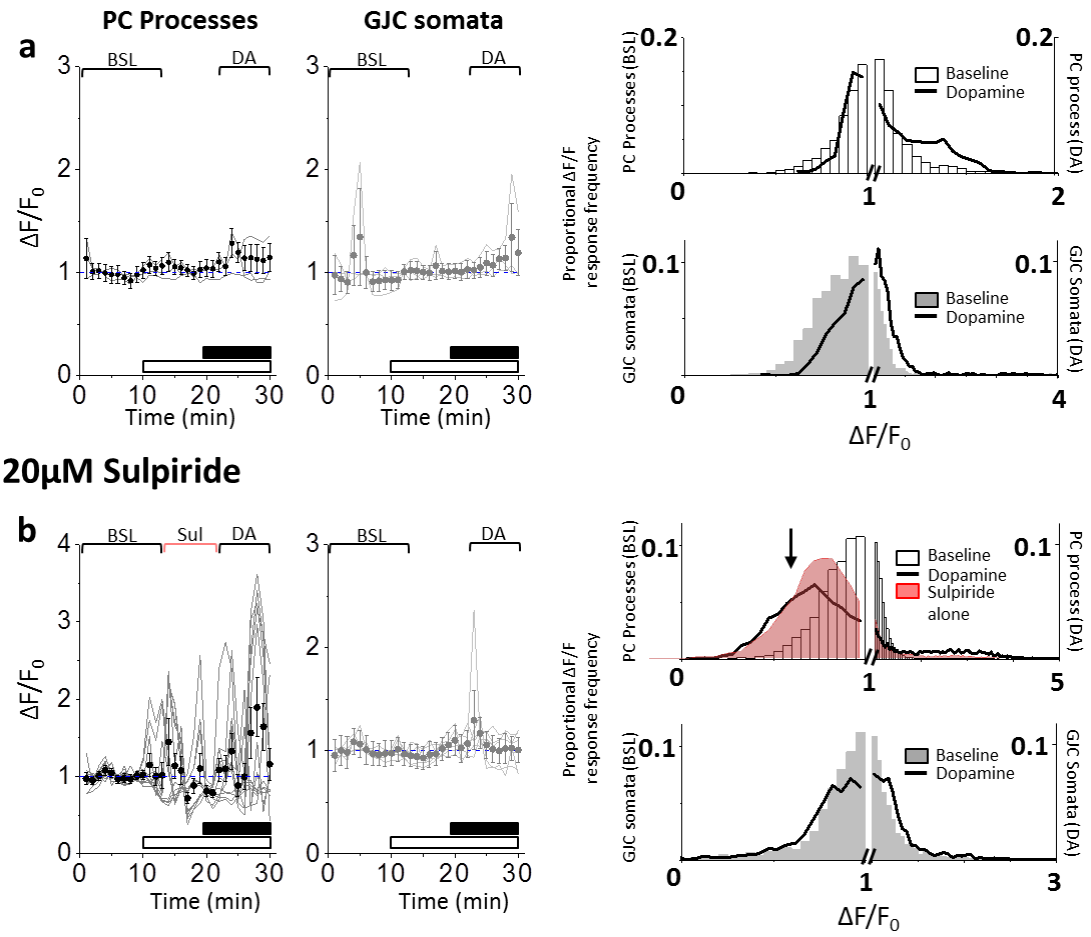

Figure 4.6 D2-type receptor blocker sulpiride has concentration-dependent effects on dopamine-induced astrocytic calcium dynamics.

a) Dopamine application (100µM) in the presence of 50µM sulpiride has little effect on $\Delta F/F_0$. Left: time course of dopamine application (hollow bar – sulpiride application, black bar – dopamine) for AC processes, black points indicate average, grey lines indicate each individual cell response. Middle: time course for GJC somata, grey points indicate average, light grey lines indicate each individual cell response. Right: histogram of $\Delta F/F_0$ data points recorded from patched cell (AC) processes (above) and Gap-junction coupled (GJC) somata (below). Bars indicate baseline distribution (t = 1-12), line indicates distribution in presence of dopamine (t = 13-20), brackets in time courses (left, middle) indicate time frames sampled for histograms. **b**) Dopamine application (100µM) in the presence of 20µM sulpiride triggers a decrease in baseline $\Delta F/F_0$ but an increase in spontaneous events. Layout: as above; red shading indicates $\Delta F/F_0$ in presence of 20µM sulpiride only. Black arrows in histogram indicate negative $\Delta F/F_0$ shoulder in the presence of dopamine, hollow circles/bars – data from AC processes, grey circles/bars – data from GJC somata.

4.3.9 Decreased blockade of the D2-type receptor continues to block GJC calcium changes, but Sulpiride itself triggers activity in AC processes.

In 20µM sulpiride, the mean fluorescence change in dopamine, from baseline, is significant for AC processes – to 1.34 ± 0.15 of baseline (p=0.046, 1-sample t-test, n=12; data from 12 processes, 3 slices, 2 animals) – but not for GJC somata (p=0.327, 1-sample t-test, n=6; data from 6 cells, 3 slices, 2 animals). However this does not capture the nature of the responses well (figure 6b, left and middle panels) – for this it is better to look at the frequency distributions. The AC process proportional frequency distribution at baseline is well modelled by a Gaussian distribution (peak x=0.97, σ=0.18, FWHM=0.43, R^2=0.99), but the distribution in dopamine, when modelled by a single Gaussian, does not capture the positive-going tail, (peak x=0.73, σ=0.24, FWHM=0.56, R^2=0.9) – for this a double Gaussian is required (x peaks=0.72/2.22, σ=0.21/1.13, FWHM=0.51/2.66, R^2=0.99). In both models, there is a clear peak below baseline peak x from data in dopamine as indicated by the black arrow in figure 4.6b. However in GJC somata both the baseline (peak x=0.99, σ=0.16, FWHM=0.38, R^2=0.98) and dopamine (peak x=1.02, σ=0.24, FWHM=0.57, R^2=0.98) distributions are well captured by similar Gaussian curves. 20µM Sulpiride on its own, before dopamine application, appears to affect AC process calcium – but the difference of the means from baseline is not significant (p=0.339, 1-sample Wilcoxon signed rank test, n=12; not normally distributed, p=0.044, Shapiro-Wilk test). However, fitting the distribution of $\Delta F/F_0$ in sulpiride alone with a single Gaussian gives a very good fit (peak x=0.78, σ=0.19, FWHM=0.46, R^2=0.99) and peak at x=0.78, well below baseline – see supplementary figure S11.

4.3.10 Specific, coincident activation of D1 and D2 receptors stimulates a small, biphasic calcium signal in AC processes only.

Can the dopamine-receptor dependent effects reported above be replicated through dopamine-receptor activation alone? When 100µM SKF38390 (a specific D1R agonist) and 100µM quinpirole (a specific D2R agonist) are added to the bath, no significant change in $\Delta F/F_0$ was found in either the processes (p=0.421, 1-sample Wicoxon signed ranks test, n=15; data not normally distributed, p=0.002, Shapiro-Wilk test; data from 15 processes, 5 slices, 4 animals) or the GJC somata (p=0.158, 1-sample t-test, n=12; data from 12 GJCs, 5 slices, 4 animals). Although the proportional frequency distribution of GJC $\Delta F/F_0$ can be modelled equally well with a single Gaussian in both baseline (peak x=0.99, σ=0.29, FWHM=0.67, R^2=0.99) and dopamine (peak x=1.04, σ=0.29, FWHM=0.68, R^2=0.99) conditions, AC process $\Delta F/F_0$ in dopamine is worse approximated by a single Gaussian distribution (peak x=0.9, σ=0.26, FWHM=0.61, R^2=0.93) than AC process baseline $\Delta F/F_0$ (peak x=0.94, σ=0.26, FWHM=0.61, R^2=0.99). The dopamine distribution is better modelled by a double Gaussian (x peaks=0.87/1.58, σ=0.22/0.77, FWHM=0.51/1.82, R^2=0.98).

4.3.11 Activation of D2Rs alone triggers a small bidirectional calcium signal in AC processes alone, similar to D1/D2 agonist application

When 100µM quinpirole alone is added to the bath, there is a significant increase in $\Delta F/F_0$ was found in AC processes (p=0.021, 1-sample t-test, n=16; data from 16 processes, 3 slices, 1 animal) but not in GJC somata (p=0.857, 1-sample t-test, n=6; data from 6 GJCs, 3 slices, 1 animals). The proportional frequency distribution of GJC $\Delta F/F_0$ can be modelled equally well with a single Gaussian in both baseline (peak x=0.99, σ=0.14, FWHM=0.34, R^2=1) and dopamine (peak x=1, σ=0.13, FWHM=0.38, R^2=0.99) conditions. AC processes display spontaneous activity in baseline conditions, leading to a $\Delta F/F_0$ distribution that can be adequately modelled by a single Gaussian distribution (peak x=0.9, σ=0.25, FWHM=0.59, R^2=0.97) but better modelled with a double Gaussian (x peaks=0.86/1.26, σ=0.21/0.39,

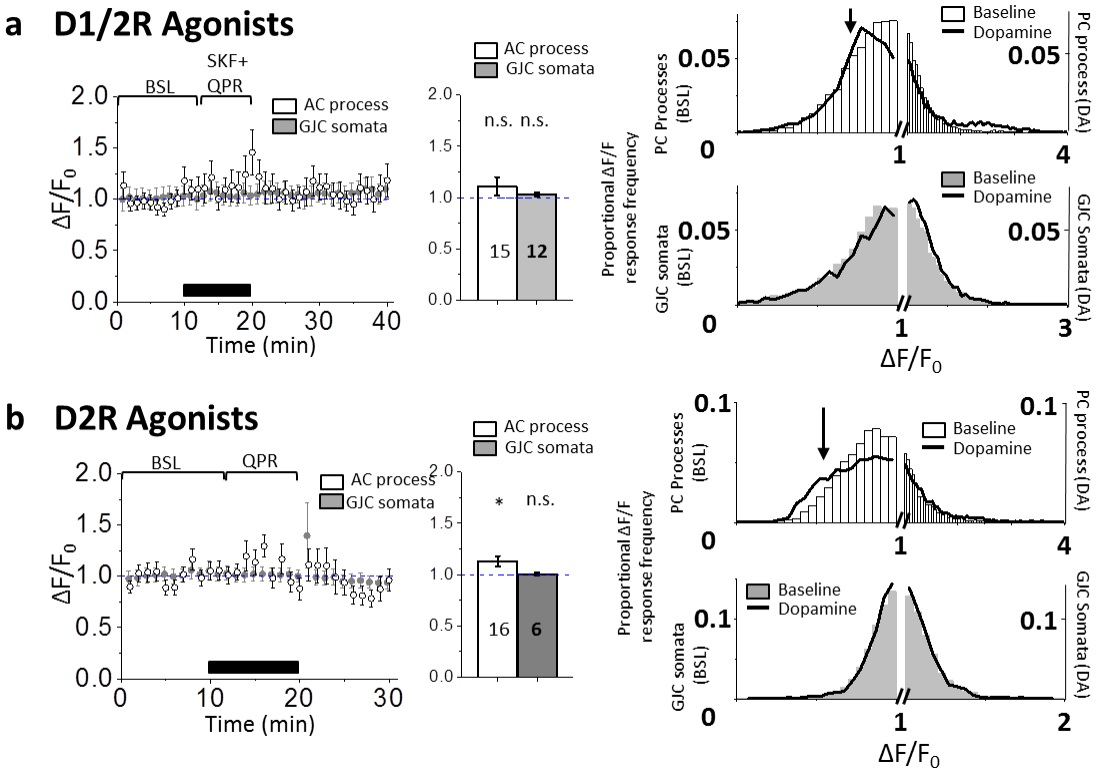

Figure 4.7 Specific dopamine receptor agonist application triggers small, biphasic calcium dynamics in astrocytic processes.

a) SKF38390 (100µM) and Quinpirole (100µM) has a small effect on process $\Delta F/F_0$. Left: time course of dopamine application (black bar – SKF and QPR application), brackets indicate time frames sampled for histograms; middle: fluorescence change average over t = 13-17; right: histogram of $\Delta F/F_0$ data points recorded from patched cell (AC) processes (above) and Gap-junction coupled (GJC) somata (below) – bars indicate baseline distribution (t = 1-12), line indicates distribution in presence of dopamine (t = 13-20). **b**) Quinpirole alone (150µM) has a similar, small effect on process $\Delta F/F_0$. Layout: as in **a**).

FWHM=0.49/0.91, R^2=1) – see supplementary figure S12. Similarly, AC process $\Delta F/F_0$ in dopamine can be modelled with a single Gaussian (peak x=0.96, σ=0.35, FWHM=0.83, R^2=0.96) but is better fitted with a double Gaussian (x peaks=0.83/1.36, σ=0.28/0.47, FWHM=0.66/1.1, R^2=0.98) – see supplementary figure S13.

4.4 Discussion

4.4.1 Why is the response to dopamine different between the patched cell and gap junction-coupled cells? The creation of an astrocyte 'perforated-patch'.

The first aim of this chapter is to assess whether dopamine has similar effects on astrocytic calcium in non-treated slices to those that have been bulk-loaded with SR101 and fluo-4-AM (as in chapter 3). I achieved this by whole-cell patch-clamping single astrocytes and loading them with cell-impermeant calcium-indicator (Fluo 4). The greatly improved dye-loading and signal to noise ratio afforded by this technique allowed me to image astrocyte processes – key to understanding dopamine induced calcium dynamics. AC process calcium dynamics in response to dopamine stimulation have yet to be studied (given all previous studies have been in culture). A striking, if well-known phenomenon that occurs upon whole-cell patch-clamp of an astrocyte is the appearance of nearby, non-patched astrocytes when viewed under fluorescence excitation imaging. Astrocytes are intimately linked to each other by gap junctions, channels formed primarily from connexin 43 and connexin 30 proteins (Giaume and Theis 2010) *in situ*. These gap-junctions are permeable to molecules up to around 1-1.2kDA in size, including important intracellular signalling ions (Na^+, K^+ and Ca^{2+}) (Ransom and Ye 2005) and some second messangers and amino acids (Tabernero et al. 2006; Theis and Giaume 2012). These inter-cellular pores are permeable to both the morphological dye and calcium-indicator that I am using: Alexa 594 (MW: 909 Da) and Fluo-4 (MW: 737 Da) respectively and it is the diffusion of these dyes into neighbouring astrocytes that makes them visible (see figure 1a). Indeed this phenomenon is so robust that its presence is used as an indicator of patched cell health, as undesirable intracellular conditions (high calcium, pH change) interfere with gap junction coupling (Crow et al. 1994; Giaume and Venance 1998; Rackauskas et al. 2010). I have decided to put this phenomenon to use throughout this thesis by imaging concurrently

from both patched astrocyte (AC) processes and gap-junction coupled astrocyte (GJC) somata. The patched astrocyte can be regarded as a filter between the patch pipette and the GJCs – both limiting the size of molecules dialysing into, or washing out from GJCs (through gap-junction pores) and limiting the diffusion rate between the pipette and GJCs, by increasing the spatial distance and environmental complexity (proteins, cell-membrane, etc.) between the patch-pipette and the imaged cell. This recording configuration can be likened to electrophysiological perforated-patch recordings (Horn and Marty 1988), as both methods seek to leave the recorded cell's intracellular milieu as close to its original state as possible – hence the 'astrocyte perforated patch'.

As is clear from figure 4.1, in all but AC somata, dopamine triggers average intracellular cytosolic free calcium increases. The lack of response in the AC somata is to be expected – it is a relatively small structure (8-10µM diameter) which will dialyse rapidly with pipette solution, washing out most small endogenous signalling molecules that could be vital for dopamine-induced calcium increase. The mechanical stimulation from pipette tip vibration could also trigger calcium signalling (Charles et al. 1991), further confounding any possible calcium response recordings. Therefore, for the remainder of this thesis I have not reported fluorescence changes at the AC soma.

AC processes are currently considered the most interesting area of inquiry regarding astrocytic calcium signalling, given their proximity to the synapse and the compartmentalization of their calcium responses (Di Castro et al. 2011). Here, I discuss the large processes imaged in the above results – smaller, synapse-ensheathing processes are too small to contain the endoplasmic reticulum required for internal calcium release upon dopamine stimulation. Unlike the AC soma, they show an effect of dopamine on cytosolic free Ca^{2+} – the fact that this is proportionally smaller than both the average fluorescence increase recorded in bulk-loaded cells (chapter 3) and in GJCs, suggests that there is a

residual effect of the nearby patch-pipette on the AC processes. The effect is not due to functional difference in process vs. soma calcium signalling: there is no significant or obvious difference between the calcium response in GJC somata and GJC processes (figure 4.1). Dopamine-induced calcium changes are reported relative to average baseline fluorescence so two, non-exclusive, explanations are possible: firstly, dialysis of the AC with the patch-pipette solution and washout of the existing intracellular milieu decreases the sensitivity of the AC to dopamine-induced calcium increase; secondly, the mechanical stimulation and dialysis of the AC with residual patch-pipette Ca^{2+} increases the baseline free calcium levels and spontaneous calcium dynamics. Thus, even if the same absolute concentration of calcium is reached upon dopamine stimulation, the relative increase from baseline will be reported as lower. Of the two, the second seems more likely: baseline spontaneous activity in AC processes was often observed to be higher than in GJCs (see example in figure 1**a**) and even than that observed in bulk loaded cells; this activity would increase the baseline average and is also indicative of a greater probability in intracellular CICR, itself increased by a higher resting free cytosolic calcium concentration. Whilst it is tempting to speculate that washout of small molecular components of the dopamine receptor-linked intracellular signalling cascade (e.g. cAMP, IP_3) decreases AC process sensitivity to dopamine, whilst sparing GJC somatic sensitivity, it has been shown that IP_3-mediated spontaneous activity is still present in patched astrocytes (Di Castro et al. 2011; Sun et al. 2014), arguing against a strong effect of washout on the intracellular signalling milieu.

Overall, the data from this initial result shows a startling effect of patch-clamping on the astrocytic dopamine response. Although the effect of dopamine is the subject of this thesis, the implications of this result are not limited to investigations of dopamine's effects on calcium. Whole-cell patch-clamping of astrocytes dramatically interferes with the nature of their intracellular calcium dynamics, a result which is supported by more data coming out

of our group (Zheng and Bard – personal communication). This is problematic as it is only the processes of patched astrocytes that can be imaged for calcium dynamics with sufficient spatiotemporal resolution. When studying the effect of long-lasting, global dopamine stimulation, as used in this chapter, it is possible to take calcium dynamics recorded from the soma as a general indication of the effects of stimulation. Highly localized events of a short time-period, for example synaptic stimulation and spontaneous activity (Henneberger et al. 2010; Di Castro et al. 2011; Panatier et al. 2011), that are only visible in astrocyte processes, are generally a result of more spatially and temporally precise stimuli – hence the viability of the 'astrocyte perforated-patch' as a recording method for this chapter. This method relies on the gap-junction coupling of astrocytes across the syncytium. These gap-junctions are pores, created by connexin proteins, which allow small molecules (~1.2kDa) across the astrocytic plasma membrane into neighouring astrocytes. Alexa594 molecules have a molecular weight of 820 Da and fluo-4 of 930 Da, allowing them to diffuse from the patched astrocyte into the surrounding astrocytes, allowing them to be imaged.

4.4.2 A novel astrocytic calcium decrease.

Perhaps the most surprising finding of this chapter is dopamine's ability to decrease astrocytic cytosolic free calcium concentration (Ca^{2+}-decrease) as well as increasing it (Ca^{2+}-increase) (figure 4.2). Such Ca^{2+}-decrease in response to dopamine is not unprecedented, but has not been discussed in detail in the literature. Khan et al. (2001) report Ca^{2+}-decrease upon stimulation of the D2R with quinpirole, in the presence of the D2R antagonist raclopride. This is a surprising result – given that quinpirole alone is reported to increase calcium – that Khan et al. explain via raclopride blockade of constitutive D2R pathway activity (although such constitutive activity has not been reported in the literature

and could also be explained by hetero/homomeric receptor expression – see section 4.3.6). Zhang et al. (2009) show example traces of Ca^{2+}-decrease in individual striatal astrocytes following stimulation with both SKF38393 and quinpirole – although they do not comment on it. Dopamine-induced Ca^{2+}-decrease is not reported by Vaarmann et al. (2010) or Requardt et al. (2012). Hence it is fair to say that this is the first detailed report of dopamine-induced Ca^{2+}-decrease in astrocytes – although this is not to say that the addition of dopamine is not simply interfering with underlying Ca^{2+} homeostasis, by blocking Ca^{2+} entry, or stimulating Ca^{2+} extrusion. In neurons, dopamine has been reported to decrease intracellular free calcium levels in snail neurons (Gerschenfeld et al. 1989), lactotrophs of the hypothalamus (Malgaroli et al. 1987) do so via decreased voltage-gated Ca^{2+} channel activity and cone-photoreceptors via D4 receptors (Ivanova et al. 2008). In the rodent prefrontal cortical neurons, D4Rs decrease NMDAR mediated calcium-currents (Wang et al. 2003). Astrocytes express VGCCs (Barres et al. 1989; D'Ascenzo et al. 2004; Burgos et al. 2007; Padmashri and Sikdar 2007) so it is possible that dopamine receptor activation could modulate resting calcium through interference with VGCC opening from spontaneous neuronal activity-induced local depolarization. In astrocytes, excepting the above results, the only report of inducible Ca^{2+}-decrease is from Shigetomi et al. 2011, who report that TRPA1 channels regulate astrocyte basal calcium, and that specific blockade of these channels decreases resting calcium levels. Very interestingly, in peripheral neurons, apomorphine – a non-selective dopamine receptor agonist with a slight preference toward D2-type receptor activiation – triggered concentration-dependent activation (low concentrations) or inhibition (higher concentrations) of the TRPA1 channel (Schulze et al. 2013) – although see (Aman et al. 2007). This novel site of potential dopamine action could be another explanation for the Ca^{2+}-decrease reported here from dopamine application.

Are Ca^{2+}-decrease and Ca^{2+}-increase inter-dependent? This can be resolved by answering two questions: are decreases always preceded by transient increases – i.e. are

they some kind of extended negative rebound? And do large increases only occur riding on small, obscured decreases? Calcium decreases almost always follow dopamine-induced increases – although this trend can be reversed with the application of the D1/5R blocker SCH23390, arguing against dopamine autoxidation as the cause (table 4.1): AC processes and GJC somata can exhibit dopamine-induced calcium decreases without concomitant increases, as can be seen in D1-type receptor blockers (figure 4.5) and in some 100µM recordings not shown in the single cell examples in figure 2. Given that the ratio of cells exhibiting a decrease before an increase can be shifted (though D1/5R blockade – it seems that Ca^{2+}-decrease is not solely a knock-on effect of a

Protocol	Figure data taken from	cell population	First DA-induced Ca^{2+} response direction	
			+	-
100µM DA	4.2	AC process	13	2
		GJC somata	7	0
50µM DA	4.3c	AC process	12	0
		GJC somata	4	0
20µM DA	4.3b	AC process	21	3
		GJC somata	9	2
100µM DA + 10µM SCH23390	4.5a	AC process	7	4
		GJC somata	1	7
100µM DA + 5 µM SCH23390	4.5b	AC process	14	6
		GJC somata	7	3

Table 4.1 Direction of first clear effect of dopamine on astrocytic Ca^{2+} in protocols where a Ca^{2+} decrease has been recorded

Table indicates the number of cells responding to dopamine either first with an increase (+) or a decrease (-) in either AC processes or GJC somata, which protocol was used to elicit the Ca^{2+} changes, and which figures the data are displayed in.

Ca^{2+}-increase. As the Ca^{2+}-decrease has slower kinetics and smaller amplitude than the Ca^{2+}-increases, is seems likely that a Ca^{2+}-increase often appears first because it more easily distinguished from baseline F/F_0, whereas a Ca^{2+}-decrease may have already begun but not be visible under these recording conditions. As discussed later, it is certainly possible to induce Ca^{2+}-increase without a visible Ca^{2+}-decrease – although given the small amplitude of Ca^{2+}-decrease, it may be present, but not sensed with the fluorescent indicators used. This possible lack of sensitivity is discussed below, but it could be remedied in future by the use of higher sensitivity dyes (e.g. OGB-1). The reason for continued use of Fluo-4 is that it provides the high dynamic range required to record all of the calcium increase.

The dopamine-induced Ca^{2+}-decrease is not always clearly visible, but can occur at any point after the initial addition of dopamine to the perfusion solution. It constitutes a far smaller relative shift in fluorescence intensity than the dopamine-induced Ca^{2+}-increase – but this could be because the recording configuration is set up to best record calcium increases (Fluo-4 has a high dynamic range, but lower sensitivity than OGB-1; the laser power for each recording is adjusted to make the resting fluo-4 fluorescence only very slightly greater than background). The kinetics of Ca^{2+}-decrease are very different from Ca^{2+}-increase – Ca^{2+}-decrease onset is very slow (minutes) compared to Ca^{2+}-increase, which has a sharp onset (1-2 seconds), whether it is the beginning of a sustained increase or many shorter transients. On the basis of these features the dopamine-induced Ca^{2+}-decrease can be classified as a change in the resting calcium concentration, whereas the Ca^{2+}-increase are more transient signals, riding on top of the baseline decrease. The fact that Ca^{2+}-decrease persists after the washout of dopamine and takes 10s of minutes to return to baseline indicates that it is working through a different, slower system to the Ca^{2+}-increase. This might be a concentration-dependent effect, stimulation by residual dopamine, post-

washout, of high-affinity receptors or other highly sensitive pathways – but this was not found to be the case when concentration effects were directly investigated (figure 4.3). Apart from the examples in figure 4.2a, b I have chosen not to analyse the fluorescence from the washout period with regard to dopamine-induced calcium decrease: this is because the potential interaction of both residual dopamine in the slice and longer lasting, previously stimulated, intracellular mechanisms affecting astrocytic calcium, make clear inferences as to the mechanism and function of Ca^{2+}-decrease hard to draw. It is important to note that Fluo-4 is highly pH sensitive – an increase in alkalinity of ~0.2 could account for the decrease in recorded fluorescence described here – however there are no reports in the literature of dopamine triggering such an increase in alkalinity.

Given the much larger $\Delta F/F_0$ value that Ca^{2+}-increase command over Ca^{2+}-decrease, and their stochastic nature, averaging the fluorescence data over time would eradicate any recorded decrease in fluorescence, even when they spend most of their time at decreased fluorescence (see figure 4. 5b and figure 4. 2a, c3 for a good example). Presenting the proportional frequency distribution of $\Delta F/F_0$ values gathered at both phases of dopamine application experiment (baseline vs. in the presence of dopamine) allows the pooling of all data points from all the recorded cells for each epoch, and visualization of all general shifts in $\Delta F/F_0$ caused by dopamine. The distributions of the decrease and the increase can be well modelled by the sum of two Gaussians – one with the peak x location below the mean, one with peak above – this implies the presence of two biological processes, one responsible for Ca^{2+}-decrease, one for Ca^{2+}-increase. In fact, this Gaussian analysis may slightly underestimate the amplitude of Ca^{2+}-decrease: the sampling area for the 'dopamine' epoch shown in all the histograms has an arbitrary start point (the beginning of the 3rd minute post addition of dopamine to the perfusion solution), which may not correspond perfectly to the beginning of the dopamine effect – hence each histogram will display some proportion of baseline $\Delta F/F_0$, which will slightly positively skew the peak of

the first Gaussian. The negative going 'shoulders' on each histogram in figure 2 indicated that there may in fact be an even greater negative-going component, not completely captured in these Gaussian fits.

4.4.3 Why does changing dopamine concentration affect the relative proportion of decreasing and increasing fluorescence?

To distinguish between stimulation of dopamine-induced decreases and increase, I gradually increased the concentration of applied dopamine (figure 4.3), starting at 10µM – which elicits neither an increase nor a decrease in fluorescence. Interestingly, 20µM dopamine has different effects on GJCs compared to AC processes: in GJCs, only F_i visible, but in AC processes both Ca^{2+}-increase and Ca^{2+}-decrease are apparent. This could be explained by two obvious differences between AC process recordings and GJC somata recordings: better signal to noise ratio from AC processes, and increased resting calcium in AC processes compared to GJC somata. Thus, with respect to a decreased signal to noise ratio, an overall reduction in both dopamine-induced calcium increase and decrease processes, from decreased dopamine stimulation, would lead to smaller $\Delta F/F_0$ for Ca^{2+}-increase and Ca^{2+}-decrease (see the average time course in figure 3b): given the higher concentration of dye in the AC processes and the better signal to noise ratio, the decrease might only visible here and not in the GJC somata. If initial resting calcium is the cause, it is possible that an increased resting cytosolic calcium concentration in the AC processes could potentiate dopamine's ability to decrease astrocytic calcium. An ideal experiment to test this would be to artificially increase the resting calcium in GJCs (by increasing external Ca^{2+} concentration, for example) and see if that mimics the dopamine-decreasing effect of 20µM dopamine in GJCs.

At 50µM, dopamine induces an even clearer decrease in AC processes (the Gaussian modelling decrease shifts from x peak 0.9 in 20µM to 0.86 in 50µM) and a decrease in GJCs (when modelled with a triple Gaussian, x peak of decrease is 0.77). This is consistent with a calcium decrease in GJCs at 20µM dopamine being present, but out of sensitivity range, especially as the observed decrease in AC processes is larger in 50µM than 20µM dopamine – but does not rule out a potentiation of the dopamine-induced decrease at higher intracellular resting calcium levels. At 100µM dopamine, both AC processes and GJC somata show populations of decreased fluorescence, but not to the same extent as at 50µM (first fitted Gaussian peaks are at 0.9 and 0.95 respectively) – indicating that, at higher concentrations, the dopamine-induced fluorescence increase begins to overwhelm the decrease.

A biphasic concentration-dependent response such as seen in these data is consistent with the biphasic activation of TRPA1 channels – activated at lower DAR agonist concentrations and antagonized at higher ones (Schulze et al. 2013). Another possible explanation is astrocytic D2-type receptor inhibition of baseline-activatied VGCCs. The concomitant calcium increase could be triggered by D2R-mediated IP_3 increase (Hernandez-Lopez et al. 2000) in conjunction with other DA-sensitive pathways (see below).

4.4.4 Pharmacological dissection of the calcium increase and decrease.

Interestingly, simultaneous blockade of mGluRs, $GABA_BRs$ and Na^+ channels during 100µM dopamine application blocks the calcium decrease but not the increase (consistent with the similar result in TTX alone from bulk-loaded slices – see chapter 3). This implies a dopaminergic activation of neuronal activity and a concomitant release of a glioactive substance that decreases astrocytic calcium. To date, there are no reports of mGluR or $GABA_BR$-mediated astrocytic calcium decreases in the literature, so the candidate substance

is likely to be released by dopamine-induced hippocampal neuronal activity itself. An intriguing possibility is that Ca^{2+} itself is the active extracellular signalling molecule: Torres et al. (2012) recently reported that increasing neuronal calcium dynamics (as dopamine has been reported to do – (Gulledge and Jaffe 2001; Lezcano and Bergson 2002) – decreases extracellular calcium concentration. This was reported to trigger astrocytic calcium increases via ATP release – a result that is consistent with the partial blockade of Ca^{2+}-increase by PPADS discussed below – but over an extended time-period could decrease astrocytic intracellular calcium through decreased calcium entry from the extracellular space and slow draining of the intracellular stores. The alternative is a dopamine-induced release of endocannabinoids, acetylcholine or serotonin (none of which have been reported in hippocampal slices) and their subsequent induction of a Ca^{2+} decrease. Neither of these phenomena have been reported – in fact, regarding the latter, the opposite has (Cai et al. 2000; Araque et al. 2002; Navarrete and Araque 2008).

In GJCs, blockade of P2 purinergic receptors eliminates the calcium decrease whilst sparing part of the calcium increase (there is a strong negative going peak in AC processes – but the sample size is small and more prone to random variation). Therefore ATP, either through tonic activation or through dopamine-induced release is responsible for part of the astrocytic calcium rise – a well-described phenomenon (McCarthy and Salm 1991; Koizumi et al. 2002; Fumagalli et al. 2003; Navarrete et al. 2013). ATP has been reported to stimulate dopamine release in the striatum (Zhang et al. 1995) raising the intriguing possibility of a positive feedback mechanism between local dopamine release and astrocytes via astrocytic release of ATP. More puzzling is the blockade Ca^{2+}-decrease by PPADS – calcium reduction through a direct action of P2 receptors would contradict the consensus in the literature that P2R activation invokes only calcium increases in astrocytes. It also argues against the involvement of TRPA1 channels in the calcium decrease – and there are no reports of PPADS affecting TRPA1 channels. The PPADS data do bear a striking

resemblance to those from 20μM dopamine application. P2Y receptors are Gq-coupled, operating through PLC activation (Pirotton et al. 1996), as do D2Rs (Hernandez-Lopez et al. 2000) and the PI-linked D1-like receptor (Hasbi et al. 2009); it is possible that PPADS depresses the activity of this D2R pathway through P2YR antagonism, thereby indirectly decreasing the effects of dopamine on astrocytic calcium: the reverse has been shown (dopamine receptor modulation of ATP-evoked calcium increase) in striatal neurons, indicating a functional link between the two receptor pathways (Rubini et al. 2008). This could push the dopamine-induced Ca^{2+}-decrease out of the recording sensitivity range (as discussed above) in GJCs, leaving a Ca^{2+}-increase visible – this would account for a Ca^{2+}-decrease visible in AC processes but not GJC somata. Another possibility is that PPADS, in blocking the P2YR, blocks tonic ATP-induced reactive oxygen species-generation in the recorded astrocytes (Kahlert et al. 2007), which blocks part of the calcium increase; this would be consistent with the partial inhibition of the calcium response seen in the presence of selegiline in bulk-loaded cells (chapter 3). PPADS has been reported to interfere with amphetamine-like psychostimulant administration-induced behaviour (Kittner et al. 2001) – as these drugs increase dopamine concentration in the brain, it may be that there exists a previously undocumented interaction between dopamine, dopamine-receptors and PPADS.

As with bulk-loaded slices, strong, simultaneous blockade of both D1 and D2-type receptors completely inihibits both the Ca^{2+}-decrease and Ca^{2+}-increase. As this includes the PPADS-insensitive portion of Ca^{2+}-increase (an increase also insensitive to neuronal blocker cocktail), it can be assumed that astrocytically localized dopamine receptors can trigger a calcium increase – as has been reported previously (Khan et al. 2001; Liu et al. 2009a; Requardt et al. 2012). Inhibition of Ca^{2+}-decrease by dopamine receptor blockers could be explained by the inhibition of neuronal calcium response to dopamine – stopping extracellular calcium decrease, the blockade of TRPA1 activation by non-selective action

dopamine receptor blockers (although this is yet to be reported in the literature) or by a previously unreported calcium-decreasing action of dopamine receptors.

4.4.5 How does stimulation of individual dopamine receptor types change the nature of the astrocytic calcium response?

Blockade of D1/5Rs alone inhibits dopamine-induced Ca^{2+}-increase – consistent with Requardt et al. (2012) and Liu et al. (2009) – but spares the Ca^{2+}-decrease (figure 5). This strongly implies not only a D1-mediated mechanism of calcium increase, but also separate mechanisms of calcium increase and decrease. Decreasing the concentration of SCH23390 used to block D1/5Rs increased the excitatory effect of dopamine, without affecting the scale of the fluorescence decrease from baseline (the rough x-co-ordinate of the peak) i.e. only changing the proportion of time spent at decreased baseline – consistent with the above hypothesis. From these data one would assume therefore, that Ca^{2+}-decrease is mediated by D2Rs – but the data from D2R blockade indicates a more complex picture.

Addition of the D2/3R blocker sulpiride to the bath (figure 6) has no direct effect on AC process cytosolic calcium or GJC somatic calcium at 50µM. However, at 20µM, it seems to trigger massive spontaneous calcium dynamics in AC processes, but not GJC somata. Sulpiride can block D2 inhibitory autoreceptors in the striatum (el Mestikawy et al. 1986), leading to increased dopaminergic tonus (Tanaka et al. 1996). Hence it is possible that this triggered calcium dynamics in astrocytes, which was visible only in the more sensitive AC processes – however the dopamine-induced Ca^{2+}-increase was entirely blocked by Sulpiride at both concentrations and in both GJC somata and AC processes (as the distribution of AC process activity in 20µM sulpiride and 100µM dopamine simultaneously was similar to that in 20µM sulpiride alone), implying that any effect of increased tonus would be blocked. The

blockade of both dopamine-induced calcium increase and decrease in GJC somata at both sulpiride concentrations might be considered the stronger evidence, given the sensitivity of AC process recordings to mechanical stimulation and cytosolic solution exchange from the patch-pipette. Examining only the data GJC recordings suggests that Ca^{2+}-decrease and Ca^{2+}-increase are both under the control of D2-type receptors, whereas Ca^{2+}-increase is under the control of D1/5Rs. There is evidence for this function of D2-type receptors in the literature: the non-selective dopaminergic receptor agonist apomorphine can decrease calcium in chromaffin cells through PLC (a recognized downstream signalling molecule of D2/3Rs) inhibition and calcium entry into the cell (Sontag et al. 1990); D2/3 receptor activation has been shown to decrease calcium dynamics through modulation of L-type VGCCs in rat Nucleus Accumbens neurons (Perez et al. 2011), rat and frog pituitary melanotropes (Desrues et al. 1993; Fass et al. 1999) and neuroblastoma cells(Vallar et al. 1990; Brown and Seabrook 1995). The consensus from this literature is that D2/3R-mediated calcium decrease operates through inhibition of VGCC activity – as astrocytes are known to express functional VGCCs (Barres et al. 1989; D'Ascenzo et al. 2004; Burgos et al. 2007; Padmashri and Sikdar 2007), this could well be the mechanism of dopamine-induced calcium decrease. Interestingly, the level of oxidative stress in cultured neurons has been found to control the effect of dopamine on calcium levels, with higher oxidative stress (such as may be found in the presence of high concentrations of dopamine – see Vaarmann et al. 2010) – which could trigger D2/3R-dependent inhibition of local VGCC opening (Steullet et al. 2008), although higher oxidative stress also triggers TRP channel opening (Kim and Hwang 2013). Given dopamine receptor blockers' ability to completely eradicate the astrocytic calcium response, the actions of selegiline as a partial blocker of the calcium increase seen in chapter 3 have not been investigated further here.

Very interestingly, specific co-stimulation of both D1 and D2 dopamine receptors with the D1 agonist SKF83983 and the D2 agonist quinpirole triggers both a slight Ca^{2+}

increase and decrease, only visible in the astrocytic processes. One possibility to explain this, in conjunction with the finding that large astrocyte Ca^{2+} dynamics are SCH23390-sensitive (figure 4.5), is that astrocytes preferentially express D5 receptors – astrocytes have been found to express D5Rs in culture (Brito et al. 2004) – and these are partially activated by SKF38393. Another, more intriguing, possibility is that activation of dopamine receptors alone is necessary but not sufficient to trigger the magnitude of the dopamine responses seen upon stimulation with dopamine itself – it requires non-receptor signalling as well. This is consistent with MAOb blockade-induced inhibition seen in chapter 3 – it is possible that, while D1/2 activation provides a calcium 'spark', the IP_3 generated by MAO activity (through PLC activation) amplifies the Ca^{2+} released from intracellular stores. This idea of a dopamine receptor mediated calcium 'spark' is also consistent with only seeing dopamine receptor agonist activity in the AC processes – it is possible that dopamine receptor-mediated signalling is spatially localized, whilst MAOb-mediated large-amplitude Ca^{2+} signalling is a more synchronous whole-cell Ca^{2+} discharge (Rusakov et al. 2014).

The Ca^{2+} response seen upon dual dopamine receptor agonist stimulation is consistent with both a solely D1-type receptor mediated dopamine-induced calcium increase, and a heteromeric D1/D2 receptor activation (Hasbi et al. 2010). However more results seem to rule out a large, solely D2R mediated response (although D3 and D4 activation is still a possible route) – as discussed below.

I have found that astrocytic stimulation with the specific D2 dopamine receptor agonist quinpirole does not change astrocytic calcium levels from their baseline (figure 4.7) – unlike the results reported from Khan et al. (2001). This could be due to stimulation of hippocampal astrocytes in this study as opposed to PFC astrocytes in theirs, or due to the nature of the culture conditions. I used the same concentration of quinpirole as was used in their study (150μM) however it is difficult to know what the necessary concentration

required to stimulate astrocytes *in situ* is, given that I have no positive control. Hence it may be that there was an astrocytic effect but I could not pick it up – given the small nature of the original reported effect (a 10s increase of 20% ΔF/F) in low noise culture recording conditions, this is a definite possibility.

4.4.6 A putative model of astrocytic dopaminergic signalling

The fact that both D1-type and D2-type receptor blockers can separately inhibit the dopamine-induced calcium increase suggests the presence of a D1-D2 or D2-D5 heteromer (Hasbi et al. 2010; Hasbi et al. 2011) activation of which leads to calcium increase, but which can be inhibited through blockade of either subunit. There is evidence for these types of receptor in HEK cells (Lee et al. 2004; Rashid et al. 2007) and striatal neurons (Verma et al. 2010). Simultaneous blockade of both D1 and D2-type receptors has also been found to be necessary to block dopaminergic modulation of ATP-evoked calcium increase in striatal neurons (Rubini et al. 2008). This is consistent with the reported inhibition of calcium signal through D1R blockade reported by Requardt et al. (2012). Co-expression of both D1-D2, or D2-D5 receptor heteromers and D2R homomers – or differential activation of the dopamine heteromer (Hasbi et al. 2010) – could account for the dopamine-induced calcium increases and decreases (through VGCC inhibition) reported in this chapter, although part of the reported calcium decrease may be due to TRPA1 activation, changes in external calcium through neuronal activity and ATP signalling. An excellent further experiment would be to test for a dopamine-induced Ca^{2+} decrease in the presence of TRPA1 receptor blockers – occlusion of the Ca^{2+} decrease would strongly suggest that it was TRPA1 mediated.

How does this fit with the selegiline-induced amplification of the Ca^{2+} increase seen in chapter 3? Requardt et al. (2012) suggest that D1R activation increases the ratio of NADH

to NAD^+ in astrocytes, changing the redox state of the cell (as does MAOb-mediated ROS production) and increasing the likelihood of Ca^{2+} transients through IP_3R signalling (Raturi et al. 2013). D2-type receptors also increase intracellular IP_3 (Hernandez-Lopez et al. 2000), but not through changing the redox state of the cell. Hence, another possible explanation of the receptor-sensitivity of this response is that blockade of D1-type receptors could decrease the IP_3 concentration in the cell (as does MAOb blockade) through a shift in the redox state (Raturi et al. 2013), thus decreasing the probability of a Ca^{2+} increase but not a Ca^{2+} decrease. However blockade of D2-type receptors could both inhibit TRPA1-mediated Ca^{2+} decrease and Ca^{2+} increase through inhibition of IP_3 production.

Another possibility is on off-target effect of dopamine (not directly on astrocytic D1/2 type receptors) triggering a complex metabolic change within the astrocytic syncytium, leading to the observed calcium decrease. Simultaneous direct astrocytic dopamine receptor activation could account for the two observed calcium signals. Whilst such a complex metabolic effect could be difficult to unravel, the experiments listed in the discussion above would test more thoroughly if the calcium decrease is indeed through a direct effect on astrocytes. Additionally, it would be informative to assay the astrocytic response to dopamine during the blockade of the homeostatic calcium machinery (e.g. SERCA pumps) – and even in the presence of 0mM extracellular Ca^{2+} bath solution – to ascertain whether the calcium decrease is due to an interference with homeostatic processes.

4.4.7 Physiological relevance of an astrocyte calcium decrease

Shigetomi et al. (2011) report that astrocyte resting calcium decrease through TRPA1 activation, or through buffering of internal calcium with BAPTA, decreases interneuronal miniature IPSC (mIPSC) amplitude via an increase in extracellular GABA

concentration. Dopamine has been reported to have similar inhibitory effects on interneuron activity (Gribkoff and Ashe 1984; Swant et al. 2008; Tierney et al. 2008; Paul and Cox 2013), hence astrocytic modulation of GABAergic inhibition could be another route of dopamine function in the hippocampus.

4.5 Conclusion

As in chapter 3, dopamine was found to increase astrocytic intracellular free calcium through D1/D2 receptor stimulation – although here measured in a novel 'astrocyte perforated-patch' configuration. A previously unreported effect of dopamine was also reported in the slice preparation: a decrease in astrocytic calcium through D2 receptor activation, in a neuronal activity-dependant fashion. The exact mechanism of this decrease remains unclear.

Chapter 5: Results 3

Astrocytic calcium dynamics play only a small role in dopaminergic modulation of synaptic communication in the Stratum Lacunosum-Moleculare.

5.1 Introduction

Dopamine has a strong inhibitory effect on baseline excitatory transmission in Stratum Lacunosum-Moleculare (SLM), mediated by D1/2Rs and working, at least partially, through decrease of pre-synaptic release probability (Otmakhova and Lisman 1998). Given that this inhibition is D1/2R mediated, as are the dopamine-induced astrocyte calcium transients reported in chapters 3 and 4, and astrocyte calcium transients have been proposed to modulate neuronal activity (Perea and Araque 2007; Henneberger et al. 2010), I investigated the possibility that dopamine-induced astrocytic calcium transients were responsible for the dopamine-induced inhibition of SLM synapses. Similarly, dopamine has been implicated in post-tetanic potentiation (PTP) induction (Young and Yang 2005) – a form of short term potentiation that has been found at the perforant path-CA1 synapse (Colbert and Levy 1993; Leao et al. 2012) – so I investigated the involvement of astrocytes in a dopaminergic modulation of SLM PTP.

5.2 Methods

Transverse hippocampal slices were taken from p21-25 male Sprague-Dawley rats. All experiments were conducted at 32°C. Astrocytes from the Stratum Lacunosum-Moleculare (SLM) region of CA1 were identified under DIC and patched-clamped (figure 1a-c). For 'calcium-clamp' experiments (Henneberger et al. 2010), cells were held in cell attach

mode for the indicated time before break-in. The patched cell (PC) processes and nearby gap-junction coupled cell (GJC) somata were imaged with a 2P-setup at an excitation laser power of 2-5mW, at a frame rate of 1Hz. Emitted light was collected in two channels: 515-560nm (peak Fluo-4 emission wavelength = 515nm) and 590-650nm (peak Alexa594 emission wavelength = 618nm). Fluorescence intensity for each cell, per frame, is calculated as the average fluorescence of all pixels in a manually defined region of interest (ROI). Fluorescence data is from GJCs (see results chapter 2). G/R intensity is normalized to baseline, to give a time course of cytosolic calcium dynamics ($\Delta F/F_0$) from ROIs. Cells with unstable resting calcium in the baseline condition – i.e. fluctuations unlike normally observed calcium transients (Parri et al. 2001; Aguado et al. 2002) or a constantly rising baseline – were discarded. Cells with no DA washout were discarded.

To record fEPSPs from perforant path (pp)-CA1 synapses, a recording pipette was placed in SLM of CA1 and a monopolar stimulating electrode in pp, closer to subiculum. Stimulus strength was adjusted to give 50-60% of maximal fEPSP amplitude and recordings were made at 0.067Hz (every 15s). Astrocytic fEPSPs (afEPSPs) can be recorded from the astrocyte patch pipette, and they provide an accurate readout of the local fEPSP (Henneberger et al. 2010) – although peak afEPSP amplitude has to be computed from subtracting afEPSP peak from the following upwards deflection of the voltage trace. Simultaneous afEPSP and fEPSP (from a locally positioned recording pipette) were made during 'calcium-clamp' experiments (figure 5.2c). Theta-burst-stimulation (TBS) consisted of 8 stimuli at 100Hz delivered twice at 5Hz.

The fluorescence data presented in this chapter are all from GJC somata, averagered over the total number of cells and for each experimental minute – error bars show the standard error. For the purposes of statistical analysis of imaging experiments, *n* was taken to be the total number of GJCs sampled, although total number of slices and

animals are also given. For electrophysiology data, *n* is the number of slices, although animal numbers are also given. To compare two normally distributed data populations, a two sample t-test was used.

5.3 Results

5.3.1 Unlike astrocytes from stratum radiatum, stratum lacunosm-moleculare astrocytes do not show a visible calcium response to 20µM bath-applied dopamine.

Are astrocytes throughout CA1 homogeneous in their response to dopamine? Interestingly, they do not seem to be: 20µM bath-applied dopamine does not significantly

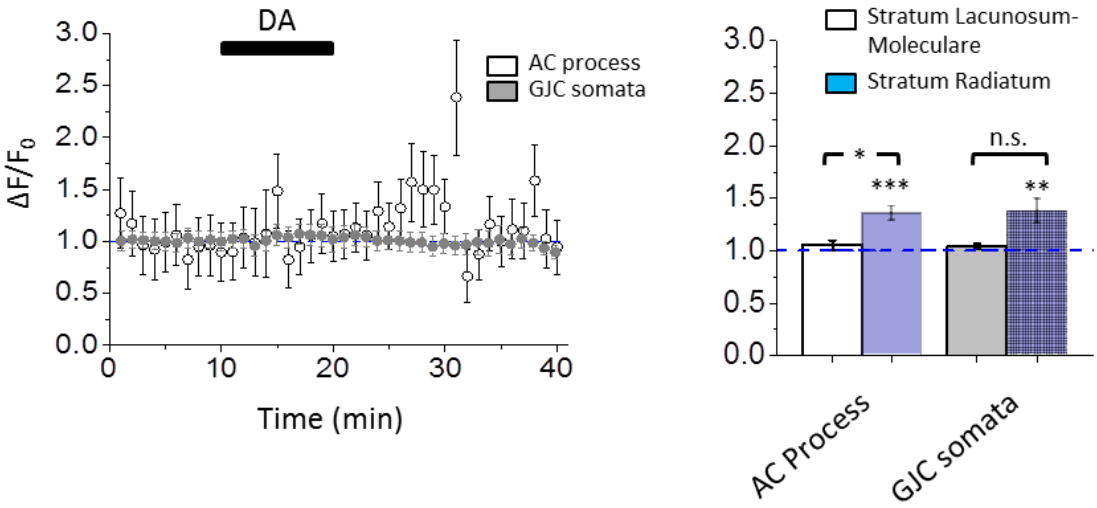

Figure 5.1 Unlike in stratum radiatum, 20uM Dopamine does not evoke astrocytic calcium transients in stratum lacunosum-moleculare

a) Time courses of astrocytic AC process (hollow circles) and GJC somata (grey circles) calcium changes in response to 20µM dopamine (black bar). **b**) Summary bar graphs showing average response in stratum lacunosm-moleculare astrocytes (white and grey) compared to stratum radiatum astrocytes (blue and blue cross-hatched) in both GJC somata (white and blue) and AC

processes (grey and blue cross-hatched). n.s. – not significant, ** - p<0.05, ** - p<0.01, *** p<0.001, t-test (1), Wilcoxon signed rank test, 2-sample t-test or Mann-Whitney test (see text).

---

change $\Delta F/F_0$ in either AC processes (p=0.29, 1-sample t-test, n=6; data from 6 processes, 2 slices, 2 animals) or GJC somata (p=0.232, 1-sample Wilcoxon signed rank test, n=10; not normally distributed, p=0.029, Shapiro-Wilk test; data from 12 cells, 4 slices, 4 animals) of the stratum lacunosum-moleculare (SLM) – see figure 5.1. $\Delta F/F_0$ of SLM AC processes is significantly less than SR AC processes (p=0.041, 2-sample t-test; SR data from figure 4.3), similarly the difference $\Delta F/F_0$ of SLM GJC somata from SR GJC somata approaches significance (p=0.052, Mann-Whitney test; SR data taken from figure 4.3)

5.3.2 Ca^{2+}-clamp blocks the dopamine-induced Ca^{2+}-decrease, but not the increase.

Ca^{2+}-clamping of astrocytic intracellular milieu has been used to block astrocyte-dependent processes (Henneberger et al. 2010); in order to inhibit astrocytic Ca^{2+}-dynamics directly I will use this method later in the chapter. But first I tested whether it can block dopamine-induced astrocyte Ca^{2+}-dynamics. Astrocyte Ca^{2+}-clamp does not block dopamine-induced Ca^{2+} increases, but it does block dopamine-evoked decreases. Thus, use of the Ca^{2+}-clamp can be used to test whether a dopamine-induced astrocytic Ca^{2+} decrease is necessary for a given electrophysiological effect. In section 5.3, although 20µM dopamine does not trigger Ca^{2+} increases, any Ca^{2+} decreases (not visible in this configuration) would be blocked. Although calcium dynamics were not imaged during the Ca^{2+}-clamp data in figure 5.3, this control experiment is displayed here (figure 2.4). In AC processes (data from 25 processes; 3 slices, 3 animals), baseline can be fitted with a single Gaussian (x peak=0.98,

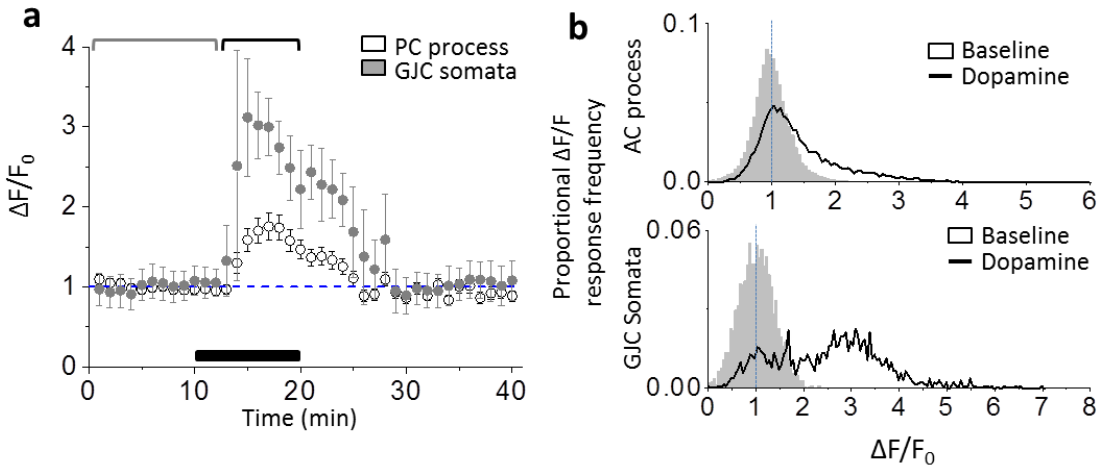

Figure 5.2 **Calcium-clamp solution in astrocytes blocks dopamine-induced calcium decreases but not increases in stratum radiatum astrocytes.**

a) time courses of astrocytic PC process (hollow circles) and GJC somata (grey circles) calcium changes in response to 20μM dopamine (black bar) whilst patched with a calcium-clamp solution; grey bracket indicates region sampled for 'baseline' in b), black bracket indicates region sampled for 'dopamine'. **b**) histogram of $\Delta F/F_0$ responses in baseline (t=1-12, grey bars) and dopamine (t=13-20, black line) conditions, for AC processes (upper right panel) and GJC somata (lower right panel).

FWHM=0.93, R^2=0.92), but requires two (x peaks=1.07/1.74, σ=0.27/0.7, FWHM=0.68/1.66, R^2=0.99) – see figure S1. GJCs were not analysed as they were beyond the distance that could be affected by the Ca^{2+}-clamp. This methodological finding is discussed further in the general discussion. σ=0.24, FWHM=0.6, R^2=0.99), dopamine cannot be well fitted with a single Gaussian (x peak=1.16, σ=0.39,

5.3.3 Dopaminergic inhibition of the perforant path-stratum lacunosum-moleculare synapse is unaffected by local clamp of astrocytic intracellular calcium.

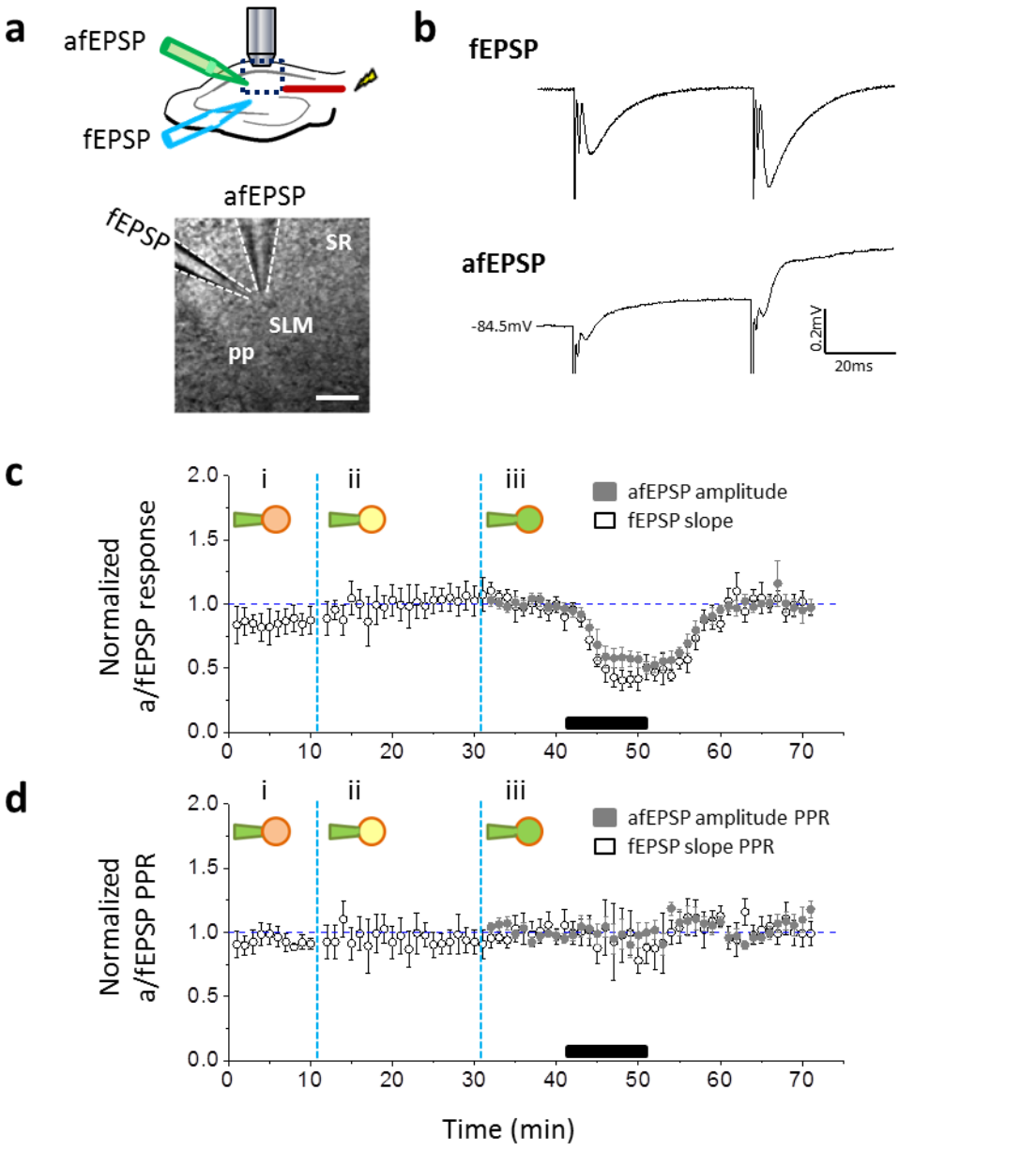

Figure 5.3 Dopaminergic inhibition of perforant path fEPSPs persists with astrocyte calcium dynamics clamped.

a) Recording configuration: above, relative positions of patch pipette (green), field electrode (blue) and stimulating electrode (red) in the hippocampal slice; below, DIC image of patch and recording pipettes, pp – perforant path, SLM – stratum lacunosum-moleculare, SR – stratum radiatum, scale bar – 50µm. **b**) example of simultaneous fEPSP (above) and afEPSP (below) recordings (averaged over 80 traces). **c**) Time course of normalized fEPSP slope (hollow circles) and normalized afEPSP peak (grey circles) for cell attach (i), whole cell equilibrating (ii) and whole cell recording (iii) followed by dopamine (20µM) application (black bar). **d**) paired-pulse ratios (50ms interval) for recordings shown in **c**).

Now, I tried to inhibit dopamine-dependent synaptic inhibition in the stratum lacunosum-moleculare (Otmakhova and Lisman 1999) with the astrocyte Ca^{2+}-clamp. The protocol for the Ca^{2+}-clamp experiment was as follows: astrocyte fEPSPs (afEPSPs) and nearby fEPSPs were simultaneously recorded (figure 5.2a, b); for the first 10 minutes, astrocytes were held in cell-attach mode; then whole-cell mode was achieved and the cell allowed to fill for 20 minutes; finally 10 minutes baseline (t=32-41) was recorded, followed by 10 minutes dopamine (20µM) application (t=42-51) and then 20 minutes washout (t=52-71). Baseline was taken as the period 10 minutes before dopamine application. There was no significant difference from baseline of fEPSP slopes in cell-attach mode (t=6-10) (p=0.316, 1-sample t-test, n=3). The inhbitory effect of DA at t=47-51 was clear (figure 5.2c): a decrease of fEPSP slope to 0.44 ± 0.05 of baseline (p=0.001, 1-sample t-test, n=4). The afEPSP showed a similar DA induced decrease (figure 5.2c), 0.56 ± 0.07 baseline (p=0.03, 1-sample t-test, n = 3). The fEPSP PPR (figure 5.2d) does not change significantly upon cell dialysis (p=0.077, 1-sample t-test, n = 3), nor upon DA application (p=0.253, 1-sample t-test, n = 4). This is consistent with the afEPSP recordings (figure 5.2d) – they show no significant PPR difference from baseline (p=0.461, 1-sample t-test, n = 3).

5.3.4 Dopamine inhibits PTP in the stratum lacunosum-moleculare.

Astrocytes are not necessary for dopaminergic inhibition of baseline fEPSPs in SLM – could they be involved in short-term plasticity? First I looked to establish an effect of dopamine on short-term plasticity. In the presence of 50µM picrotoxin (PTX), a short theta-burst stimulus (TBS) induces post-tetanic potentiation (PTP) – as shown in the example in figure 5.4a and the averaged data in figure 5.4b. Recording rate is 0.067Hz, starting at 5 seconds post-TBS. There is an interaction between control and dopamine peak amplitudes (figure 5.4**i**, upper panel) (2-way repeated measures ANOVA, F(19,171) = 2.01, p=0.01, table

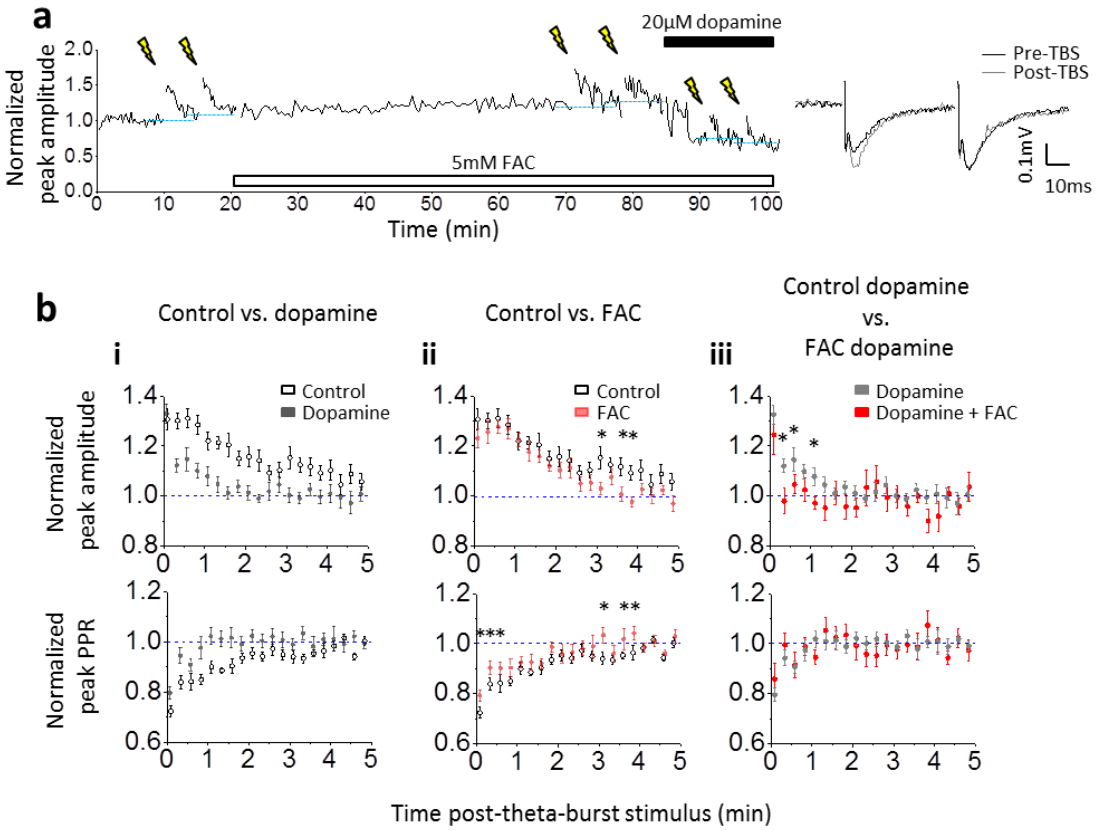

Figure 5.4 Inhibition of post-tetanic potentiation in the Stratum Lacunosum-moleculare by dopamine is enhanced after inhibition of glial Krebs' cycle with fluoroacetate.

a) Left: example experiment – peak fEPSP amplitude sampled every 15s – showing effect of dopamine (black bar) on PTP induction in fluoroacetate (FAC – hollow bar), lightning bolts indicate theta-burst stimulus (TBS), blue dashed lines indicate baselines taken for normalization of each PTP. Right: example fEPSPs recorded before (black trace) and 5s after (grey trace) TBS. **b**) **i**) Time course of PTP following TBS in 20μM dopamine (grey circles) normalized to control (hollow circles). Above: Peak amplitudes normalized to average peak amplitude of previous minute. Below: time course of paired-pulse ratio ($2^{nd}/1^{st}$ amplitude peaks) following TBS. **ii**) Time course of PTP after 50 minutes in control conditions (hollow circles) and after 50 mins FAC incubation (pink circles). Layout: as in **i**). **iii**) effect of dopamine on PTP in control (grey circles) and FAC pre-incubation conditions (red circles). Layout: as in **i**); statistics compare dopamine and FAC+dopamine data sets, * = $p < 0.05$, Fisher's test – see text.

S1) and it is clear from figure 5.4b that the control data are more greatly potentiated than the dopamine data. Comparing individual time points between the two conditions using fisher's test, all points were significantly different ($p<0.05$) except at 5, 155, 170, 215, 245, 260 and 290 seconds (see figure 5 S1). PPR changes post-TBS (figure 5.4**i**, lower panel) also interacted (2-way repeated measures ANOVA, $F(19,171) = 1.74$, $p=0.034$, table 5 S2), with smaller PPR. From 125s onwards, only 215s and 275s were significantly lower in control than dopamine; data taken from 10 stimuli, 5 slices, 5 animals. changes in visible in dopamine. At all time-points up to and including 110s – apart from 35s – dopamine PPR was significantly less than control using fisher's test, at the $p<0.05$ level.

5.3.5 Astrocytes are not required for PTP but partially alleviate dopaminergic inhibition of PTP.

Finally: are astrocytes involved in this dopaminergic modulation of PTP? Pre-incubation with 5mM of the glial poison fluoroacetate (FAC) does not significantly affect the TBS-induced PTP amplitude (figure 5.4i) (2-way repeated measures ANOVA, $F(19,133) = 0.753$, $p=0.758$, table S3) – only three time points are significantly different at $p<0.05$, using fisher's test: 185s, 215s and 230s (see figure 5 S3). However, although there is no significant interaction between the PPRs (2-way repeated measures ANOVA, $F(19,133) = 0.864$, $p=0.628$, table S4), when examining individual time points the difference in PPR reaches $p<0.05$ significance (using fisher's test) for the first three recordings, i.e. 5s, 20s and 35s – as well as at 185s, 215s and 230s.

Dopaminergic inhibition of TBS-induced PTP amplitude persists in FAC and there is no significant interaction between dopaminergic inhibition in FAC pretreated slices and inhibition observed under control conditions (2-way repeated measures ANOVA, $F(19,133) = 1.14$, $p=0.138$, table S5) – however upon individual comparison with Fisher's test, at the

$p<0.05$ level, amplitudes following TBS in dopamine at 20s, 35s, and 65s are significantly lower in FAC pre-treated slices. Regarding PPR, there is no interaction between FAC-pretreated and control slices in dopamine (2-way repeated measures ANOVA, $F(19,133) = 0.642$, $p=0.868$, table S6), nor do any of the individual time points show a significant difference at the $p<0.05$ level when tested with Fisher's test. Control data taken from 10 stimuli, 5 slices, 5 animals, Dopamine data taken from 8 stimuli, 4 slices, 4 animals.

5.4 Discussion

5.4.1 Heterogeneity in the astrocytic response to dopamine – distinct subpopulations.

Unlike the calcium responses recorded from astrocytes in stratum radiatum (S.R.) (chapter 4), there is no cytosolic calcium increase in stratum lacunosum-moleculare (SLM) astrocyte GJCs from 20µM dopamine stimulation. Given that SLM astrocytes can respond to dopamine (figure 5.3), this may indicate a sensitivity difference to dopamine between astrocytes from different hippocampal strata. Morphological differences between S.R. and SLM astrocytes have been reported before, SLM astrocytes occupying smaller synaptic territories (Ogata and Kosaka 2002). Similarly astrocytic K^+ buffering in SLM has been reported to be more gap-junction dependent than in S.R. (Wallraff et al. 2006; Hewett 2009). Subpopulations of hippocampal astrocytes have also been reported in their expression of GFAP and NPY (St-Pierre et al. 2000) and RNA expression (Yeh et al. 2009). Cortical astrocytes display population-specific volume changes (Benesova et al. 2009) and also subpopulations that are responsive to Sonic Hedgehog (Garcia et al. 2010).

Very interestingly, (Reuss et al. 2000) describe a subpopulation of cortical astrocytes, functionally distinct in that they respond to D1R stimulation with calcium

transients – and they show that incubation with FGF-2 increases the proportion of these cells. FGF-2 is present in the hippocampus (Ernfors et al. 1990; Zechel et al. 2010), involved in memory formation (Preissler et al. 2007), is known to modulate astrocytic response to different ligands (Song and Ghosh 2004) and has been found to be modulated by the dopaminergic system in rat hippocampus and prefrontal cortex (Turner et al. 2008; Giannotti et al. 2013) A decreasing gradient of FGF-2 expression from SR to SLM could be responsible for this observed change in astrocyte sensitivity to dopamine – but such a gradient has yet to be reported. It is also intriguing that this astrocytic sensitivity difference occurs between two CA1 strata with such different functional responses to dopamine: whereas dopamine is strongly inhibitory at SLM synapses (Otmakhova and Lisman 1998) – suggested to gate information flow from the entorhinal cortex – in the SR it is far less inhibitory (Otmakhova and Lisman 1998) and promotes synaptic l-LTP formation (Frey et al. 1989; Matthies et al. 1997; Kwon et al. 2008). As astrocytes are necessary for e-LTP formation (Henneberger et al. 2010), this increased SR sensitivity could well suggest a role for astrocytes in the functional division of dopamine action across CA1.

5.4.2 Astrocytes are not involved in dopaminergic inhibition of the perforant path-stratum lacunosum-moleculare synapse.

Although no calcium responses were recorded at 20µM dopamine in SLM astrocytes, one cannot be sure of the calcium dynamics in the fine, synapse-enwrapping, processes. Hence, I 'clamped' the calcium through intracellular dialysis of both Ca^{2+} and calcium buffers in order to deactivate astrocyte-calcium mediated processes at nearby synapses – a technique that has been shown to work for LTP induction in stratum radiatum astrocytes (Henneberger et al. 2010). This has no clear effect on the inhibitory action of dopamine (figure 5.2), as reported by Otmakhova and Lisman (1998) – whereas they report

a decrease to 60% of synaptic strength in dopamine, I observe a decrease to 45 ± 5%. However, Otmakhova and Lisman (1998) also report high variability in the strength of the inhibition and it seems likely that, with the relatively small sample size in my experiments, the inhibitory effect I see is comparable to theirs. Ideally, now that I have shown that afEPSPs are an accurate measure of the fEPSP changes due to dopamine, I would repeat these experiments with the fEPSP electrode over 200µM away. At this distance the calcium clamp no longer has traction – at least over LTP induction (Henneberger et al. 2010). Here I would record non astrocyte calcium-clamped synaptic responses to verify. This would identify the presence of any small contributory action of astrocytic on this dopaminergic inhibition. This experiment does not rule out dopamine affecting synaptic inhibition through non-calcium mediated astrocyte pathways. The calcium-clamp protocol was tested for its effectiveness in chapter 2: it was found that it inhibited dopamine-induced calcium decreases but not increases. Hence it is possible that the dopamine induced inhibition is still due to astrocyte invoked calcium increases, but the massive change in calcium conditions within the cell should have had some effect on the inhibition if they were important for it.

5.4.3 Dopaminergic inhibition of post-tetanic potentiation.

As discussed in chapter 1, potentiation at the perforant path-SLM synapse is controversial in the literature, having been reported as possible only under GABAR blockade by Colbert and Levy (1993), but possible under normal conditions by Leao et al. (2012). I could only induce very short potentiation under strong repetitive TBS (data not shown), but in the GABAR blocker picrotoxin, it was possible to induced both PTP and LTP. In fact, many of the recordings were discarded because long-lasting potentiation was induced (fEPSP amplitude did not return to baseline after 5 minutes), hence only a weak

version of TBS was used to induce PTP (figure 5.4). This PTP had a strong presynaptic component, demonstrated by the PPR change, similar to other reported short term-potentiation (Zucker and Regehr 2002). Consistent with dopamine's inhibitory, presynaptic effect on baseline transmission (Otmakhova and Lisman 1998), it inhibited the amplitude (post 5s) and duration of PTP induction through (at least partial) inhibition of the presynaptic component – as witnessed by the inhibition of the PTP evoked PPR decrease. This all fits with an overall inhibitory function for dopamine at this synapse.

5.4.4 What role do astrocytes play in both control and dopamine-modulated PTP?

Inhibition of the astrocytic Krebs cycle with fluoroacetate (FAC) does not change the relative amplitude of TBS evoked PTP (although the responses tend to be non-significantly smaller) but it marginally increases the duration of the PTP by ~1 minute (figure 5.4bii). Interestingly, there is a clear difference in PPR change evoked by TBS – a PPR significantly closer to baseline for the first three recordings (5s, 20s and 35s). It appears that astrocytes secrete a presynaptically active excitatory signalling molecule upon TBS (Agulhon et al. 2008), release of which could be triggered through extracellular K^+ build-up and subsequent astrocytic cAMP increase (Choi et al. 2012). Another possibility is that FAC is interfering with astrocyte K^+ conductance (Largo et al. 1997) and hence with short-term potentiation (Sibille et al. 2014). If the effect is due to gliotransmission, the signalling molecules released could include glutamate (Fiacco and McCarthy 2004; Perea and Araque 2007) or ATP, acting on presynaptic A2 receptors after extracellular breakdown to adenosine, as previously reported by Panatier et al. (2011); this would explain a FAC-induced inhibition of the TBS-induced PPR decrease. Astrocytic calcium has been reported to be necessary for short-term plasticity at the Schaffer collateral synapse (Andersson and

Hanse 2010) – but this was short-term depression – and astrocyte control of both short-term facilitation and depression has been postulated (De Pitta et al. 2011). A decrease in presynaptic release probability would predict a smaller amplitude response to TBS – but I did not observe this; a possible explanation is compromised astrocytic glutamate buffering in the synaptic cleft from FAC poisoning, this would increase the amplitude of the post-synaptic response, potentially obscuring the decrease in amplitude from decreased presynaptic release.

Addition of dopamine to FAC-incubated slices completely inhibits PTP past 5s, remaining smaller than PTP in dopamine from control slices for ~1min (at 20s, 35s, and 65s). However there is not the significant inhibition of the PPR decrease that we would expect from FAC-incubated slices compared to control. The PPR result is perhaps unsurprising, as dopamine in control conditions has such a strong inhibitory effect on post-TBS PPR decrease that it may completely obscure any further significant PPR shift (for example, the normalized PPR at 20s is at 1 for FAC slices already). The further depression of the PTP by dopamine in FAC pre-treated slices is the most exciting result: it suggests that, upon TBS in the presence of dopamine, astrocytes release an excitatory neuroactive compound that moderates the inhibitory effect of dopamine – possibly an increase release of the presynaptically active molecule postulated above – an effect not present in FAC pre-treated slices.

A methodological caveat to this result is the function of FAC: although in this chapter it is assumed that FAC has disrupted astrocytic function and normal Ca^{2+} dynamics, it is important to note that this disruption is not complete. FAC inhibits the Krebs' cycle by binding to coenzyme A, which reacts with citrate synthase to produce fluorocitrate which inhibits aconitase function and therefore aerobic respiration. However, astrocytes could

still respire anaerobically and there is no data to suggest whether, in this state, they could still respond with similar calcium changes to dopamine.

Although astrocytes are clearly not involved in dopaminergic modulation of baseline synaptic transmission – they are in transient synaptic potentiation. Is this phenomenon dependent on astrocytic calcium? Although no calcium responses are seen in SLM astrocytes in response to the 20µM dopamine used throughout this chapter, it may be that only synergistic stimulation with both synaptically released glutamate and bath applied dopamine triggers visible astrocytic calcium responses in this astrocyte population – this would be a fruitful area for further study. It has been reported that SLM synaptic inputs at theta frequency, when coupled with Schaffer-Collateral stimulation (preceding by half a theta-cycle), can preferentially stimulate the pyramidal cell soma (Ang et al. 2005): this presents another potential area for astrocytic involvement and would certainly be worth investigating.

5.5 Conclusion

Astrocytes of the stratum lacunosum-moleculare form a functionally distinct subset, in regard to their response to dopamine, in comparison to astrocytes of the stratum radiatum – they display decreased dopamine sensitivity. Although stratum lacunosum-moleculare astrocytes do not mediate the established dopaminergic inhibition of the perforant path input to CA1, their health is necessary to achieve the full degree of potentiation when post-tetanic potentiation is induced at this synapse.

Chapter 6: Results 4

Astrocytes are not necessary for either dopaminergic modulation of baseline transmission or post-tetanic potentiation in stratum radiatum.

6.1 Introduction

Dopamine is now recognized as an important neuromodulator in Stratum Radiatum (SR) of the hippocampus – it can moderately inhibit basal transmission (Otmakhova and Lisman 1998) and is necessary for l-LTP induction (Matthies et al. 1997) and also for spatial memory formation (Li et al. 2003). Dopamine has been reported to modulated cortical PTP in an input frequency-specific manner (Young and Yang 2005) and may be involved with hippocampal PTP deficiencies in the Mecp2-disrupted mouse model of Rett syndrome (Weng et al. 2011). Given astrocytes' increased sensitivity to dopamine in CA1 stratum radiatum, compared to stratum oriens (chapter 5), I decided to test whether dopamine's effects on baseline transmission were astrocyte-mediated. I then tested for a dopaminergic modulation of PTP at schaffer-collateral synapses and for an astrocytic component to any such modulation.

6.2 Methods

Transverse hippocampal slices were taken from p21-25 male Sprague-Dawley rats. All experiments were conducted at 32°C. To record fEPSPs from Schaffer collateral synapses, a recording pipette was placed in stratum radiatum of CA1 and a bipolar stimulating electrode also in stratum radiatum, but closer to CA3 (>200µm apart). To record NMDAR-mediated fEPSPs in stratum oriens, the field electrode was placed in stratum

oriens, among the basal dendrites, and the stimulation electrode in the alveus, toward the subiculum; for these recordings, CA3 was removed from the slice, picrotoxin (50µM) and NBQX (100µM) were added and 0.1mM Mg^{2+} recording solution was used. Stimulus strength was adjusted to give 50-60% of maximal fEPSP slope and recordings were made at 0.067Hz (every 15s). fEPSP slope was measured either from 20-60% of the upward phase or from 30-70%, depending on the nature of the fEPSP. Theta-burst-stimulation (TBS) consisted of 8 stimuli at 100Hz delivered twice at 5Hz. Recordings were discarded if baseline was unstable or fEPSP slope did not return to baseline after 10 minutes recording from the first TBS. Unless otherwise stated, all data was normally distributed (as measured with the Shapiro-Wilk test). Paired-pulse ratio (PPR) refers to the ratio of the second slope compared to the first. fEPSP are reported after normalization to baseline, as were PPRs – traces were discarded if the PPR of the first recording post TBS (15s) was not beneath the antecedent value.

6.3 Results

6.3.1 Glial poisoning with fluoroacetate does not affect the dopaminergic inhibition of stratum radiatum fEPSPs.

In the previous chapter I found that inhibiting astrocytes in stratum lacunosum-moleculare (SLM) with fluoroacetate did not affect dopamine's ability to inhibit fEPSPs – but I have also shown that astrocytic Ca^{2+} responsiveness to dopamine is different between SLM and stratum radiatum (SR): could there also be a difference in astrocytic involvement in dopaminergic signalling? I tested this here. Bath application of 20µM dopamine transiently inhibits excitatory synaptic communication (figure 6.1). At t=16-20, fEPSP slope – as normalized to baseline – is significantly decreased to 0.8±0.03 ($p=0.028$, 1-sample t-test, n=3), but PPR is not significantly changed ($p=0.327$, 1-sample t-test, n=3). Hippocampal

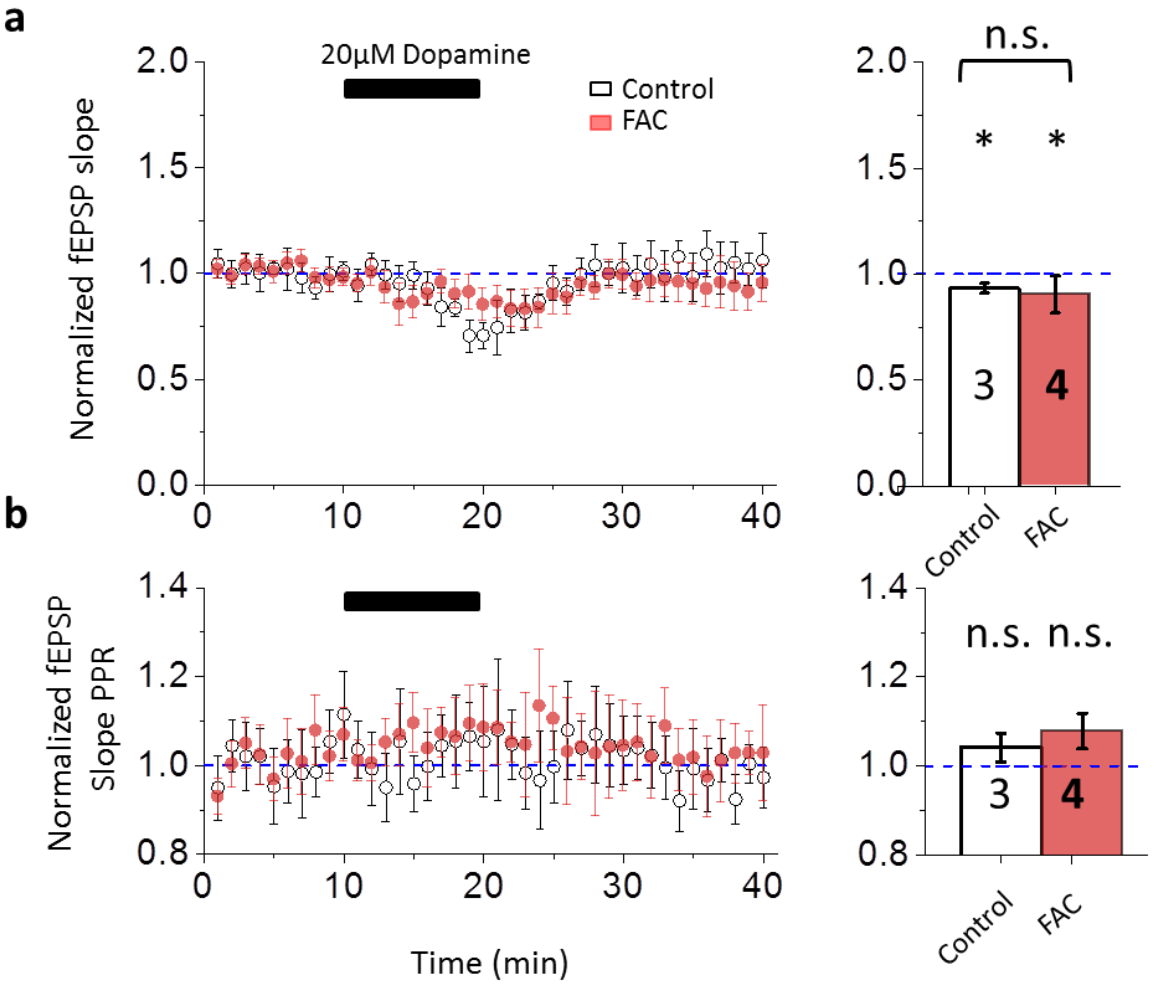

Figure 6.1 Glial poisoning with fluoroacetate does not affect the inhibition of Stratum Radiatum fEPSPs by dopamine.

a) Stratum Radiatum fEPSP slopes in response to 20µM dopamine. Left: time courses normalized to baseline (t=1-10) in control conditions (hollow circles) and after 50 mins fluoroacetate (FAC) incubation (red circles), dopamine application indicated by black bar. Right: summary bar chart of dopamine effect on fEPSP slope (average of t=16-20). **b**) Paired-pulse ratio of Stratum Radiatum fEPSP slopes in response to 20µM dopamine. Layout: as in **a**); * - $p < 0.05$, n.s. – non-significant, 1-sample t-test (1).

---

slices pre-incubated with 5mM fluoroacetate (FAC) still displayed dopamine-induced inhibition, to 0.86±0.04 (p=0.04, 1-sample t-test, n=4) and no PPR change (p=0.103, 1-

sample t-test, n=3). The dopamine-induced slope decreases in control and FAC were not significantly different (p=0.284, 2-sample t-test).

6.3.2 Description of a reproducible form of transient post-tetanic potentiation at Schaffer collateral synapses.

Given the lack of a clear involvement of astrocytes in dopaminergic modulation of basal transmission, I next wanted to investigate whether astrocytes were necessary for dopaminergic modulation of short-term potentiation – but first I needed to describe a reliable short-term plasticity protocol in slices, one that could be used twice at the same synapses to control for variation between synaptic populations. A short TBS protocol can induce transient, reproducible PTP at Schaffer collateral synapses (Figure 6.2): normalized fEPSP slope 15s post-TBS is significantly larger – 1.6 of baseline – for 1st TBS (p=0.004, 1-sample t-test, n=8) and also – to 1.73 of baseline – for 2nd TBS (p=0.01, 1-sample t-test, n=8). These two TBS-induced increases are not significantly different (p=0.368, paired t-test). This coincides with a decrease in PPR: PPR 15s post 1st TBS is not significantly decreased (p=0.107, 1-sample t-test, n=8), but 30s post TBS is (p=0.009, 1-sample t-test, n=8); PPR 15s post 2nd TBS is significantly lower than baseline (p=0.004, 1-sample t-test, n=8) as it is at 30s (p=0.048, 1-sample t-test, n=8). There is no significant difference in PPR between 15s post 1st and 2nd TBS (p=0.114, 1-sample t-test, n=8) or 30s (p=0.824, 1-sample t-test, n=8). By 16-20 minutes post-1st TBS (t=21-25) the fEPSP had returned to baseline – it was not significantly different (p=0.75, 1-sample t-test, n=8); likewise PPR had returned to baseline (p=0.705, 1-sample Wilcoxon signed rank test, n=8; not normally distributed, p=0.003, Shapiro-Wilk). There is no interaction between 1st and 2nd PTP fEPSP slopes (2-way repeated measures ANOVA, F(19,133) = 0.68, p=0.836, table S7), nor between 1st and 2nd PTP PPRs (2-way repeated measures ANOVA, F(19,133) = 0.61, p=0.894, table S8), for 5

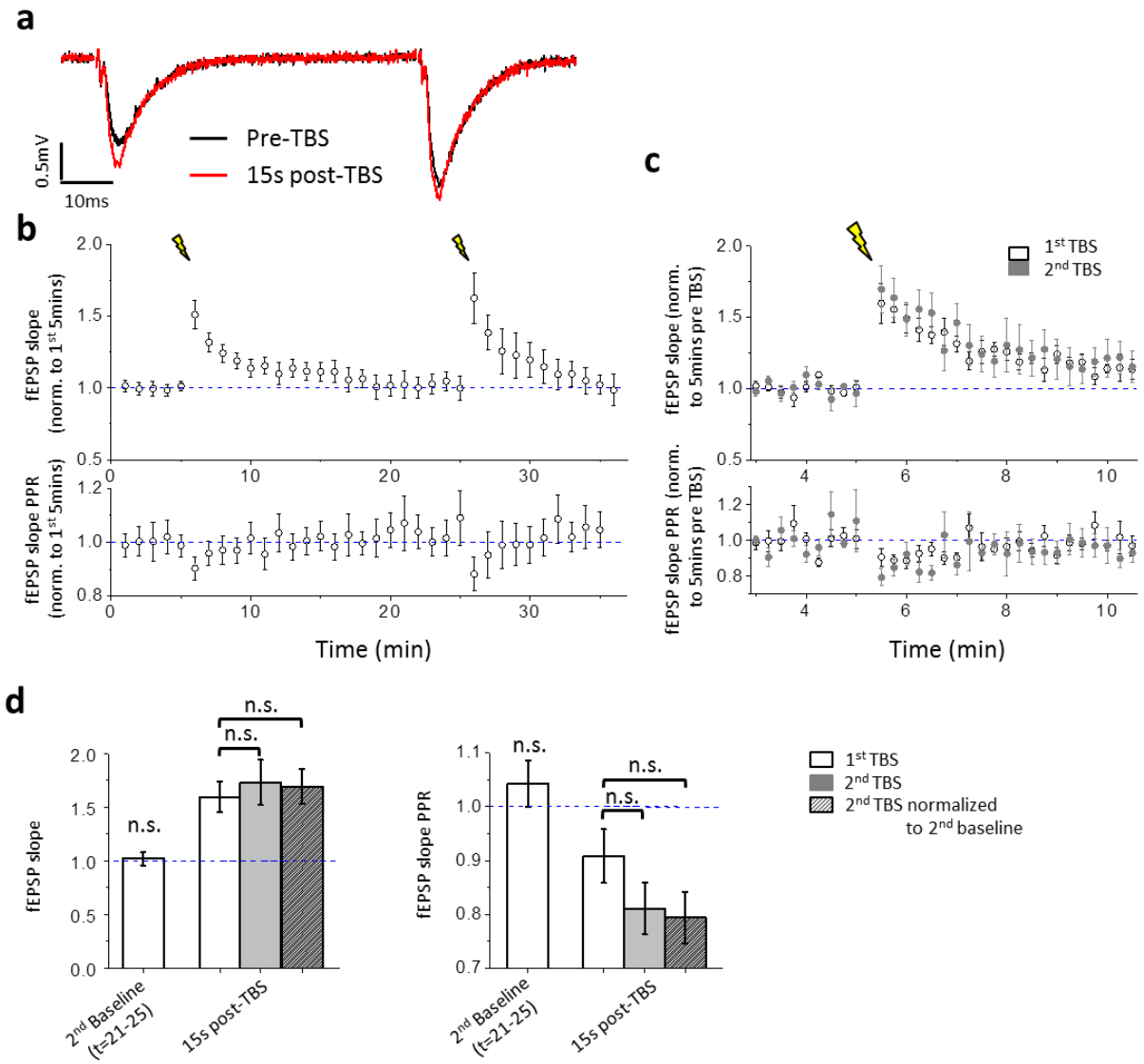

Figure 6.2 TBS induced PTP reproducibly returns to baseline and has a pre-synaptic component.

a) Example fEPSP traces from double stimulation; black trace – baseline, red trace – first recording (15s) after theta-burst stimulation (TBS). **b**) Above: time course (average per minute) of Stratum Radiatum fEPSP slopes in response to two TBSs (lightning bolts), 20 minutes apart. Below: paired-pulse ratios (PPR) for the above fEPSPs. Both time courses normalized to baseline (t=1-5). **c**) Above: fEPSPs recorded 5 minutes either side of both TBS at higher time resolution (1 rec / 15s), normalized to the 5 minutes preceding each TBS respectively; hollow circles – 1st TBS, grey circles – 2nd TBS. Below: PPRs of the above fEPSPs. **d**) Summary bar charts for fEPSP slopes (left) and fEPSP PPRs (right), showing average baseline for 2nd TBS and first recording (15s) post-TBS of both 1st and 2nd TBS (grey bars) normalized to 1st baseline, and first recording post-2nd TBS normalized to 2nd baseline (grey hatched bars); n.s. – non-significant, 1-sample t-test (1) or 1-sample wilcoxon signed rank test – see text.

minutes post-TBS; no single time-points are significantly different – fisher test.

6.3.3 In the presence of dopamine receptor blockers fEPSPs at 2nd baseline are larger than the original baseline average, but not larger than fEPSPs recorded at the 2nd baseline in the previous control experiment

Does blockade of dopamine signalling affect fEPSPs recorded at baseline? When 20µM SCH23390 (D1R antagonist) and 50µM Sulpiride (D2R antagonist) are added to the bath solution at t=16, the 2nd baseline fEPSP slope (figure 6.3) – before the 2nd TBS (t=21-25) – is significantly larger than the average fEPSP at the experiment start (t=1-5) – it is 1.12 ± 0.05 of the baseline (p=0.035, 1-sample t-test, n=9); PPR is significantly decreased from 1 at t=21-25 to 0.95 ± 0.01 of baseline (p=0.005, 1-sample t-test, n=9). The average fEPSP slope at 2nd baseline in dopamine antagonists is not significantly different to that recorded at the 2nd baseline in control conditions (p=0.204, two-sample t-test), although the average PPR was significantly lower in DR antagonists (p=0.024, Mann-Whitney test) – figure 6.4c.

6.3.4 Blockade of dopamine receptors occludes initial, pre-synaptic component of relative post-tetanic potentiation, but does not affect the latter components.

Is this PTP dopamine-dependent? Is it dependent on tonic dopamine in the slice? To check this I induced PTP in the presence of dopamine-receptor blockers. Comparing fEPSP slopes of the 1st and 2nd TBS-evoked PTPs (Figure 6.4), both normalized to the baseline taken at the start of the recording (1-5mins), shows no significant interaction (2-

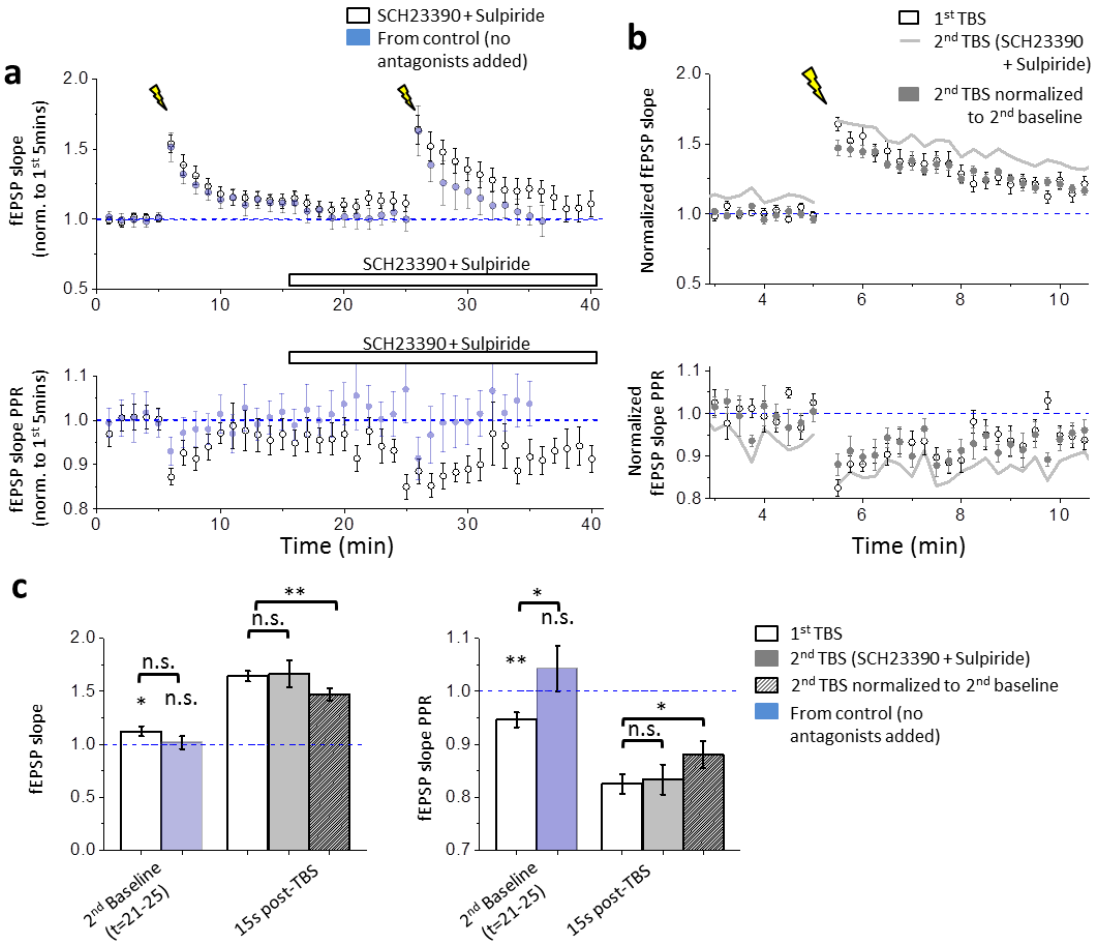

Figure 6.3 Dopamine receptor blockade potentiates baseline fEPSP presynaptically which partially occludes PTP.

a) Dopamine blockade raises post-TBS baseline transmission. Above: time course (average per minute) of stratum radiatum fEPSP slopes in response to two TBSs (lightning bolts), 20 minutes apart; hollow bar indicates SCH23390 (20µM) and Sulpiride (50µM) application. Below: paired-pulse ratios (PPR) for the above fEPSPs. Both time courses normalized to baseline (t=1-5); hollow circles – SCH23390 and Sulpiride added, blue circles – data from previous control experiment (figure 6.3a). **b**) Above: fEPSPs recorded 5 minutes either side of both TBS at higher time resolution (1 rec / 15s), normalized to the 5 minutes preceding each TBS respectively; hollow circles – 1st TBS, grey circles – 2nd TBS (in SCH23390 and Sulpiride), light grey line – 2nd TBS normalized to 1st TBS baseline. Below: PPRs of the above fEPSPs. **c**) Summary bar charts for fEPSP slopes (left) and fEPSP PPRs (right), showing average baseline for 2nd TBS and first recording (15s) post-TBS of both 1st and 2nd TBS (grey bars) normalized to 1st baseline, and first recording post-2nd TBS normalized to 2nd baseline (grey hatched bars); n.s. – non-significant, 1-sample t-test (1).

way repeated measures ANOVA, F(19,152) = 1.28, p=0.203, table S9); comparing individual time points, with the fisher test, shows some significant difference at specific time points, more in the final 2.5 mins. Examining only the first recording post-TBS (15s), there is no difference between evoked 1st and 2nd TBS (p=0.819, paired t-test, n=9). When each 2nd TBS is renormalized to the 5 minute baseline preceding it, there is a significant interaction between 1st and 2nd TBS fEPSP (2-way repeated measures ANOVA, F(19,152) = 1.74, p=0.034, table S10), but only one significant difference when individual points are compared (with fisher test), at 15s. At 15s, the fEPSP post-2nd TBS (in dopamine receptor blockers) is significantly smaller than the fEPSP post-1st TBS (p=0.001, paired t-test, n=9)

Comparing PPRs in the same fashion, there is a significant interaction between 1st and 2nd TBS-evoked PTP PPRs, when both normalized to the beginning baseline (2-way repeated measures ANOVA, F(19,152) = 1.8, p=0.027, table S11) – there are some significantly different individual differences (fisher test), but none in the first minute (see table S12); at 15s, the 1st and 2nd PPRs are not significantly different (0.668, paired t-test, n=9). When the 2nd PPR is normalized to the previous 5 minutes, there is still a significant interaction (2-way repeated measures ANOVA, F(19,152) = 1.72, p=0.038, table S6) – there are no significant individual differences apart from at 270s post-TBS; at 15s, the PPR is significantly different (p=0.026, paired t-test, n=9).

6.3.5 Prolonged recording after post-tetanic potentiation results in fEPSP rundown.

FAC takes 50 minutes incubation to have an effect on glial activity – is it possible to record PTP before FAC application and again after FAC incubation? Unfortunately fEPSPs exhibit significant rundown after such a long time: fEPSP slopes (figure 6.4a) recorded at t=61-65 (56-60 minutes post-TBS) approach a significant decrease to 0.76 ± 0.08 of baseline

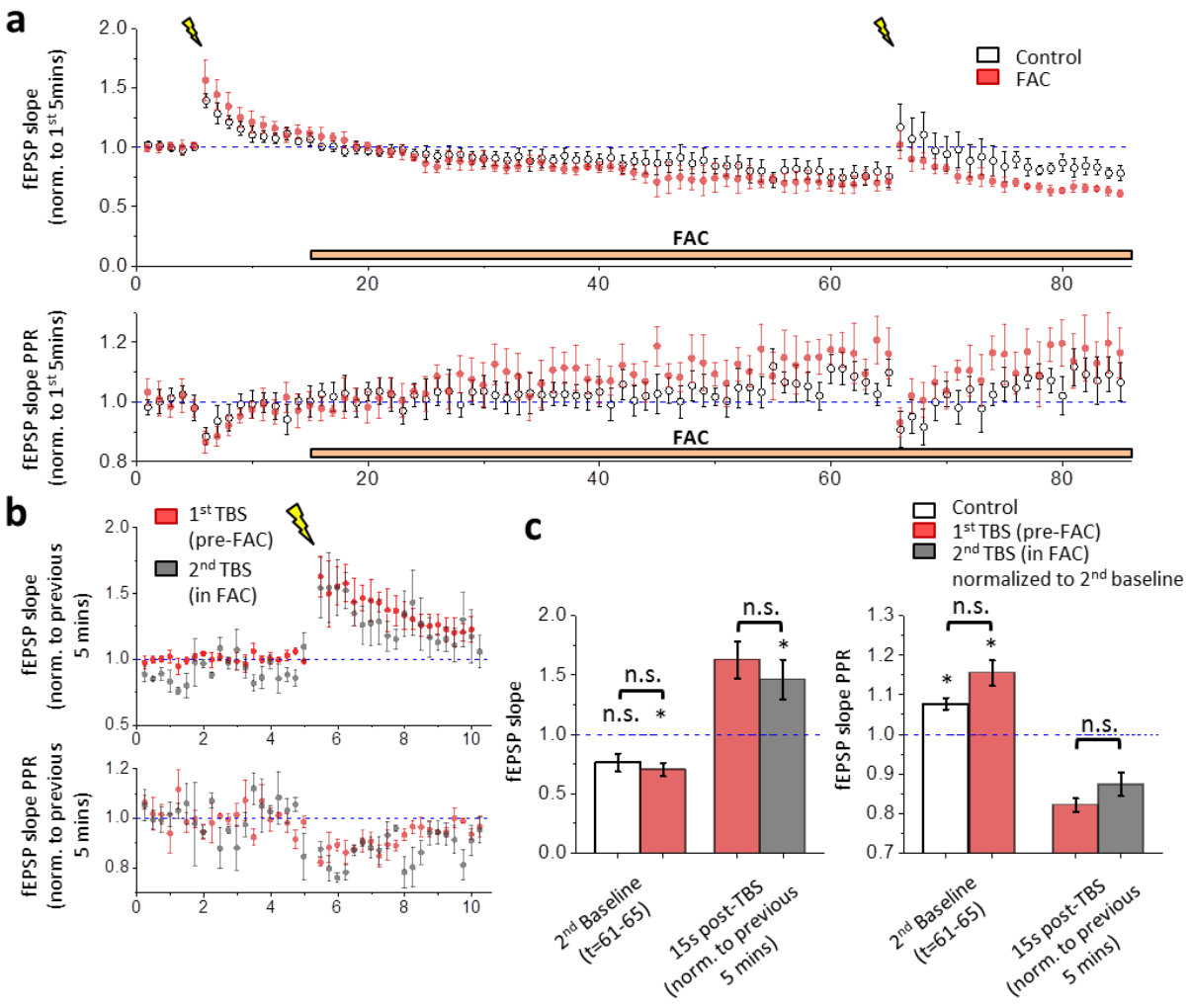

Figure 6.4 **FAC incubation does not affect the size of PTP proportional to recent baseline, but rundown is apparent 50 minutes post-TBS in both control and FAC conditions.**

a) Prolonged recording post TBS decreases baseline fEPSP slope and increases PPR both in control conditions and after incubation with fluoracetate (FAC). Above: time course (average per minute) of Stratum Radiatum fEPSP slopes in response to two TBSs (lightning bolts), 60 minutes apart; hollow circles – control conditions, red circles – FAC added at t=16, orange bar indicates FAC (5mM) application. Below: paired-pulse ratios (PPR) for the above fEPSPs. Both time courses normalized to baseline (t=1-5). **b**) Above: fEPSPs recorded 5 minutes either side of both TBS at higher time resolution (1 rec / 15s), normalized to the 5 minutes preceding each TBS respectively; hollow circles – 1st TBS, red circles – 2nd TBS (in FAC). Below: PPRs of the above fEPSPs. **c**) Summary bar charts for fEPSP slopes (left) and fEPSP PPRs (right), showing average baseline for 2nd TBS (t=61-65) in control (hollow bar)

and FAC incubation (red bar) conditions, and first recording (15s) post-TBS for both 1st (red bar) and 2nd (grey bar) TBS normalized to previous 5 minutes; * - $p < 0.05$, n.s. – non-significant, 1-sample t-test (1).

(p=0.052, 1-sample t-test, n=4), the PPR values are significantly higher – 1.08 ± 0.01 – than baseline (p=0.013, 1-sample t-test, n=4).

6.3.6 Relative post-tetanic potentiation before and after fluoroacetate incubation is unchanged.

I go on to FAC to isolate and inhibit astrocytic Krebs' cycle function – but first I checked to see if glial poisoning alone would affect fEPSPs. In control conditions, the 2nd baseline period (61-65 mins) has approached a significant decrease in fEPSP slope to 0.76 ± 0.08 of baseline (p=0.052, 1-sample t-test, n=4) and has a significantly increased PPR to 1.08 ± 0.01 of baseline (p=0.013, 1-sample t-test, n=4). In slices where fluoroacetate (FAC) was added at t=15 mins, the 2nd baseline fEPSP was significantly decreased to 0.7 ± 0.06 of baseline (p=0.035, 1-sample t-test, n=3) and PPR was increased to 1.15 ± 0.03 (p=0.041, 1-sample t-test, n=3). The fEPSP changes were not different between control and FAC conditions (p=0.582, 2-sample t-test), although PPR approached a significant increase (+0.08) in FAC compared to control conditions (0.062, 1-sample t-test)

When each 2nd TBS (in FAC) is renormalized to the 5 minute baseline preceding it, there is no significant interaction between 1st and 2nd TBS PPR (2-way repeated measures ANOVA, $F(19,57) = 0.75$, p=0.748, table S13), but only one significant difference when individual points are compared (with fisher test), at 135s; there is no significant difference between the two at 15s (p=0.662, paired t-test, n=4). When the 2nd PPR is normalized to the previous 5 minutes, there is still no significant interaction (2-way repeated measures

ANOVA, F(19,57) = 0.84, p=0.658, table S14) – there are some significant individual differences occurring after 2.5 minutes post-TBS; at 15s, the PPR is not significantly different (p=0.721, paired t-test, n=4).

6.3.7 Glial poisoning increases the modulation of baseline by dopamine receptor blockers, but does not affect post-tetanic potentiation by dopamine receptor blockers.

Does glial poisoning with FAC change the way in which dopamine receptor blockade affects baseline fEPSPs, or reveal an effect on PTP? The average 2nd baseline fEPSP slope, after addition of DR antagonists (20µM SCH23390, 50µM Sulpiride) in slices pre-incubated in FAC (5mM) (figure 6.5) before the 2nd TBS (t=21-25) is significantly larger than that at the experiment start (t=1-5) – its median (it is not normally distributed – p=0.019, Shapiro-Wilk test) is 1.18 of the baseline (p=0.035, 1-sample Wilcoxon signed rank test, n=11). This average fEPSP slope increase at 2nd baseline is significantly greater than that recorded in control conditions (no FAC or DR antagonists – figure 6.3) (p=0.023, Mann-Whitney test) but not than that recorded in DR antagonists alone (figure 6.4) (p=0.362, Mann-Whitney test). It is important to note that there is a significant interaction between the 1st PTP recorded in control conditions and that recorded in FAC pre-incubated slices (2-way ANOVA, F(1,19) =38.7, p<0.001), although there is no significant difference between both fEPSP slopes at 15s (p=0.24, 2-sample t-test). The average PPR at the 2nd baseline is significantly decreased from 1 to 0.9 ± 0.03 of baseline (p=0.007, 1-sample t-test, n=11). This is significantly lower than that recorded in control conditions (p=0.009, Mann-Whitney test) but not lower than that recorded in antagonists alone (p=0.191, two-sample t-test).

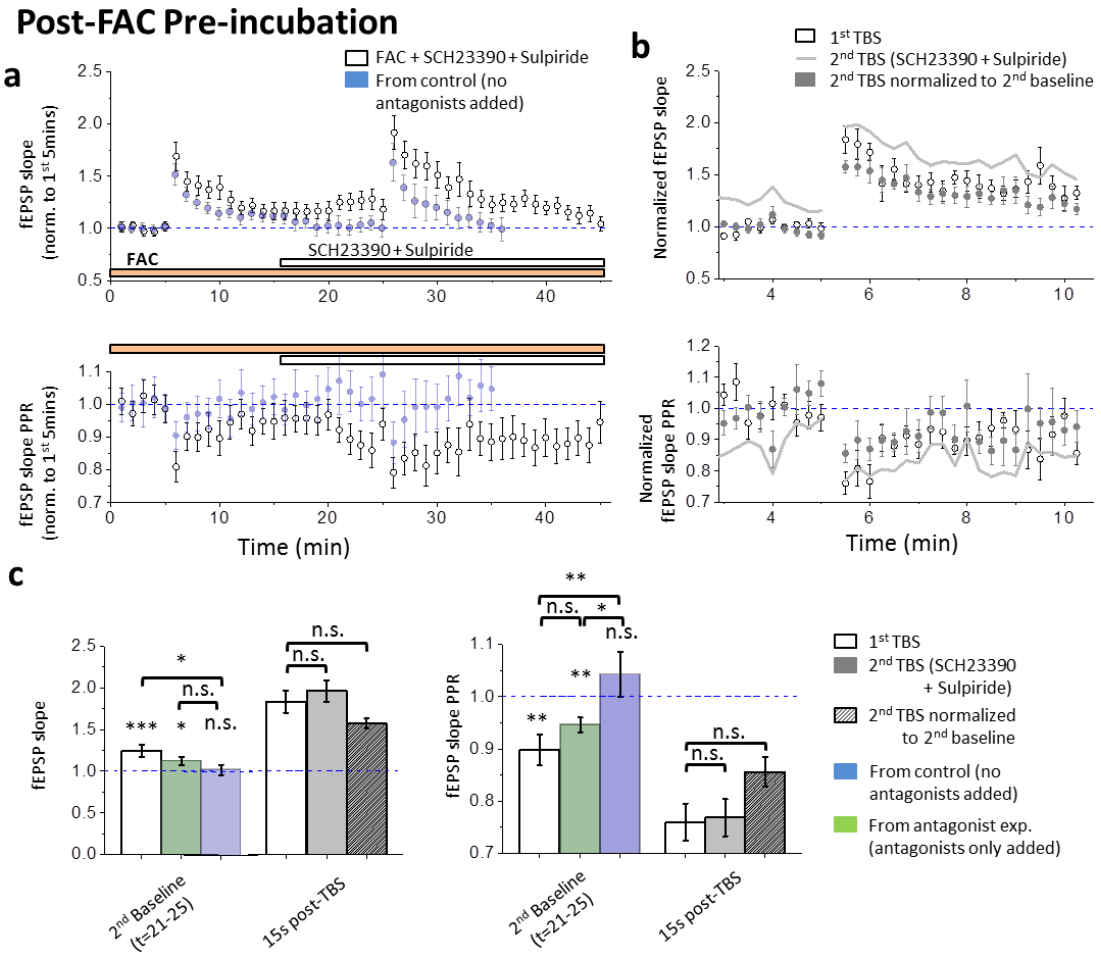

Figure 6.5 Pre-incubation with FAC does not interfere with the effect of Dopamine blockers on baseline transmission or PTP.

a) Glial poisoning with FAC does not significantly modify the effect of dopamine receptor blockade in stratum radiatum fEPSPs. Above: time course (average per minute) of Stratum Radiatum fEPSP slopes in response to two TBSs (lightning bolts), 20 minutes apart; hollow bar indicates SCH23390 (20µM) and Sulpiride (50µM) application, orange bar indicates presence of FAC (5mM). Below: paired-pulse ratios (PPR) for the above fEPSPs. Both time courses normalized to baseline (t=1-5); hollow circles – FAC pre-incubation and SCH23390 and Sulpiride added, blue circles – data from previous control experiment (figure 6.3a). **b**) Above: fEPSPs recorded 5 minutes either side of both TBS at higher time resolution (1 rec / 15s), normalized to the 5 minutes preceding each TBS respectively; hollow circles – 1st TBS, grey circles – 2nd TBS (in SCH23390 and Sulpiride), light grey line – 2nd TBS normalized to 1st TBS baseline. Below: PPRs of the above fEPSPs. **c**) Summary bar charts for fEPSP slopes (left) and fEPSP PPRs (right), showing average baseline for 2nd TBS and first recording (15s) post-TBS of both 1st and 2nd TBS (grey bars) normalized to 1st baseline, and first recording post-2nd TBS normalized to 2nd baseline (grey hatched bars); * - $p < 0.05$, ** - $p < 0.01$, *** - $p < 0.01$, n.s. – non-significant, 1-sample t-test (1) or wilcoxon signed ranks test – see text.

Comparing fEPSP slopes of the 1st and 2nd TBS-evoked PTPs (Figure 6.5), both normalized to the baseline taken at the start of the recording (1-5mins), there is no significant interaction (2-way repeated measures ANOVA, F(19,171) = 1.25, p=0.227, table S15); comparing individual time points, with the Fisher test, shows some significant difference at specific time points, more in the final 2.5 mins. Examining only the first recording post TBS (15s), there is no difference between evoked 1st and 2nd TBS (p=0.272, paired t-test, n=11). When each 2nd TBS is renormalized to the 5 minute baseline preceding it, there is no significant interaction between 1st and 2nd TBS PPR (2-way repeated measures ANOVA, F(19,171) = 1.3, p=0.187, table S16), but only one significant difference when individual points are compared (with fisher test), at 255s. At 15s the normalized fEPSP slopes are not significantly different (p=0.079, paired t-test, n=11). Comparing PPRs in the same fashion, there is no significant interaction between 1st and 2nd TBS-evoked PTP PPRs, when both normalized to the beginning baseline (2-way repeated measures ANOVA, F(19,171) = 1.26, p=0.219, table S17) – there are some significantly different individual differences (fisher test), but none in the first minute; at 15s, the 1st and 2nd PPRs are not significantly different (0.833, Kolmogorov-smirnov). When the 2nd PPR is normalized to the previous 5 minutes, there is still no significant interaction (2-way repeated measures ANOVA, F(19,171) = 1.24, p=0.228, table S18) – there are no significant individual differences; at 15s, the PPR is not significantly different (p=0.075, Kolmogorov-smirnov).

6.3.8 Blockade of putative tonic dopaminergic activity does not affect astrocyte-derived-d-serine-modulated NMDAR-mediated fEPSPs.

Bath application of SCH23390 (20µM) whilst recording NMDAR-mediated fEPSPs (in presence of low Mg^{2+} (0.1mM), NBQX (100µM) and picrotoxin (50µM)) had no significant effect on NMDAR-mediated fEPSP slopes (p=0.528, 1-sample t-test, n=5) – see figure 6.6.

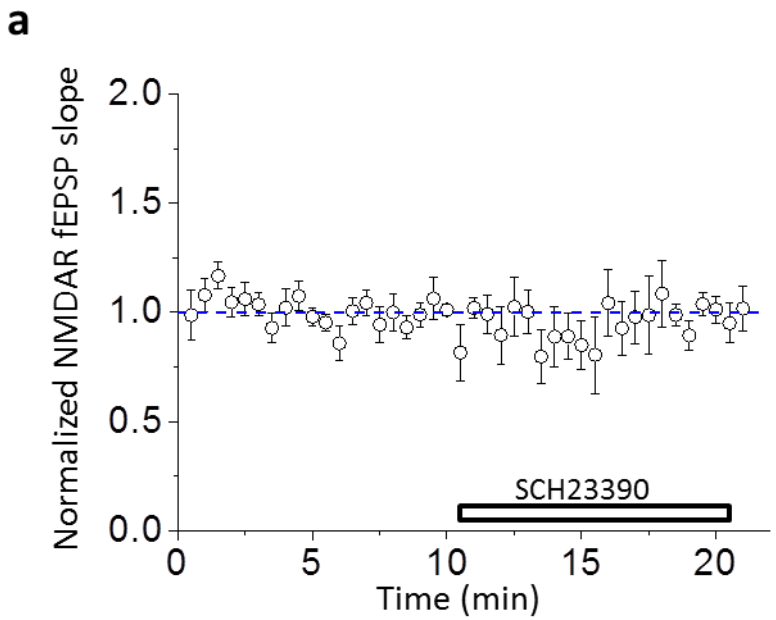

Figure 6.6 Blockade of D1-type receptors does not affect NMDAR-mediated currents in the stratum radiatum.

NMDAR-mediated fEPSPs normalized to baseline (t=1-10), recorded from stratum oriens in low (0.1mM) Mg^{2+},10µM NBQX and 50µM picrotoxin; SCH23390 (20µM) added at t=11 mins (hollow bar).

6.4 Discussion

6.4.1 I find no evidence to suggest that astrocytes play role in dopaminergic modulation of baseline synaptic transmission in stratum radiatum.

Investigation of different types of baseline synaptic activity that could be dopamine-modulated has revealed a possible role for astrocytes in baseline transmission (figure 6.1) but not in NMDAR-mediated currents (figure 6.6). Bath application of 20µM dopamine has a small but highly significant inhibitory effect on baseline, primarily AMPAR-mediated, currents at the Schaffer collateral synapse (Otmakhova and Lisman 1999). Consistent with the lack of an astrocyte component in this dopaminergic inhibition in the stratum lacunosum-moleculare (Chapter 5), astrocyte metabolic poisoning does not affect the inhibition of fEPSP slopes in CA1 (figure 6.1). This reliably repeats Otmakhova and Lisman's result (1999): although I see no significant change in PPR, their reported increase may be due to a constantly rising PPR, as it is not washed out with dopamine, whereas my PPR values are still at baseline after dopamine washout.

6.4.2 What role does dopamine play in PTP?

Given the lack of astrocytic interaction with dopamine at basal activity levels, I next investigated their involvement in synaptic potentiation. Surprisingly, studies of dopaminergic modulation of post-tetanic potentiation (PTP) are scarce, only Young and Yang (2005) in the cortex and the possibility of a dopaminergic involvement in the PTP deficit in a mouse model of Rett syndrome – given that dopamine tonus is increased in these mice (Weng et al. 2011). This is the first investigation I am aware of into dopaminergic modulation of PTP at the CA1 synapse. PTP in the hippocampus is very well studied (Zucker and Regehr 2002) and my PTP phenomenon is at the longer lasting end of

potentiation that qualifies as 'PTP' and not 'STP' (short-term potentiation) – a phenomenon defined by the stimulation of protein production. Given this, I will discuss two facets of the PTP described here: early PTP (ePTP) (<30s) that will contain a fast acting, presynaptic component – controlled by calcium concentration-dependent release probability increase at the presynaptic bouton (Zucker and Regehr 2002) – and late PTP (lPTP) that I postulate is primarily post-synaptic. Evidence for the validity of this classification comes from the faster return to baseline of the PPR than of the fEPSP slope (figure 6.3), indicating a proportion of the potentiation is not reliant on increased release probability. It is likely that there is also a post-synaptic component to the ePTP as a post-TBS increase in the 2nd fEPSP slope is visible (see example in figure 6.3a). After 20 minutes the fEPSP slope has returned to baseline and a second TBS can be given, which displays identical characteristics. This experimental protocol controls for variability in slice quality, animal differences and stimulation and recording electrode placement, making it sensitive to slight changes caused by pharmacological interrogation. Blockade of D1/2Rs has two effects: firstly, it decreases the baseline paired-pulse ratio, and secondly it partially occludes ePTP (when normalized to the new baseline. I will discuss each of these phenomena in turn.

6.4.2.1 Putative dopaminergic modulation of baseline transmission

Although dopamine receptor blockade alone significantly decreases only PPR (figure 6.3) from control, when dopamine receptors are blocked after FAC incubation both baseline fEPSP slope and PPR are significantly different from baseline. Hence it is possible that FAC enhances a pre-existing action of dopamine receptor blockers – an idea supported by the fact that the direction of the effect is the same for both manipulations and additive (increasing fEPSP slope and decreasing PPR) – see figure 6.5c.

If this is the case, then could the non-significant increase in baseline fEPSP under dopamine receptor blockade be indicative of a real effect? Such an increase in baseline could potentially be due to either blockade of tonic dopaminergic inhibition in stratum radiatum, or could possibly be an effect of dopaminergic blockade on the decaying tail of the 1st PTP. To answer the latter first – there is little evidence to suggest that increasing the decay rate of potentiation is a function of tonic dopamine in the hippocampus (although there is in Aplysia (Newlin et al. 1980)) ; given that many studies have reported that dopamine enhances hippocampal lLTP (Frey et al. 1990; Swanson-Park et al. 1999) and inhibits low frequency stimulation induced depotentiation (Otmakhova and Lisman 1998), one would in fact expect the opposite. One group has, however, demonstrated a direct depotentiating effect of phasically released dopamine (Kwon et al. 2008) after LTP induction, if this effect could be caused by tonic dopamine, or by dopamine release from the 1st TBS, this could provide a potential mechanism – although their phenomenon is D4R mediated and my blockade of D1/2-type receptors should leave D4Rs unblocked (although the concentrations of antagonist are high – potentially high enough to block all dopamine receptors). High-frequency stimulation has been shown to trigger dopamine release in the hippocampus (Frey et al. 1990), so it is possible that the 1st TBS triggers a dopamine release that depotentiates the induced PTP, although the stimulus I used is far weaker than that used by Frey et al. and the time between any putative dopamine release and the start of dopamine receptor blockade is long (~15 minutes) – probably long enough for full dopamine clearance from the extracellular space. This, coupled with the apparent dip towards baseline at t=18-19 (figure 6.4a) and subsequent rise at t=21-23 (if depotentiation were being inhibited, one would expect a constant decay as seen in figure 6.3), makes a direct effect of D1/2-type receptor blockade on baseline transmission more plausible.

Regarding tonic dopaminergic inhibition of baseline, addition of D1-type receptors blockers alone has not been reported to increase baseline transmission (Frey et al. 1991;

Huang and Kandel 1995), but there is no report yet of a disinhibitory effect of combined D1/2-type receptor blockade on baseline transmission in CA1. Such a result is consistent with studies that report an inhibitory effect of dopamine application on Schaffer collateral synapses (Hsu 1996; Otmakhova and Lisman 1999); these studies have both found evidence for a presynaptic locus – as I have with the PPR decrease upon D1/2-type receptor blockade. Hsu (1996) reports D2R-mediated inhibition of presynaptic transmitter release (although D2R mediated increase in CA1 pyramidal firing rate was previously reported (Smialowski and Bijak 1987), such a presynaptic D2 receptor, tonically activated, could explain the antagonist-induced transmission potentiation. In PFC, D2R activation triggers GABA-mediated EPSP inhibition in deep layer pyramidal neurons from superficial but not deep layer stimulation – raising the possibility of layer specific effects of D2R activation on inhibition (Tseng and O'Donnell 2007); alleviating such inhibition through D2 blockade could contribute to baseline potentiation witnessed. However this D2R could also be astrocytic – D2R activation could trigger release of presynaptically inhibitory gliotransmitter, such as adenosine (Halassa et al. 2009) or ATP (Panatier et al. 2011).

The ideal and simple experiment to test whether simultaneous D1/2-type receptor blockade can potentiate baseline synaptic transmission is to add D1/2R antagonists to the slice whilst recording fEPSPs at baseline, without giving any kind of TBS.

6.4.2.2 Increased early PTP

When renormalized to the observed baseline increase, D1/2-type receptor blockade attenuates the slope increase and PPR decrease seen on the first recording post-TBS, an effect which then slips away. This is a clear effect on the relative presynaptic ePTP (figure 6.3). This result has two interpretations: the first is that tonic dopaminergic inhibition of presynaptic release is transiently overcome by TBS-induced ePTP, acting

through the same presynaptic pathways – alleviation of this tonic inhibition through DR blockade decreases the relative possible TBS-induced ePTP increase; the second is that TBS-induced dopamine release transiently potentiates presynaptic release, a potentiation blocked by DR antagonism.

There is some evidence for both possible mechanisms in the literature – both Frey et al. (1991) and Huang and Kandel (1996) see a decrease in mean fEPSP response at 1 minute post LTP induction during D1/5R blockade compared to control (although this does not reach significance); given their greater stimulus strength (100 stimuli at 100Hz), it is plausible that more dopamine would be released and any presynaptic excitatory effect of released dopamine would last longer than the 15-30s observed in this chapter. The work of Hsu (1996), however, would support a relative occlusion of ePTP by blockade of tonic D2R activation.

What is striking is the lack of effect on relative PTP that dopamine receptor blockers have. Given the importance of dopamine in the hippocampus for synaptic plasticity and behaviour (Li et al. 2003), and its reported role in PTP in the PFC (Young and Yang 2005), one might have expected some effect of dopamine blockade on hippocampal PTP, but this highly sensitive double TBS protocol uncovers very little difference made by DR antagonism. This result is consistent with the bulk of the literature in suggesting the dopamine is important for the later stages of LTP, possibly via translation and transcription through ERK signalling (Kaphzan et al. 2006; Sarantis et al. 2009).

6.4.3 What role do astrocytes play in PTP?

Given that FAC takes 50 minutes to affect astrocytes (Henneberger et al. 2010), this protocol required a 60 minute interval from the 1st to the 2nd TBS to measure the effect of

astrocyte poisoning at the same set of synapses. This had the unexpected effect of decreasing fEPSP slopes and increasing PPR at baseline stimulation rate. This could constitute synaptic rundown, always a potential hazard in slice recordings, or it could be due to the 1st PTP – it is possible that this short term potentiating stimulus could cause LTD, via a decrease in presynaptic release probability, and it would be interesting to pharmacologically probe this phenomenon further. However it is clear, comparing control and FAC traces, that the ability of TBS to induce relative PTP is unchanged without astrocytes (figure 6.5). Healthy astrocyte K^+ uptake decreases the magnitude of PTP in control conditions (Sibille et al. 2014), so one might expect a PTP increase after FAC incubation – which I do not see – but the exact effect of FAC on K^+ transport is still unknown.

6.4.4 Could compromising astrocyte function have changed the dopamine-receptor-mediated effects on post-tetanic-potentiation?

The putative additive effect of glial poisoning on DAR blockade-induced baseline fEPSP increase and PPR decrease, this would suggest either that tonic dopaminergic stimulation of astrocytes causes an astrocytic release of presynaptically active inhibitory gliotransmitter – adenosine for example (Florian et al. 2011). Another possibility is that FAC incubation itself changes the post-TBS return to baseline synaptic transmission in the slice. Given there is a significant interaction between the control 1st PTP and the pre-incubated FAC and DAR antagonist 1st PTP, this may indicate the latter (although the 1st fEPSP amplitude post TBS, at 15s, was not significantly different between the two) – if this is the case, then although the effects of DAR blockade and FAC incubation are both similar, they may be independent i.e. astrocytes are not affected by tonic dopamine.

If astrocytes were modulating baseline activity through tonic dopamine activation, such a change would be consistent with astrocytes having a moderating effect on the dopaminergic inhibition of Schaffer collateral synapses at baseline – consistent with the moderating effect they were found to have post-PTP in SLM (chapter 5). More recordings would have to be made to be confident of such a delicate effect.

As commented on in Chapter 5, section 5.4.4, FAC is not a complete inhibitor of astrocytic function (although in this chapter it is assumed to inhibit the astrocytic calcium response to dopamine). FAC inhibits aerobic respiration (through creation of fluorocitrate and the inhibition of aconitase) – but there is no data to show whether astrocytes could still respond with normal calcium signals whilst respiring solely anaerobically.

6.4.5 NMDAR-mediated currents are not regulated by tonic D1/5R activation.

D1 receptor activation has been strongly linked to NMDAR activity, having been reported to both increase and decrease NMDAR-mediated currents (Chetkovich and Sweatt 1993; Castro et al. 1999; Seamans et al. 2001; Lee et al. 2002; Chen et al. 2004; Pei et al. 2004) , modulate ERK signalling (Kaphzan et al. 2006; Sarantis et al. 2009), control NMDAR-mediated LTP (Stramiello and Wagner 2008; Roggenhofer et al. 2013) and NMDAR-mediated behaviour (Li et al. 2003; Roggenhofer et al. 2010; Xing et al. 2010; Zarrindast et al. 2012). Given dopaminergic calcium increases in astrocytes are D1-mediated (Chapter 3, 4) and the astrocytic control of NMDAR responses via D-serine release (Panatier et al. 2006; Oliet and Mothet 2009; Fossat et al. 2012) is mediated by astrocytic calcium (Henneberger et al. 2010) and similarly that D1R blockade blocks Ca^{2+} dependent processes in neurons (Chen et al. 2007) – I tested whether baseline NMDAR-mediated transmission was sensitive to D1-blockade. The lack of a significant effect of SCH23390 on NMDAR-mediated fEPSPs suggests that any astrocytic activation by tonic dopamine release in the hippocampal slice

does not control tonic release of D-serine (consistent with the data from chapter 4) or activate D1R/NMDAR interaction on neurons. Recently, it has been reported that D4Rs modulate NMDAR-mediated currents during LTP induction in stratum oriens (Herwerth et al. 2012) – where the above data is recorded –a repeat of this experiment with D4R blockade would be an interesting further investigation.

6.5 Conclusion

As has been previously shown, direct application of dopamine can inhibit Schaffer collateral synapses. However, this is the first time it has been reported that blockade of tonic dopamine in the hippocampal slice can potentiate baseline synaptic transmission at the Schaffer collaterals. Similarly this is the first study to show that dopamine receptor blockade can interfere with the early phase of PTP in the hippocampal slice, although the later phase is unaffected. It is clear, however, that none of these dopaminergic phenomena are mediated by astrocytes.

When this chapter is taken into account with the previous chapter, apart from the small role of astrocytes in PTP-modulation at the pp-SLM synapse, the data indicate no role for astrocytes in the dopaminergic modulation of synaptic transmission in CA1 of the hippocampus. This suggests that the robust dopamine induced Ca^{2+} changes in astrocytes are not obviously linked to synaptic activity – although whether they have any physiological function is still unsure.

Chapter 7: Results 5.

Viral delivery of a channelrhodopsin transgene to dopaminergic hippocampal afferents the does not work if under the control of a CaMKII promoter.

7.1 Introduction

Dopaminergic projections from the ventral tegmental area (VTA) innervate the hippocampus in rat (Swanson 1982; Gasbarri et al. 1994a; Gasbarri et al. 1994b) and in mouse (Herwerth et al. 2012) in the Stratum Oriens and Stratum Lacunosum-Moleculare. Although bath application of dopamine has been shown to affect hippocampal slice activity (Frey et al. 1990; Huang and Kandel 1995; Otmakhova and Lisman 1999), we can only be sure of the physiological relevance of dopamine action *in vivo* (Li et al. 2003) because only here is dopamine released from dopaminergic terminals at a physiological level. Although it is possible to release dopamine by LTP-inducing electrical stimuli (Frey et al. 1989), it is not possible to do so without this extremely powerful stimulus.

Over the last ten years, optogenetic control of neuronal activity has become the most versatile and powerful tool to selectively control specific populations of cells (Fenno et al. 2011). Channelrhodopsins are light-sensitive proteins that, upon activation, create an ion-permeable pore in the plasma membrane. CaMKII has been reported to be expressed in the dopaminergic neurons of the VTA (Fog et al. 2006; Padmanabhan and Prasad 2009) as well as in most principal neurons of the brain (Griffith 2004; Wayman et al. 2011). In order to selectively control dopaminergic projections to the hippocampus, I injected the VTA with a viral vector that would express excitatory channelrhodopsin under the CaMKII promoter: transport of the channelrhodopsin protein throughout the axonal arborisation of

dopaminergic cells should allow release of dopamine in a physiological manner upon stimulation with light.

7.2 Methods

50-60g juvenile male Sprague-Dawley rats were anaesthetised with a mixture of ketamine (60 mg/kg) and medetomidine (250 mg/kg) intra-muscular. Additional anaesthesia was administered depending on the duration of the surgery. The head was shaved and cleaned with chlorohexidine. The head was positioned in a stereotaxic frame and protective ophthalmic gel was applied. A midline incision was made and the skull was cleaned and dried. A small craniotomy was performed within the right parietal bone. The surface of the brain was flushed with aCSF to remove any blood products. The virus (AAVsCaMKII-ChR2(H134R)-Venus YFP suspended in filtered saline (1:10) was injected into two sites in the Ventral Tegmental Area (VTA) (2µl per injection). The skin was sutured. Buprenorphonine was administered (0.05 mg/kg s.c.) and the anaesthesia was reversed with atipemazole (1mg/kg i.m.). Post-operative care was given. The animals were allowed to recover for 14/21 days to allow transgene expression. For immunocytochemistry, rats were terminally anesthatised (urethane, 1.5 g/kg i.p.) and intracardially perfused with saline followed by ice cold 4% paraformaldehyde. The brains were removed and post-fixed overnight at 4°C. The brains were soaked sucrose (30%, 4°C) for a further 24 hours. The brains were sliced into 60µm thick sections and serially mounted. Mounting medium containing dapi (Vectashield) was applied and the coverslips secured. For immunohistochemical identification of dopaminergic neurons and axons, tissue was incubated in sheep anti-Tyrosine Hydroxylase antibody (1:250, Abcam) overnight at 4°C, then again in secondary donkey anti-sheep Alexa 568 (1:500, Molecular probes). Fluorescence of YFP and Alexa 568 were imaged on a Zeiss AX10 bright-field microscope.

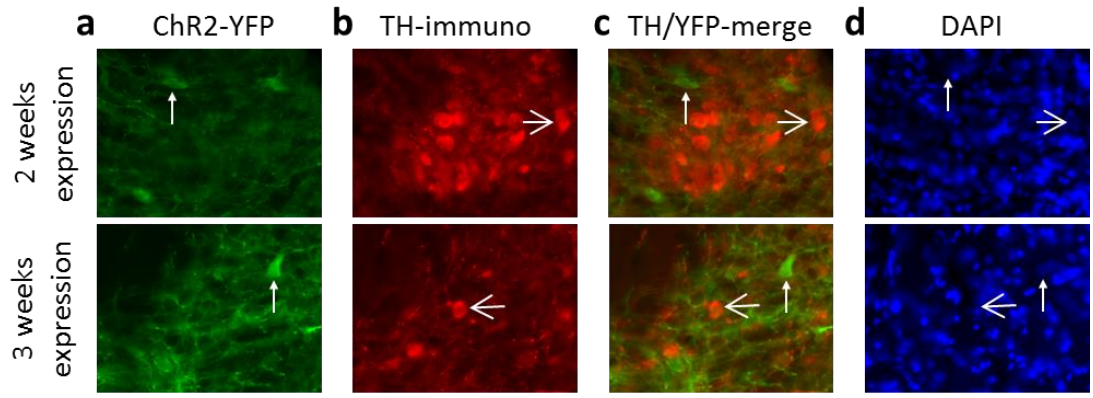

Figure 7.1 Principle cells of the Ventral Tegmental Area that express the ChR2-CamKII virus are not from the dopaminergic cell population.

a) ChR2-YFP protein expression in VTA cells (green), small vertical white arrows indicate principle cell somata. Above: animal sacrificed 2 weeks post-injection. Below: 3 weeks post-injection. **b**) anti-tyrosine-hydroxylase reactivity (red) in the same area of tissue, large horizontal white arrows indicate principle cell somata. Layout as in **a**). **c**) red and green images merged to show no overlap in fluorescence (yellow). Layout: as in **a**). **d**) DAPI staining shows cell nuclei – DAPI staining is weak, but present in principle cells indicated in **a**) – **c**).

7.3 Results

7.3.1 Principle cells of the Ventral-Tegmental Area can express ChR2-YFP under the CaMKII promotor, but these are not the dopaminergic cells.

In PFA-fixed midbrain slices, large cell bodies are visible at ~535nm light wavelength in the animal sacrificed at 2 weeks and that at 3 weeks (figure 7.1a). Staining with antibodies for tyrosine hydroxylase (TH) reveals large numbers of dopaminergic neurons in the same imaging field as the YFP –positive cells (figure 7.1b), but no cells are positive for both TH and YFP (figure 7.1c). DAPI staining shows weak but positive staining for nuclear material in all YFP and TH-labelled cells (figure 7.1d.

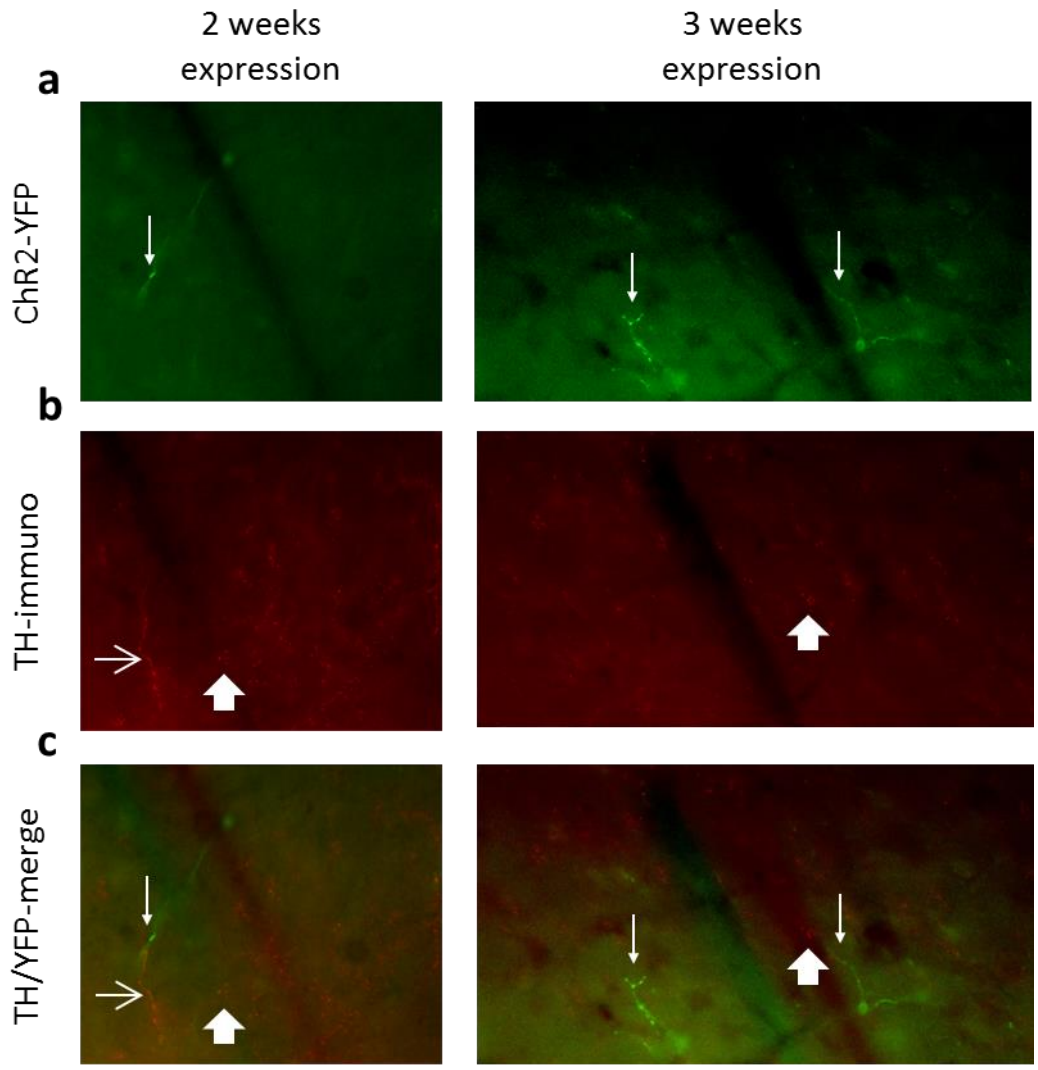

Figure 7.2 **Both dopaminergic and ChR2-CamKII expressing axons from VTA innervate Stratum Lacunosum-Moleculare of the hippocampus but dopaminergic axons do not express ChR2-CamKII.**

a) ChR2-YFP protein expression in axons in Stratum Lacunosum-Moleculare of the hippocampus (green), small vertical white arrows indicate axons. Left: animal sacrificed 2 weeks post-injection. Right: 3 weeks post-injection. **b**) anti-tyrosine-hydroxylase reactivity (red) in the same area of tissue, thin, horizontal white arrows indicate axons;,thick, vertical white arrows indicate groups of fluorescent puncta. Layout as in **a**). **c**) red and green images merged to show no overlap in fluorescence (yellow). Layout: as in **a**).

7.3.2 Both cell types project from VTA to hippocampus, but the populations do not overlap.

In hippocampal slices taken from the same animals, thin YFP-positive structures, identified as axons based on their sparse distribution and characteristic morphology, innervate stratum Lacunosum-Moleculare (figure 7.2a). Similarly axonal structures and large amounts of punctate staining (putative axonal terminals) are TH-positive in the same regions of the hippocampus (figure 7.2b). However, as with the neuronal cell bodies, there is no overlap in the fluorescence (figure 7.2c)

7.4 Discussion

7.4.1 Which neurons were transfected?

The expression of channelrhodopsin in cell bodies in the VTA (identified by the presence and characteristic distribution of TH positive cells and baso-medial location) of both animals, none of which co-express tyrosine hydroxylase, is strong evidence to suggest that this specific CaMKII promotor AAV vector does not transfect dopaminergic neurons. The VTA contains both GABAergic (Bonci and Malenka 1999; Koyama et al. 2005; Cohen et al. 2012; Tolu et al. 2013) and glutamatergic (Yamaguchi et al. 2007; Yamaguchi et al. 2011). GABAergic neurons in rat striatum and cortex do not express CaMKII (Benson et al. 1992; Jones et al. 1994; Liu and Jones 1996; Wang et al. 2013b), but those in rat cerebellum (Borodinsky et al. 2003) and nucleus accumbens (Liu et al. 2009c; Avalos-Fuentes et al. 2013) can – so it is unsure whether these could be GABAergic cells transduced. VTA glutamatergic cells express CaMKII throughout the brain, so these form a likely potential target for viral infection.

Given that there is clear innervation of the hippocampus by axons transfected with ChR2, then the transfected VTA cell types must be those that project to the hippocampus. There is no evidence to suggest a GABAergic projection to the hippocampus in the literature; there is evidence for both dopaminergic (Gasbarri et al. 1994a) and glutamatergic (Yamaguchi et al. 2011) innervation of the hippocampus from VTA. This is consistent with the results from this chapter – I have found TH-positive axonal innervation of the hippocampus, which could correspond to dopaminergic innervation from the VTA (or noradrenaline from the locus coeruleus, which also sends many projections to the hippocampus (Swanson et al. 1987), and non-TH-positive axons in very close proximity, suggesting they belong to the same fibre tract. I suggest that the results show ChR2 transfection of glutamatergic cells of the VTA, not dopaminergic cells, and their projections to the hippocampus. Although I did not test whether these projections could be functionally activated by light, this result shows that, in principle, it is possible to specifically transfect VTA inputs – up to and including the axonal terminals – to the hippocampus with channelrhodopsin.

7.4.2 Why were no dopaminergic neurons transfected?

It is possible to transduce dopaminergic neurons with adeno-associated viruses (AAV) such as used here (Oh et al. 2009; Bass et al. 2013), similarly CamKII can be used as a promotor for transgenic expression of channelrhodopsins (Land et al. 2014). So why did I observe no transfected dopaminergic cells? One possibility is that dopaminergic cells were transfected, but died before the animals' brains were sliced: the viral injection may be slightly cytotoxic, either through the immune response (Martino et al. 2011) or through protein overexpression in the infected cells. Dopaminergic cells are more vulnerable to cytotoxic stimuli than the surrounding cell types (Gonzalez-Hernandez et al. 2010) – hence

they may not have survived while the glutamatergic cells did. Another possibility, given that Oh et al. (2009) use AAVs to transfect dopaminergic neurons, is that the CaMKIIα promoter, the specific CaMKII subtype in this virus, is not in fact suited to transfecting dopaminergic neurons. Although there is evidence from cultured dopaminergic neurons to support CaMKIIα expression (Fog et al. 2006), other studies have found expression of other CaMKII subtypes, but not CaMKIIα (Kamata et al. 2006). Expression of CaMKIIα in dopaminergic brainstem nuclei regions as a whole is high (Erondu and Kennedy 1985; Ochiishi et al. 1998), consistent with the strong expression that I have seen, but my results suggest that either the particular vector I was using was ineffectual or that dopaminergic neurons are not amenable to transfection.

Had the transfection worked, it would still have been non-specific: any light flash to a slice with transfected VTA afferents would have stimulated both glutamate and dopamine release. Recently, a transgenic, tyrosine hydroxylase::Cre rat has been created in which transgenes can be expressed selectively and reliably in dopaminergic neurons (Witten et al. 2011) and has already been used to study learning (Steinberg et al. 2013) and depression (Chaudhury et al. 2013; Tye et al. 2013). Were I to try this experimental method again, I would choose this elegant system or, if possible, the TH-promotor AAV system (Oh et al. 2009) to transfect dopaminergic neurons.

7.5 Conclusion

Hippocampal afferents from the ventral tegmental area can be specifically transfected by midbrain viral injection – but these projections were not dopaminergic.

Chapter 8: General Discussion

In this final chapter I will discuss the overall findings from this thesis, the questions yet unanswered and possible ways to tackle them. I will then consider some methodological issues and discuss the physiological relevance of the effects of dopamine on astrocytes and other possible areas of astrocyte-dopamine interaction.

8.1 Dopamine triggers astrocyte calcium increases

The first, most consistent and least controversial observation made in this thesis is that dopamine can stimulate increased astrocyte calcium (Ca^{2+}) activity *in situ* (chapters 3, 4, 5), in agreement with the culture literature also describing such an increase (Parpura and Haydon 2000; Liu et al. 2009a; Vaarmann et al. 2010; Requardt et al. 2012). In probing the mechanisms of this Ca^{2+} increase, it becomes apparent how varied the potential routes of dopamine action on astrocytes are – a problem I believe underlies much of the dopamine literature in neurons as well. I have provided evidence for D1-type receptor, D2-type receptor and IP_3 receptor control of dopamine-induced astrocytic Ca^{2+} increase, as well is modulation through monoamine oxidase and purinergic receptor activity. One explanation is activation of an astrocytic D1-D2 heteromer (figure 8.1), a receptor type that is known to exist on neurons (Hasbi et al. 2011), that exerts its effects through PLC activation and IP_3 release. The best test for this hypothesis would be to image astrocyte Ca^{2+} upon challenge with SKF83959, the specific D1-D2 heterooligomer agonist used by the group championing this research (Hasbi et al. 2009), with a large Ca^{2+} increase (and no decrease) predicted.

How do my results compare to the literature? The most reliable of the myriad results reported in cultures is that stimulation of astrocytes with dopamine itself produces

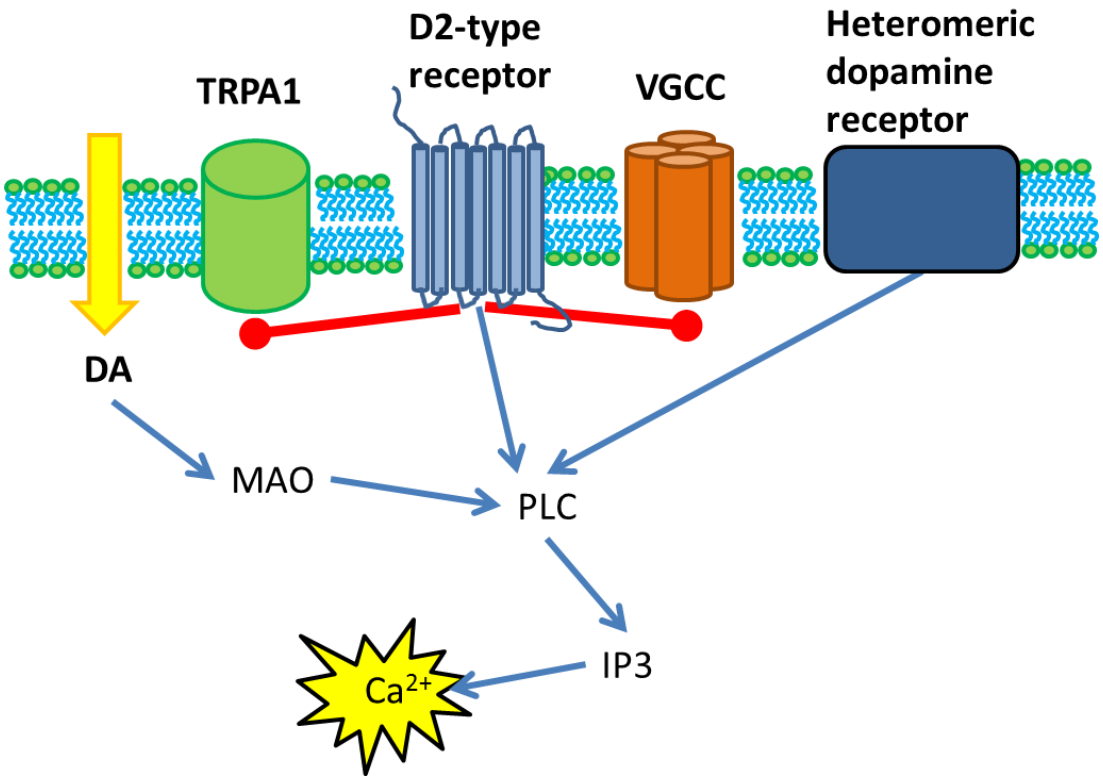

Figure 8.1 Possible dopaminergic signalling pathways in astrocytes

Heteromeric dopamine receptors activate PLC which produces IP_3 and facilitates release of Ca^{2+} from intracellular stores; DA breakdown by monoamine oxidase amplifies the PLC response through lipid peroxidation; activation of the D2-type receptor can decrease resting calcium levels, possibly through voltage-gated calcium channel or TRPA1 channel inhibition.

---

overall cytosolic Ca^{2+} concentration increase. Unfortunately, the pharmacology reported here is inconclusive, although a potential unifying mechanism based on my results is described in figure 8.1. The unusual sensitivity of the dopaminergic increase to both D1 and D2-type receptor blockers (chapter 4) has not been reported in the previous culture studies. It is possible that culture conditions known to change expression profiles of another monoamine receptor, the 5-HT receptor (Kimelberg et al. 1997), could be having similar, unique, actions on astrocytes cultured in different labs. An interesting result

reported here that could shed light on this culture/slice difference, was the striking response difference between astrocytes of the SR and the SLM. Not only is the functional relevance of this worth investigating, but if such differences are visible between two very similar populations of astrocytes, the massive differences seen in culture studies could be explained by slight differences in astrocyte harvesting or culturing technique.

An interesting result in the light of recent reports is the inhibitory effect of MAOb blockade on the dopamine-induced Ca^{2+} increase, as reported first by Vaarmann et al. (2010). This, coupled to reports of astrocytic D1-mediated control of NAD^+/NADH ratio (Requardt et al. 2012), is compatible with an important role for reactive oxygen species (ROS) in the amplification of intracellular Ca^{2+} signals. Lipid peroxidation activates PLC and triggers intracellular IP_3 increase, a previously reported route of ROS-mediated astrocytic Ca^{2+} increase (Vaarmann et al. 2010) that is consistent with selegline sensitivity and possible 2-APB sensitivity of the dopamine-induced astrocye Ca^{2+} increase reported here (chapter 3). But another, as yet unexplored mechanism of ROS induced Ca^{2+} signalling in astrocytes, is through TRP channel activation. TRPA1 (Shigetomi et al. 2011) and TRPV4 (Dunn et al. 2013) activation has been shown to mediated astrocyte calcium increase, and TRP channels are sensitive to oxidative stress (Naziroglu 2012). As a further experiment, imaging astrocyte Ca^{2+} and selective blockade of either of these TRP channel types during dopaminergic stimulation could reveal a new, ROS-mediated form of astrocyte calcium signalling.

8.2 Dopamine triggers astrocyte calcium decreases

The second major finding, one that I believe is the most interesting and most worthy of further investigation, is that dopamine can reliably induce decreases in astrocytic cytosolic Ca^{2+} concentration. There has been only one other report in the literature of a

pharmacologically tractable astrocyte Ca^{2+} decrease (Shigetomi et al. 2011) and no report of a dopamine-mediated Ca^{2+} decrease – the question is: what is the function of this Ca^{2+} drop? A tantalizing prospect comes from the methods of this thesis: the Ca^{2+}-clamp protocol (chapters 2, 6) was found to block specifically dopamine-induced Ca^{2+} decreases, but not increases. I found no effect of the clamp on dopaminergic inhibition of SLM synapses, but the clamp is capable of inhibiting both LTP (Henneberger et al. 2010) and LTD (Min and Nevian 2012). Given dopamine's well publicised involvement in LTP induction and maintenance in the hippocampus (Frey et al. 1990; Li et al. 2003), it is exciting to speculate that clamp of a dopamine-induced Ca^{2+} decrease (dopamine released from the LTP-inducing HFS) that appears concomitantly with the observed HFS-induced Ca^{2+} increase could play a part in the Ca^{2+}-mediated inhibition of LTP. TRPA1 blockade decreases astrocyte basal calcium levels and HFS-induced LTP in CA1 of the hippocampus (Shigetomi et al. 2013); I have shown that blockade of D1/5 receptors also decreases basal calcium – in the presence of dopamine (chapter 4) – could this be an explanation for the inhibitory effects of D1/5 receptor blockade on LTP induction (Frey et al. 1991)? If so, one might expect selective inhibition of the astrocytic dopamine-induced Ca^{2+} decrease, but not the Ca^{2+} increase, seen upon Ca^{2+}-clamp, to paradoxically preserve LTP in the presence of simultaneous dopamine and Ca^{2+}-clamp. That said, the multiple possible forms of calcium signalling in astrocytes (spatially and temporally – Rusakov et al. 2014) may indicate that simply raising global Ca^{2+} (as dopamine has been shown to do) does not activate the correct Ca^{2+}-sensitive astrocytic machinery, as in the case of Fiacco et al. (2007). This could be easily tested by attempting to rescue LTP induction during Ca^{2+}-clamp with dopamine application. Apomorphine has recently been shown to inhibit TRPA1 channels in high concentrations (Schulze et al. 2013), hence another prediction would be that apomorphine dose dependently inhibits hippocampal LTP through decrease of astrocyte basal calcium levels – a theory that would be relatively simple to test.

8.3 Dopamine, astrocytes and LTP.

In the hippocampus, dopamine is most often linked to LTP induction and maintenance (Frey et al. 1991; Matthies et al. 1997; Li et al. 2003). Similarly, astrocytes have been convincingly shown to mediate LTP induction (Henneberger et al. 2010). Therefore it is my lasting regret that I have not managed to test for a possible interaction between the two in this process. To do so one would have to be able to manipulate dopaminergic signalling in astrocytes without interfering with the internal Ca^{2+} state that allows them to gate LTP. The most elegant solution would be astrocyte-specific knockout (or viral knockdown) of either D1 or D2 receptors. This would block the dopamine induced Ca^{2+} increase, but leave the decrease intact in a D2-KO sensitive fashion – dopaminergic LTP modulation could then be probed between control and knockout animals. Such animals could also be used to probe known dopamine-sensitive behaviours. Failing these, admittedly fancy, techniques, one could replace the astrocytically-derived d-serine (release of which allows LTP induction) with bath applied d-serine, clamp astrocytic Ca^{2+} (or use FAC) and probe LTP-induction between healthy astrocyte and clamped/poisoned astrocyte slices. There are some potential problems with this approach: the correct concentration of D-serine to add to the perfusion solution to provide adequate NMDAR co-agonism without complete saturation (and hence overstimulation) of the receptor is not known; it may also be the case that an astrocytic role in dopaminergic modulation of LTP works through modulation of d-serine release.

8.4 Tonic dopamine action in the hippocampus

An intriguing, unexpected result of chapter 6 is the astrocyte-modulated inhibition of baseline synaptic transmission. This result has not been previously documented in the literature, although potential mechanisms for it have (Hsu 1996; Otmakhova and Lisman 1999). One possible reason for this information blackspot could be that an increase requires dual blockade of both D1/5 and D2/3 receptors; if true, the culprit could be a dopamine receptor heteroligomer – although these receptors have yet to be described and characterized in the hippocampus. Two simple experiments could shed light on the DR-blockade induced baseline release probability increase: addition of SCH23390 and sulpiride without prior TBS, to ensure no complicating interaction and addition of SKF83959 to baseline Schaffer collateral responses to witness an increase in fEPSP slope. I saw no clear effect of blockade of tonic dopaminergic signalling on astrocyte calcium activity (See chapters 3 and 4), although a may have had I used a calcium indicator more sensitive in the resting calcium range (e.g. OGB-1). If astrocytes are involved in tonic dopaminergic modulation of synaptic transmission, one would expect some sort of intracellular signalling linking sensation of dopamine to release of inhibitory gliotransmitter. It is possible that this is not Ca^{2+} or that it works through a different intracellular signalling cascade (e.g. cAMP signalling). I would also be interested to see the effect of simultaneous application of both DR blockers on NMDAR-mediated currents – any effect could indicate a role for astrocytes in baseline NMDAR modulation through dopamine.

8.5 Imaging astrocytic Ca^{2+} signals.

This thesis makes use of two popular Ca^{2+}-imaging techniques: bulk AM-dye loading and cell-impermeable dye loading through a patch-pipette: I will now briefly discuss the merits and drawbacks of each technique. AM-dyes have many advantages: they have a

simple loading protocol (see chapter 2); the technique is high-throughput – multiple cells can be imaged at a time and viable cells can be identified quickly. Perhaps the greatest advantage of bulk-loading is that cells can be imaged with no physical interference – although this is a weakness in another sense: it offers no specific control over the intracellular milieu (unlike whole-cell patch-clamp). There are, however some serious drawbacks: the signal to noise ratio drastically decreases as AM-dyes load non-specifically: astrocytes, neurons and other glial cells will take up the dye. This necessitates addition of astrocyte-specific markers to ensure data is gathered from the correct cell population. Such cell type-specific staining can be achieved with genetically encoded fluorescent proteins under the control of astrocyte-specific promoters (e.g. GFAP, S100β), fluorescent dyes that label astrocytes specifically (Nimmerjahn et al. 2004) or with post-hoc immuncytochemsitry. The necessity of labelling cells is problematic – genetic labelling can only be done in certain transgenic animals (mice are the only mammals for which these methods are widespread, although some transgenic rats are starting to be used (Witten et al. 2011)), or over a small area when virally transfecting non-transgenic animals (the act of injection can also cause gliosis, changing the nature of astrocytic physiology). SR101 is the most commonly used astrocyte-specific fluorescent dye, but it can induce neuronal plasticity change (Kang et al. 2010). Simply being able to identify cells post-hoc is clearly suboptimal. But perhaps most importantly when considering the use of AM-dyes, astrocytes *in situ* have huge numbers of very fine processes that make up most of their volume (Bushong et al. 2002; Halassa et al. 2007) and display great variety and number of Ca^{2+} events that are uncoupled from the soma (Di Castro et al. 2011) – but these fine processes cannot be resolved with AM-dyes (figure 2c). Studies using these dyes can often report Ca^{2+} activity only from the soma and the very large adjacent primary processes (e.g. Porter and McCarthy, 1996) (see chapter 2): but it is vital to understand the Ca^{2+} activity in the fine processes, as it is at the fine processes, enwrapping individual synapses, that local

release of neurotransmitter is most likely to trigger a Ca^{2+} response (Rusakov et al. 2011) and indeed local calcium signalling may form a parallel information processing pathway (Rusakov et al. 2014).

Whole-cell patch clamp offers a clear solution to this problem. This technique greatly increases the signal to noise ratio and allows imaging of the free Ca^{2+} activity in the finer processes. However this method can also lead to artefacts in ascertaining intracellular free Ca^{2+} concentration – mechanical stimulation from the pipette tip can cause Ca^{2+} transients (Charles et al. 1991), the intracellular milieu is dialysed (an effect that the Ca^{2+}-clamp takes advantage of) and the widely used 2-photon excitation imaging systems used for intact tissue still cannot image the smallest astrocytic compartments – although new fluorescent techniques, PALM, STORM and STED, can provide increased spatial resolution at the cost of temporal resolution and laser light intensity increase, respectively. Genetically encoded Ca^{2+} indicators may soon become the Ca^{2+} reporter of choice (Shigetomi et al. 2011; Tong et al. 2013) given that no patch-clamping is necessary – and they are of clear use for *in* vivo studies (Atkin et al. 2009) and TIRF studies of Ca^{2+} microactivity in cultured astrocytes (Shigetomi et al. 2011) – but their current lack of temporal sensitivity (Yamada and Mikoshiba 2012) and heterogenous subcellular expression of the proteins (concentrated in organelles) makes their current incarnation suboptimal for slice work.

8.6 Analysis of astrocyte Ca^{2+} Signals

A major challenge in understanding astrocyte Ca^{2+} signalling lies in the huge variety of Ca^{2+} activity they can display and in the heterogeneity of their response to a given stimulus (Bernardinelli et al. 2011). Unlike neurons, whose stereotyped output – the action potential – is a physiological reference point to judge the efficacy of a given stimulation, astrocytes have no clear 'spike'-like signal. Hence judging the purpose, relative magnitude

or physiological relevance of a stimulus by its Ca^{2+} response is challenging and this has led to confusion in the literature. Figure 1.3 shows some examples of the astrocytic Ca^{2+} signals that have been published: clearly there is great spatial, temporal and magnitudal variety, even between neighbouring astrocytes in the same preparation, and there is no consensus as to either what constitutes a stereotypical astrocytic Ca^{2+} signal, or what is a physiologically relevant Ca^{2+} increase to experimentally evoke when attempting to stimulate a change in neuronal activity.

In vivo recording of spontaneous (Hirase et al. 2004; Takata and Hirase 2008; Kuchibhotla et al. 2009; Sasaki et al. 2011) and evoked astrocyte Ca^{2+} activity (Gourine et al. 2010; Takata et al. 2011) have shed some light on physiologically relevant astrocytic Ca^{2+} signals, although spontaneous activity is still highly variable and difficult to quantify (but see Sasaki et al. and Takata and Hirase). Two caveats of the current *in vivo* literature: firstly, all studies have been done under anaesthetic and secondly, current imaging technology only allows accurate fluorescent measurement from astrocyte somata *in vivo* and at with low temporal resolution (seconds). Not only do astrocytes display large amounts of Ca^{2+} activity in their finer processes – which may have more relevance to synaptic physiology (Rusakov et al. 2014) – but also that their Ca^{2+} activity can occur on a timescale of hundreds of milliseconds and less.

These difficulties have led many studies to simply describe astrocytic Ca^{2+} qualitatively – as stimulation of an obvious change in Ca^{2+} concentration or dynamics. Attempts in the literature to apply a rigorous quantification of Ca^{2+} activity are always reliant on either an arbitrary numerical definition of an 'event', or manual selection of 'events', which amounts to the same thing: Takata et al. (2012) quantify their evoked Ca2+ 'surges' as beginning when change in fluorescence ($\Delta F/F_0$) exceeds 50% increase from a baseline (defined, arbitrarily, as the mean of the lower 2/3s of the fluorescence intensity

histogram) and ending when $\Delta F/F_0$ drops beneath 2SD of the baseline – again an arbitrary value; di Castro et al. (2011) quantify their spontaneous activity by frequency, rise time and duration of events – but the threshold for classification of an event in the fluorescence signal is 'operator' chosen; Tanaka et al. (2013) compare the integral and duration of $\Delta F/F_0$ over time of each event, after a DHPG (mGluR1 agonist) puff, but again the events measured are manually selected.

The highly non-stereotyped responses to stimulation often recorded in this thesis have led to my choice of simple, impartial forms of fluorescence analysis: average $\Delta F/F_0$ over a given time; relative 'oscillatory activity' change from baseline; differences in $\Delta F/F_0$ frequency distribution between baseline and presence-of-dopamine epochs. Although this risks losing some detail of the signal and possibly some biological effect that could be found in individual event analysis (Tanaka et al. 2013), it provides a solid, quantitative base upon which to report any overall change in astrocytic free Ca^{2+} concentration.

8.7 Caveats of studying dopaminergic activity in slice

A serious problem facing all previous *in vitro* studies, and the experiments from this thesis, is the nature of the dopaminergic stimulation. Topical application of dopamine, or dopamine agonists, is by far the most commonly used way of stimulating cells dopaminergically *in vitro*: this is because dopaminergic innervation of forebrain regions is sparse so electrically stimulated release is not possible without resorting to overly powerful stimulation protocols (Frey et al. 1989). Unfortunately, my brief foray into optogentics, with the aim of overcoming this problem, was fruitless, preventing me from solving the problem. Dopamine is released phasically in response to environmental stimulus, but it also maintains a tonus throughout brain tissue (consistent with my results in chapter 6) – the prolonged addition of dopamine, or dopamine agonists, to the slice (or culture) perfusion

solution creates a kind of 'dopamine clamp' on the recorded cellular activity. Whereas this would not be a great problem if the pharmacology was simple, given the antagonistic nature of the two dopamine receptor types and the non-receptor-mediated effects of dopamine, the summation of all of these activities that occurs over this prolonged stimulation time makes untangling the causes especially hard. Coupled to this, we cannot be sure of the physiological concentration of dopamine reached at any time in living brain tissue – as dopamine receptors have different affinities, this would drastically alter the overall effect of dopamine in the extracellular space (given all of these potential problems, it is interesting that application of only D1 or D2 antagonists can fully block the powerful Ca^{2+} response to dopamine – this suggests that dopamine receptors are strongly linked to the workings of astrocytic Ca^{2+}). The most pressing of all further experiments on this subject would be the recording of astrocytic Ca^{2+} response to optogenetic stimulation of the dopaminergic innervating input, using TH-CRE rats, or the AAV TH-promoter described by Oh et al. (2009). Without these tools, it would also be possible to use high-frequency stimulation (HFS) protocols (such as used by Frey et al. 1989) during the blockade of ionotropic and metabotropic glutamate, GABA, endocannabinoid, serotonin, acetylcholine and adrenergic receptors to record only the dopamine receptor mediated response to a more physiological release of dopamine.

Another factor to take into account is the age of animals used in this thesis – animals were sacrificed at post-natal day 21-25: there is some evidence to suggest that (in the prefrontal cortex) dopamine changes its effects throughout development – at p12-20, dopamine triggers a D2R-dependent inhibition, one which is smaller at p30-40 and gone at p70-100 (Paul and Cox 2013). Hence it is possible that astrocytes also exhibit developmental changes in dopamine sensitivity or involvement in dopaminergic function – repetition of the above experiments in adult slices would address this.

8.8 Physiological relevance

There is a body of evidence that questions the relevance of astrocytic Ca^{2+} transients, such as the ones I have catalogued here in response to dopamine, to astrocyte-neuron communication (Fiacco et al. 2007; Agulhon et al. 2010). Given the large, complex and long-lasting nature of the astrocyte Ca^{2+} responses to dopamine, the total lack of observed effect on neurons (both in this thesis and the literature) begs the question: how can astrocyte Ca^{2+} activity be so radically changed and yet there be no visible effect on neuronal activity? Previous studies have reported LTP induction (Perea and Araque 2007) and glutamate release (Wang et al. 2013a) upon triggering of similar levels of Ca^{2+} increase – where was this in my recordings, or throughout the hippocampal dopamine literature? It could possibly be due to activation of separate Ca^{2+} signalling pathways, perhaps it was overstimulation of intracellular Ca^{2+} activity. But the results best fit with the observations that Ca^{2+} increases in astrocytes are not necessarily a marker for neuron-glia interaction or necessarily mediate any effect on local neuronal activity. A conceptual difference is evolving in the literature between widespread, whole-cell astrocyte Ca^{2+} increases and localized Ca^{2+} dynamics (Rusakov et al. 2014). It is clearly possible to stimulate widespread Ca^{2+} increase in astrocytes with dopamine – the challenge is now to modulate localized calcium dynamics; the limiting factor here (as mentioned in section 8.7) is the method of dopaminergic stimulation. This is not to say that large-scale Ca^{2+} transients have no effect on astrocyte dynamics – there are many physiological pathways not investigated in this thesis – i.e. the possibility of longer term change of their Ca^{2+} oscillation dynamics.

8.9 Astrocytes and dopamine: Unexplored avenues

Dopamine has actions on astrocytes that are not mediated by intracellular Ca^{2+} – and these alternative signalling cascades could prove more important in dopaminergic modulation of astrocyte activity (and hence potentially neuronal activity). Classically, dopamine receptors are defined by their control of the cAMP signalling pathway, control which they exert in astrocytes (Zanassi et al. 1999; Li et al. 2006), and this could be a fruitful area of investigation, given that cAMP can control capacitative Ca^{2+} entry in astrocytes (Wu et al. 1999), change aquaporin expression (through PKA activation)(Yamamoto et al. 2002) and has been reported to control astrocytic membrane potential (Bolton et al. 2006) – although if this happened upon dopamine stimulation I would expect to have seen it in the astrocytes I patched and I did not. Consistent with a role for astrocytic cAMP activity, fluorocitrate poisoning has been shown to decrease overall cAMP levels in cortex (Stone and John 1991). Other dopamine signalling pathways that have been found in astrocytes – αβcrystallin (Shao et al. 2013), FGF-2 (Reuss and Unsicker 2001) – would also be interesting to study. The dopaminergic agonist apomorphine has been reported to decrease S100β secretion from astrocytes (Nardin et al. 2011) and increased metabolic stress has been reported to increase S100β secretion (Gerlach et al. 2006) – could this be a TRP channel mediated effect as discussed above? Also, as S100β is Ca^{2+} buffer there may be effects of dopamine on astrocyte control of extracellular Ca^{2+} concentrations (or longer term intracellular astrocyte Ca^{2+} buffering) which, given the recent description of extracellular Ca^{2+} as a signalling molecule (Torres et al. 2012), is an exciting potential area for research.

Another fascinating question is whether astrocytes play a role in the release of dopamine. In the striatum, astrocytes have been reported to control dopamine release through their release of (release inhibiting) kynurenic acid (Wu et al. 2007). In the hippocampus, NMDAR activity modulates extracellular dopamine concentration (Schroder

and Reymann 1990; Whitton et al. 1994; Chaki et al. 1998) and astrocytes modulate NMDAR activity (Henneberger et al. 2010) through d-serine release – d-serine has been shown to be important in some dopamine-mediated behaviour (Horio et al. 2012; Hammond et al. 2013). Hence it seems likely that astrocytes exert some level of control over the concentration of dopamine in the hippocampus. One could use cyclic voltammetry to compare hippocampal dopamine levels in astrocyte-IP_3 KO mice with wild types. Another, unusual, possibility is that astrocytes could produce dopamine themselves – d-amino oxidase, expressed in astrocytes (Urai et al. 2002), can break down D-DOPA to form dopamine (Kawazoe et al. 2007), although this would presuppose the presence of D-DOPA in hippocampal astrocytes.

A final unexplored area in this thesis is the prefrontal cortex (PFC): there is plenty of research showing an important role for astrocytes in the cortex (Reyes and Parpura 2008; Perea et al. 2014) and dopamine exerts strong modulation of neuronal activity in the PFC (Schultz 2001) – given the difference in dopamine response in astrocytes from the same hippocampal zone (chapter 4, 5), one could surely expect some novel and exciting dopamine response from PFC astrocytes.

8.10 Conclusion

This thesis adds to the expanding literature detailing astrocytic calcium increases in response to dopamine. It details a dopamine receptor mediated increase in astrocytic calcium *in situ*, and reveals a novel D2-type receptor mediated astrocytic calcium response – a cytosolic concentration decrease. However it can provide little evidence to suggest that astrocytic dopaminergic signalling is involved in hippocampal synaptic transmission.

Chapter 9: Supplementary figures

9.1 Supplementary figures

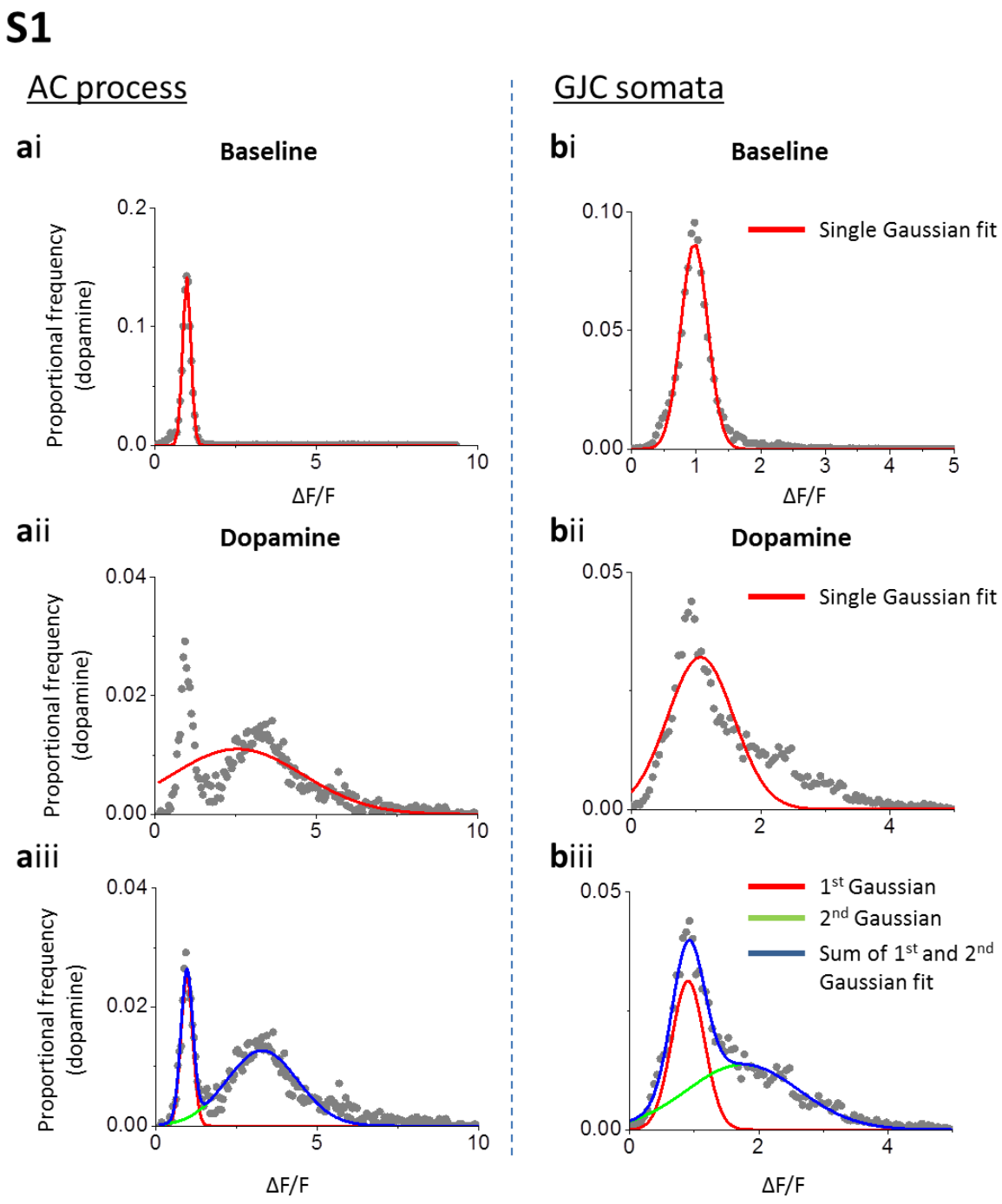

Figure S1 Gaussian fits for 100µM dopamine application in Figure 2

ai) Baseline $\Delta F/F_0$ proportional distribution and fitted single Gaussian curve in AC processes; grey circles indicate recorded data, red line indicates modelled data. **a**ii) as in **a**i) but in dopamine. **a**iii) double Gaussian fit of dopamine proportional $\Delta F/F_0$ distribution; grey circles indicate recorded data,

red line indicates 1st of 2 modelled gaussian curves, green line indicates 2nd of 2, blue line indicates sum of 1st and 2nd Gaussians, giving modelled distribution. **b**) As in **a**) but recordings from GJC somata. Data taken from figure 2c, d.

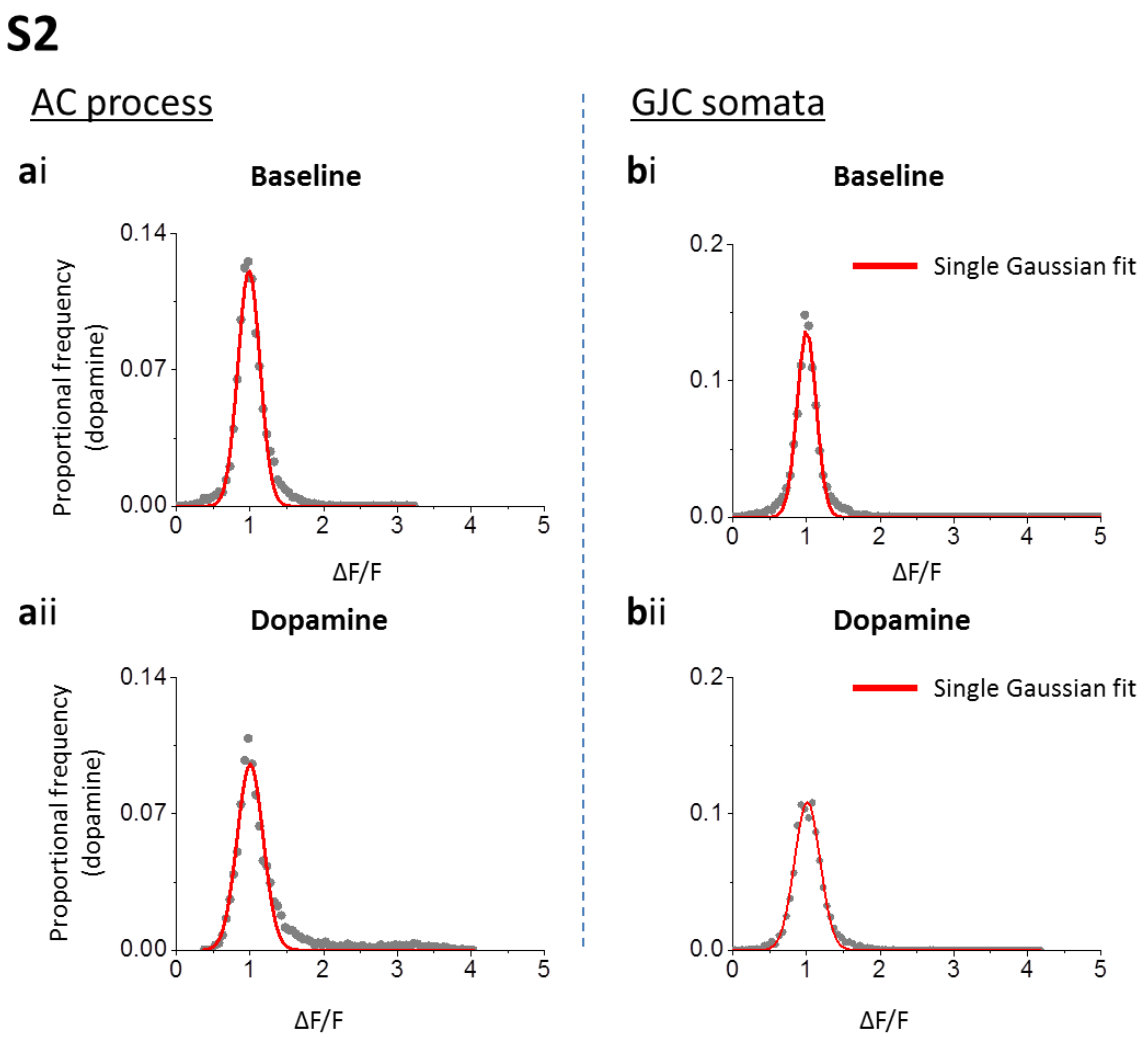

Figure S2 Gaussian fits for 10µM dopamine application in Figure 3a

ai) Baseline $\Delta F/F_0$ proportional distribution and fitted single Gaussian curve in AC processes; grey circles indicate recorded data, red line indicates modelled data. **a**ii) as in **a**i) but in dopamine. **b**) As in **a**) but recordings from GJC somata. Data taken from figure 3a.

S3

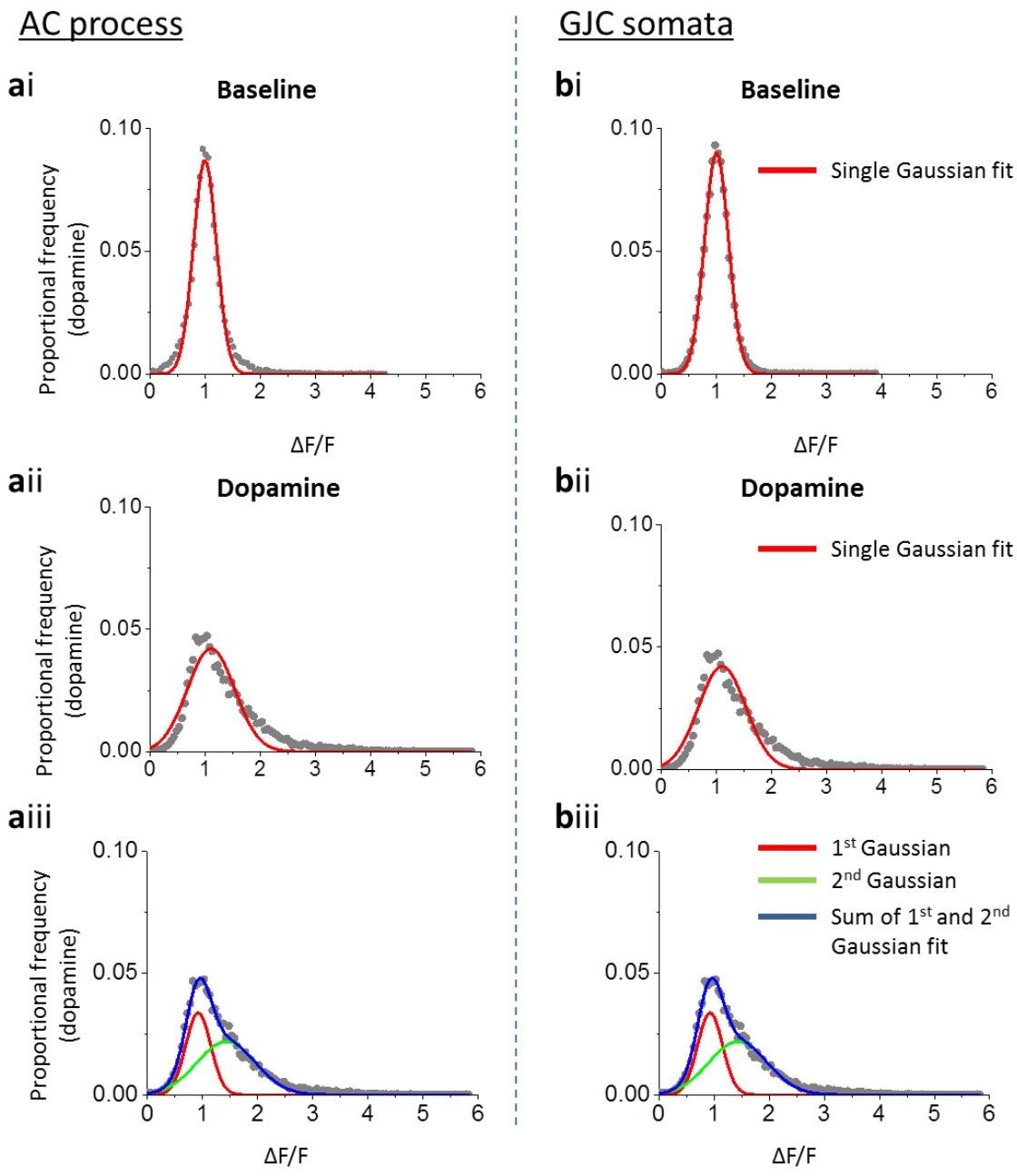

Figure S3 Gaussian fits for 20µM dopamine application in Figure 3b

ai) Baseline $\Delta F/F_0$ proportional distribution and fitted single Gaussian curve in AC processes; grey circles indicate recorded data, red line indicates modelled data. aii) as in ai) but in dopamine. aiii) double Gaussian fit of dopamine proportional $\Delta F/F_0$ distribution; grey circles indicate recorded data, red line indicates 1st of 2 modelled gaussian curves, green line indicates 2nd of 2, blue line indicates sum of 1st and 2nd Gaussians, giving modelled distribution. b) As in a) but recordings from GJC somata. Data taken from figure 3b.

S4

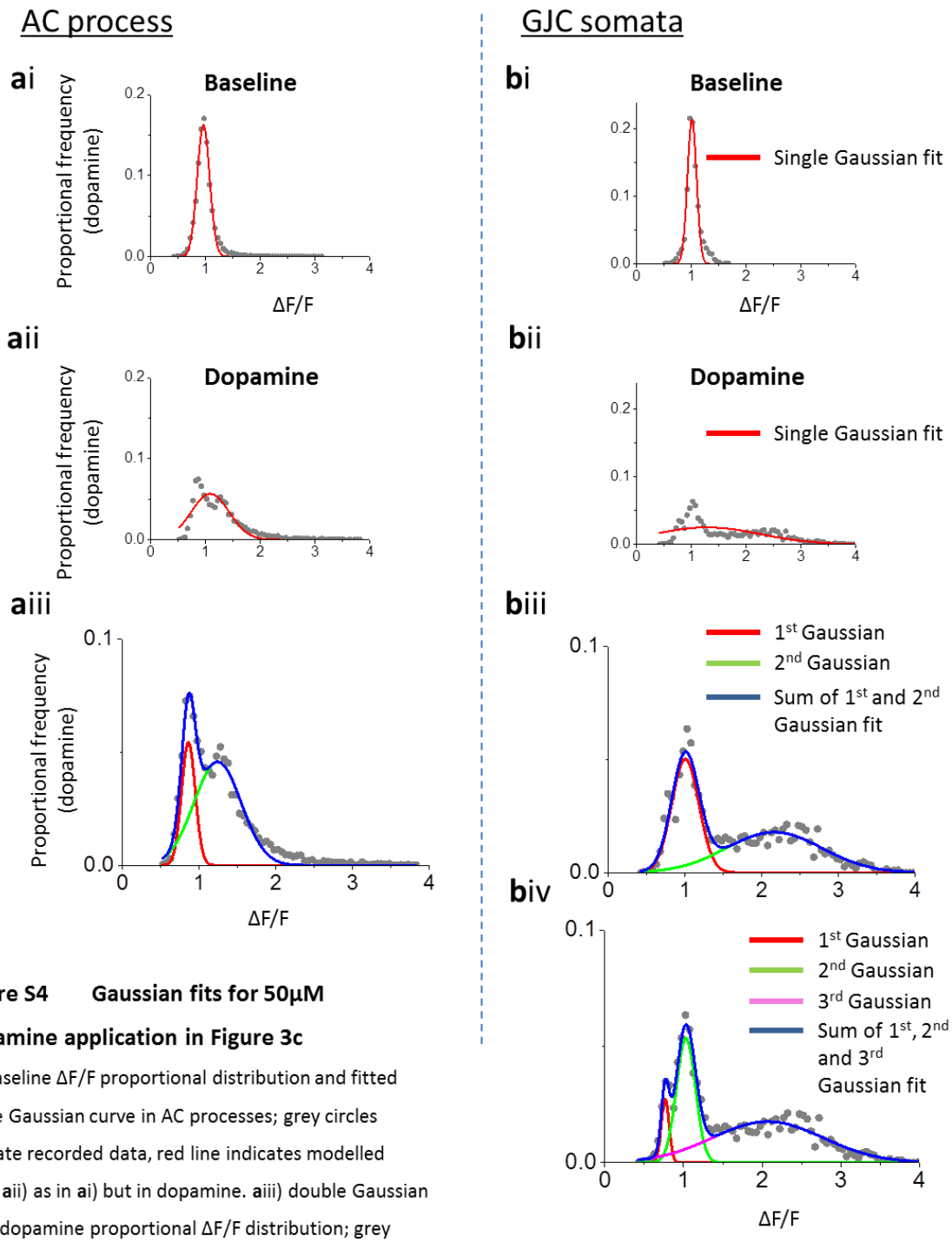

Figure S4 Gaussian fits for 50µM dopamine application in Figure 3c

ai) Baseline ΔF/F proportional distribution and fitted single Gaussian curve in AC processes; grey circles indicate recorded data, red line indicates modelled data. **a**ii) as in **a**i) but in dopamine. **a**iii) double Gaussian fit of dopamine proportional ΔF/F distribution; grey circles indicate recorded data, red line indicates 1st of 2 modelled gaussian curves, green line indicates 2nd of 2, blue line indicates sum of 1st and 2nd Gaussians, giving modelled distribution. **b**) As in **a**) but recordings from GJC somata. **b**iv) triple Gaussian fit of dopamine proportional $\Delta F/F_0$ distribution; magenta line indicates 3rd modelled gaussian curve. Data taken from figure 3c.

S5

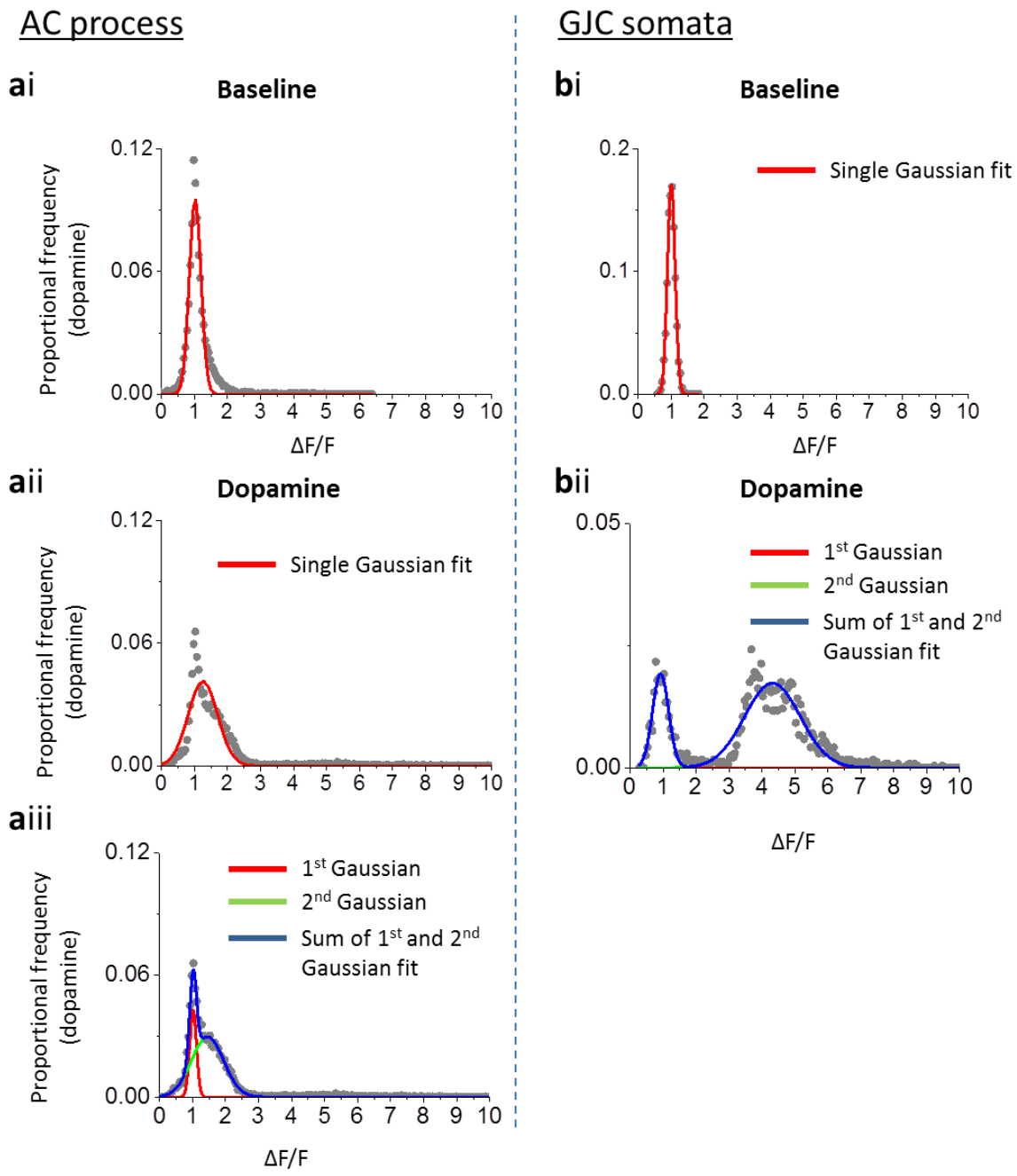

Figure S5 **Gaussian fits for 100µM dopamine application during neuronal blocker cocktail in Figure 4a**

ai) Baseline $\Delta F/F_0$ proportional distribution and fitted single Gaussian curve in AC processes; grey circles indicate recorded data, red line indicates modelled data. **a**ii) as in **a**i) but in dopamine. **a**iii) double Gaussian fit of dopamine proportional $\Delta F/F_0$ distribution; grey circles indicate recorded data, red line indicates 1st of 2 modelled gaussian curves, green line indicates 2nd of 2, blue line indicates

sum of 1st and 2nd Gaussians, giving modelled distribution. **b**) As in **a**) but recordings from GJC somata. Data taken from figure 4a.

S6

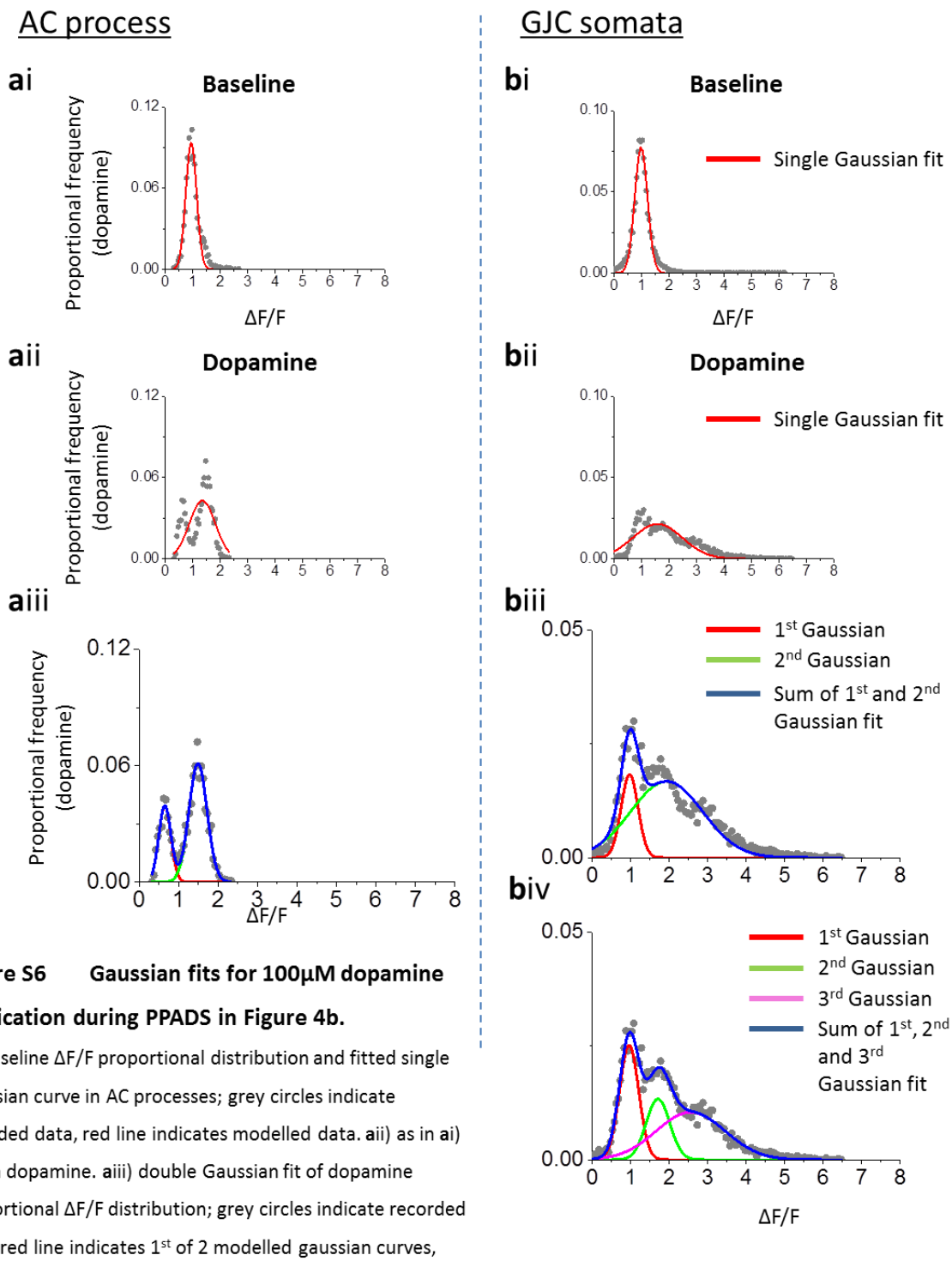

Figure S6 Gaussian fits for 100µM dopamine application during PPADS in Figure 4b.

ai) Baseline ΔF/F proportional distribution and fitted single Gaussian curve in AC processes; grey circles indicate recorded data, red line indicates modelled data. **a**ii) as in **a**i) but in dopamine. **a**iii) double Gaussian fit of dopamine proportional ΔF/F distribution; grey circles indicate recorded data, red line indicates 1st of 2 modelled gaussian curves, green line indicates 2nd of 2, blue line indicates sum of 1st and 2nd Gaussians, giving modelled distribution. **b**) As in **a**) but recordings from GJC somata. **b**iv) triple Gaussian fit of dopamine proportional ΔF/F distribution; magenta line indicates 3rd modelled gaussian curve. Data taken from figure 4b.

S7

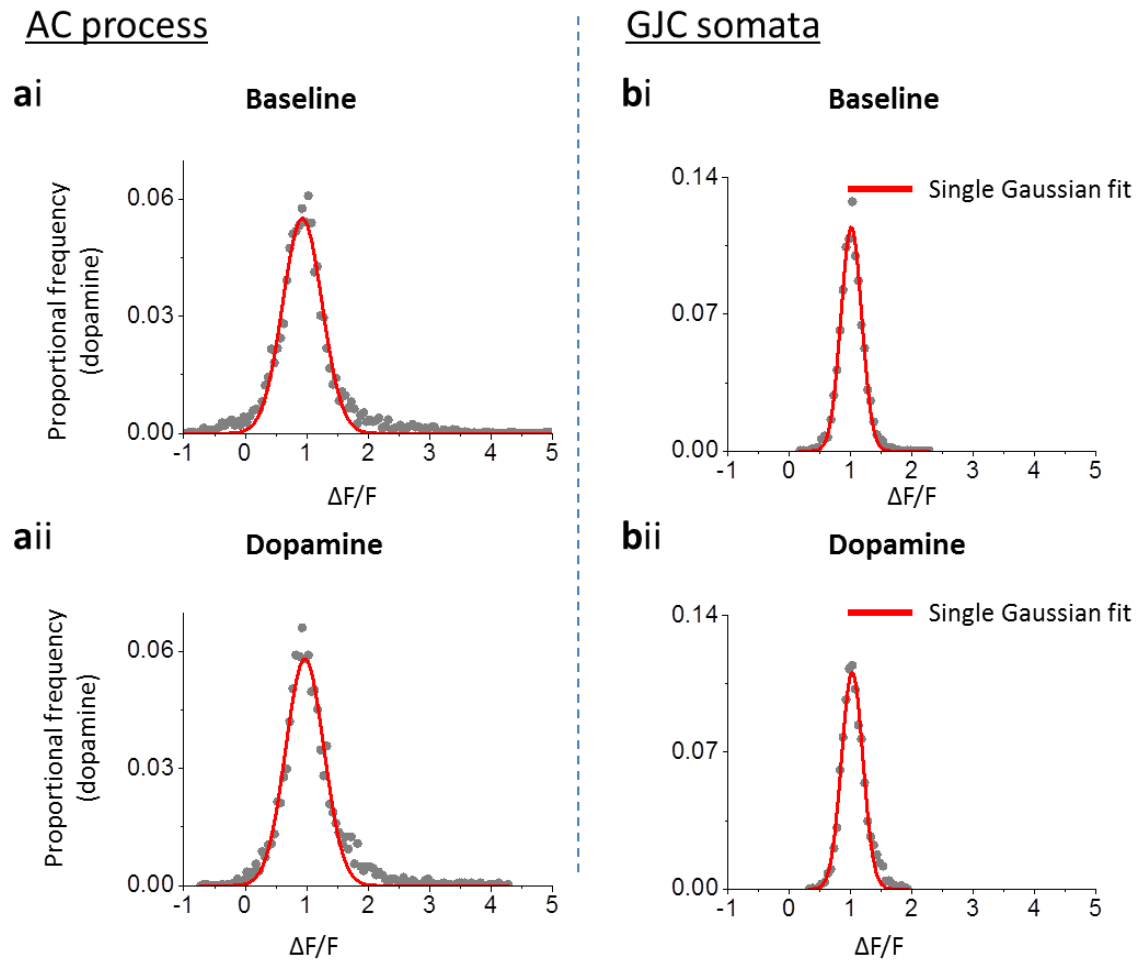

Figure S7 **Gaussian fits for 100µM dopamine application during dopamine receptor blockerade in Figure 4c**

ai) Baseline $\Delta F/F_0$ proportional distribution and fitted single Gaussian curve in AC processes; grey circles indicate recorded data, red line indicates modelled data. **a**ii) as in **a**i) but in dopamine. **b**) As in **a**) but recordings from GJC somata. Data taken from figure 4c.

S8

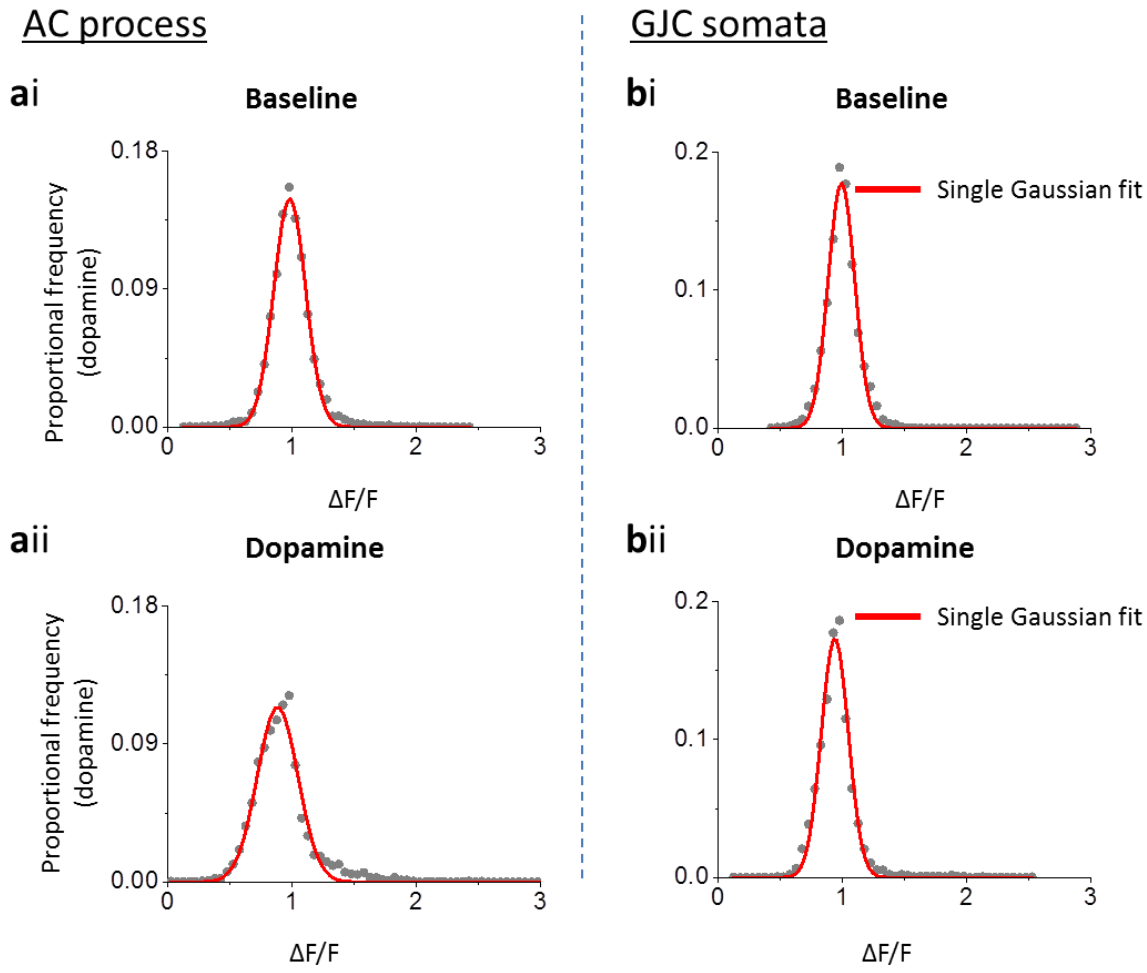

Figure S8 **Gaussian fits for 100µM dopamine application in the presence of 10µM SCH23390 Figure 5a**

ai) Baseline $\Delta F/F_0$ proportional distribution and fitted single Gaussian curve in AC processes; grey circles indicate recorded data, red line indicates modelled data. **a**ii) as in **a**i) but in dopamine. **b**) As in **a**) but recordings from GJC somata. Data taken from figure 5a.

S9

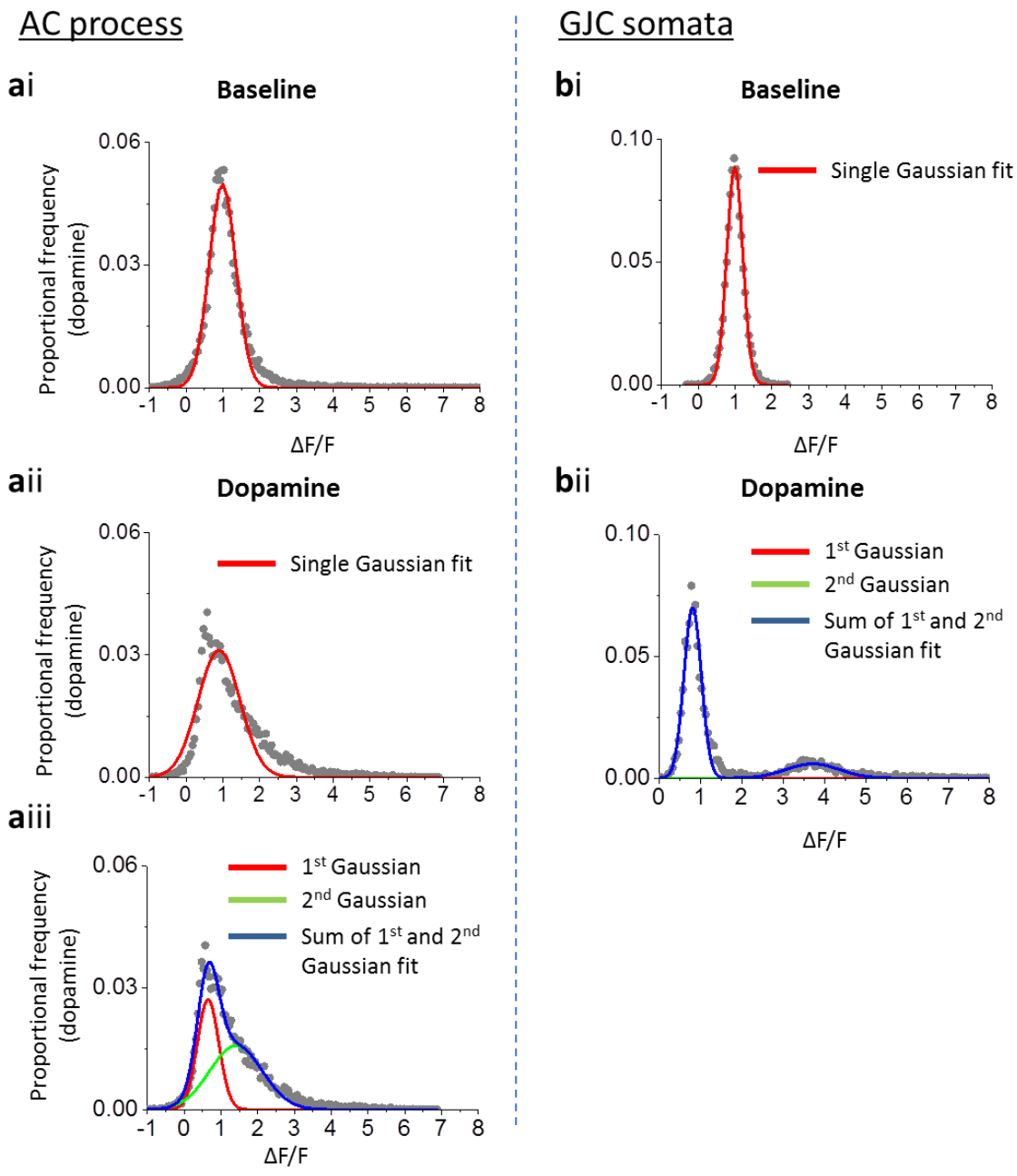

Figure S9 **Gaussian fits for 100µM dopamine application during 5µM SCH 23390 in Figure 5b**

ai) Baseline $\Delta F/F_0$ proportional distribution and fitted single Gaussian curve in AC processes; grey circles indicate recorded data, red line indicates modelled data. **a**ii) as in **a**i) but in dopamine. **a**iii) double Gaussian fit of dopamine proportional $\Delta F/F_0$ distribution; grey circles indicate recorded data, red line indicates 1st of 2 modelled gaussian curves, green line indicates 2nd of 2, blue line indicates sum of 1st and 2nd Gaussians, giving modelled distribution. **b**) As in **a**) but recordings from GJC somata. Data taken from figure 5b.

S10

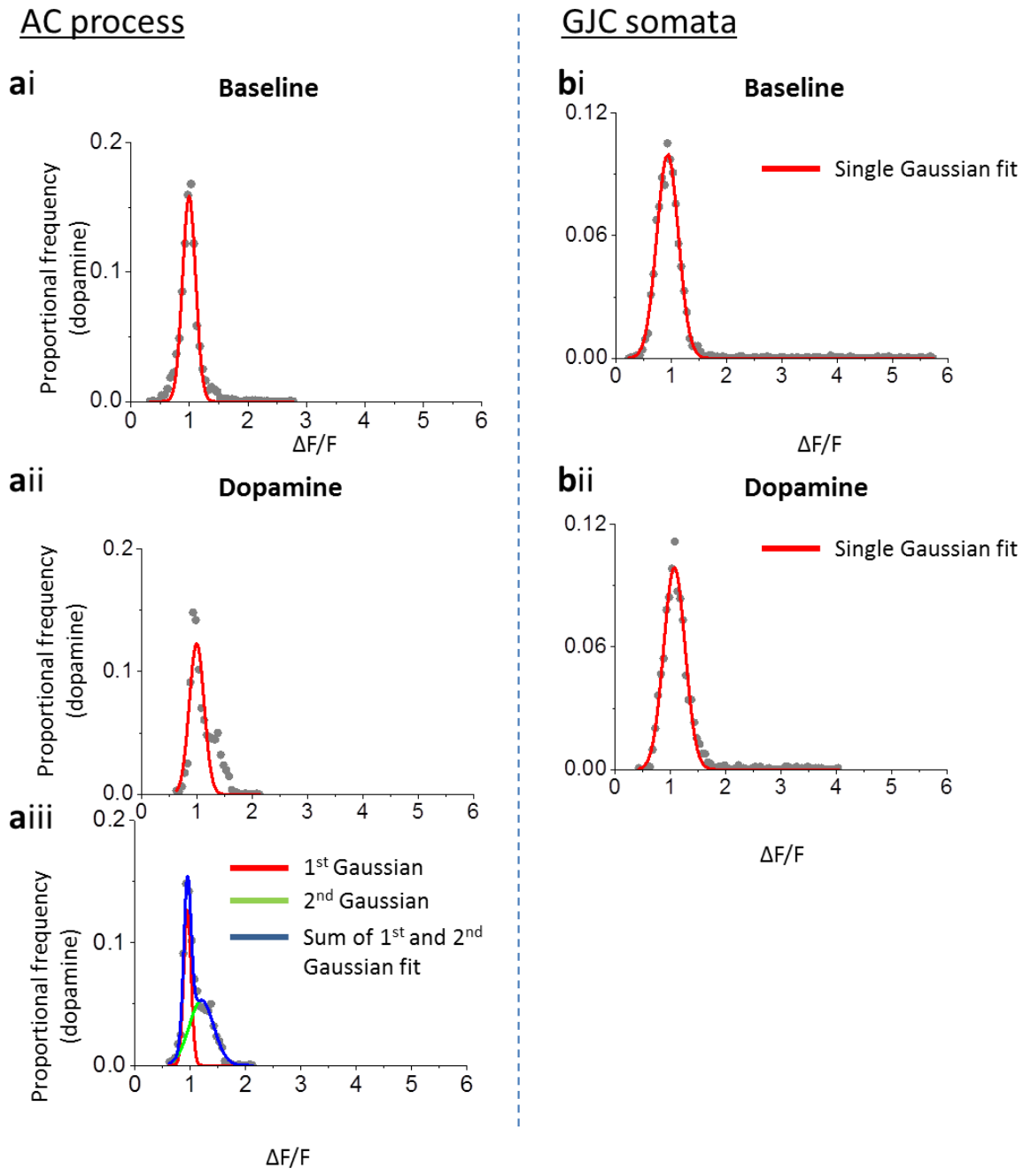

Figure S10 **Gaussian fits for 100µM dopamine application during 50µM sulpiride in Figure 6a.**

ai) Baseline $\Delta F/F_0$ proportional distribution and fitted single Gaussian curve in AC processes; grey circles indicate recorded data, red line indicates modelled data. **a**ii) as in **a**i) but in dopamine. **a**iii) double Gaussian fit of dopamine proportional $\Delta F/F_0$ distribution; grey circles indicate recorded data, red line indicates 1st of 2 modelled gaussian curves, green line indicates 2nd of 2, blue line indicates

sum of 1st and 2nd Gaussians, giving modelled distribution. **b**) As in **a**) but recordings from GJC somata. Data taken from figure 6a.

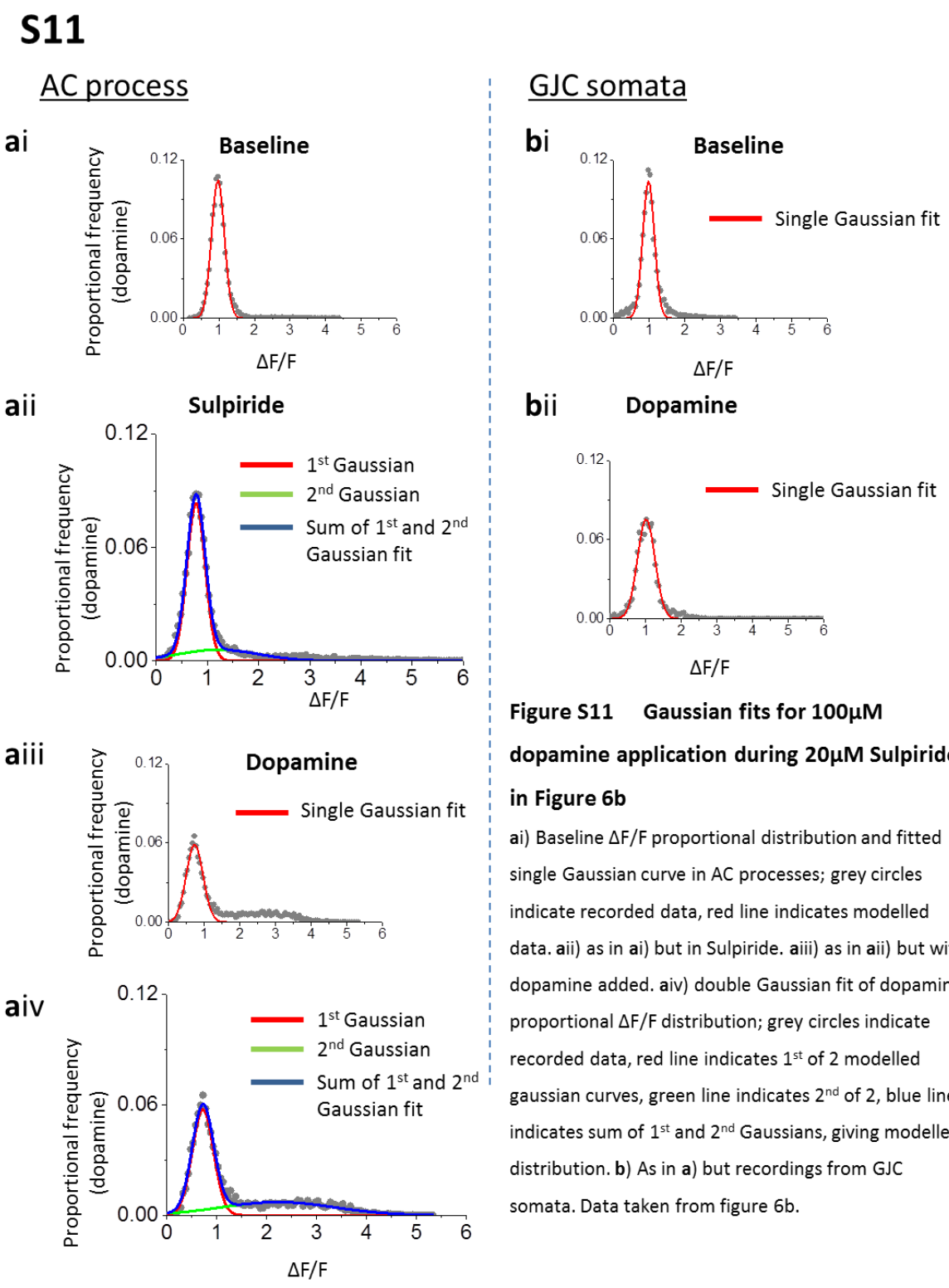

Figure S11 Gaussian fits for 100µM dopamine application during 20µM Sulpiride in Figure 6b

ai) Baseline ΔF/F proportional distribution and fitted single Gaussian curve in AC processes; grey circles indicate recorded data, red line indicates modelled data. **a**ii) as in **a**i) but in Sulpiride. **a**iii) as in **a**ii) but with dopamine added. **a**iv) double Gaussian fit of dopamine proportional ΔF/F distribution; grey circles indicate recorded data, red line indicates 1st of 2 modelled gaussian curves, green line indicates 2nd of 2, blue line indicates sum of 1st and 2nd Gaussians, giving modelled distribution. **b**) As in **a**) but recordings from GJC somata. Data taken from figure 6b.

S12

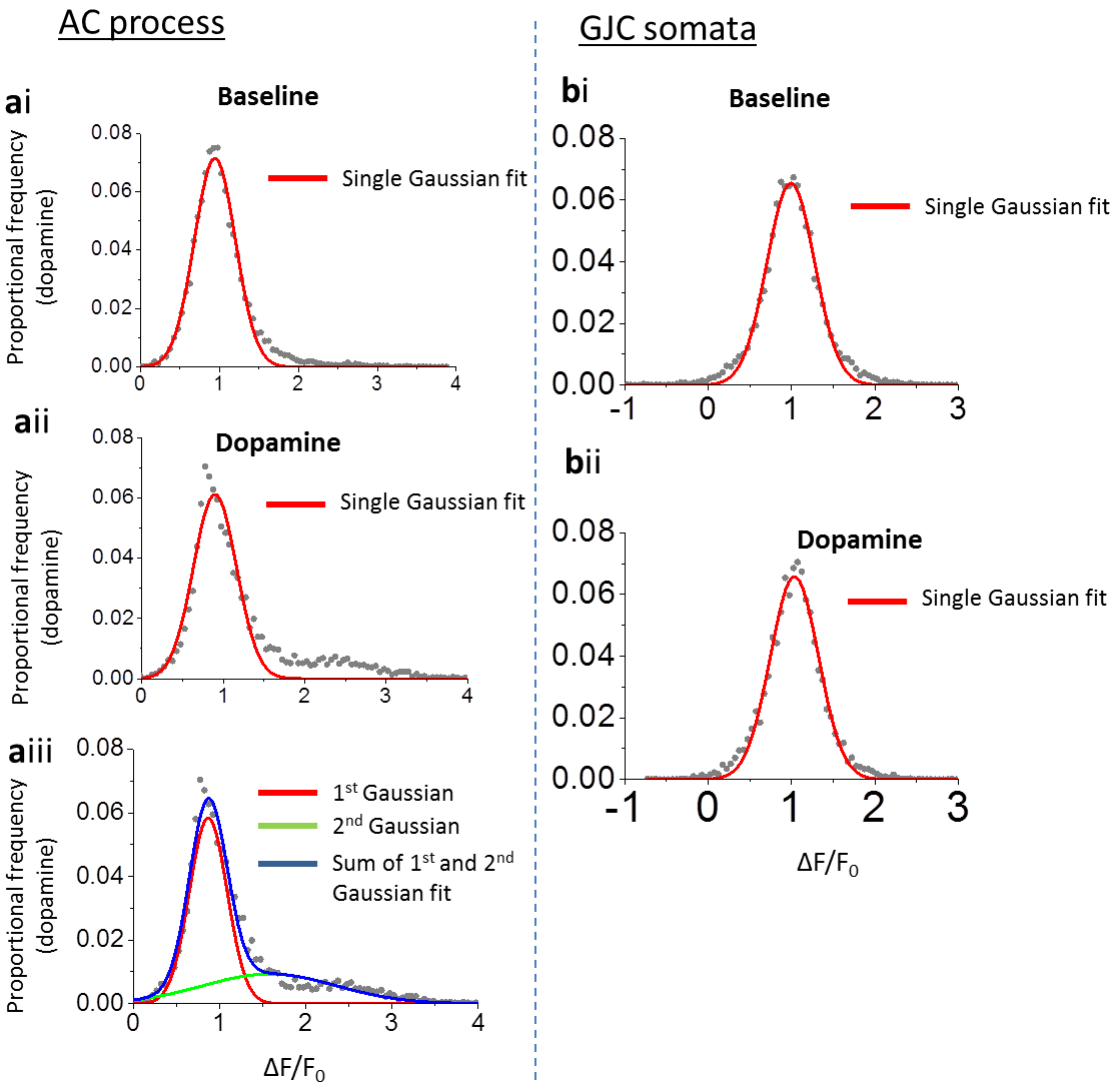

Figure S12 **Gaussian fits for simultaneous 100µM SKF38390 and 100µM quinpirole application in Figure 7a.**

ai) Baseline $\Delta F/F_0$ proportional distribution and fitted single Gaussian curve in AC processes; grey circles indicate recorded data, red line indicates modelled data. **a**ii) as in **a**i) but in dopamine. **a**iii) double Gaussian fit of dopamine proportional $\Delta F/F_0$ distribution; grey circles indicate recorded data, red line indicates 1st of 2 modelled gaussian curves, green line indicates 2nd of 2, blue line indicates sum of 1st and 2nd Gaussians, giving modelled distribution. **b**) As in **a**) but recordings from GJC somata. Data taken from figure 7a.

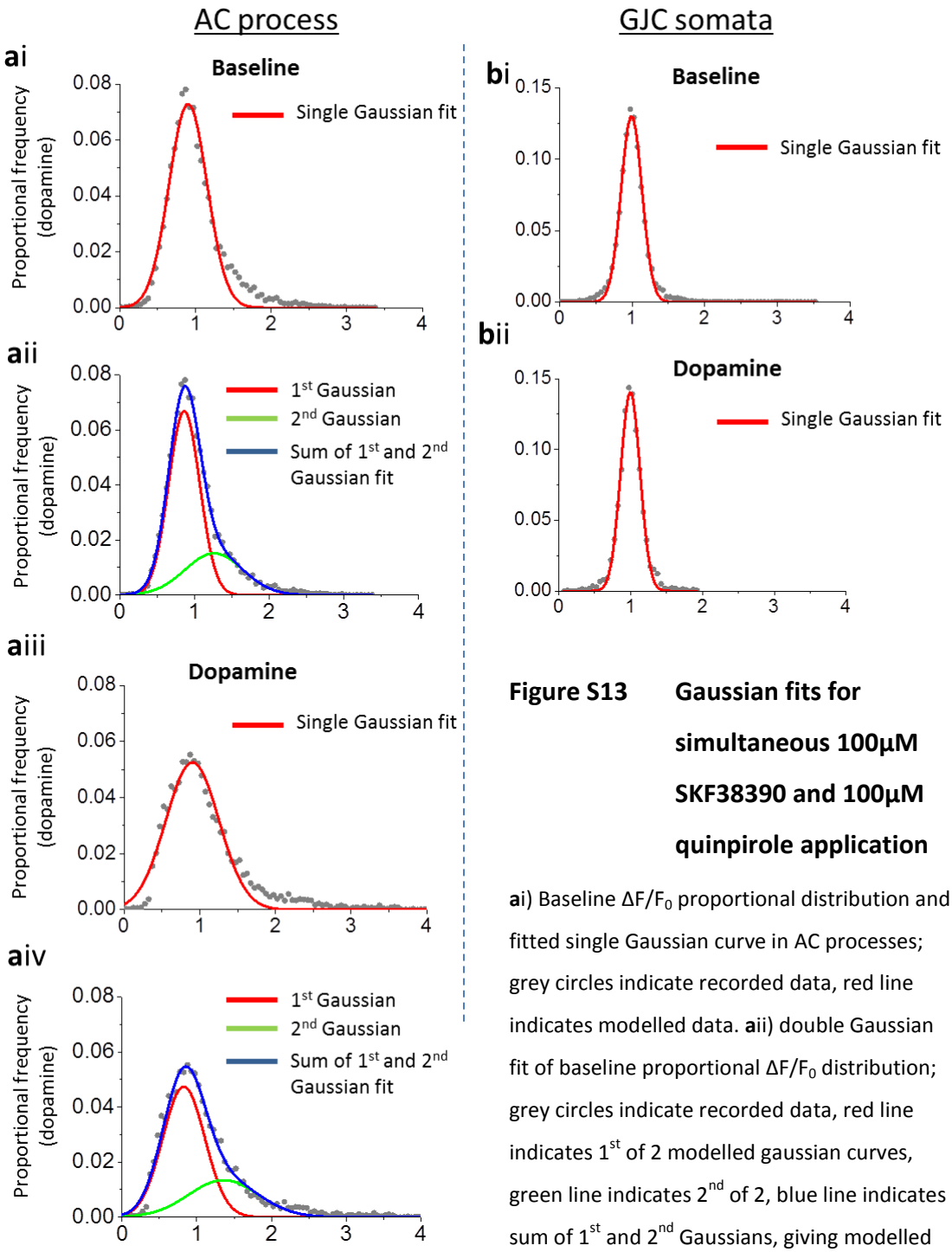

Figure S13 **Gaussian fits for simultaneous 100µM SKF38390 and 100µM quinpirole application**

ai) Baseline $\Delta F/F_0$ proportional distribution and fitted single Gaussian curve in AC processes; grey circles indicate recorded data, red line indicates modelled data. **a**ii) double Gaussian fit of baseline proportional $\Delta F/F_0$ distribution; grey circles indicate recorded data, red line indicates 1st of 2 modelled gaussian curves, green line indicates 2nd of 2, blue line indicates sum of 1st and 2nd Gaussians, giving modelled distribution. as in **a**i) but in dopamine. **a**iii) as in **a**i) but in dopamine. **a**iv) double Gaussian fit of dopamine proportional $\Delta F/F_0$ distribution; grey circles indicate recorded data, red line indicates 1st of 2 modelled gaussian curves, green line indicates 2nd of 2, blue line indicates sum of 1st and 2nd Gaussians, giving modelled distribution. **b**i) As in **a**i) but recordings from GJC somata. **b**ii) as in **a**iii) but recordings from GJC somata. Data taken from figure 7b.

9.2 Supplementary tables

Time (s)	Mean Dif.	Std. Error	DF	|t|value	Prob>|t|	Sig.	95% LCL	95% UCL
5	-0.01898	0.0407	171	0.46633	0.64157		-0.09933	0.06136
20	0.17186	0.0407	171	4.22222	3.92E-05	*	0.09151	0.2522
35	0.14187	0.0407	171	3.48557	6.24E-04	*	0.06153	0.22222
50	0.14859	0.0407	171	3.65055	3.47E-04	*	0.06824	0.22893
65	0.11506	0.0407	171	2.82681	0.00526	*	0.03471	0.1954
80	0.14851	0.0407	171	3.64853	3.50E-04	*	0.06816	0.22885
95	0.17309	0.0407	171	4.25258	3.47E-05	*	0.09275	0.25344
110	0.10042	0.0407	171	2.46727	0.0146	*	0.02008	0.18077
125	0.12242	0.0407	171	3.00763	0.00303	*	0.04207	0.20276
140	0.14539	0.0407	171	3.57202	4.60E-04	*	0.06505	0.22574
155	0.07096	0.0407	171	1.74327	0.08308		-0.00939	0.1513
170	0.06337	0.0407	171	1.55693	0.12134		-0.01697	0.14372
185	0.12222	0.0407	171	3.00285	0.00308	*	0.04188	0.20257
200	0.129	0.0407	171	3.16929	0.00181	*	0.04865	0.20934
215	0.07428	0.0407	171	1.82483	0.06977		-0.00607	0.15462
230	0.08482	0.0407	171	2.08389	0.03866	*	0.00448	0.16516
245	0.07565	0.0407	171	1.85869	0.06479		-0.00469	0.156
260	0.04704	0.0407	171	1.1558	0.24938		-0.0333	0.12739
275	0.10457	0.0407	171	2.56915	0.01105	*	0.02423	0.18492
290	0.03656	0.0407	171	0.8983	0.37029		-0.04378	0.11691

Table S1 ANOVA for post-TBS fEPSP amplitudes in control and dopamine conditions.

Time - seconds post-TBS stimulus; Mean Dif. – dopamine fEPSP amplitude subtracted from control fEPSP amplitude; std. error – standard error; DF – degrees of freedom; t value – statistical t-value; prob>t – probability that t value is the same as expected; Sig. – does prob>t reach a significance of <0.05; 95% LCL – 95% lower confidence interval; 95% UCL – 95% upper confidence interval.

Time	Mean Dif.	Std. Error	DF	|t|value	Prob>|t|	Sig.	95% LCL	95% UCL
5	-0.07132	0.03438	171	2.07419	0.03956	*	-0.13919	-0.00345
20	-0.10373	0.03438	171	3.01679	2.94E-03	*	-0.17159	-0.03586
35	-0.06564	0.03438	171	1.90922	5.79E-02		-0.13351	0.00223
50	-0.12416	0.03438	171	3.61102	4.01E-04	*	-0.19203	-0.05629
65	-0.11968	0.03438	171	3.48095	6.34E-04	*	-0.18755	-0.05182
80	-0.12352	0.03438	171	3.59257	4.28E-04	*	-0.19139	-0.05565
95	-0.10971	0.03438	171	3.19075	1.69E-03	*	-0.17758	-0.04184
110	-0.05315	0.03438	171	1.54578	0.12401		-0.12102	0.01472
125	-0.06723	0.03438	171	1.9553	0.05218		-0.1351	6.41E-04
140	-0.05972	0.03438	171	1.73705	8.42E-02		-0.12759	0.00814
155	-0.0463	0.03438	171	1.34672	0.17985		-0.11417	0.02157
170	-0.05523	0.03438	171	1.60629	0.11005		-0.1231	0.01264
185	-0.047	0.03438	171	1.36685	0.17347		-0.11487	0.02087
200	-0.09716	0.03438	171	2.82594	0.00528	*	-0.16503	-0.02929
215	-0.02584	0.03438	171	0.7516	0.45333		-0.09371	0.04203
230	-0.0432	0.03438	171	1.25653	0.21064		-0.11107	0.02467
245	-0.02472	0.03438	171	0.71893	0.47316		-0.09259	0.04315
260	0.02661	0.03438	171	0.77398	0.44001		-0.04126	0.09448
275	-0.07641	0.03438	171	2.2223	0.02757	*	-0.14428	-0.00854
290	0.01177	0.03438	171	0.34234	0.73251		-0.0561	0.07964

Table S2 ANOVA for post-TBS PPR in control and dopamine conditions.

Time - seconds post-TBS stimulus; Mean Dif. – dopamine PPR subtracted from control PPR; std. error – standard error; DF – degrees of freedom; t value – statistical t-value; prob>t – probability that t value is the same as expected; Sig. – does prob>t reach a significance of <0.05; 95% LCL – 95% lower confidence interval; 95% UCL – 95% upper confidence interval.

Time	Mean Dif.	Std. Error	DF	|t|value	Prob>|t|	Sig.	95% LCL	95% UCL
5	0.05358	0.0486	133	1.10255	0.27221		-0.04254	0.14971
20	0.04528	0.0486	133	0.93171	3.53E-01		-0.05085	0.14141
35	0.03391	0.0486	133	0.69771	4.87E-01		-0.06222	0.13004
50	0.01523	0.0486	133	0.31341	7.54E-01		-0.0809	0.11136
65	-0.00501	0.0486	133	0.10303	9.18E-01		-0.10114	0.09112
80	0.03638	0.0486	133	0.74863	4.55E-01		-0.05975	0.13251
95	0.0444	0.0486	133	0.91367	3.63E-01		-0.05172	0.14053
110	0.02866	0.0486	133	0.5898	0.55632		-0.06746	0.12479
125	0.05251	0.0486	133	1.08037	0.28193		-0.04362	1.49E-01
140	0.02712	0.0486	133	0.5581	5.78E-01		-0.06901	0.12325
155	0.03991	0.0486	133	0.8212	0.413		-0.05622	0.13604
170	0.0465	0.0486	133	0.95685	0.34038		-0.04963	0.14263
185	0.12085	0.0486	133	2.48661	0.01414	*	0.02472	0.21698
200	0.0474	0.0486	133	0.97538	0.33114		-0.04873	0.14353
215	0.1075	0.0486	133	2.21193	0.02868	*	0.01137	0.20363
230	0.11239	0.0486	133	2.3125	0.02229	*	0.01626	0.20852
245	0.07251	0.0486	133	1.49192	0.13809		-0.02362	0.16864
260	0.04151	0.0486	133	0.8542	0.39453		-0.05462	0.13764
275	0.06144	0.0486	133	1.26426	0.20835		-0.03469	0.15757
290	0.08426	0.0486	133	1.73382	0.08527		-0.01187	0.18039

Table S3 ANOVA for post-TBS fEPSPs in control and FAC conditions.

Time - seconds post-TBS stimulus; Mean Dif. – FAC fEPSP subtracted from control fEPSP; std. error – standard error; DF – degrees of freedom; t value – statistical t-value; prob>t – probability that t value is the same as expected; Sig. – does prob>t reach a significance of <0.05; 95% LCL – 95% lower confidence interval; 95% UCL – 95% upper confidence interval.

Time	Mean Dif.	Std. Error	DF	|t|value	Prob>|t|	Sig.	95% LCL	95% UCL
5	-0.07146	0.03539	133	2.0193	0.04547	*	-0.14146	-0.00146
20	-0.07304	0.03539	133	2.06387	4.10E-02	*	-0.14303	-0.00304
35	-0.07675	0.03539	133	2.16881	3.19E-02	*	-0.14675	-0.00675
50	-0.06078	0.03539	133	1.71757	8.82E-02		-0.13078	0.00921
65	-0.01936	0.03539	133	0.54708	5.85E-01		-0.08936	0.05064
80	-0.05792	0.03539	133	1.63657	1.04E-01		-0.12791	0.01208
95	-0.0087	0.03539	133	0.24571	8.06E-01		-0.07869	0.0613
110	-0.04842	0.03539	133	1.36822	0.17355		-0.11842	0.02158
125	0.01209	0.03539	133	0.34167	0.73314		-0.05791	8.21E-02
140	-0.01775	0.03539	133	0.50172	6.17E-01		-0.08775	0.05224
155	-0.00399	0.03539	133	0.11268	0.91045		-0.07398	0.06601
170	-0.03229	0.03539	133	0.91244	0.36319		-0.10229	0.03771
185	-0.08629	0.03539	133	2.43836	0.01607	*	-0.15629	-0.01629
200	-0.0297	0.03539	133	0.83936	0.40277		-0.0997	0.04029
215	-0.07181	0.03539	133	2.02913	0.04444	*	-0.1418	-0.00181
230	-0.08075	0.03539	133	2.2817	0.0241	*	-0.15074	-0.01075
245	-0.0033	0.03539	133	0.09334	0.92578		-0.0733	0.06669
260	0.00309	0.03539	133	0.08725	0.93061		-0.06691	0.07308
275	-0.01447	0.03539	133	0.40903	0.68317		-0.08447	0.05552
290	-0.03461	0.03539	133	0.97797	0.32987		-0.10461	0.03539

Table S4 ANOVA for post-TBS PPR in control and FAC conditions.

Time - seconds post-TBS stimulus; Mean Dif. – FAC PPR subtracted from control PPR; std. error – standard error; DF – degrees of freedom; t value – statistical t-value; prob>t – probability that t value is the same as expected; Sig. – does prob>t reach a significance of <0.05; 95% LCL – 95% lower confidence interval; 95% UCL – 95% upper confidence interval.

Time	Mean Dif.	Std. Error	DF	|t|value	Prob>|t|	Sig.	95% LCL	95% UCL
5	0.08104	0.05773	133	1.40371	0.16274		-0.03315	0.19524
20	0.14563	0.05773	133	2.52232	1.28E-02	*	0.03143	0.25982
35	0.12048	0.05773	133	2.08684	3.88E-02	*	0.00629	0.23468
50	0.07865	0.05773	133	1.36229	1.75E-01		-0.03555	0.19285
65	0.12313	0.05773	133	2.13264	3.48E-02	*	0.00893	0.23732
80	0.07102	0.05773	133	1.2301	2.21E-01		-0.04318	0.18522
95	-0.01796	0.05773	133	0.31101	7.56E-01		-0.13215	0.09624
110	0.0697	0.05773	133	1.20726	0.22947		-0.0445	0.1839
125	0.04866	0.05773	133	0.84287	0.40082		-0.06553	1.63E-01
140	-0.06232	0.05773	133	1.07949	2.82E-01		-0.17652	0.05187
155	-0.05533	0.05773	133	0.95841	0.3396		-0.16953	0.05886
170	0.03064	0.05773	133	0.53068	0.59653		-0.08356	0.14484
185	-0.02049	0.05773	133	0.35495	0.72319		-0.13469	0.0937
200	0.03737	0.05773	133	0.64732	0.51854		-0.07682	0.15157
215	0.03743	0.05773	133	0.64828	0.51792		-0.07677	0.15163
230	0.08312	0.05773	133	1.43969	0.1523		-0.03108	0.19732
245	0.09787	0.05773	133	1.69509	0.0924		-0.01633	0.21206
260	-0.02529	0.05773	133	0.43808	0.66204		-0.13949	0.0889
275	-0.01246	0.05773	133	0.21576	0.8295		-0.12665	0.10174
290	-0.05355	0.05773	133	0.92756	0.35532		-0.16775	0.06064

Table S5 ANOVA for post-TBS fEPSP in dopamine and dopamine + FAC conditions.

Time - seconds post-TBS stimulus; Mean Dif. – dopamine fEPSP subtracted from dopamine + FAC fEPSP; std. error – standard error; DF – degrees of freedom; t value – statistical t-value; prob>t – probability that t value is the same as expected; Sig. – does prob>t reach a significance of <0.05; 95% LCL – 95% lower confidence interval; 95% UCL – 95% upper confidence interval.

Time	Mean Dif.	Std. Error	DF	|t|value	Prob>|t|	Sig.	95% LCL	95% UCL
5	-0.05856	0.05536	133	1.05778	0.29207		-0.16805	0.05094
20	-0.06643	0.05536	133	1.20007	2.32E-01		-0.17593	0.04306
35	-0.02107	0.05536	133	0.38063	7.04E-01		-0.13057	0.08842
50	-0.01771	0.05536	133	0.31994	7.50E-01		-0.12721	0.09178
65	0.08006	0.05536	133	1.44631	1.50E-01		-0.02943	0.18956
80	-0.02927	0.05536	133	0.52866	5.98E-01		-0.13876	0.08023
95	-0.00883	0.05536	133	0.15954	8.73E-01		-0.11833	0.10066
110	-0.04745	0.05536	133	0.85711	0.39292		-0.15694	0.06205
125	0.02055	0.05536	133	0.37125	0.71105		-0.08894	1.30E-01
140	0.0309	0.05536	133	0.55817	5.78E-01		-0.0786	0.14039
155	0.04279	0.05536	133	0.77303	0.44088		-0.0667	0.15229
170	0.01043	0.05536	133	0.1884	0.85085		-0.09907	0.11992
185	0.01043	0.05536	133	0.1884	0.85085		-0.09907	0.11992
200	0.02923	0.05536	133	0.52808	0.59832		-0.08026	0.13873
215	-0.04227	0.05536	133	0.76363	0.44644		-0.15177	0.06722
230	-0.06558	0.05536	133	1.1847	0.23825		-0.17508	0.04391
245	-0.0236	0.05536	133	0.42624	0.67062		-0.13309	0.0859
260	0.03809	0.05536	133	0.68799	0.49266		-0.07141	0.14758
275	-0.0041	0.05536	133	0.074	0.94112		-0.11359	0.1054
290	0.02844	0.05536	133	0.51371	0.60831		-0.08106	0.13793

Table S6 ANOVA for post-TBS PPR in dopamine and dopamine + FAC conditions.

Time - seconds post-TBS stimulus; Mean Dif. – dopamine fEPSP subtracted from dopamine + FAC fEPSP; std. error – standard error; DF – degrees of freedom; t value – statistical t-value; prob>t – probability that t value is the same as expected; Sig. – does prob>t reach a significance of <0.05; 95% LCL – 95% lower confidence interval; 95% UCL – 95% upper confidence interval.

Time	Mean Dif.	Std. Error	DF	|t|value	Prob>|t|	Sig.	95% LCL	95% UCL
15	-0.13597	0.12896	133	1.05433	0.29364		-0.39105	0.11911
30	-0.11814	0.12896	133	0.91611	0.36127		-0.37322	0.13694
45	-0.04044	0.12896	133	0.31355	0.75436		-0.29552	0.21464
60	-0.16477	0.12896	133	1.27766	0.2036		-0.41985	0.09031
75	-0.16395	0.12896	133	1.27134	0.20583		-0.41903	0.09113
90	0.1423	0.12896	133	1.10341	0.27184		-0.11278	0.39738
105	-0.15233	0.12896	133	1.1812	0.23963		-0.40741	0.10275
120	-0.09656	0.12896	133	0.74872	0.45535		-0.35164	0.15852
135	0.00102	0.12896	133	0.00793	0.99368		-0.25406	0.2561
150	0.06915	0.12896	133	0.53621	0.59271		-0.18593	0.32423
165	-0.04562	0.12896	133	0.35371	0.72411		-0.30069	0.20946
180	-0.0841	0.12896	133	0.6521	0.51546		-0.33918	0.17098
195	-0.01264	0.12896	133	0.098	0.92208		-0.26772	0.24244
210	-0.14197	0.12896	133	1.10089	0.27293		-0.39705	0.11311
225	2.81E-04	0.12896	133	0.00218	0.99826		-0.2548	0.25536
240	-0.00169	0.12896	133	0.01308	0.98959		-0.25677	0.25339
255	0.05133	0.12896	133	0.398	0.69127		-0.20375	0.30641
270	-0.12275	0.12896	133	0.95186	0.34289		-0.37783	0.13233
285	-0.08625	0.12896	133	0.6688	0.50478		-0.34133	0.16883
300	-0.07914	0.12896	133	0.6137	0.54046		-0.33422	0.17594

Table S7 ANOVA for PTP fEPSP amplitudes comparing post 1st and 2nd TBS.

Time - seconds post-TBS; Mean Dif. – 1st TBS fEPSP amplitude subtracted from 2nd TBS fEPSP amplitude; std. error – standard error; DF – degrees of freedom; t value – statistical t-value; prob>t – probability that t value is the same as expected; Sig. – does prob>t reach a significance of <0.05; 95% LCL – 95% lower confidence interval; 95% UCL – 95% upper confidence interval.

Time	Mean Dif.	Std. Error	DF	|t|value	Prob>|t|	Sig.	95% LCL	95% UCL
15	0.08618	0.08935	133	0.96446	0.33657		-0.09056	0.26291
30	0.00926	0.08935	133	0.10368	0.91758		-0.16747	0.186
45	-0.08585	0.08935	133	0.96081	0.33839		-0.26258	0.09088
60	0.07486	0.08935	133	0.83778	0.40365		-0.10188	0.25159
75	0.10474	0.08935	133	1.17227	0.24318		-0.07199	0.28148
90	-0.15199	0.08935	133	1.70104	0.09127		-0.32872	0.02474
105	0.01603	0.08935	133	0.17945	0.85785		-0.1607	0.19277
120	0.05883	0.08935	133	0.65845	0.51139		-0.1179	0.23557
135	-0.0033	0.08935	133	0.03694	0.97059		-0.18003	0.17343
150	-0.07009	0.08935	133	0.78444	0.43418		-0.24682	0.10664
165	0.01456	0.08935	133	0.16301	0.87076		-0.16217	0.1913
180	-0.0191	0.08935	133	0.21377	0.83105		-0.19583	0.15763
195	-0.02904	0.08935	133	0.325	0.74569		-0.20577	0.14769
210	0.05918	0.08935	133	0.66231	0.50892		-0.11755	0.23591
225	-0.05844	0.08935	133	0.65401	0.51423		-0.23517	0.1183
240	-0.05688	0.08935	133	0.63658	0.52549		-0.23361	0.11985
255	-0.03533	0.08935	133	0.39545	0.69315		-0.21207	0.1414
270	0.0824	0.08935	133	0.92226	0.35806		-0.09433	0.25914
285	-0.03464	0.08935	133	0.38767	0.69888		-0.21137	0.14209
300	0.08513	0.08935	133	0.95271	0.34247		-0.09161	0.26186

Table S8 ANOVA for PTP PPR amplitudes comparing post 1st and 2nd TBS.

Time - seconds post-TBS; Mean Dif. – 1st TBS PPR amplitude subtracted from 2nd TBS PPR amplitude; std. error – standard error; DF – degrees of freedom; t value – statistical t-value; prob>t – probability that t value is the same as expected; Sig. – does prob>t reach a significance of <0.05; 95% LCL – 95% lower confidence interval; 95% UCL – 95% upper confidence interval.

Time	Mean Dif.	Std. Error	DF	|t|value	Prob>|t|	Sig.	95% LCL	95% UCL
15	-0.02294	0.08317	152	0.27579	0.78308		-0.18727	0.14139
30	-0.12277	0.08317	152	1.47603	0.142		-0.28709	0.04156
45	-0.07287	0.08317	152	0.87606	0.38238		-0.23719	0.09146
60	-0.18289	0.08317	152	2.19883	0.0294	*	-0.34721	-0.01856
75	-0.07179	0.08317	152	0.86312	0.38943		-0.23612	0.09254
90	-0.13062	0.08317	152	1.57041	0.1184		-0.29494	0.03371
105	-0.20294	0.08317	152	2.43994	0.01584	*	-0.36727	-0.03861
120	-0.12389	0.08317	152	1.48956	0.13841		-0.28822	0.04043
135	-0.14576	0.08317	152	1.75248	0.08171		-0.31009	0.01857
150	-0.16336	0.08317	152	1.96408	0.05134		-0.32769	9.66E-04
165	-0.1187	0.08317	152	1.42707	0.15561		-0.28302	0.04563
180	-0.24727	0.08317	152	2.97297	0.00343	*	-0.4116	-0.08295
195	-0.16634	0.08317	152	1.99986	0.0473	*	-0.33066	-0.00201
210	-0.20582	0.08317	152	2.47458	0.01444	*	-0.37015	-0.04149
225	-0.2014	0.08317	152	2.42143	0.01664	*	-0.36573	-0.03707
240	-0.13791	0.08317	152	1.65812	0.09936		-0.30224	0.02641
255	-0.12792	0.08317	152	1.53796	0.12614		-0.29224	0.03641
270	-0.26298	0.08317	152	3.16181	0.00189	*	-0.42731	-0.09865
285	-0.1255	0.08317	152	1.50882	0.13342		-0.28982	0.03883
300	-0.18405	0.08317	152	2.21283	0.0284	*	-0.34838	-0.01972

Table S9 ANOVA for PTP fEPSP amplitudes comparing post 1st and 2nd TBS in control vs. SCH23390 and Sulpiride – both normalized to 1st baseline.

Time - seconds post-TBS; Mean Dif. – 1st TBS fEPSP amplitude subtracted from 2nd TBS fEPSP amplitude; std. error – standard error; DF – degrees of freedom; t value – statistical t-value; prob>t – probability that t value is the same as expected; Sig. – does prob>t reach a significance of <0.05; 95% LCL – 95% lower confidence interval; 95% UCL – 95% upper confidence interval.

Time	Mean Dif.	Std. Error	DF	|t|value	Prob>|t|	Sig.	95% LCL	95% UCL
15	0.17179	0.06186	152	2.77722	0.00617	*	0.04958	0.294
30	0.06062	0.06186	152	0.98007	0.32861		-0.06159	0.18283
45	0.11209	0.06186	152	1.81215	0.07194		-0.01012	0.2343
60	-0.01016	0.06186	152	0.16426	0.86975		-0.13237	0.11205
75	0.09752	0.06186	152	1.57649	0.11699		-0.02469	0.21973
90	0.03944	0.06186	152	0.63753	0.52474		-0.08277	0.16164
105	-0.01555	0.06186	152	0.25145	0.8018		-0.13776	0.10666
120	0.04692	0.06186	152	0.75845	0.44936		-0.07529	0.16912
135	0.02756	0.06186	152	0.44558	0.65654		-0.09465	0.14977
150	0.00925	0.06186	152	0.14957	0.8813		-0.11296	0.13146
165	0.03949	0.06186	152	0.63837	0.52419		-0.08272	0.1617
180	-0.09422	0.06186	152	1.52323	0.12978		-0.21643	0.02799
195	-0.00756	0.06186	152	0.12215	0.90294		-0.12977	0.11465
210	-0.0438	0.06186	152	0.70808	0.47998		-0.16601	0.07841
225	-0.04146	0.06186	152	0.67024	0.50372		-0.16367	0.08075
240	0.01863	0.06186	152	0.30125	0.76363		-0.10358	0.14084
255	0.02759	0.06186	152	0.44604	0.6562		-0.09462	0.1498
270	-0.10583	0.06186	152	1.71086	0.08915		-0.22804	0.01638
285	0.0262	0.06186	152	0.42351	0.67252		-0.09601	0.14841
300	-0.03787	0.06186	152	0.61219	0.54133		-0.16008	0.08434

Table S10 ANOVA for PTP fEPSP amplitudes comparing post 1st and 2nd TBS in control vs. SCH23390 and Sulpiride – renormalized.

Time - seconds post-TBS; Mean Dif. – 1st TBS fEPSP amplitude subtracted from 2nd TBS fEPSP amplitude; std. error – standard error; DF – degrees of freedom; t value – statistical t-value; prob>t – probability that t value is the same as expected; Sig. – does prob>t reach a significance of <0.05; 95% LCL – 95% lower confidence interval; 95% UCL – 95% upper confidence interval.

Time	Mean Dif.	Std. Error	DF	|t|value	Prob>|t|	Sig.	95% LCL	95% UCL
15	-0.00841	0.03489	152	0.24115	0.80977		-0.07734	0.06052
30	0.01819	0.03489	152	0.52135	0.60288		-0.05074	0.08712
45	0.03199	0.03489	152	0.9169	0.36065		-0.03694	0.10092
60	0.04872	0.03489	152	1.39644	0.16462		-0.02021	0.11765
75	0.01134	0.03489	152	0.3251	0.74555		-0.05759	0.08027
90	0.05283	0.03489	152	1.51413	0.13207		-0.0161	0.12176
105	0.07994	0.03489	152	2.29138	0.02332	*	0.01101	0.14887
120	0.02237	0.03489	152	0.64127	0.52231		-0.04656	0.0913
135	0.0669	0.03489	152	1.91761	0.05704		-0.00203	0.13583
150	0.04459	0.03489	152	1.27816	0.20314		-0.02434	0.11352
165	0.02687	0.03489	152	0.77021	0.44237		-0.04206	0.0958
180	0.10431	0.03489	152	2.98989	0.00326	*	0.03538	0.17324
195	0.05455	0.03489	152	1.56362	0.11999		-0.01438	0.12348
210	0.09301	0.03489	152	2.66575	0.00851	*	0.02408	0.16194
225	0.05761	0.03489	152	1.65113	0.10078		-0.01132	0.12654
240	0.05943	0.03489	152	1.70329	0.09056		-0.0095	0.12836
255	0.06206	0.03489	152	1.77892	0.07725		-0.00687	0.13099
270	0.18683	0.03489	152	5.35492	3.10E-07	*	0.1179	0.25576
285	0.06068	0.03489	152	1.73912	0.08404		-0.00825	0.12961
300	0.0453	0.03489	152	1.29843	0.19611		-0.02363	0.11423

Table S11 ANOVA for PTP PPR amplitudes comparing post 1st and 2nd TBS in control vs. SCH23390 and Sulpiride – both normalized to 1st baseline.

Time - seconds post-TBS; Mean Dif. – 1st TBS PPR amplitude subtracted from 2nd TBS PPR amplitude; std. error – standard error; DF – degrees of freedom; t value – statistical t-value; prob>t – probability that t value is the same as expected; Sig. – does prob>t reach a significance of <0.05; 95% LCL – 95% lower confidence interval; 95% UCL – 95% upper confidence interval.

Time	Mean Dif.	Std. Error	DF	|t|value	Prob>|t|	Sig.	95% LCL	95% UCL
15	-0.0554	0.03597	152	1.54005	0.12563		-0.12646	0.01567
30	-0.0307	0.03597	152	0.85334	0.39482		-0.10176	0.04037
45	-0.01692	0.03597	152	0.4703	0.63882		-0.08798	0.05415
60	-0.00108	0.03597	152	0.0301	0.97603		-0.07215	0.06998
75	-0.03983	0.03597	152	1.10723	0.26994		-0.1109	0.03124
90	8.84E-04	0.03597	152	0.02457	0.98043		-0.07018	0.07195
105	0.03246	0.03597	152	0.90237	0.36829		-0.03861	0.10353
120	-0.02884	0.03597	152	0.80179	0.42393		-0.09991	0.04223
135	0.01868	0.03597	152	0.51924	0.60435		-0.05239	0.08975
150	-0.00412	0.03597	152	0.11447	0.90901		-0.07519	0.06695
165	-0.02248	0.03597	152	0.62507	0.53286		-0.09355	0.04858
180	0.05166	0.03597	152	1.43614	0.15302		-0.01941	0.12273
195	0.00269	0.03597	152	0.07473	0.94053		-0.06838	0.07376
210	0.04383	0.03597	152	1.21859	0.22489		-0.02723	0.1149
225	0.00811	0.03597	152	0.22543	0.82194		-0.06296	0.07918
240	0.0095	0.03597	152	0.26407	0.79208		-0.06157	0.08057
255	0.01053	0.03597	152	0.29276	0.77011		-0.06054	0.0816
270	0.13827	0.03597	152	3.84403	1.77E-04	*	0.06721	0.20934
285	0.00919	0.03597	152	0.25555	0.79864		-0.06188	0.08026
300	-0.00792	0.03597	152	0.22021	0.826		-0.07899	0.06315

Table S12 ANOVA for PTP PPR amplitudes comparing post 1st and 2nd TBS in control vs. SCH23390 and Sulpiride – renormalized.

Time - seconds post-TBS; Mean Dif. – 1st TBS PPR amplitude subtracted from 2nd TBS PPR amplitude; std. error – standard error; DF – degrees of freedom; t value – statistical t-value; prob>t – probability that t value is the same as expected; Sig. – does prob>t reach a significance of <0.05; 95% LCL – 95% lower confidence interval; 95% UCL – 95% upper confidence interval.

Time	Mean Dif.	Std. Error	DF	|t|value	Prob>|t|	Sig.	95% LCL	95% UCL
15	-0.0485	0.14875	57	0.32603	0.7456		-0.34636	0.24937
30	-0.16108	0.14875	57	1.0829	0.28341		-0.45894	0.13678
45	-0.12328	0.14875	57	0.82875	0.4107		-0.42114	0.17459
60	-0.2247	0.14875	57	1.5106	0.13641		-0.52256	0.07316
75	-0.12522	0.14875	57	0.84181	0.40341		-0.42308	0.17265
90	-0.13604	0.14875	57	0.91454	0.36428		-0.4339	0.16183
105	-0.14408	0.14875	57	0.96863	0.33682		-0.44195	0.15378
120	-0.08912	0.14875	57	0.59911	0.55147		-0.38698	0.20875
135	-0.34667	0.14875	57	2.3306	0.02334	*	-0.64454	-0.04881
150	-0.22685	0.14875	57	1.52504	0.13278		-0.52471	0.07102
165	-0.12941	0.14875	57	0.87002	0.38794		-0.42728	0.16845
180	-0.24559	0.14875	57	1.65105	0.10423		-0.54346	0.05227
195	-0.13077	0.14875	57	0.87914	0.38302		-0.42863	0.16709
210	-0.15522	0.14875	57	1.04348	0.30113		-0.45308	0.14265
225	-0.0916	0.14875	57	0.61581	0.54047		-0.38947	0.20626
240	-0.0916	0.14875	57	0.61581	0.54047		-0.38947	0.20626
255	-0.10632	0.14875	57	0.71473	0.47769		-0.40418	0.19155
270	-0.08151	0.14875	57	0.54799	0.58584		-0.37938	0.21635
285	-0.2553	0.14875	57	1.71631	0.09154		-0.55316	0.04257
300	-0.07661	0.14875	57	0.51505	0.60851		-0.37448	0.22125

Table S13 ANOVA for PTP fEPSP amplitudes comparing post 1st and 2nd TBS in control and FAC – renormalized.

Time - seconds post-TBS; Mean Dif. – 1st TBS fEPSP amplitude subtracted from 2nd TBS fEPSP amplitude; std. error – standard error; DF – degrees of freedom; t value – statistical t-value; prob>t – probability that t value is the same as expected; Sig. – does prob>t reach a significance of <0.05; 95% LCL – 95% lower confidence interval; 95% UCL – 95% upper confidence interval.

Time	Mean Dif.	Std. Error	DF	|t|value	Prob>|t|	Sig.	95% LCL	95% UCL
15	0.02018	0.059	57	0.34197	0.73363		-0.09797	0.13833
30	0.07188	0.059	57	1.21825	0.22815		-0.04627	0.19003
45	-0.0198	0.059	57	0.33554	0.73845		-0.13795	0.09835
60	0.09063	0.059	57	1.53596	0.13008		-0.02753	0.20878
75	0.03591	0.059	57	0.60854	0.54525		-0.08225	0.15406
90	0.04923	0.059	57	0.83442	0.40753		-0.06892	0.16739
105	0.07759	0.059	57	1.31508	0.19375		-0.04056	0.19575
120	0.04635	0.059	57	0.78557	0.43537		-0.0718	0.1645
135	0.09182	0.059	57	1.55615	0.12521		-0.02633	0.20997
150	0.12395	0.059	57	2.10068	0.0401	*	0.00579	0.2421
165	0.03855	0.059	57	0.65329	0.5162		-0.07961	0.1567
180	0.12722	0.059	57	2.15612	0.03531	*	0.00907	0.24537
195	0.12172	0.059	57	2.06293	0.04369	*	0.00357	0.23987
210	0.05788	0.059	57	0.98099	0.33074		-0.06027	0.17603
225	0.05134	0.059	57	0.87005	0.38792		-0.06682	0.16949
240	0.02352	0.059	57	0.39864	0.69165		-0.09463	0.14167
255	0.04714	0.059	57	0.79886	0.42769		-0.07102	0.16529
270	0.0074	0.059	57	0.1254	0.90065		-0.11075	0.12555
285	0.14168	0.059	57	2.40117	0.01963	*	0.02352	0.25983
300	-0.04216	0.059	57	0.71459	0.47778		-0.16031	0.07599

Table S14 ANOVA for PTP PPR amplitudes comparing post 1st and 2nd TBS in control and FAC – renormalized.

Time - seconds post-TBS; Mean Dif. – 1st TBS PPR amplitude subtracted from 2nd TBS PPR amplitude; std. error – standard error; DF – degrees of freedom; t value – statistical t-value; prob>t – probability that t value is the same as expected; Sig. – does prob>t reach a significance of <0.05; 95% LCL – 95% lower confidence interval; 95% UCL – 95% upper confidence interval.

Time	Mean Dif.	Std. Error	DF	|t|value	Prob>|t|	Sig.	95% LCL	95% UCL
15	-0.13196	0.12461	171	1.05894	0.29112		-0.37793	0.11402
30	-0.19996	0.12461	171	1.60463	0.11042		-0.44594	0.04602
45	-0.15296	0.12461	171	1.22752	0.22131		-0.39894	0.09301
60	-0.13137	0.12461	171	1.05421	0.29327		-0.37735	0.11461
75	-0.19823	0.12461	171	1.59077	0.11351		-0.44421	0.04775
90	-0.2592	0.12461	171	2.08007	0.03901	*	-0.50518	-0.01323
105	-0.18885	0.12461	171	1.51553	0.13148		-0.43483	0.05712
120	-0.14988	0.12461	171	1.20277	0.23073		-0.39586	0.0961
135	-0.26707	0.12461	171	2.14324	0.03351	*	-0.51305	-0.0211
150	-0.05826	0.12461	171	0.4675	0.64074		-0.30423	0.18772
165	-0.09429	0.12461	171	0.75663	0.45032		-0.34026	0.15169
180	-0.24776	0.12461	171	1.98827	0.04838	*	-0.49374	-0.00179
195	-0.16825	0.12461	171	1.35022	0.17873		-0.41423	0.07772
210	-0.39978	0.12461	171	3.20815	0.0016	*	-0.64575	-0.1538
225	-0.16387	0.12461	171	1.31504	0.19026		-0.40985	0.08211
240	-0.10341	0.12461	171	0.82983	0.40779		-0.34938	0.14257
255	0.15832	0.12461	171	1.27048	0.20564		-0.08766	0.4043
270	-0.14643	0.12461	171	1.17504	0.24161		-0.3924	0.09955
285	-0.24678	0.12461	171	1.98037	0.04927	*	-0.49276	-8.02E-04
300	-0.05861	0.12461	171	0.47035	0.63871		-0.30459	0.18737

Table S15 ANOVA for PTP fEPSP amplitudes, preincubated in FAC, comparing post 1st and 2nd TBS in control vs. SCH23390 and Sulpiride – both normalized to 1st baseline.

Time - seconds post-TBS; Mean Dif. – 1st TBS fEPSP amplitude subtracted from 2nd TBS fEPSP amplitude; std. error – standard error; DF – degrees of freedom; t value – statistical t-value; prob>t – probability that t value is the same as expected; Sig. – does prob>t reach a significance of <0.05; 95% LCL – 95% lower confidence interval; 95% UCL – 95% upper confidence interval.

Time	Mean Dif.	Std. Error	DF	|t|value	Prob>|t|	Sig.	95% LCL	95% UCL
15	0.20473	0.12592	171	1.62588	0.10582		-0.04383	0.45328
30	0.14305	0.12592	171	1.13606	0.25752		-0.1055	0.3916
45	0.16544	0.12592	171	1.31386	0.19065		-0.08311	0.41399
60	0.16741	0.12592	171	1.3295	0.18545		-0.08115	0.41596
75	0.10029	0.12592	171	0.7965	0.42684		-0.14826	0.34885
90	0.01883	0.12592	171	0.14956	0.88129		-0.22972	0.26738
105	0.08053	0.12592	171	0.63953	0.52334		-0.16802	0.32908
120	0.1069	0.12592	171	0.84898	0.39708		-0.14165	0.35545
135	-0.0062	0.12592	171	0.04926	0.96077		-0.25476	0.24235
150	0.19919	0.12592	171	1.5819	0.11552		-0.04936	0.44774
165	0.15694	0.12592	171	1.24636	0.21434		-0.09161	0.40549
180	0.02195	0.12592	171	0.17435	0.8618		-0.2266	0.27051
195	0.08182	0.12592	171	0.64978	0.5167		-0.16673	0.33037
210	-0.12752	0.12592	171	1.01276	0.31261		-0.37608	0.12103
225	0.09703	0.12592	171	0.7706	0.44201		-0.15152	0.34558
240	0.15474	0.12592	171	1.22888	0.2208		-0.09381	0.40329
255	0.40265	0.12592	171	3.19774	0.00165	*	0.1541	0.6512
270	0.10928	0.12592	171	0.86785	0.38669		-0.13927	0.35783
285	0.00645	0.12592	171	0.05124	0.95919		-0.2421	0.255
300	0.18474	0.12592	171	1.46713	0.14418		-0.06381	0.43329

Table S16 ANOVA for PTP fEPSP amplitudes, preincubated in FAC, comparing post 1st and 2nd TBS in control vs. SCH23390 and Sulpiride – renormalized.

Time - seconds post-TBS; Mean Dif. – 1st TBS fEPSP amplitude subtracted from 2nd TBS fEPSP amplitude; std. error – standard error; DF – degrees of freedom; t value – statistical t-value; prob>t – probability that t value is the same as expected; Sig. – does prob>t reach a significance of <0.05; 95% LCL – 95% lower confidence interval; 95% UCL – 95% upper confidence interval.

Time	Mean Dif.	Std. Error	DF	|t|value	Prob>|t|	Sig.	95% LCL	95% UCL
15	0.00133	0.06294	171	0.02111	0.98319		-0.12291	0.12556
30	-0.01074	0.06294	171	0.17057	0.86476		-0.13497	0.1135
45	-0.02116	0.06294	171	0.33626	0.73709		-0.1454	0.10307
60	0.06636	0.06294	171	1.05443	0.29317		-0.05787	0.1906
75	0.0763	0.06294	171	1.21233	0.22706		-0.04793	0.20054
90	0.0209	0.06294	171	0.332	0.74029		-0.10334	0.14513
105	0.04991	0.06294	171	0.79306	0.42884		-0.07432	0.17415
120	0.06067	0.06294	171	0.96398	0.33642		-0.06356	0.18491
135	0.03808	0.06294	171	0.60506	0.54594		-0.08615	0.16232
150	0.0286	0.06294	171	0.45441	0.65011		-0.09564	0.15283
165	-0.01999	0.06294	171	0.31768	0.75112		-0.14423	0.10424
180	0.11851	0.06294	171	1.88299	0.0614		-0.00572	0.24275
195	0.14559	0.06294	171	2.3133	0.0219	*	0.02136	0.26983
210	0.18162	0.06294	171	2.88567	0.00441	*	0.05738	0.30585
225	0.11363	0.06294	171	1.80535	0.07278		-0.01061	0.23786
240	-0.01016	0.06294	171	0.1615	0.87189		-0.1344	0.11407
255	-0.0403	0.06294	171	0.64037	0.52279		-0.16454	0.08393
270	0.0449	0.06294	171	0.71336	0.47659		-0.07934	0.16913
285	0.13119	0.06294	171	2.08439	0.03861	*	0.00695	0.25542
300	-0.02058	0.06294	171	0.32691	0.74413		-0.14481	0.10366

Table S17 ANOVA for PTP PPR amplitudes, preincubated in FAC, comparing post 1st and 2nd TBS in control vs. SCH23390 and Sulpiride – both normalized to 1st baseline.

Time - seconds post-TBS; Mean Dif. – 1st TBS PPR amplitude subtracted from 2nd TBS PPR amplitude; std. error – standard error; DF – degrees of freedom; t value – statistical t-value; prob>t – probability that t value is the same as expected; Sig. – does prob>t reach a significance of <0.05; 95% LCL – 95% lower confidence interval; 95% UCL – 95% upper confidence interval.

Time	Mean Dif.	Std. Error	DF	|t|value	Prob>|t|	Sig.	95% LCL	95% UCL
15	-0.0627	0.07202	171	0.87054	0.38522		-0.20486	0.07947
30	-0.08991	0.07202	171	1.24838	0.2136		-0.23207	0.05225
45	-0.09373	0.07202	171	1.30137	0.19488		-0.23589	0.04844
60	-0.01124	0.07202	171	0.15613	0.87612		-0.15341	0.13092
75	0.00624	0.07202	171	0.08661	0.93108		-0.13593	0.1484
90	-0.06335	0.07202	171	0.87956	0.38033		-0.20551	0.07882
105	-0.0263	0.07202	171	0.36517	0.71544		-0.16846	0.11586
120	-0.02538	0.07202	171	0.35245	0.72494		-0.16755	0.11678
135	-0.04519	0.07202	171	0.62747	0.53119		-0.18735	0.09697
150	-0.04333	0.07202	171	0.6016	0.54824		-0.18549	0.09884
165	-0.1122	0.07202	171	1.5579	0.1211		-0.25436	0.02996
180	0.0454	0.07202	171	0.63041	0.52927		-0.09676	0.18757
195	0.07932	0.07202	171	1.10138	0.27228		-0.06284	0.22148
210	0.12125	0.07202	171	1.68355	0.09409		-0.02091	0.26341
225	0.03836	0.07202	171	0.53257	0.59502		-0.10381	0.18052
240	-0.10483	0.07202	171	1.45556	0.14735		-0.24699	0.03733
255	-0.11984	0.07202	171	1.66404	0.09794		-0.26201	0.02232
270	-0.04578	0.07202	171	0.63569	0.52583		-0.18795	0.09638
285	0.0569	0.07202	171	0.79004	0.4306		-0.08526	0.19906
300	-0.09922	0.07202	171	1.37761	0.17013		-0.24138	0.04295

Table S18 ANOVA for PTP PPR amplitudes, preincubated in FAC, comparing post 1st and 2nd TBS in control vs. SCH23390 and Sulpiride – renormalized.

Time - seconds post-TBS; Mean Dif. – 1st TBS PPR amplitude subtracted from 2nd TBS PPR amplitude; std. error – standard error; DF – degrees of freedom; t value – statistical t-value; prob>t – probability that t value is the same as expected; Sig. – does prob>t reach a significance of <0.05; 95% LCL – 95% lower confidence interval; 95% UCL – 95% upper confidence interval.

Chapter 10: References

Abraham, W. C., B. Logan, J. M. Greenwood and M. Dragunow (2002). "Induction and experience-dependent consolidation of stable long-term potentiation lasting months in the hippocampus." J Neurosci **22**(21): 9626-9634.

Adermark, L., R. B. Clarke, T. Olsson, E. Hansson, B. Soderpalm and M. Ericson (2011). "Implications for glycine receptors and astrocytes in ethanol-induced elevation of dopamine levels in the nucleus accumbens." Addict Biol **16**(1): 43-54.

Aguado, F., J. F. Espinosa-Parrilla, M. A. Carmona and E. Soriano (2002). "Neuronal activity regulates correlated network properties of spontaneous calcium transients in astrocytes in situ." J Neurosci **22**(21): 9430-9444.

Agulhon, C., T. A. Fiacco and K. D. McCarthy (2010). "Hippocampal short- and long-term plasticity are not modulated by astrocyte Ca2+ signaling." Science **327**(5970): 1250-1254.

Agulhon, C., J. Petravicz, A. B. McMullen, E. J. Sweger, S. K. Minton, S. R. Taves, K. B. Casper, T. A. Fiacco and K. D. McCarthy (2008). "What is the role of astrocyte calcium in neurophysiology?" Neuron **59**(6): 932-946.

Agulhon, C., M. Y. Sun, T. Murphy, T. Myers, K. Lauderdale and T. A. Fiacco (2012). "Calcium Signaling and Gliotransmission in Normal vs. Reactive Astrocytes." Front Pharmacol **3**: 139.

Akam, T., I. Oren, L. Mantoan, E. Ferenczi and D. M. Kullmann (2012). "Oscillatory dynamics in the hippocampus support dentate gyrus-CA3 coupling." Nat Neurosci **15**(5): 763-768.

Aly, M., C. Ranganath and A. P. Yonelinas (2013). "Detecting changes in scenes: the hippocampus is critical for strength-based perception." Neuron **78**(6): 1127-1137.

Aman, T. K., R. Y. Shen and S. Haj-Dahmane (2007). "D2-like dopamine receptors depolarize dorsal raphe serotonin neurons through the activation of nonselective cationic conductance." J Pharmacol Exp Ther **320**(1): 376-385.

Andersen P, Morris R, Amaral D, Bliss T, O'Keefe J (2007) The Hippocampus Book. Oxford University Press.

Andersson, M. and E. Hanse (2010). "Astrocytes impose postburst depression of release probability at hippocampal glutamate synapses." J Neurosci **30**(16): 5776-5780.

Andersson, R. H., A. Johnston, P. A. Herman, U. H. Winzer-Serhan, I. Karavanova, D. Vullhorst, A. Fisahn and A. Buonanno (2012). "Neuregulin and dopamine modulation of hippocampal gamma oscillations is dependent on dopamine D4 receptors." Proc Natl Acad Sci U S A **109**(32): 13118-13123.

Andrade, R., R. C. Malenka and R. A. Nicoll (1986). "A G protein couples serotonin and GABAB receptors to the same channels in hippocampus." Science **234**(4781): 1261-1265.

Ang, C. W., G. C. Carlson and D. A. Coulter (2005). "Hippocampal CA1 circuitry dynamically gates direct cortical inputs preferentially at theta frequencies." J Neurosci **25**(42): 9567-9580.

Araque, A., N. Li, R. T. Doyle and P. G. Haydon (2000). "SNARE protein-dependent glutamate release from astrocytes." J Neurosci **20**(2): 666-673.

Araque, A., E. D. Martin, G. Perea, J. I. Arellano and W. Buno (2002). "Synaptically released acetylcholine evokes Ca2+ elevations in astrocytes in hippocampal slices." J Neurosci **22**(7): 2443-2450.

Arcuino, G., J. H. Lin, T. Takano, C. Liu, L. Jiang, Q. Gao, J. Kang and M. Nedergaard (2002). "Intercellular calcium signaling mediated by point-source burst release of ATP." Proc Natl Acad Sci U S A **99**(15): 9840-9845.

Atkin, S. D., S. Patel, A. Kocharyan, L. A. Holtzclaw, S. H. Weerth, V. Schram, J. Pickel and J. T. Russell (2009). "Transgenic mice expressing a cameleon fluorescent Ca2+ indicator in astrocytes and Schwann cells allow study of glial cell Ca2+ signals in situ and in vivo." J Neurosci Methods **181**(2): 212-226.

Avalos-Fuentes, A., S. Loya-Lopez, A. Flores-Perez, S. Recillas-Morales, H. Cortes, F. Paz-Bermudez, J. Aceves, D. Erlij and B. Floran (2013). "Presynaptic CaMKIIalpha modulates dopamine D3 receptor activation in striatonigral terminals of the rat brain in a Ca(2)(+) dependent manner." Neuropharmacology **71**: 273-281.

Bai, J. Z. and J. Lipski (2010). "Differential expression of TRPM2 and TRPV4 channels and their potential role in oxidative stress-induced cell death in organotypic hippocampal culture." Neurotoxicology **31**(2): 204-214.

Bal, A., T. Bachelot, M. Savasta, M. Manier, J. M. Verna, A. L. Benabid and C. Feuerstein (1994). "Evidence for dopamine D2 receptor mRNA expression by striatal astrocytes in culture: in situ hybridization and polymerase chain reaction studies." Brain Res Mol Brain Res **23**(3): 204-212.

Barres, B. A., L. L. Chun and D. P. Corey (1989). "Calcium current in cortical astrocytes: induction by cAMP and neurotransmitters and permissive effect of serum factors." J Neurosci **9**(9): 3169-3175.

Bass, C. E., V. P. Grinevich, D. Gioia, J. D. Day-Brown, K. D. Bonin, G. D. Stuber, J. L. Weiner and E. A. Budygin (2013). "Optogenetic stimulation of VTA dopamine neurons reveals that tonic but not phasic patterns of dopamine transmission reduce ethanol self-administration." Front Behav Neurosci **7**: 173.

Basu, J., K. V. Srinivas, S. K. Cheung, H. Taniguchi, Z. J. Huang and S. A. Siegelbaum (2013). "A cortico-hippocampal learning rule shapes inhibitory microcircuit activity to enhance hippocampal information flow." Neuron **79**(6): 1208-1221.

Beckstead, R. M., V. B. Domesick and W. J. Nauta (1979). "Efferent connections of the substantia nigra and ventral tegmental area in the rat." Brain Res **175**(2): 191-217.

Benedetti, B., V. Matyash and H. Kettenmann (2011). "Astrocytes control GABAergic inhibition of neurons in the mouse barrel cortex." J Physiol **589**(Pt 5): 1159-1172.

Benesova, J., M. Hock, O. Butenko, I. Prajerova, M. Anderova and A. Chvatal (2009). "Quantification of astrocyte volume changes during ischemia in situ reveals two populations of astrocytes in the cortex of GFAP/EGFP mice." J Neurosci Res **87**(1): 96-111.

Benson, D. L., P. J. Isackson, C. M. Gall and E. G. Jones (1992). "Contrasting patterns in the localization of glutamic acid decarboxylase and Ca2+/calmodulin protein kinase gene expression in the rat central nervous system." Neuroscience **46**(4): 825-849.

Bergles, D. E. and C. E. Jahr (1997). "Synaptic activation of glutamate transporters in hippocampal astrocytes." Neuron **19**(6): 1297-1308.

Bernardinelli, Y., C. Salmon, E. V. Jones, W. T. Farmer, D. Stellwagen and K. K. Murai (2011). "Astrocytes display complex and localized calcium responses to single-neuron stimulation in the hippocampus." J Neurosci **31**(24): 8905-8919.

Berridge, K. C. (2007). "The debate over dopamine's role in reward: the case for incentive salience." Psychopharmacology (Berl) **191**(3): 391-431.

Bethus, I., D. Tse and R. G. Morris (2010). "Dopamine and memory: modulation of the persistence of memory for novel hippocampal NMDA receptor-dependent paired associates." J Neurosci **30**(5): 1610-1618.

Bezzi, P., G. Carmignoto, L. Pasti, S. Vesce, D. Rossi, B. L. Rizzini, T. Pozzan and A. Volterra (1998). "Prostaglandins stimulate calcium-dependent glutamate release in astrocytes." Nature **391**(6664): 281-285.

Bilmen, J. G. and F. Michelangeli (2002). "Inhibition of the type 1 inositol 1,4,5-trisphosphate receptor by 2-aminoethoxydiphenylborate." Cell Signal **14**(11): 955-960.

Bliss, T. V. and T. Lomo (1973). "Long-lasting potentiation of synaptic transmission in the dentate area of the anaesthetized rabbit following stimulation of the perforant path." J Physiol **232**(2): 331-356.

Bolton, S., K. Greenwood, N. Hamilton and A. M. Butt (2006). "Regulation of the astrocyte resting membrane potential by cyclic AMP and protein kinase A." Glia **54**(4): 316-328.

Bonansco, C., A. Couve, G. Perea, C. A. Ferradas, M. Roncagliolo and M. Fuenzalida (2011). "Glutamate released spontaneously from astrocytes sets the threshold for synaptic plasticity." Eur J Neurosci **33**(8): 1483-1492.

Bonci, A. and R. C. Malenka (1999). "Properties and plasticity of excitatory synapses on dopaminergic and GABAergic cells in the ventral tegmental area." J Neurosci **19**(10): 3723-3730.

Bootman MD1, Collins TJ, Mackenzie L, Roderick HL, Berridge MJ, Peppiatt CM (2002). "2-aminoethoxydiphenyl borate (2-APB) is a reliable blocker of store-operated Ca2+ entry but an inconsistent inhibitor of InsP3-induced Ca2+ release." FASEB J. Aug;16(10):1145-50..

Borgkvist, A., T. Malmlof, K. Feltmann, M. Lindskog and B. Schilstrom (2012). "Dopamine in the hippocampus is cleared by the norepinephrine transporter." Int J Neuropsychopharmacol **15**(4): 531-540.

Borodinsky, L. N., D. O'Leary, J. H. Neale, S. Vicini, O. A. Coso and M. L. Fiszman (2003). "GABA-induced neurite outgrowth of cerebellar granule cells is mediated by GABA(A) receptor activation, calcium influx and CaMKII and erk1/2 pathways." J Neurochem **84**(6): 1411-1420.

Bouron, A. and H. Reuter (1999). "The D1 dopamine receptor agonist SKF-38393 stimulates the release of glutamate in the hippocampus." Neuroscience **94**(4): 1063-1070.

Bowser, D. N. and B. S. Khakh (2004). "ATP excites interneurons and astrocytes to increase synaptic inhibition in neuronal networks." J Neurosci **24**(39): 8606-8620.

Brito, V., C. Beyer and E. Kuppers (2004). "BDNF-dependent stimulation of dopamine D5 receptor expression in developing striatal astrocytes involves PI3-kinase signaling." Glia **46**(3): 284-295.

Brown, N. A. and G. R. Seabrook (1995). "Phosphorylation- and voltage-dependent inhibition of neuronal calcium currents by activation of human D2(short) dopamine receptors." Br J Pharmacol **115**(3): 459-466.

Bruner, G. and S. Murphy (1990). "ATP-evoked arachidonic acid mobilization in astrocytes is via a P2Y-purinergic receptor." J Neurochem **55**(5): 1569-1575.

Burgos, M., M. D. Pastor, J. C. Gonzalez, J. R. Martinez-Galan, C. F. Vaquero, N. Fradejas, A. Benavides, J. M. Hernandez-Guijo, P. Tranque and S. Calvo (2007). "PKCepsilon upregulates voltage-dependent calcium channels in cultured astrocytes." Glia **55**(14): 1437-1448.

Bushong, E. A., M. E. Martone, Y. Z. Jones and M. H. Ellisman (2002). "Protoplasmic astrocytes in CA1 stratum radiatum occupy separate anatomical domains." J Neurosci **22**(1): 183-192.

Butt, A. M. and A. Kalsi (2006). "Inwardly rectifying potassium channels (Kir) in central nervous system glia: a special role for Kir4.1 in glial functions." J Cell Mol Med **10**(1): 33-44.

Buzsaki, G. (1989). "Two-stage model of memory trace formation: a role for "noisy" brain states." Neuroscience **31**(3): 551-570.

Cai, Z., G. P. Schools and H. K. Kimelberg (2000). "Metabotropic glutamate receptors in acutely isolated hippocampal astrocytes: developmental changes of mGluR5 mRNA and functional expression." Glia **29**(1): 70-80.

Cameron, D. L. and J. T. Williams (1993). "Dopamine D1 receptors facilitate transmitter release." Nature **366**(6453): 344-347.

Cantrell, A. R., R. D. Smith, A. L. Goldin, T. Scheuer and W. A. Catterall (1997). "Dopaminergic modulation of sodium current in hippocampal neurons via cAMP-dependent phosphorylation of specific sites in the sodium channel alpha subunit." J Neurosci **17**(19): 7330-7338.

Cao, X., L. P. Li, Q. Wang, Q. Wu, H. H. Hu, M. Zhang, Y. Y. Fang, J. Zhang, S. J. Li, W. C. Xiong, H. C. Yan, Y. B. Gao, J. H. Liu, X. W. Li, L. R. Sun, Y. N. Zeng, X. H. Zhu and T. M. Gao (2013). "Astrocyte-derived ATP modulates depressive-like behaviors." Nat Med **19**(6): 773-777.

Capogna, M. (2011). "Neurogliaform cells and other interneurons of stratum lacunosum-moleculare gate entorhinal-hippocampal dialogue." J Physiol **589**(Pt 8): 1875-1883.

Carboni, E., G. L. Tanda, R. Frau and G. Di Chiara (1990). "Blockade of the noradrenaline carrier increases extracellular dopamine concentrations in the prefrontal cortex: evidence that dopamine is taken up in vivo by noradrenergic terminals." J Neurochem **55**(3): 1067-1070.

Castro, N. G., M. C. de Mello, F. G. de Mello and Y. Aracava (1999). "Direct inhibition of the N-methyl-D-aspartate receptor channel by dopamine and (+)-SKF38393." Br J Pharmacol **126**(8): 1847-1855.

Cavelier, P. and D. Attwell (2005). "Tonic release of glutamate by a DIDS-sensitive mechanism in rat hippocampal slices." J Physiol **564**(Pt 2): 397-410.

Chaki, S., S. Okuyama, S. Ogawa and K. Tomisawa (1998). "Regulation of NMDA-induced [3H]dopamine release from rat hippocampal slices through sigma-1 binding sites." Neurochem Int **33**(1): 29-34.

Chang, M. S., L. M. Ariah, A. Marks and E. C. Azmitia (2005). "Chronic gliosis induced by loss of S-100B: knockout mice have enhanced GFAP-immunoreactivity but blunted response to a serotonin challenge." Brain Res **1031**(1): 1-9.

Charles, A. C., E. R. Dirksen, J. E. Merrill and M. J. Sanderson (1993). "Mechanisms of intercellular calcium signaling in glial cells studied with dantrolene and thapsigargin." Glia **7**(2): 134-145.

Charles, A. C., J. E. Merrill, E. R. Dirksen and M. J. Sanderson (1991). "Intercellular signaling in glial cells: calcium waves and oscillations in response to mechanical stimulation and glutamate." Neuron **6**(6): 983-992.

Chaudhury, D., J. J. Walsh, A. K. Friedman, B. Juarez, S. M. Ku, J. W. Koo, D. Ferguson, H. C. Tsai, L. Pomeranz, D. J. Christoffel, A. R. Nectow, M. Ekstrand, A. Domingos, M. S. Mazei-Robison, E. Mouzon, M. K. Lobo, R. L. Neve, J. M. Friedman, S. J. Russo, K. Deisseroth, E. J. Nestler and M. H. Han (2013). "Rapid regulation of depression-related behaviours by control of midbrain dopamine neurons." Nature **493**(7433): 532-536.

Chen, G., P. Greengard and Z. Yan (2004). "Potentiation of NMDA receptor currents by dopamine D1 receptors in prefrontal cortex." Proc Natl Acad Sci U S A **101**(8): 2596-2600.

Chen, L., J. D. Bohanick, M. Nishihara, J. K. Seamans and C. R. Yang (2007). "Dopamine D1/5 receptor-mediated long-term potentiation of intrinsic excitability in rat

prefrontal cortical neurons: Ca2+-dependent intracellular signaling." J Neurophysiol **97**(3): 2448-2464.

Chen, X., L. Wang, Y. Zhou, L. H. Zheng and Z. Zhou (2005). ""Kiss-and-run" glutamate secretion in cultured and freshly isolated rat hippocampal astrocytes." J Neurosci **25**(40): 9236-9243.

Chen, Z., K. Ito, S. Fujii, M. Miura, H. Furuse, H. Sasaki, K. Kaneko, H. Kato and H. Miyakawa (1996). "Roles of dopamine receptors in long-term depression: enhancement via D1 receptors and inhibition via D2 receptors." Receptors Channels **4**(1): 1-8.

Chetkovich, D. M. and J. D. Sweatt (1993). "nMDA receptor activation increases cyclic AMP in area CA1 of the hippocampus via calcium/calmodulin stimulation of adenylyl cyclase." J Neurochem **61**(5): 1933-1942.

Choi, H. B., G. R. Gordon, N. Zhou, C. Tai, R. L. Rungta, J. Martinez, T. A. Milner, J. K. Ryu, J. G. McLarnon, M. Tresguerres, L. R. Levin, J. Buck and B. A. MacVicar (2012). "Metabolic communication between astrocytes and neurons via bicarbonate-responsive soluble adenylyl cyclase." Neuron **75**(6): 1094-1104.

Chun, M. M. and E. A. Phelps (1999). "Memory deficits for implicit contextual information in amnesic subjects with hippocampal damage." Nat Neurosci **2**(9): 844-847.

Ciccarelli, R., P. Di Iorio, V. Bruno, G. Battaglia, I. D'Alimonte, M. D'Onofrio, F. Nicoletti and F. Caciagli (1999). "Activation of A(1) adenosine or mGlu3 metabotropic glutamate receptors enhances the release of nerve growth factor and S-100beta protein from cultured astrocytes." Glia **27**(3): 275-281.

Clarke, L. E. and B. A. Barres (2013). "Emerging roles of astrocytes in neural circuit development." Nat Rev Neurosci **14**(5): 311-321.

Cohen, J. Y., S. Haesler, L. Vong, B. B. Lowell and N. Uchida (2012). "Neuron-type-specific signals for reward and punishment in the ventral tegmental area." Nature **482**(7383): 85-88.

Colbert, C. M. and W. B. Levy (1993). "Long-term potentiation of perforant path synapses in hippocampal CA1 in vitro." Brain Res **606**(1): 87-91.

Collingridge, G. L., S. J. Kehl and H. McLennan (1983). "Excitatory amino acids in synaptic transmission in the Schaffer collateral-commissural pathway of the rat hippocampus." J Physiol **334**: 33-46.

Contreras, J. E., H. A. Sanchez, E. A. Eugenin, D. Speidel, M. Theis, K. Willecke, F. F. Bukauskas, M. V. Bennett and J. C. Saez (2002). "Metabolic inhibition induces opening of unapposed connexin 43 gap junction hemichannels and reduces gap

junctional communication in cortical astrocytes in culture." Proc Natl Acad Sci U S A **99**(1): 495-500.

Cornell-Bell, A. H., S. M. Finkbeiner, M. S. Cooper and S. J. Smith (1990). "Glutamate induces calcium waves in cultured astrocytes: long-range glial signaling." Science **247**(4941): 470-473.

Cotrina, M. L., J. H. Lin, A. Alves-Rodrigues, S. Liu, J. Li, H. Azmi-Ghadimi, J. Kang, C. C. Naus and M. Nedergaard (1998). "Connexins regulate calcium signaling by controlling ATP release." Proc Natl Acad Sci U S A **95**(26): 15735-15740.

Crow, J. M., M. M. Atkinson and R. G. Johnson (1994). "Micromolar levels of intracellular calcium reduce gap junctional permeability in lens cultures." Invest Ophthalmol Vis Sci **35**(8): 3332-3341.

D'Ascenzo, M., M. Vairano, C. Andreassi, P. Navarra, G. B. Azzena and C. Grassi (2004). "Electrophysiological and molecular evidence of L-(Cav1), N- (Cav2.2), and R-(Cav2.3) type Ca2+ channels in rat cortical astrocytes." Glia **45**(4): 354-363.

da Silva, W. C., C. C. Kohler, A. Radiske and M. Cammarota (2012). "D1/D5 dopamine receptors modulate spatial memory formation." Neurobiol Learn Mem **97**(2): 271-275.

Danbolt, N. C. (2001). "Glutamate uptake." Prog Neurobiol **65**(1): 1-105.

Davies, C. H., S. J. Starkey, M. F. Pozza and G. L. Collingridge (1991). "GABA autoreceptors regulate the induction of LTP." Nature **349**(6310): 609-611.

De Pitta, M., V. Volman, H. Berry and E. Ben-Jacob (2011). "A tale of two stories: astrocyte regulation of synaptic depression and facilitation." PLoS Comput Biol **7**(12): e1002293.

Defagot, M. C., E. L. Malchiodi, M. J. Villar and M. C. Antonelli (1997). "Distribution of D4 dopamine receptor in rat brain with sequence-specific antibodies." Brain Res Mol Brain Res **45**(1): 1-12.

Demchyshyn, L. L., F. McConkey and H. B. Niznik (2000). "Dopamine D5 receptor agonist high affinity and constitutive activity profile conferred by carboxyl-terminal tail sequence." J Biol Chem **275**(31): 23446-23455.

Desrues, L., M. Lamacz, B. G. Jenks, H. Vaudry and M. C. Tonon (1993). "Effect of dopamine on adenylate cyclase activity, polyphosphoinositide metabolism and cytosolic calcium concentrations in frog pituitary melanotrophs." J Endocrinol **136**(3): 421-429.

Devaraju, P., M. Y. Sun, T. L. Myers, K. Lauderdale and T. A. Fiacco (2013). "Astrocytic group I mGluR-dependent potentiation of astrocytic glutamate and potassium uptake." J Neurophysiol **109**(9): 2404-2414.

Di Castro, M. A., J. Chuquet, N. Liaudet, K. Bhaukaurally, M. Santello, D. Bouvier, P. Tiret and A. Volterra (2011). "Local Ca2+ detection and modulation of synaptic release by astrocytes." Nat Neurosci **14**(10): 1276-1284.

Dimpfel, W. and J. A. Hoffmann (2011). "Effects of rasagiline, its metabolite aminoindan and selegiline on glutamate receptor mediated signalling in the rat hippocampus slice in vitro." BMC Pharmacol **11**: 2.

Ding, S., T. Fellin, Y. Zhu, S. Y. Lee, Y. P. Auberson, D. F. Meaney, D. A. Coulter, G. Carmignoto and P. G. Haydon (2007). "Enhanced astrocytic Ca2+ signals contribute to neuronal excitotoxicity after status epilepticus." J Neurosci **27**(40): 10674-10684.

Duffy, A. M., M. L. Fitzgerald, J. Chan, D. C. Robinson, T. A. Milner, K. Mackie and V. M. Pickel (2011). "Acetylcholine alpha7 nicotinic and dopamine D2 receptors are targeted to many of the same postsynaptic dendrites and astrocytes in the rodent prefrontal cortex." Synapse **65**(12): 1350-1367.

Duffy, S. and B. A. MacVicar (1994). "Potassium-dependent calcium influx in acutely isolated hippocampal astrocytes." Neuroscience **61**(1): 51-61.

Dunlap, K., J. I. Luebke and T. J. Turner (1995). "Exocytotic Ca2+ channels in mammalian central neurons." Trends Neurosci **18**(2): 89-98.

Dunn, K. M., D. C. Hill-Eubanks, W. B. Liedtke and M. T. Nelson (2013). "TRPV4 channels stimulate Ca2+-induced Ca2+ release in astrocytic endfeet and amplify neurovascular coupling responses." Proc Natl Acad Sci U S A **110**(15): 6157-6162.

Ekblom, J., S. S. Jossan, M. Bergstrom, L. Oreland, E. Walum and S. M. Aquilonius (1993). "Monoamine oxidase-B in astrocytes." Glia **8**(2): 122-132.

el Mestikawy, S., J. Glowinski and M. Hamon (1986). "Presynaptic dopamine autoreceptors control tyrosine hydroxylase activation in depolarized striatal dopaminergic terminals." J Neurochem **46**(1): 12-22.

Eldridge, L. L., B. J. Knowlton, C. S. Furmanski, S. Y. Bookheimer and S. A. Engel (2000). "Remembering episodes: a selective role for the hippocampus during retrieval." Nat Neurosci **3**(11): 1149-1152.

Emptage, N. J., C. A. Reid, A. Fine and T. V. Bliss (2003). "Optical quantal analysis reveals a presynaptic component of LTP at hippocampal Schaffer-associational synapses." Neuron **38**(5): 797-804.

Ernfors, P., P. Lonnerberg, C. Ayer-LeLievre and H. Persson (1990). "Developmental and regional expression of basic fibroblast growth factor mRNA in the rat central nervous system." J Neurosci Res **27**(1): 10-15.

Erondu, N. E. and M. B. Kennedy (1985). "Regional distribution of type II Ca2+/calmodulin-dependent protein kinase in rat brain." J Neurosci **5**(12): 3270-3277.

Everitt, B. J., J. A. Parkinson, M. C. Olmstead, M. Arroyo, P. Robledo and T. W. Robbins (1999). "Associative processes in addiction and reward. The role of amygdala-ventral striatal subsystems." Ann N Y Acad Sci **877**: 412-438.

Fagni, L., P. Chavis, F. Ango and J. Bockaert (2000). "Complex interactions between mGluRs, intracellular Ca2+ stores and ion channels in neurons." Trends Neurosci **23**(2): 80-88.

Fass, D. M., K. Takimoto, R. E. Mains and E. S. Levitan (1999). "Tonic dopamine inhibition of L-type Ca2+ channel activity reduces alpha1D Ca2+ channel gene expression." J Neurosci **19**(9): 3345-3352.

Fatatis, A. and J. T. Russell (1992). "Spontaneous changes in intracellular calcium concentration in type I astrocytes from rat cerebral cortex in primary culture." Glia **5**(2): 95-104.

Fellin, T., O. Pascual, S. Gobbo, T. Pozzan, P. G. Haydon and G. Carmignoto (2004). "Neuronal synchrony mediated by astrocytic glutamate through activation of extrasynaptic NMDA receptors." Neuron **43**(5): 729-743.

Fenno, L., O. Yizhar and K. Deisseroth (2011). "The development and application of optogenetics." Annu Rev Neurosci **34**: 389-412.

Fernandez de Sevilla, D. and W. Buno (2003). "Presynaptic inhibition of Schaffer collateral synapses by stimulation of hippocampal cholinergic afferent fibres." Eur J Neurosci **17**(3): 555-558.

Ferroni, S., C. Marchini, T. Ogata and P. Schubert (2002). "Recovery of deficient cholinergic calcium signaling by adenosine in cultured rat cortical astrocytes." J Neurosci Res **68**(5): 615-621.

Fiacco, T. A., C. Agulhon, S. R. Taves, J. Petravicz, K. B. Casper, X. Dong, J. Chen and K. D. McCarthy (2007). "Selective stimulation of astrocyte calcium in situ does not affect neuronal excitatory synaptic activity." Neuron **54**(4): 611-626.

Fiacco, T. A. and K. D. McCarthy (2004). "Intracellular astrocyte calcium waves in situ increase the frequency of spontaneous AMPA receptor currents in CA1 pyramidal neurons." J Neurosci **24**(3): 722-732.

Fields, R. D. (2011). "Nonsynaptic and nonvesicular ATP release from neurons and relevance to neuron-glia signaling." Semin Cell Dev Biol **22**(2): 214-219.

Fischer, R., F. Schliess and D. Haussinger (1997). "Characterization of the hypo-osmolarity-induced Ca2+ response in cultured rat astrocytes." Glia **20**(1): 51-58.

Flores-Hernandez, J., S. Hernandez, G. L. Snyder, Z. Yan, A. A. Fienberg, S. J. Moss, P. Greengard and D. J. Surmeier (2000). "D(1) dopamine receptor activation reduces GABA(A) receptor currents in neostriatal neurons through a PKA/DARPP-32/PP1 signaling cascade." J Neurophysiol **83**(5): 2996-3004.

Florian, C., C. G. Vecsey, M. M. Halassa, P. G. Haydon and T. Abel (2011). "Astrocyte-derived adenosine and A1 receptor activity contribute to sleep loss-induced deficits in hippocampal synaptic plasticity and memory in mice." J Neurosci **31**(19): 6956-6962.

Fog, J. U., H. Khoshbouei, M. Holy, W. A. Owens, C. B. Vaegter, N. Sen, Y. Nikandrova, E. Bowton, D. G. McMahon, R. J. Colbran, L. C. Daws, H. H. Sitte, J. A. Javitch, A. Galli and U. Gether (2006). "Calmodulin kinase II interacts with the dopamine transporter C terminus to regulate amphetamine-induced reverse transport." Neuron **51**(4): 417-429.

Foskett, J. K., C. White, K. H. Cheung and D. O. Mak (2007). "Inositol trisphosphate receptor Ca2+ release channels." Physiol Rev **87**(2): 593-658.

Fossat, P., F. R. Turpin, S. Sacchi, J. Dulong, T. Shi, J. M. Rivet, J. V. Sweedler, L. Pollegioni, M. J. Millan, S. H. Oliet and J. P. Mothet (2012). "Glial D-serine gates NMDA receptors at excitatory synapses in prefrontal cortex." Cereb Cortex **22**(3): 595-606.

Frey, U., S. Hartmann and H. Matthies (1989). "Domperidone, an inhibitor of the D2-receptor, blocks a late phase of an electrically induced long-term potentiation in the CA1-region in rats." Biomed Biochim Acta **48**(7): 473-476.

Frey, U., H. Matthies, K. G. Reymann and H. Matthies (1991). "The effect of dopaminergic D1 receptor blockade during tetanization on the expression of long-term potentiation in the rat CA1 region in vitro." Neurosci Lett **129**(1): 111-114.

Frey, U., H. Schroeder and H. Matthies (1990). "Dopaminergic antagonists prevent long-term maintenance of posttetanic LTP in the CA1 region of rat hippocampal slices." Brain Res **522**(1): 69-75.

Fumagalli, M., R. Brambilla, N. D'Ambrosi, C. Volonte, M. Matteoli, C. Verderio and M. P. Abbracchio (2003). "Nucleotide-mediated calcium signaling in rat cortical astrocytes: Role of P2X and P2Y receptors." Glia **43**(3): 218-203.

Fuxe, K., A. B. Dahlstrom, G. Jonsson, D. Marcellino, M. Guescini, M. Dam, P. Manger and L. Agnati (2010). "The discovery of central monoamine neurons gave volume transmission to the wired brain." Prog Neurobiol **90**(2): 82-100.

Gangarossa, G., S. Longueville, D. De Bundel, J. Perroy, D. Herve, J. A. Girault and E. Valjent (2012). "Characterization of dopamine D1 and D2 receptor-expressing neurons in the mouse hippocampus." Hippocampus **22**(12): 2199-2207.

Garcia, A. D., R. Petrova, L. Eng and A. L. Joyner (2010). "Sonic hedgehog regulates discrete populations of astrocytes in the adult mouse forebrain." J Neurosci **30**(41): 13597-13608.

Gasbarri, A., M. G. Packard, E. Campana and C. Pacitti (1994a). "Anterograde and retrograde tracing of projections from the ventral tegmental area to the hippocampal formation in the rat." Brain Res Bull **33**(4): 445-452.

Gasbarri, A., A. Sulli, R. Innocenzi, C. Pacitti and J. D. Brioni (1996). "Spatial memory impairment induced by lesion of the mesohippocampal dopaminergic system in the rat." Neuroscience **74**(4): 1037-1044.

Gasbarri, A., A. Sulli and M. G. Packard (1997). "The dopaminergic mesencephalic projections to the hippocampal formation in the rat." Prog Neuropsychopharmacol Biol Psychiatry **21**(1): 1-22.

Gasbarri, A., C. Verney, R. Innocenzi, E. Campana and C. Pacitti (1994b). "Mesolimbic dopaminergic neurons innervating the hippocampal formation in the rat: a combined retrograde tracing and immunohistochemical study." Brain Res **668**(1-2): 71-79.

Geppert, M., Y. Goda, R. E. Hammer, C. Li, T. W. Rosahl, C. F. Stevens and T. C. Sudhof (1994). "Synaptotagmin I: a major Ca2+ sensor for transmitter release at a central synapse." Cell **79**(4): 717-727.

Gerlach, R., G. Demel, H. G. Konig, U. Gross, J. H. Prehn, A. Raabe, V. Seifert and D. Kogel (2006). "Active secretion of S100B from astrocytes during metabolic stress." Neuroscience **141**(4): 1697-1701.

Gerschenfeld, H. M., D. Paupardin-Tritsch, C. Hammond and R. Harris-Warrick (1989). "Intracellular mechanism of neurotransmitter-induced modulations of voltage-dependent Ca current in snail neurons." Cell Biol Int Rep **13**(12): 1141-1154.

Ghanbarian, E. and F. Motamedi (2013). "Ventral tegmental area inactivation suppresses the expression of CA1 long term potentiation in anesthetized rat." PLoS One **8**(3): e58844.

Giannotti, G., L. Caffino, F. Calabrese, G. Racagni and F. Fumagalli (2013). "Dynamic modulation of basic Fibroblast Growth Factor (FGF-2) expression in the rat brain following repeated exposure to cocaine during adolescence." Psychopharmacology (Berl) **225**(3): 553-560.

Giaume, C., L. Leybaert, C. C. Naus and J. C. Saez (2013). "Connexin and pannexin hemichannels in brain glial cells: properties, pharmacology, and roles." Front Pharmacol **4**: 88.

Giaume, C. and M. Theis (2010). "Pharmacological and genetic approaches to study connexin-mediated channels in glial cells of the central nervous system." Brain Res Rev **63**(1-2): 160-176.

Giaume, C. and L. Venance (1998). "Intercellular calcium signaling and gap junctional communication in astrocytes." Glia **24**(1): 50-64.

Gines, S., J. Hillion, M. Torvinen, S. Le Crom, V. Casado, E. I. Canela, S. Rondin, J. Y. Lew, S. Watson, M. Zoli, L. F. Agnati, P. Verniera, C. Lluis, S. Ferre, K. Fuxe and R. Franco (2000). "Dopamine D1 and adenosine A1 receptors form functionally interacting heteromeric complexes." Proc Natl Acad Sci U S A **97**(15): 8606-8611.

Glaum, S. R., J. A. Holzwarth and R. J. Miller (1990). "Glutamate receptors activate Ca2+ mobilization and Ca2+ influx into astrocytes." Proc Natl Acad Sci U S A **87**(9): 3454-3458.

Goldsmith, S. K. and J. N. Joyce (1994). "Dopamine D2 receptor expression in hippocampus and parahippocampal cortex of rat, cat, and human in relation to tyrosine hydroxylase-immunoreactive fibers." Hippocampus **4**(3): 354-373.

Golovina, V. A. (2005). "Visualization of localized store-operated calcium entry in mouse astrocytes. Close proximity to the endoplasmic reticulum." J Physiol **564**(Pt 3): 737-749.

Gonzalez-Hernandez, T., I. Cruz-Muros, D. Afonso-Oramas, J. Salas-Hernandez and J. Castro-Hernandez (2010). "Vulnerability of mesostriatal dopaminergic neurons in Parkinson's disease." Front Neuroanat **4**: 140.

Gonzalez-Islas, C. and J. J. Hablitz (2003). "Dopamine enhances EPSCs in layer II-III pyramidal neurons in rat prefrontal cortex." J Neurosci **23**(3): 867-875.

Gourine, A. V., V. Kasymov, N. Marina, F. Tang, M. F. Figueiredo, S. Lane, A. G. Teschemacher, K. M. Spyer, K. Deisseroth and S. Kasparov (2010). "Astrocytes control breathing through pH-dependent release of ATP." Science **329**(5991): 571-575.

Gribkoff, V. K. and J. H. Ashe (1984). "Modulation by dopamine of population responses and cell membrane properties of hippocampal CA1 neurons in vitro." Brain Res **292**(2): 327-338.

Griffith, L. C. (2004). "Calcium/calmodulin-dependent protein kinase II: an unforgettable kinase." J Neurosci **24**(39): 8391-8393.

Grimaldi, M., M. Maratos and A. Verma (2003). "Transient receptor potential channel activation causes a novel form of [Ca 2+]I oscillations and is not involved in capacitative Ca 2+ entry in glial cells." J Neurosci **23**(11): 4737-4745.

Grosche, J., V. Matyash, T. Moller, A. Verkhratsky, A. Reichenbach and H. Kettenmann (1999). "Microdomains for neuron-glia interaction: parallel fiber signaling to Bergmann glial cells." Nat Neurosci **2**(2): 139-143.

Gulledge, A. T. and D. B. Jaffe (2001). "Multiple effects of dopamine on layer V pyramidal cell excitability in rat prefrontal cortex." J Neurophysiol **86**(2): 586-595.

Guthrie, P. B., J. Knappenberger, M. Segal, M. V. Bennett, A. C. Charles and S. B. Kater (1999). "ATP released from astrocytes mediates glial calcium waves." J Neurosci **19**(2): 520-528.

Haak, L. L., H. C. Heller and A. N. van den Pol (1997). "Metabotropic glutamate receptor activation modulates kainate and serotonin calcium response in astrocytes." J Neurosci **17**(5): 1825-1837.

Halassa, M. M., T. Fellin, H. Takano, J. H. Dong and P. G. Haydon (2007). "Synaptic islands defined by the territory of a single astrocyte." J Neurosci **27**(24): 6473-6477.

Halassa, M. M., C. Florian, T. Fellin, J. R. Munoz, S. Y. Lee, T. Abel, P. G. Haydon and M. G. Frank (2009). "Astrocytic modulation of sleep homeostasis and cognitive consequences of sleep loss." Neuron **61**(2): 213-219.

Hammad, H. and J. J. Wagner (2006). "Dopamine-mediated disinhibition in the CA1 region of rat hippocampus via D3 receptor activation." J Pharmacol Exp Ther **316**(1): 113-120.

Hammond, S., C. M. Seymour, A. Burger and J. J. Wagner (2013). "D-Serine facilitates the effectiveness of extinction to reduce drug-primed reinstatement of cocaine-induced conditioned place preference." Neuropharmacology **64**: 464-471.

Hansen, N. and D. Manahan-Vaughan (2012). "Dopamine D1/D5 Receptors Mediate Informational Saliency that Promotes Persistent Hippocampal Long-Term Plasticity." Cereb Cortex.

Hasbi, A., T. Fan, M. Alijaniaram, T. Nguyen, M. L. Perreault, B. F. O'Dowd and S. R. George (2009). "Calcium signaling cascade links dopamine D1-D2 receptor heteromer to

striatal BDNF production and neuronal growth." Proc Natl Acad Sci U S A **106**(50): 21377-21382.

Hasbi, A., B. F. O'Dowd and S. R. George (2010). "Heteromerization of dopamine D2 receptors with dopamine D1 or D5 receptors generates intracellular calcium signaling by different mechanisms." Curr Opin Pharmacol **10**(1): 93-99.

Hasbi, A., B. F. O'Dowd and S. R. George (2011). "Dopamine D1-D2 receptor heteromer signaling pathway in the brain: emerging physiological relevance." Mol Brain **4**: 26.

Hassinger, T. D., P. B. Guthrie, P. B. Atkinson, M. V. Bennett and S. B. Kater (1996). "An extracellular signaling component in propagation of astrocytic calcium waves." Proc Natl Acad Sci U S A **93**(23): 13268-13273.

Heinonen, E. H. and R. Lammintausta (1991). "A review of the pharmacology of selegiline." Acta Neurol Scand Suppl **136**: 44-59.

Heinrich, A., R. D. Ando, G. Turi, B. Rozsa and B. Sperlagh (2012). "K+ depolarization evokes ATP, adenosine and glutamate release from glia in rat hippocampus: a microelectrode biosensor study." Br J Pharmacol **167**(5): 1003-1020.

Henneberger, C., T. Papouin, S. H. Oliet and D. A. Rusakov (2010). "Long-term potentiation depends on release of D-serine from astrocytes." Nature **463**(7278): 232-236.

Henneberger, C. and D. A. Rusakov (2012). "Monitoring local synaptic activity with astrocytic patch pipettes." Nat Protoc **7**(12): 2171-2179.

Hepp, R., M. Perraut, S. Chasserot-Golaz, T. Galli, D. Aunis, K. Langley and N. J. Grant (1999). "Cultured glial cells express the SNAP-25 analogue SNAP-23." Glia **27**(2): 181-187.

Herlinger E, Jameson RF, Linert J (1995) Spontaneous autoxidation of dopamine. J Chem Soc Perkin Trans 2, 259-263

Hernandez-Lopez, S., T. Tkatch, E. Perez-Garci, E. Galarraga, J. Bargas, H. Hamm and D. J. Surmeier (2000). "D2 dopamine receptors in striatal medium spiny neurons reduce L-type Ca2+ currents and excitability via a novel PLC[beta]1-IP3-calcineurin-signaling cascade." J Neurosci **20**(24): 8987-8995.

Herron, C. E., R. A. Lester, E. J. Coan and G. L. Collingridge (1986). "Frequency-dependent involvement of NMDA receptors in the hippocampus: a novel synaptic mechanism." Nature **322**(6076): 265-268.

Hertz, L. (1965). "Possible role of neuroglia: a potassium-mediated neuronal--neuroglial--neuronal impulse transmission system." Nature **206**(989): 1091-1094.

Herwerth, M., V. Jensen, M. Novak, W. Konopka, O. Hvalby and G. Kohr (2012). "D4 dopamine receptors modulate NR2B NMDA receptors and LTP in stratum oriens of hippocampal CA1." Cereb Cortex **22**(8): 1786-1798.

Hewett, J. A. (2009). "Determinants of regional and local diversity within the astroglial lineage of the normal central nervous system." J Neurochem **110**(6): 1717-1736.

Higashi, K., A. Fujita, A. Inanobe, M. Tanemoto, K. Doi, T. Kubo and Y. Kurachi (2001). "An inwardly rectifying K(+) channel, Kir4.1, expressed in astrocytes surrounds synapses and blood vessels in brain." Am J Physiol Cell Physiol **281**(3): C922-931.

Hirase, H., L. Qian, P. Bartho and G. Buzsaki (2004). "Calcium dynamics of cortical astrocytic networks in vivo." PLoS Biol **2**(4): E96.

Hirrlinger J1, Hülsmann S, Kirchhoff F. (2004). " Astroglial processes show spontaneous motility at active synaptic terminals in situ." Eur J Neurosci 20(*):2235-9Hogerton, A. L. and M. T. Bowser (2013). "Monitoring neurochemical release from astrocytes using in vitro microdialysis coupled with high-speed capillary electrophoresis." Anal Chem **85**(19): 9070-9077.

Hokfelt T, Martensson R, Bjorklund A, Kleinau S, Goldstein M. (1984) Distributional maps of tyrosine-hydroxylase immunoreactive neurons in the rat brain. In: Bjorklund A, Hokfelt T, eds Handbook of Chemical Neuroanatomy, Vol II: Classical Neurotransmitters in the CNS, Part I. Amsterdam: Elsevier, 277-379.

Holtzclaw LA, Pandhit S, Bare DJ, Mignery GA, Russell JT. (2002) Astrocytes in adult rat brain express type 2 inositol 1,4,5-trisphosphate receptors. Glia. 2002 Jul;39(1):69-84.

Horio, M., M. Kohno, Y. Fujita, T. Ishima, R. Inoue, H. Mori and K. Hashimoto (2012). "Role of serine racemase in behavioral sensitization in mice after repeated administration of methamphetamine." PLoS One **7**(4): e35494.

Horn, R. and A. Marty (1988). "Muscarinic activation of ionic currents measured by a new whole-cell recording method." J Gen Physiol **92**(2): 145-159.

Hosli, E. and L. Hosli (1986). "Binding sites for [3H]dopamine and dopamine-antagonists on cultured astrocytes of rat striatum and spinal cord: an autoradiographic study." Neurosci Lett **65**(2): 177-182.

Hsu, K. S. (1996). "Characterization of dopamine receptors mediating inhibition of excitatory synaptic transmission in the rat hippocampal slice." J Neurophysiol **76**(3): 1887-1895.

Huang, C., J. Wu, R. Liao and W. Zhang (2012). "SKF83959, an agonist of phosphatidylinositol-linked D(1)-like receptors, promotes ERK1/2 activation and cell migration in cultured rat astrocytes." PLoS One **7**(11): e49954.

Huang, C. C., J. J. Tsai and K. S. Hsu (1997). "L-deprenyl (selegiline) limits the repetitive firing of action potentials in rat hippocampal CA1 neurons via a dopaminergic mechanism." Brain Res **753**(1): 27-35.

Huang, Y. Y. and E. R. Kandel (1995). "D1/D5 receptor agonists induce a protein synthesis-dependent late potentiation in the CA1 region of the hippocampus." Proc Natl Acad Sci U S A **92**(7): 2446-2450.

Hubbard JA1, Hsu MS, Fiacco TA, Binder DK. (2013) "Glial cell changes in epilepsy: overview of the clinical problem and therapeutic opportunities" Neurochem Int. 2013 Dec;63(7):638-51.

Ihalainen, J. A., P. Riekkinen, Jr. and M. G. Feenstra (1999). "Comparison of dopamine and noradrenaline release in mouse prefrontal cortex, striatum and hippocampus using microdialysis." Neurosci Lett **277**(2): 71-74.

Illes, P., A. Verkhratsky, G. Burnstock and H. Franke (2012). "P2X receptors and their roles in astroglia in the central and peripheral nervous system." Neuroscientist **18**(5): 422-438.

Inazu, M., N. Kubota, H. Takeda, J. Zhang, Y. Kiuchi, K. Oguchi and T. Matsumiya (1999). "Pharmacological characterization of dopamine transport in cultured rat astrocytes." Life Sci **64**(24): 2239-2245.

Inazu, M., H. Takeda and T. Matsumiya (2003). "Functional expression of the norepinephrine transporter in cultured rat astrocytes." J Neurochem **84**(1): 136-144.

Ivanova, T. N., A. L. Alonso-Gomez and P. M. Iuvone (2008). "Dopamine D4 receptors regulate intracellular calcium concentration in cultured chicken cone photoreceptor cells: relationship to dopamine receptor-mediated inhibition of cAMP formation." Brain Res **1207**: 111-119.

Iversen LL, Iversen SD, Dunnett SB, Bjorklund A. (2010). Dopamine Handbook. Oxford University Press.

Jalonen, T. O., R. R. Margraf, D. B. Wielt, C. J. Charniga, M. L. Linne and H. K. Kimelberg (1997). "Serotonin induces inward potassium and calcium currents in rat cortical astrocytes." Brain Res **758**(1-2): 69-82.

Janigro, D., R. Wender, G. Ransom, D. L. Tinklepaugh and H. R. Winn (1996). "Adenosine-induced release of nitric oxide from cortical astrocytes." Neuroreport **7**(10): 1640-1644.

Jensen, A. M. and S. Y. Chiu (1990). "Fluorescence measurement of changes in intracellular calcium induced by excitatory amino acids in cultured cortical astrocytes." J Neurosci **10**(4): 1165-1175.

Jones, E. G., G. W. Huntley and D. L. Benson (1994). "Alpha calcium/calmodulin-dependent protein kinase II selectively expressed in a subpopulation of excitatory neurons in monkey sensory-motor cortex: comparison with GAD-67 expression." J Neurosci **14**(2): 611-629.

Judge, S. J. and M. E. Hasselmo (2004). "Theta rhythmic stimulation of stratum lacunosum-moleculare in rat hippocampus contributes to associative LTP at a phase offset in stratum radiatum." J Neurophysiol **92**(3): 1615-1624.

Kahlert, S., T. Blaser, M. Tulapurkar and G. Reiser (2007). "P2Y receptor-activating nucleotides modulate cellular reactive oxygen species production in dissociated hippocampal astrocytes and neurons in culture independent of parallel cytosolic Ca(2+) rise and change in mitochondrial potential." J Neurosci Res **85**(15): 3443-3456.

Kamata, A., Y. Takeuchi and K. Fukunaga (2006). "Identification of the isoforms of Ca2+/calmodulin-dependent protein kinase II and expression of brain-derived neurotrophic factor mRNAs in the substantia nigra." J Neurochem **96**(1): 195-203.

Kanemaru, K., Y. Okubo, K. Hirose and M. Iino (2007). "Regulation of neurite growth by spontaneous Ca2+ oscillations in astrocytes." J Neurosci **27**(33): 8957-8966.

Kang, J., L. Jiang, S. A. Goldman and M. Nedergaard (1998). "Astrocyte-mediated potentiation of inhibitory synaptic transmission." Nat Neurosci **1**(8): 683-692.

Kang, J., N. Kang, D. Lovatt, A. Torres, Z. Zhao, J. Lin and M. Nedergaard (2008). "Connexin 43 hemichannels are permeable to ATP." J Neurosci **28**(18): 4702-4711.

Kang, J., N. Kang, Y. Yu, J. Zhang, N. Petersen, G. F. Tian and M. Nedergaard (2010). "Sulforhodamine 101 induces long-term potentiation of intrinsic excitability and synaptic efficacy in hippocampal CA1 pyramidal neurons." Neuroscience **169**(4): 1601-1609.

Kaphzan, H., K. J. O'Riordan, K. P. Mangan, J. M. Levenson and K. Rosenblum (2006). "NMDA and dopamine converge on the NMDA-receptor to induce ERK activation and synaptic depression in mature hippocampus." PLoS One **1**: e138.

Kastritsis, C. H., A. K. Salm and K. McCarthy (1992). "Stimulation of the P2Y purinergic receptor on type 1 astroglia results in inositol phosphate formation and calcium mobilization." J Neurochem **58**(4): 1277-1284.

Kawazoe, T., H. Tsuge, T. Imagawa, K. Aki, S. Kuramitsu and K. Fukui (2007). "Structural basis of D-DOPA oxidation by D-amino acid oxidase: alternative pathway for dopamine biosynthesis." Biochem Biophys Res Commun **355**(2): 385-391.

Kearn, C. S., K. Blake-Palmer, E. Daniel, K. Mackie and M. Glass (2005). "Concurrent stimulation of cannabinoid CB1 and dopamine D2 receptors enhances heterodimer formation: a mechanism for receptor cross-talk?" Mol Pharmacol **67**(5): 1697-1704.

Khan, Z. U., A. Gutierrez, R. Martin, A. Penafiel, A. Rivera and A. de la Calle (2000). "Dopamine D5 receptors of rat and human brain." Neuroscience **100**(4): 689-699.

Khan, Z. U., P. Koulen, M. Rubinstein, D. K. Grandy and P. S. Goldman-Rakic (2001). "An astroglia-linked dopamine D2-receptor action in prefrontal cortex." Proc Natl Acad Sci U S A **98**(4): 1964-1969.

Kim, S. and S. W. Hwang (2013). "Emerging roles of TRPA1 in sensation of oxidative stress and its implications in defense and danger." Arch Pharm Res **36**(7): 783-791.

Kimelberg, H. K., Z. Cai, P. Rastogi, C. J. Charniga, S. Goderie, V. Dave and T. O. Jalonen (1997). "Transmitter-induced calcium responses differ in astrocytes acutely isolated from rat brain and in culture." J Neurochem **68**(3): 1088-1098.

Kittel-Schneider, S., G. Kenis, J. Schek, D. van den Hove, J. Prickaerts, K. P. Lesch, H. Steinbusch and A. Reif (2012). "Expression of monoamine transporters, nitric oxide synthase 3, and neurotrophin genes in antidepressant-stimulated astrocytes." Front Psychiatry **3**: 33.

Kittner, H., U. Krugel and P. Illes (2001). "The purinergic P2 receptor antagonist pyridoxalphosphate-6-azophenyl-2'4'-disulphonic acid prevents both the acute locomotor effects of amphetamine and the behavioural sensitization caused by repeated amphetamine injections in rats." Neuroscience **102**(2): 241-243.

Klausberger, T. and P. Somogyi (2008). "Neuronal diversity and temporal dynamics: the unity of hippocampal circuit operations." Science **321**(5885): 53-57.

Koizumi, S., Y. Saito, K. Nakazawa, K. Nakajima, J. I. Sawada, S. Kohsaka, P. Illes and K. Inoue (2002). "Spatial and temporal aspects of Ca2+ signaling mediated by P2Y receptors in cultured rat hippocampal astrocytes." Life Sci **72**(4-5): 431-442.

Koller, H., K. Thiem and M. Siebler (1996). "Tumour necrosis factor-alpha increases intracellular Ca2+ and induces a depolarization in cultured astroglial cells." Brain **119 (Pt 6)**: 2021-2027.

Kotecha, S. A., J. N. Oak, M. F. Jackson, Y. Perez, B. A. Orser, H. H. Van Tol and J. F. MacDonald (2002). "A D2 class dopamine receptor transactivates a receptor tyrosine kinase to inhibit NMDA receptor transmission." Neuron **35**(6): 1111-1122.

Koyama, S., Y. Kanemitsu and F. F. Weight (2005). "Spontaneous activity and properties of two types of principal neurons from the ventral tegmental area of rat." J Neurophysiol **93**(6): 3282-3293.

Kuchibhotla, K. V., C. R. Lattarulo, B. T. Hyman and B. J. Bacskai (2009). "Synchronous hyperactivity and intercellular calcium waves in astrocytes in Alzheimer mice." Science **323**(5918): 1211-1215.

Kwon, O. B., D. Paredes, C. M. Gonzalez, J. Neddens, L. Hernandez, D. Vullhorst and A. Buonanno (2008). "Neuregulin-1 regulates LTP at CA1 hippocampal synapses through activation of dopamine D4 receptors." Proc Natl Acad Sci U S A **105**(40): 15587-15592.

Lachowicz, J. E. and D. R. Sibley (1997). "Chimeric D2/D3 dopamine receptor coupling to adenylyl cyclase." Biochem Biophys Res Commun **237**(2): 394-399.

Lalo, U., O. Palygin, S. Rasooli-Nejad, J. Andrew, P. G. Haydon and Y. Pankratov (2014). "Exocytosis of ATP from astrocytes modulates phasic and tonic inhibition in the neocortex." PLoS Biol **12**(1): e1001747.

Land, B. B., N. S. Narayanan, R. J. Liu, C. A. Gianessi, C. E. Brayton, M. G. D, M. Sarhan, D. J. Guarnieri, K. Deisseroth, G. K. Aghajanian and R. J. Dileone (2014). "Medial prefrontal D1 dopamine neurons control food intake." Nat Neurosci **17**(2): 248-253.

Largo, C., J. M. Ibarz and O. Herreras (1997). "Effects of the gliotoxin fluorocitrate on spreading depression and glial membrane potential in rat brain in situ." J Neurophysiol **78**(1): 295-307.

Leao, R. N., S. Mikulovic, K. E. Leao, H. Munguba, H. Gezelius, A. Enjin, K. Patra, A. Eriksson, L. M. Loew, A. B. Tort and K. Kullander (2012). "OLM interneurons differentially modulate CA3 and entorhinal inputs to hippocampal CA1 neurons." Nat Neurosci **15**(11): 1524-1530.

Lee, F. J., S. Xue, L. Pei, B. Vukusic, N. Chery, Y. Wang, Y. T. Wang, H. B. Niznik, X. M. Yu and F. Liu (2002). "Dual regulation of NMDA receptor functions by direct protein-protein interactions with the dopamine D1 receptor." Cell **111**(2): 219-230.

Lee, M., E. G. McGeer and P. L. McGeer (2011). "Mechanisms of GABA release from human astrocytes." Glia **59**(11): 1600-1611.

Lee, S., B. E. Yoon, K. Berglund, S. J. Oh, H. Park, H. S. Shin, G. J. Augustine and C. J. Lee (2010). "Channel-mediated tonic GABA release from glia." Science **330**(6005): 790-796.

Lee, S. P., C. H. So, A. J. Rashid, G. Varghese, R. Cheng, A. J. Lanca, B. F. O'Dowd and S. R. George (2004). "Dopamine D1 and D2 receptor Co-activation generates a novel phospholipase C-mediated calcium signal." J Biol Chem **279**(34): 35671-35678.

Lemon, N. and D. Manahan-Vaughan (2006). "Dopamine D1/D5 receptors gate the acquisition of novel information through hippocampal long-term potentiation and long-term depression." J Neurosci **26**(29): 7723-7729.

Lezcano, N. and C. Bergson (2002). "D1/D5 dopamine receptors stimulate intracellular calcium release in primary cultures of neocortical and hippocampal neurons." J Neurophysiol **87**(4): 2167-2175.

Li, A., H. Guo, X. Luo, J. Sheng, S. Yang, Y. Yin, J. Zhou and J. Zhou (2006). "Apomorphine-induced activation of dopamine receptors modulates FGF-2 expression in astrocytic cultures and promotes survival of dopaminergic neurons." Faseb j **20**(8): 1263-1265.

Li, S., W. K. Cullen, R. Anwyl and M. J. Rowan (2003). "Dopamine-dependent facilitation of LTP induction in hippocampal CA1 by exposure to spatial novelty." Nat Neurosci **6**(5): 526-531.

Lin, R. C. and R. H. Scheller (2000). "Mechanisms of synaptic vesicle exocytosis." Annu Rev Cell Dev Biol **16**: 19-49.

Lim D1, Ronco V, Grolla AA, Verkhratsky A, Genazzani AA. (2014) " Glial Calcium Signalling in Alzheimer's disease" Rev Physiol Biochem Pharmacol. Jun 17.

Liu, J., F. Wang, C. Huang, L. H. Long, W. N. Wu, F. Cai, J. H. Wang, L. Q. Ma and J. G. Chen (2009a). "Activation of phosphatidylinositol-linked novel D1 dopamine receptor contributes to the calcium mobilization in cultured rat prefrontal cortical astrocytes." Cell Mol Neurobiol **29**(3): 317-328.

Liu, J., W. Wang, F. Wang, F. Cai, Z. L. Hu, Y. J. Yang, J. Chen and J. G. Chen (2009b). "Phosphatidylinositol-linked novel D(1) dopamine receptor facilitates long-term depression in rat hippocampal CA1 synapses." Neuropharmacology **57**(2): 164-171.

Liu, X. B. and E. G. Jones (1996). "Localization of alpha type II calcium calmodulin-dependent protein kinase at glutamatergic but not gamma-aminobutyric acid (GABAergic) synapses in thalamus and cerebral cortex." Proc Natl Acad Sci U S A **93**(14): 7332-7336.

Liu, X. Y., X. P. Chu, L. M. Mao, M. Wang, H. X. Lan, M. H. Li, G. C. Zhang, N. K. Parelkar, E. E. Fibuch, M. Haines, K. A. Neve, F. Liu, Z. G. Xiong and J. Q. Wang (2006). "Modulation of D2R-NR2B interactions in response to cocaine." Neuron **52**(5): 897-909.

Liu, X. Y., L. M. Mao, G. C. Zhang, C. J. Papasian, E. E. Fibuch, H. X. Lan, H. F. Zhou, M. Xu and J. Q. Wang (2009c). "Activity-dependent modulation of limbic dopamine D3 receptors by CaMKII." Neuron **61**(3): 425-438.

Luciana, M. and P. F. Collins (1997). "Dopaminergic modulation of working memory for spatial but not object cues in normal humans." J Cogn Neurosci **9**(3): 330-347.

Luo, Y., G. C. Kokkonen, A. Hattori, F. J. Chrest and G. S. Roth (1999). "Dopamine stimulates redox-tyrosine kinase signaling and p38 MAPK in activation of astrocytic C6-D2L cells." Brain Res **850**(1-2): 21-38.

MacDermott, A. B., L. W. Role and S. A. Siegelbaum (1999). "Presynaptic ionotropic receptors and the control of transmitter release." Annu Rev Neurosci **22**: 443-485.

Malarkey, E. B., Y. Ni and V. Parpura (2008). "Ca2+ entry through TRPC1 channels contributes to intracellular Ca2+ dynamics and consequent glutamate release from rat astrocytes." Glia **56**(8): 821-835.

Malarkey, E. B. and V. Parpura (2008). "Mechanisms of glutamate release from astrocytes." Neurochem Int **52**(1-2): 142-154.

Malgaroli, A., L. Vallar, F. R. Elahi, T. Pozzan, A. Spada and J. Meldolesi (1987). "Dopamine inhibits cytosolic Ca2+ increases in rat lactotroph cells. Evidence of a dual mechanism of action." J Biol Chem **262**(29): 13920-13927.

Marin, P., M. Tence, J. C. Delumeau, J. Glowinski and J. Premont (1993). "Adenosine and somatostatin potentiate the alpha 1-adrenergic activation of phospholipase C in striatal astrocytes through a mechanism involving arachidonic acid and glutamate." Biochem Soc Trans **21**(4): 1114-1119.

Martig, A. K. and S. J. Mizumori (2011). "Ventral tegmental area disruption selectively affects CA1/CA2 but not CA3 place fields during a differential reward working memory task." Hippocampus **21**(2): 172-184.

Martino, A. T., R. W. Herzog, I. Anegon and O. Adjali (2011). "Measuring immune responses to recombinant AAV gene transfer." Methods Mol Biol **807**: 259-272.

Matthies, H., A. Becker, H. Schroeder, J. Kraus, V. Hollt and M. Krug (1997). "Dopamine D1-deficient mutant mice do not express the late phase of hippocampal long-term potentiation." Neuroreport **8**(16): 3533-3535.

McCarthy, K. D. and A. K. Salm (1991). "Pharmacologically-distinct subsets of astroglia can be identified by their calcium response to neuroligands." Neuroscience **41**(2-3): 325-333.

Meier, S. D., K. W. Kafitz and C. R. Rose (2008). "Developmental profile and mechanisms of GABA-induced calcium signaling in hippocampal astrocytes." Glia **56**(10): 1127-1137.

Miller, R. H. and M. C. Raff (1984). "Fibrous and protoplasmic astrocytes are biochemically and developmentally distinct." J Neurosci **4**(2): 585-592.

Miller, R. J. (1998). "Presynaptic receptors." Annu Rev Pharmacol Toxicol **38**: 201-227.

Min, R. and T. Nevian (2012). "Astrocyte signaling controls spike timing-dependent depression at neocortical synapses." Nat Neurosci **15**(5): 746-753.

Ming, Y., H. Zhang, L. Long, F. Wang, J. Chen and X. Zhen (2006). "Modulation of Ca2+ signals by phosphatidylinositol-linked novel D1 dopamine receptor in hippocampal neurons." J Neurochem **98**(4): 1316-1323.

Mintz, I. M. and B. P. Bean (1993). "GABAB receptor inhibition of P-type Ca2+ channels in central neurons." Neuron **10**(5): 889-898.

Mirenowicz, J. and W. Schultz (1996). "Preferential activation of midbrain dopamine neurons by appetitive rather than aversive stimuli." Nature **379**(6564): 449-451.

Miyazaki, I., M. Asanuma, F. J. Diaz-Corrales, K. Miyoshi and N. Ogawa (2004). "Direct evidence for expression of dopamine receptors in astrocytes from basal ganglia." Brain Res **1029**(1): 120-123.

Mizuta, I., M. Ohta, K. Ohta, M. Nishimura, E. Mizuta, K. Hayashi and S. Kuno (2000). "Selegiline and desmethylselegiline stimulate NGF, BDNF, and GDNF synthesis in cultured mouse astrocytes." Biochem Biophys Res Commun **279**(3): 751-755.

Mockett, B. G., D. Guevremont, J. M. Williams and W. C. Abraham (2007). "Dopamine D1/D5 receptor activation reverses NMDA receptor-dependent long-term depression in rat hippocampus." J Neurosci **27**(11): 2918-2926.

Molofsky, A. V., R. Krencik, E. M. Ullian, H. H. Tsai, B. Deneen, W. D. Richardson, B. A. Barres and D. H. Rowitch (2012). "Astrocytes and disease: a neurodevelopmental perspective." Genes Dev **26**(9): 891-907.

Montagu, K. A. (1957). "Catechol compounds in rat tissues and in brains of different animals." Nature **180**(4579): 244-245.

Morris, R. G., E. Anderson, G. S. Lynch and M. Baudry (1986). "Selective impairment of learning and blockade of long-term potentiation by an N-methyl-D-aspartate receptor antagonist, AP5." Nature **319**(6056): 774-776.

Murphy, S. and G. Welk (1990). "Serotonin inhibits ATP-induced mobilization of arachidonic acid but not phosphoinositide turnover in astrocytes." Neurosci Lett **109**(1-2): 152-156.

Nardin, P., A. C. Tramontina, A. Quincozes-Santos, L. S. Tortorelli, P. Lunardi, P. R. Klein, K. M. Wartchow, L. D. Bobermin, C. Gottfried, E. Elisabetsky and C. A. Goncalves (2011). "In vitro S100B secretion is reduced by apomorphine: effects of antipsychotics and antioxidants." Prog Neuropsychopharmacol Biol Psychiatry **35**(5): 1291-1296.

Navarrete, M. and A. Araque (2008). "Endocannabinoids mediate neuron-astrocyte communication." Neuron **57**(6): 883-893.

Navarrete, M. and A. Araque (2010). "Endocannabinoids potentiate synaptic transmission through stimulation of astrocytes." Neuron **68**(1): 113-126.

Navarrete, M., G. Perea, L. Maglio, J. Pastor, R. Garcia de Sola and A. Araque (2013). "Astrocyte calcium signal and gliotransmission in human brain tissue." Cereb Cortex **23**(5): 1240-1246.

Naziroglu, M. (2012). "Molecular role of catalase on oxidative stress-induced Ca(2+) signaling and TRP cation channel activation in nervous system." J Recept Signal Transduct Res **32**(3): 134-141.

Nett, W. J., S. H. Oloff and K. D. McCarthy (2002). "Hippocampal astrocytes in situ exhibit calcium oscillations that occur independent of neuronal activity." J Neurophysiol **87**(1): 528-537.

Neusch, C., S. Schnierle and A. Moser (1997). "Selegiline induces dopamine release through ATP-sensitive potassium channels in the rat caudate-putamen in vitro." Neurochem Int **31**(2): 307-311.

Newlin, S. A., W. T. Schlapfer and S. H. Barondes (1980). "Separate serotonin and dopamine receptors modulate the duration of post-tetanic potentiation at an Aplysia synapse without affecting other aspects of synaptic transmission." Brain Res **181**(1): 89-106.

Nilsson, M., P. S. Eriksson, L. Ronnback and E. Hansson (1993). "GABA induces Ca2+ transients in astrocytes." Neuroscience **54**(3): 605-614.

Nilsson, M., E. Hansson and L. Ronnback (1991). "Heterogeneity among astroglial cells with respect to 5HT-evoked cytosolic Ca2+ responses. A microspectrofluorimetric study on single cells in primary culture." Life Sci **49**(18): 1339-1350.

Nilsson, M., E. Hansson and L. Ronnback (1992). "Agonist-evoked Ca2+ transients in primary astroglial cultures--modulatory effects of valproic acid." Glia **5**(3): 201-209.

Nimmerjahn, A., F. Kirchhoff, J. N. Kerr and F. Helmchen (2004). "Sulforhodamine 101 as a specific marker of astroglia in the neocortex in vivo." Nat Methods **1**(1): 31-37.

O'Carroll, C. M. and R. G. Morris (2004). "Heterosynaptic co-activation of glutamatergic and dopaminergic afferents is required to induce persistent long-term potentiation." Neuropharmacology **47**(3): 324-332.

O'keefe and Nadel, (1978), The Hippocampus as a Cognitive Map. Oxford University Press.

Ochiishi, T., T. Yamauchi and T. Terashima (1998). "Regional differences between the immunohistochemical distribution of Ca2+/calmodulin-dependent protein kinase II alpha and beta isoforms in the brainstem of the rat." Brain Res **790**(1-2): 129-140.

Ogata, K. and T. Kosaka (2002). "Structural and quantitative analysis of astrocytes in the mouse hippocampus." Neuroscience **113**(1): 221-233.

Ogata, T., Y. Nakamura and P. Schubert (1996). "Potentiated cAMP rise in metabotropically stimulated rat cultured astrocytes by a Ca2+-related A1/A2 adenosine receptor cooperation." Eur J Neurosci **8**(6): 1124-1131.

Ogata, T., Y. Nakamura, K. Tsuji, T. Shibata, K. Kataoka and P. Schubert (1994). "Adenosine enhances intracellular Ca2+ mobilization in conjunction with metabotropic glutamate receptor activation by t-ACPD in cultured hippocampal astrocytes." Neurosci Lett **170**(1): 5-8.

Oh, M. S., S. J. Hong, Y. Huh and K. S. Kim (2009). "Expression of transgenes in midbrain dopamine neurons using the tyrosine hydroxylase promoter." Gene Ther **16**(3): 437-440.

Ohta, K., S. Kuno, S. Inoue, E. Ikeda, A. Fujinami and M. Ohta (2010). "The effect of dopamine agonists: the expression of GDNF, NGF, and BDNF in cultured mouse astrocytes." J Neurol Sci **291**(1-2): 12-16.

Olds, J. and P. Milner (1954). "Positive reinforcement produced by electrical stimulation of septal area and other regions of rat brain." J Comp Physiol Psychol **47**(6): 419-427.

Oliet, S. H. and J. P. Mothet (2009). "Regulation of N-methyl-D-aspartate receptors by astrocytic D-serine." Neuroscience **158**(1): 275-283.

Oliet, S. H., R. Piet and D. A. Poulain (2001). "Control of glutamate clearance and synaptic efficacy by glial coverage of neurons." Science **292**(5518): 923-926.

Ortiz, O., J. M. Delgado-Garcia, I. Espadas, A. Bahi, R. Trullas, J. L. Dreyer, A. Gruart and R. Moratalla (2010). "Associative learning and CA3-CA1 synaptic plasticity are

impaired in D1R null, Drd1a-/- mice and in hippocampal siRNA silenced Drd1a mice." J Neurosci **30**(37): 12288-12300.

Otmakhova, N. A. and J. E. Lisman (1996). "D1/D5 dopamine receptor activation increases the magnitude of early long-term potentiation at CA1 hippocampal synapses." J Neurosci **16**(23): 7478-7486.

Otmakhova, N. A. and J. E. Lisman (1998). "D1/D5 dopamine receptors inhibit depotentiation at CA1 synapses via cAMP-dependent mechanism." J Neurosci **18**(4): 1270-1279.

Otmakhova, N. A. and J. E. Lisman (1999). "Dopamine selectively inhibits the direct cortical pathway to the CA1 hippocampal region." J Neurosci **19**(4): 1437-1445.

Otmakhova, N. A. and J. E. Lisman (2000). "Dopamine, serotonin, and noradrenaline strongly inhibit the direct perforant path-CA1 synaptic input, but have little effect on the Schaffer collateral input." Ann N Y Acad Sci **911**: 462-464.

Otto, T. and H. Eichenbaum (1992). "Neuronal activity in the hippocampus during delayed non-match to sample performance in rats: evidence for hippocampal processing in recognition memory." Hippocampus **2**(3): 323-334.

Packard, M. G. and N. M. White (1991). "Dissociation of hippocampus and caudate nucleus memory systems by posttraining intracerebral injection of dopamine agonists." Behav Neurosci **105**(2): 295-306.

Padmanabhan, S. and B. M. Prasad (2009). "Sustained depolarization decreases calcium/calmodulin-dependent protein kinase II activity and gene expression in dopamine neurons." Neuroscience **163**(1): 277-285.

Padmashri, R. and S. K. Sikdar (2007). "Glutamate pretreatment affects Ca2+ signaling in processes of astrocyte pairs." J Neurochem **100**(1): 105-117.

Panatier, A., D. T. Theodosis, J. P. Mothet, B. Touquet, L. Pollegioni, D. A. Poulain and S. H. Oliet (2006). "Glia-derived D-serine controls NMDA receptor activity and synaptic memory." Cell **125**(4): 775-784.

Panatier, A., J. Vallee, M. Haber, K. K. Murai, J. C. Lacaille and R. Robitaille (2011). "Astrocytes are endogenous regulators of basal transmission at central synapses." Cell **146**(5): 785-798.

Parpura, V., T. A. Basarsky, F. Liu, K. Jeftinija, S. Jeftinija and P. G. Haydon (1994). "Glutamate-mediated astrocyte-neuron signalling." Nature **369**(6483): 744-747.

Parpura, V., Y. Fang, T. Basarsky, R. Jahn and P. G. Haydon (1995). "Expression of synaptobrevin II, cellubrevin and syntaxin but not SNAP-25 in cultured astrocytes." FEBS Lett **377**(3): 489-492.

Parpura, V., V. Grubisic and A. Verkhratsky (2011). "Ca(2+) sources for the exocytotic release of glutamate from astrocytes." Biochim Biophys Acta **1813**(5): 984-991.

Parpura, V. and P. G. Haydon (2000). "Physiological astrocytic calcium levels stimulate glutamate release to modulate adjacent neurons." Proc Natl Acad Sci U S A **97**(15): 8629-8634.

Parpura V, Haydon P G. (2009) Astrocytes in (Patho)physiology of the nervous system. Springer Science and Business Media

Parri, H. R. and V. Crunelli (2003). "The role of Ca2+ in the generation of spontaneous astrocytic Ca2+ oscillations." Neuroscience **120**(4): 979-992.

Parri, H. R., T. M. Gould and V. Crunelli (2001). "Spontaneous astrocytic Ca2+ oscillations in situ drive NMDAR-mediated neuronal excitation." Nat Neurosci **4**(8): 803-812.

Pascual, O., K. B. Casper, C. Kubera, J. Zhang, R. Revilla-Sanchez, J. Y. Sul, H. Takano, S. J. Moss, K. McCarthy and P. G. Haydon (2005). "Astrocytic purinergic signaling coordinates synaptic networks." Science **310**(5745): 113-116.

Paul, K. and C. L. Cox (2013). "Age-dependent actions of dopamine on inhibitory synaptic transmission in superficial layers of mouse prefrontal cortex." J Neurophysiol **109**(5): 1323-1332.

Pearce, B., J. Albrecht, C. Morrow and S. Murphy (1986a). "Astrocyte glutamate receptor activation promotes inositol phospholipid turnover and calcium flux." Neurosci Lett **72**(3): 335-340.

Pearce, B., C. Morrow and S. Murphy (1986b). "Receptor-mediated inositol phospholipid hydrolysis in astrocytes." Eur J Pharmacol **121**(2): 231-243.

Pei, L., F. J. Lee, A. Moszczynska, B. Vukusic and F. Liu (2004). "Regulation of dopamine D1 receptor function by physical interaction with the NMDA receptors." J Neurosci **24**(5): 1149-1158.

Pellerin, L. (2005). "How astrocytes feed hungry neurons." Mol Neurobiol **32**(1): 59-72.

Perea, G. and A. Araque (2005). "Properties of synaptically evoked astrocyte calcium signal reveal synaptic information processing by astrocytes." J Neurosci **25**(9): 2192-2203.

Perea, G. and A. Araque (2007). "Astrocytes potentiate transmitter release at single hippocampal synapses." Science **317**(5841): 1083-1086.

Perea, G., M. Navarrete and A. Araque (2009). "Tripartite synapses: astrocytes process and control synaptic information." Trends Neurosci **32**(8): 421-431.

Perea, G., A. Yang, E. S. Boyden and M. Sur (2014). "Optogenetic astrocyte activation modulates response selectivity of visual cortex neurons in vivo." Nat Commun **5**: 3262.

Perez, M. F., K. A. Ford, I. Goussakov, G. E. Stutzmann and X. T. Hu (2011). "Repeated cocaine exposure decreases dopamine D(2)-like receptor modulation of Ca(2+) homeostasis in rat nucleus accumbens neurons." Synapse **65**(2): 168-180.

Perreault, M. L., A. Hasbi, M. Alijaniaram, B. F. O'Dowd and S. R. George (2012). "Reduced striatal dopamine D1-D2 receptor heteromer expression and behavioural subsensitivity in juvenile rats." Neuroscience **225**: 130-139.

Petravicz, J., T. A. Fiacco and K. D. McCarthy (2008). "Loss of IP3 receptor-dependent Ca2+ increases in hippocampal astrocytes does not affect baseline CA1 pyramidal neuron synaptic activity." J Neurosci **28**(19): 4967-4973.

Pirotton, S., D. Communi, S. Motte, R. Janssens and J. M. Boeynaems (1996). "Endothelial P2-purinoceptors: subtypes and signal transduction." J Auton Pharmacol **16**(6): 353-356.

Porter, J. T. and K. D. McCarthy (1995a). "Adenosine receptors modulate [Ca2+]i in hippocampal astrocytes in situ." J Neurochem **65**(4): 1515-1523.

Porter, J. T. and K. D. McCarthy (1995b). "GFAP-positive hippocampal astrocytes in situ respond to glutamatergic neuroligands with increases in [Ca2+]i." Glia **13**(2): 101-112.

Porter, J. T. and K. D. McCarthy (1996). "Hippocampal astrocytes in situ respond to glutamate released from synaptic terminals." J Neurosci **16**(16): 5073-5081.

Poskanzer, K. E. and R. Yuste (2011). "Astrocytic regulation of cortical UP states." Proc Natl Acad Sci U S A **108**(45): 18453-18458.

Preissler, T., T. Luft, F. Kapczinski, J. Quevedo, G. Schwartsmann and R. Roesler (2007). "Basic fibroblast growth factor prevents the memory impairment induced by gastrin-releasing peptide receptor antagonism in area CA1 of the rat hippocampus." Neurochem Res **32**(8): 1381-1386.

Quandt FN, MacVicar BA. (1986) Calcium activated potassium channels in cultured astrocytes. Neuroscience 19, 29-41.

Queiroz, G., D. K. Meyer, A. Meyer, K. Starke and I. von Kugelgen (1999). "A study of the mechanism of the release of ATP from rat cortical astroglial cells evoked by activation of glutamate receptors." Neuroscience **91**(3): 1171-1181.

Rackauskas, M., V. Neverauskas and V. A. Skeberdis (2010). "Diversity and properties of connexin gap junction channels." Medicina (Kaunas) **46**(1): 1-12.

Ransom B. R., Ye Z. (2005) Gap junctions and hemichannels. In Neuroglia, Kettenmann H., Ransom B. R., editors. , eds (New York, Oxford University Press;), pp. 177–189.

Rashid, A. J., C. H. So, M. M. Kong, T. Furtak, M. El-Ghundi, R. Cheng, B. F. O'Dowd and S. R. George (2007). "D1-D2 dopamine receptor heterooligomers with unique pharmacology are coupled to rapid activation of Gq/11 in the striatum." Proc Natl Acad Sci U S A **104**(2): 654-659.

Raturi, A., C. Ortiz-Sandoval and T. Simmen (2013). "Redox dependence of endoplasmic reticulum (ER) Ca(2)(+) signaling." Histol Histopathol.

Requardt, R. P., P. G. Hirrlinger, F. Wilhelm, U. Winkler, S. Besser and J. Hirrlinger (2012). "Ca(2)(+) signals of astrocytes are modulated by the NAD(+)/NADH redox state." J Neurochem **120**(6): 1014-1025.

Requardt, R. P., F. Wilhelm, J. Rillich, U. Winkler and J. Hirrlinger (2010). "The biphasic NAD(P)H fluorescence response of astrocytes to dopamine reflects the metabolic actions of oxidative phosphorylation and glycolysis." J Neurochem **115**(2): 483-492.

Reuss, B., D. S. Leung, C. Ohlemeyer, H. Kettenmann and K. Unsicker (2000). "Regionally distinct regulation of astroglial neurotransmitter receptors by fibroblast growth factor-2." Mol Cell Neurosci **16**(1): 42-58.

Reuss, B. and K. Unsicker (2000). "Survival and differentiation of dopaminergic mesencephalic neurons are promoted by dopamine-mediated induction of FGF-2 in striatal astroglial cells." Mol Cell Neurosci **16**(6): 781-792.

Reuss, B. and K. Unsicker (2001). "Atypical neuroleptic drugs downregulate dopamine sensitivity in rat cortical and striatal astrocytes." Mol Cell Neurosci **18**(2): 197-209.

Reyes, R. C. and V. Parpura (2008). "Mitochondria modulate Ca2+-dependent glutamate release from rat cortical astrocytes." J Neurosci **28**(39): 9682-9691.

Reyes, R. C., A. Verkhratsky and V. Parpura (2012). "Plasmalemmal Na+/Ca2+ exchanger modulates Ca2+-dependent exocytotic release of glutamate from rat cortical astrocytes." ASN Neuro **4**(1).

Reyes, R. C., A. Verkhratsky and V. Parpura (2013). "TRPC1-mediated Ca2+ and Na+ signalling in astroglia: differential filtering of extracellular cations." Cell Calcium **54**(2): 120-125.

Rice, M. E. and S. J. Cragg (2008). "Dopamine spillover after quantal release: rethinking dopamine transmission in the nigrostriatal pathway." Brain Res Rev **58**(2): 303-313.

Richtand, N. M., Y. Liu, R. Ahlbrand, J. R. Sullivan, A. H. Newman and R. K. McNamara (2010). "Dopaminergic regulation of dopamine D3 and D3nf receptor mRNA expression." Synapse **64**(8): 634-643.

Riva, M. A., R. Molteni and G. Racagni (1997). "L-deprenyl potentiates cAMP-induced elevation of FGF-2 mRNA levels in rat cortical astrocytes." Neuroreport **8**(9-10): 2165-2168.

Rivas, J., J. M. Gaztelu and E. Garcia-Austt (1996). "Changes in hippocampal cell discharge patterns and theta rhythm spectral properties as a function of walking velocity in the guinea pig." Exp Brain Res **108**(1): 113-118.

Roche, K. W., R. J. O'Brien, A. L. Mammen, J. Bernhardt and R. L. Huganir (1996). "Characterization of multiple phosphorylation sites on the AMPA receptor GluR1 subunit." Neuron **16**(6): 1179-1188.

Roggenhofer, E., P. Fidzinski, J. Bartsch, F. Kurz, O. Shor and J. Behr (2010). "Activation of dopamine D1/D5 receptors facilitates the induction of presynaptic long-term potentiation at hippocampal output synapses." Eur J Neurosci **32**(4): 598-605.

Roggenhofer, E., P. Fidzinski, O. Shor and J. Behr (2013). "Reduced threshold for induction of LTP by activation of dopamine D1/D5 receptors at hippocampal CA1-subiculum synapses." PLoS One **8**(4): e62520.

Rojas, H., C. Colina, M. Ramos, G. Benaim, E. H. Jaffe, C. Caputo and R. DiPolo (2007). "Na+ entry via glutamate transporter activates the reverse Na+/Ca2+ exchange and triggers Ca(i)2+-induced Ca2+ release in rat cerebellar Type-1 astrocytes." J Neurochem **100**(5): 1188-1202.

Rossato, J. I., L. R. Bevilaqua, I. Izquierdo, J. H. Medina and M. Cammarota (2009). "Dopamine controls persistence of long-term memory storage." Science **325**(5943): 1017-1020.

Rubini, P., J. Engelhardt, K. Wirkner and P. Illes (2008). "Modulation by D1 and D2 dopamine receptors of ATP-induced release of intracellular Ca2+ in cultured rat striatal neurons." Neurochem Int **52**(1-2): 113-118.

Rusakov, D. A., L. Bard, M. G. Stewart and C. Henneberger (2014). "Diversity of astroglial functions alludes to subcellular specialisation." Trends Neurosci.

Rusakov, D. A., K. Zheng and C. Henneberger (2011). "Astrocytes as regulators of synaptic function: a quest for the Ca2+ master key." Neuroscientist **17**(5): 513-523.

Russ, H., K. Staust, F. Martel, M. Gliese and E. Schomig (1996). "The extraneuronal transporter for monoamine transmitters exists in cells derived from human central nervous system glia." Eur J Neurosci **8**(6): 1256-1264.

Safiulina, V. F., R. Afzalov, L. Khiroug, E. Cherubini and R. Giniatullin (2006). "Reactive oxygen species mediate the potentiating effects of ATP on GABAergic synaptic transmission in the immature hippocampus." J Biol Chem **281**(33): 23464-23470.

Sainsbury, R. S., J. L. Harris and G. L. Rowland (1987). "Sensitization and hippocampal type 2 theta in the rat." Physiol Behav **41**(5): 489-493.

Salm, A. K. and K. D. McCarthy (1990). "Norepinephrine-evoked calcium transients in cultured cerebral type 1 astroglia." Glia **3**(6): 529-538.

Santello, M., P. Bezzi and A. Volterra (2011). "TNFalpha controls glutamatergic gliotransmission in the hippocampal dentate gyrus." Neuron **69**(5): 988-1001.

Sarantis, K., N. Matsokis and F. Angelatou (2009). "Synergistic interactions of dopamine D1 and glutamate NMDA receptors in rat hippocampus and prefrontal cortex: involvement of ERK1/2 signaling." Neuroscience **163**(4): 1135-1145.

Sasaki, T., N. Kuga, S. Namiki, N. Matsuki and Y. Ikegaya (2011). "Locally synchronized astrocytes." Cereb Cortex **21**(8): 1889-1900.

Savasta, M., A. Dubois and B. Scatton (1986). "Autoradiographic localization of D1 dopamine receptors in the rat brain with [3H]SCH 23390." Brain Res **375**(2): 291-301.

Scemes, E. and C. Giaume (2006). "Astrocyte calcium waves: what they are and what they do." Glia **54**(7): 716-725.

Schenk, F. and R. G. Morris (1985). "Dissociation between components of spatial memory in rats after recovery from the effects of retrohippocampal lesions." Exp Brain Res **58**(1): 11-28.

Schipke, C. G., A. Heidemann, A. Skupin, O. Peters, M. Falcke and H. Kettenmann (2008). "Temperature and nitric oxide control spontaneous calcium transients in astrocytes." Cell Calcium **43**(3): 285-295.

Schroder, H. and K. G. Reymann (1990). "N-methyl-D-aspartate stimulates the release of dopamine from rat hippocampal slices." Biomed Biochim Acta **49**(4): 281-284.

Schultz, W. (2001). "Reward signaling by dopamine neurons." Neuroscientist **7**(4): 293-302.

Schultz, W., P. Dayan and P. R. Montague (1997). "A neural substrate of prediction and reward." Science **275**(5306): 1593-1599.

Schulze, A., B. Oehler, N. Urban, M. Schaefer and K. Hill (2013). "Apomorphine is a bimodal modulator of TRPA1 channels." Mol Pharmacol **83**(2): 542-551.

Scoville, W. B. and B. Milner (1957). "Loss of recent memory after bilateral hippocampal lesions." J Neurol Neurosurg Psychiatry **20**(1): 11-21.

Seamans, J. K., D. Durstewitz, B. R. Christie, C. F. Stevens and T. J. Sejnowski (2001). "Dopamine D1/D5 receptor modulation of excitatory synaptic inputs to layer V prefrontal cortex neurons." Proc Natl Acad Sci U S A **98**(1): 301-306.

Shao, W., S. Z. Zhang, M. Tang, X. H. Zhang, Z. Zhou, Y. Q. Yin, Q. B. Zhou, Y. Y. Huang, Y. J. Liu, E. Wawrousek, T. Chen, S. B. Li, M. Xu, J. N. Zhou, G. Hu and J. W. Zhou (2013). "Suppression of neuroinflammation by astrocytic dopamine D2 receptors via alphaB-crystallin." Nature **494**(7435): 90-94.

Shao, Y. and K. D. McCarthy (1993). "Regulation of astroglial responsiveness to neuroligands in primary culture." Neuroscience **55**(4): 991-1001.

Shao, Y. and K. D. McCarthy (1995). "Receptor-mediated calcium signals in astroglia: multiple receptors, common stores and all-or-nothing responses." Cell Calcium **17**(3): 187-196.

Shelton, M. K. and K. D. McCarthy (2000). "Hippocampal astrocytes exhibit Ca2+-elevating muscarinic cholinergic and histaminergic receptors in situ." J Neurochem **74**(2): 555-563.

Shigetomi, E., O. Jackson-Weaver, R. T. Huckstepp, T. J. O'Dell and B. S. Khakh (2013). "TRPA1 channels are regulators of astrocyte basal calcium levels and long-term potentiation via constitutive D-serine release." J Neurosci **33**(24): 10143-10153.

Shigetomi, E., X. Tong, K. Y. Kwan, D. P. Corey and B. S. Khakh (2011). "TRPA1 channels regulate astrocyte resting calcium and inhibitory synapse efficacy through GAT-3." Nat Neurosci **15**(1): 70-80.

Shohamy, D. and R. A. Adcock (2010). "Dopamine and adaptive memory." Trends Cogn Sci **14**(10): 464-472.

Sibille, J., U. Pannasch and N. Rouach (2014). "Astroglial potassium clearance contributes to short-term plasticity of synaptically evoked currents at the tripartite synapse." J Physiol **592**(Pt 1): 87-102.

Simard, M., W. T. Couldwell, W. Zhang, H. Song, S. Liu, M. L. Cotrina, S. Goldman and M. Nedergaard (1999). "Glucocorticoids-potent modulators of astrocytic calcium signaling." Glia **28**(1): 1-12.

Small, S. A., A. S. Nava, G. M. Perera, R. DeLaPaz, R. Mayeux and Y. Stern (2001). "Circuit mechanisms underlying memory encoding and retrieval in the long axis of the hippocampal formation." Nat Neurosci **4**(4): 442-449.

Smialowski, A. and M. Bijak (1987). "Excitatory and inhibitory action of dopamine on hippocampal neurons in vitro. Involvement of D2 and D1 receptors." Neuroscience **23**(1): 95-101.

Snyder, G. L., A. A. Fienberg, R. L. Huganir and P. Greengard (1998). "A dopamine/D1 receptor/protein kinase A/dopamine- and cAMP-regulated phosphoprotein (Mr 32 kDa)/protein phosphatase-1 pathway regulates dephosphorylation of the NMDA receptor." J Neurosci **18**(24): 10297-10303.

Sohl, G. and K. Willecke (2004). "Gap junctions and the connexin protein family." Cardiovasc Res **62**(2): 228-232.

Somjen, G. G. (1988). "Nervenkitt: notes on the history of the concept of neuroglia." Glia **1**(1): 2-9.

Song, M. R. and A. Ghosh (2004). "FGF2-induced chromatin remodeling regulates CNTF-mediated gene expression and astrocyte differentiation." Nat Neurosci **7**(3): 229-235.

Sontag, J. M., P. Sanderson, M. Klepper, D. Aunis, K. Takeda and M. F. Bader (1990). "Modulation of secretion by dopamine involves decreases in calcium and nicotinic currents in bovine chromaffin cells." J Physiol **427**: 495-517.

St-Pierre, J. A., D. Nouel, Y. Dumont, A. Beaudet and R. Quirion (2000). "Sub-population of cultured hippocampal astrocytes expresses neuropeptide Y Y(1) receptors." Glia **30**(1): 82-91.

Steinberg, E. E., R. Keiflin, J. R. Boivin, I. B. Witten, K. Deisseroth and P. H. Janak (2013). "A causal link between prediction errors, dopamine neurons and learning." Nat Neurosci **16**(7): 966-973.

Stella, N., M. Tence, J. Glowinski and J. Premont (1994). "Glutamate-evoked release of arachidonic acid from mouse brain astrocytes." J Neurosci **14**(2): 568-575.

Steullet, P., S. Lavoie, R. Kraftsik, R. Guidi, R. Gysin, M. Cuenod and K. Q. Do (2008). "A glutathione deficit alters dopamine modulation of L-type calcium channels via D2 and ryanodine receptors in neurons." Free Radic Biol Med **44**(6): 1042-1054.

Stevens, C. F. and T. Tsujimoto (1995). "Estimates for the pool size of releasable quanta at a single central synapse and for the time required to refill the pool." Proc Natl Acad Sci U S A **92**(3): 846-849.

Stone, E. A. and S. M. John (1991). "Further evidence for a glial localization of rat cortical beta-adrenoceptors: studies of in vivo cyclic AMP responses to catecholamines." Brain Res **549**(1): 78-82.

Stramiello, M. and J. J. Wagner (2008). "D1/5 receptor-mediated enhancement of LTP requires PKA, Src family kinases, and NR2B-containing NMDARs." Neuropharmacology **55**(5): 871-877.

Stramiello, M. and J. J. Wagner (2010). "Cocaine enhancement of long-term potentiation in the CA1 region of rat hippocampus: lamina-specific mechanisms of action." Synapse **64**(8): 644-648.

Suarez, L. M., J. Bustamante, L. M. Orensanz, R. Martin Del Rio and J. M. Solis (2013). "Cooperation of taurine uptake and dopamine D1 receptor activation facilitates the induction of protein synthesis-dependent late LTP." Neuropharmacology **79c**: 101-111.

Sul, J. Y., G. Orosz, R. S. Givens and P. G. Haydon (2004). "Astrocytic connectivity in the hippocampus." Neuron Glia Biol **1**(1): 3-11.

Sun, D. and T. C. Jakobs (2012). "Structural remodeling of astrocytes in the injured CNS." Neuroscientist **18**(6): 567-588.

Sun, M. Y., P. Devaraju, A. X. Xie, I. Holman, E. Samones, T. R. Murphy and T. A. Fiacco (2014). "Astrocyte calcium microdomains are inhibited by Bafilomycin A1 and cannot be replicated by low-level Schaffer collateral stimulation in situ." Cell Calcium **55**(1): 1-16.

Sun, W., E. McConnell, J. F. Pare, Q. Xu, M. Chen, W. Peng, D. Lovatt, X. Han, Y. Smith and M. Nedergaard (2013). "Glutamate-dependent neuroglial calcium signaling differs between young and adult brain." Science **339**(6116): 197-200.

Surmeier, D. J., J. Bargas, H. C. Hemmings, Jr., A. C. Nairn and P. Greengard (1995). "Modulation of calcium currents by a D1 dopaminergic protein kinase/phosphatase cascade in rat neostriatal neurons." Neuron **14**(2): 385-397.

Swanson-Park, J. L., C. M. Coussens, S. E. Mason-Parker, C. R. Raymond, E. L. Hargreaves, M. Dragunow, A. S. Cohen and W. C. Abraham (1999). "A double dissociation within the hippocampus of dopamine D1/D5 receptor and beta-adrenergic receptor contributions to the persistence of long-term potentiation." Neuroscience **92**(2): 485-497.

Swanson, L. W. (1982). "The projections of the ventral tegmental area and adjacent regions: a combined fluorescent retrograde tracer and immunofluorescence study in the rat." Brain Res Bull **9**(1-6): 321-353.

Swant, J., M. Stramiello and J. J. Wagner (2008). "Postsynaptic dopamine D3 receptor modulation of evoked IPSCs via GABA(A) receptor endocytosis in rat hippocampus." Hippocampus **18**(5): 492-502.

Swant, J. and J. J. Wagner (2006). "Dopamine transporter blockade increases LTP in the CA1 region of the rat hippocampus via activation of the D3 dopamine receptor." Learn Mem **13**(2): 161-167.

Tabernero, A., J. M. Medina and C. Giaume (2006). "Glucose metabolism and proliferation in glia: role of astrocytic gap junctions." J Neurochem **99**(4): 1049-1061.

Takano, K., N. Tanaka, K. Kawabe, M. Moriyama and Y. Nakamura (2013). "Extracellular superoxide dismutase induced by dopamine in cultured astrocytes." Neurochem Res **38**(1): 32-41.

Takata, N. and H. Hirase (2008). "Cortical layer 1 and layer 2/3 astrocytes exhibit distinct calcium dynamics in vivo." PLoS One **3**(6): e2525.

Takata, N., T. Mishima, C. Hisatsune, T. Nagai, E. Ebisui, K. Mikoshiba and H. Hirase (2011). "Astrocyte calcium signaling transforms cholinergic modulation to cortical plasticity in vivo." J Neurosci **31**(49): 18155-18165.

Takeda, H., M. Inazu and T. Matsumiya (2002). "Astroglial dopamine transport is mediated by norepinephrine transporter." Naunyn Schmiedebergs Arch Pharmacol **366**(6): 620-623.

Talantova, M., S. Sanz-Blasco, X. Zhang, P. Xia, M. W. Akhtar, S. Okamoto, G. Dziewczapolski, T. Nakamura, G. Cao, A. E. Pratt, Y. J. Kang, S. Tu, E. Molokanova, S. R. McKercher, S. A. Hires, H. Sason, D. G. Stouffer, M. W. Buczynski, J. P. Solomon, S. Michael, E. T. Powers, J. W. Kelly, A. Roberts, G. Tong, T. Fang-Newmeyer, J. Parker, E. A. Holland, D. Zhang, N. Nakanishi, H. S. Chen, H. Wolosker, Y. Wang, L. H. Parsons, R. Ambasudhan, E. Masliah, S. F. Heinemann, J. C. Pina-Crespo and S. A. Lipton (2013). "Abeta induces astrocytic glutamate release, extrasynaptic NMDA receptor activation, and synaptic loss." Proc Natl Acad Sci U S A **110**(27): E2518-2527.

Tanahashi, S., S. Yamamura, M. Nakagawa, E. Motomura and M. Okada (2012). "Clozapine, but not haloperidol, enhances glial D-serine and L-glutamate release in rat frontal cortex and primary cultured astrocytes." Br J Pharmacol **165**(5): 1543-1555.

Tanaka, M., P. Y. Shih, H. Gomi, T. Yoshida, J. Nakai, R. Ando, T. Furuichi, K. Mikoshiba, A. Semyanov and S. Itohara (2013). "Astrocytic Ca2+ signals are required for the functional integrity of tripartite synapses." Mol Brain **6**: 6.

Tanaka, T., M. Yoshida, H. Yokoo, K. Mizoguchi and M. Tanaka (1996). "ATP-sensitive K+ channel openers block sulpiride-induced dopamine release in the rat striatum." Eur J Pharmacol **297**(1-2): 35-41.

Taube, J. S., R. U. Muller and J. B. Ranck, Jr. (1990). "Head-direction cells recorded from the postsubiculum in freely moving rats. I. Description and quantitative analysis." J Neurosci **10**(2): 420-435.

Tecuapetla, F., L. Carrillo-Reid, J. Bargas and E. Galarraga (2007). "Dopaminergic modulation of short-term synaptic plasticity at striatal inhibitory synapses." Proc Natl Acad Sci U S A **104**(24): 10258-10263.

Theis, M. and C. Giaume (2012). "Connexin-based intercellular communication and astrocyte heterogeneity." Brain Res **1487**: 88-98.

Theodosis, D. T., D. A. Poulain and S. H. Oliet (2008). "Activity-dependent structural and functional plasticity of astrocyte-neuron interactions." Physiol Rev **88**(3): 983-1008.

Thomas, G. M. and R. L. Huganir (2004). "MAPK cascade signalling and synaptic plasticity." Nat Rev Neurosci **5**(3): 173-183.

Thompson, A. M., J. Swant and J. J. Wagner (2005). "Cocaine-induced modulation of long-term potentiation in the CA1 region of rat hippocampus." Neuropharmacology **49**(2): 185-194.

Tian, G. F., H. Azmi, T. Takano, Q. Xu, W. Peng, J. Lin, N. Oberheim, N. Lou, X. Wang, H. R. Zielke, J. Kang and M. Nedergaard (2005). "An astrocytic basis of epilepsy." Nat Med **11**(9): 973-981.

Tierney, P. L., A. M. Thierry, J. Glowinski, J. M. Deniau and Y. Gioanni (2008). "Dopamine modulates temporal dynamics of feedforward inhibition in rat prefrontal cortex in vivo." Cereb Cortex **18**(10): 2251-2262.

Tobler, P. N., J. P. O'Doherty, R. J. Dolan and W. Schultz (2007). "Reward value coding distinct from risk attitude-related uncertainty coding in human reward systems." J Neurophysiol **97**(2): 1621-1632.

Tolu, S., R. Eddine, F. Marti, V. David, M. Graupner, S. Pons, M. Baudonnat, M. Husson, M. Besson, C. Reperant, J. Zemdegs, C. Pages, Y. A. Hay, B. Lambolez, J. Caboche, B. Gutkin, A. M. Gardier, J. P. Changeux, P. Faure and U. Maskos (2013). "Co-activation of VTA DA and GABA neurons mediates nicotine reinforcement." Mol Psychiatry **18**(3): 382-393.

Tong, X., E. Shigetomi, L. L. Looger and B. S. Khakh (2013). "Genetically encoded calcium indicators and astrocyte calcium microdomains." Neuroscientist **19**(3): 274-291.

Torres, A., F. Wang, Q. Xu, T. Fujita, R. Dobrowolski, K. Willecke, T. Takano and M. Nedergaard (2012). "Extracellular Ca(2)(+) acts as a mediator of communication from neurons to glia." Sci Signal **5**(208): ra8.

Torvinen, M., L. B. Kozell, K. A. Neve, L. F. Agnati and K. Fuxe (2004). "Biochemical identification of the dopamine D2 receptor domains interacting with the adenosine A2A receptor." J Mol Neurosci **24**(2): 173-180.

Torvinen, M., D. Marcellino, M. Canals, L. F. Agnati, C. Lluis, R. Franco and K. Fuxe (2005). "Adenosine A2A receptor and dopamine D3 receptor interactions: evidence of functional A2A/D3 heteromeric complexes." Mol Pharmacol **67**(2): 400-407.

Trantham-Davidson, H., L. C. Neely, A. Lavin and J. K. Seamans (2004). "Mechanisms underlying differential D1 versus D2 dopamine receptor regulation of inhibition in prefrontal cortex." J Neurosci **24**(47): 10652-10659.

Tseng, K. Y. and P. O'Donnell (2004). "Dopamine-glutamate interactions controlling prefrontal cortical pyramidal cell excitability involve multiple signaling mechanisms." J Neurosci **24**(22): 5131-5139.

Tseng, K. Y. and P. O'Donnell (2007). "D2 dopamine receptors recruit a GABA component for their attenuation of excitatory synaptic transmission in the adult rat prefrontal cortex." Synapse **61**(10): 843-850.

Turner, C. A., S. B. Flagel, S. M. Clinton, H. Akil and S. J. Watson (2008). "Cocaine interacts with the novelty-seeking trait to modulate FGFR1 gene expression in the rat." Neurosci Lett **446**(2-3): 105-107.

Tye, K. M., J. J. Mirzabekov, M. R. Warden, E. A. Ferenczi, H. C. Tsai, J. Finkelstein, S. Y. Kim, A. Adhikari, K. R. Thompson, A. S. Andalman, L. A. Gunaydin, I. B. Witten and K. Deisseroth (2013). "Dopamine neurons modulate neural encoding and expression of depression-related behaviour." Nature **493**(7433): 537-541.

Uchiyama, T., F. Yoshikawa, A. Hishida, T. Furuichi and K. Mikoshiba (2002). "A novel recombinant hyperaffinity inositol 1,4,5-trisphosphate (IP(3)) absorbent traps IP(3), resulting in specific inhibition of IP(3)-mediated calcium signaling." J Biol Chem **277**(10): 8106-8113.

Urai, Y., O. Jinnouchi, K. T. Kwak, A. Suzue, S. Nagahiro and K. Fukui (2002). "Gene expression of D-amino acid oxidase in cultured rat astrocytes: regional and cell type specific expression." Neurosci Lett **324**(2): 101-104.

Vaarmann, A., S. Gandhi and A. Y. Abramov (2010). "Dopamine induces Ca2+ signaling in astrocytes through reactive oxygen species generated by monoamine oxidase." J Biol Chem **285**(32): 25018-25023.

Vallar, L., C. Muca, M. Magni, P. Albert, J. Bunzow, J. Meldolesi and O. Civelli (1990). "Differential coupling of dopaminergic D2 receptors expressed in different cell types. Stimulation of phosphatidylinositol 4,5-bisphosphate hydrolysis in LtK- fibroblasts, hyperpolarization, and cytosolic-free Ca2+ concentration decrease in GH4C1 cells." J Biol Chem **265**(18): 10320-10326.

Vanderwolf, C. H. (2001). "The hippocampus as an olfacto-motor mechanism: were the classical anatomists right after all?" Behav Brain Res **127**(1-2): 25-47.

Venance, L., N. Stella, J. Glowinski and C. Giaume (1997). "Mechanism involved in initiation and propagation of receptor-induced intercellular calcium signaling in cultured rat astrocytes." J Neurosci **17**(6): 1981-1992.

Verkhratsky, A. and Butt, A (2007). "Glial Neurobiology: A textbook". Wiley.

Verkhratsky, A. and V. Parpura (2010). "Recent advances in (patho)physiology of astroglia." Acta Pharmacol Sin **31**(9): 1044-1054.

Verkhratsky, A., J. J. Rodriguez and V. Parpura (2012). "Calcium signalling in astroglia." Mol Cell Endocrinol **353**(1-2): 45-56.

Verma, V., A. Hasbi, B. F. O'Dowd and S. R. George (2010). "Dopamine D1-D2 receptor Heteromer-mediated calcium release is desensitized by D1 receptor occupancy with or without signal activation: dual functional regulation by G protein-coupled receptor kinase 2." J Biol Chem **285**(45): 35092-35103.

Vermeulen, R. J., C. A. Jongenelen, C. H. Langeveld, E. C. Wolters, J. C. Stoof and B. Drukarch (1994). "Dopamine D1 receptor agonists display a different intrinsic activity in rat, monkey and human astrocytes." Eur J Pharmacol **269**(1): 121-125.

Verney, C., M. Baulac, B. Berger, C. Alvarez, A. Vigny and K. B. Helle (1985). "Morphological evidence for a dopaminergic terminal field in the hippocampal formation of young and adult rat." Neuroscience **14**(4): 1039-1052.

Villalba, R. M. and Y. Smith (2011). "Neuroglial plasticity at striatal glutamatergic synapses in Parkinson's disease." Front Syst Neurosci **5**: 68.

Virchow, R. (1856) Gesammelte A bhantllungen zur Wissenschaftlichen Medicin. Hamm, Frankfurt a.M., 1024 pp.

Wallraff, A., R. Kohling, U. Heinemann, M. Theis, K. Willecke and C. Steinhauser (2006). "The impact of astrocytic gap junctional coupling on potassium buffering in the hippocampus." J Neurosci **26**(20): 5438-5447.

Wang, F., N. A. Smith, Q. Xu, S. Goldman, W. Peng, J. H. Huang, T. Takano and M. Nedergaard (2013a). "Photolysis of caged Ca2+ but not receptor-mediated Ca2+ signaling triggers astrocytic glutamate release." J Neurosci **33**(44): 17404-17412.

Wang, J. and P. O'Donnell (2001). "D(1) dopamine receptors potentiate nmda-mediated excitability increase in layer V prefrontal cortical pyramidal neurons." Cereb Cortex **11**(5): 452-462.

Wang, T. F., C. Zhou, A. H. Tang, S. Q. Wang and Z. Chai (2006). "Cellular mechanism for spontaneous calcium oscillations in astrocytes." Acta Pharmacol Sin **27**(7): 861-868.

Wang, X., C. Zhang, G. Szabo and Q. Q. Sun (2013b). "Distribution of CaMKIIalpha expression in the brain in vivo, studied by CaMKIIalpha-GFP mice." Brain Res **1518**: 9-25.

Wang, X., P. Zhong, Z. Gu and Z. Yan (2003). "Regulation of NMDA receptors by dopamine D4 signaling in prefrontal cortex." J Neurosci **23**(30): 9852-9861.

Wang, X., P. Zhong and Z. Yan (2002). "Dopamine D4 receptors modulate GABAergic signaling in pyramidal neurons of prefrontal cortex." J Neurosci **22**(21): 9185-9193.

Wayman, G. A., H. Tokumitsu, M. A. Davare and T. R. Soderling (2011). "Analysis of CaM-kinase signaling in cells." Cell Calcium **50**(1): 1-8.

Wei, C. L., Y. H. Liu, M. H. Yang, Z. Q. Liu and W. Ren (2013). "Dopamine inhibits high-frequency stimulation-induced long-term potentiation of intrinsic excitability in CA1 hippocampal pyramidal neurons." Neurosignals **21**(3-4): 150-159.

Weng, S. M., F. McLeod, M. E. Bailey and S. R. Cobb (2011). "Synaptic plasticity deficits in an experimental model of rett syndrome: long-term potentiation saturation and its pharmacological reversal." Neuroscience **180**: 314-321.

Whitton, P. S., S. Maione, C. S. Biggs and L. J. Fowler (1994). "N-methyl-d-aspartate receptors modulate extracellular dopamine concentration and metabolism in rat hippocampus and striatum in vivo." Brain Res **635**(1-2): 312-316.

Wiener, S. I., C. A. Paul and H. Eichenbaum (1989). "Spatial and behavioral correlates of hippocampal neuronal activity." J Neurosci **9**(8): 2737-2763.

Williams, G. V. and P. S. Goldman-Rakic (1995). "Modulation of memory fields by dopamine D1 receptors in prefrontal cortex." Nature **376**(6541): 572-575.

Witten, I. B., E. E. Steinberg, S. Y. Lee, T. J. Davidson, K. A. Zalocusky, M. Brodsky, O. Yizhar, S. L. Cho, S. Gong, C. Ramakrishnan, G. D. Stuber, K. M. Tye, P. H. Janak and K. Deisseroth (2011). "Recombinase-driver rat lines: tools, techniques, and optogenetic application to dopamine-mediated reinforcement." Neuron **72**(5): 721-733.

Wu, H. Q., A. Rassoulpour and R. Schwarcz (2007). "Kynurenic acid leads, dopamine follows: a new case of volume transmission in the brain?" J Neural Transm **114**(1): 33-41.

Wu, M. L., W. H. Chen, I. H. Liu, C. D. Tseng and S. M. Wang (1999). "A novel effect of cyclic AMP on capacitative Ca2+ entry in cultured rat cerebellar astrocytes." J Neurochem **73**(3): 1318-1328.

Xing, B., H. Kong, X. Meng, S. G. Wei, M. Xu and S. B. Li (2010). "Dopamine D1 but not D3 receptor is critical for spatial learning and related signaling in the hippocampus." Neuroscience **169**(4): 1511-1519.

Xu, J. Y., J. Zhang and C. Chen (2012). "Long-lasting potentiation of hippocampal synaptic transmission by direct cortical input is mediated via endocannabinoids." J Physiol **590**(Pt 10): 2305-2315.

Xu, T. X., T. D. Sotnikova, C. Liang, J. Zhang, J. U. Jung, R. D. Spealman, R. R. Gainetdinov and W. D. Yao (2009). "Hyperdopaminergic tone erodes prefrontal long-term potential via a D2 receptor-operated protein phosphatase gate." J Neurosci **29**(45): 14086-14099.

Yamada, Y. and K. Mikoshiba (2012). "Quantitative comparison of novel GCaMP-type genetically encoded Ca(2+) indicators in mammalian neurons." Front Cell Neurosci **6**: 41.

Yamaguchi, T., W. Sheen and M. Morales (2007). "Glutamatergic neurons are present in the rat ventral tegmental area." Eur J Neurosci **25**(1): 106-118.

Yamaguchi, T., H. L. Wang, X. Li, T. H. Ng and M. Morales (2011). "Mesocorticolimbic glutamatergic pathway." J Neurosci **31**(23): 8476-8490.

Yamamoto, N., K. Sobue, M. Fujita, H. Katsuya and K. Asai (2002). "Differential regulation of aquaporin-5 and -9 expression in astrocytes by protein kinase A." Brain Res Mol Brain Res **104**(1): 96-102.

Yang, S. N. (2000). "Sustained enhancement of AMPA receptor- and NMDA receptor-mediated currents induced by dopamine D1/D5 receptor activation in the hippocampus: an essential role of postsynaptic Ca2+." Hippocampus **10**(1): 57-63.

Yeh, T. H., Y. Lee da, S. M. Gianino and D. H. Gutmann (2009). "Microarray analyses reveal regional astrocyte heterogeneity with implications for neurofibromatosis type 1 (NF1)-regulated glial proliferation." Glia **57**(11): 1239-1249.

Yokoyama, C., H. Okamura and Y. Ibata (1995). "Dopamine D2-like receptors labeled by [3H]YM-09151-2 in the rat hippocampus: characterization and autoradiographic distribution." Brain Res **681**(1-2): 153-159.

Young, C. E. and C. R. Yang (2005). "Dopamine D1-like receptor modulates layer- and frequency-specific short-term synaptic plasticity in rat prefrontal cortical neurons." Eur J Neurosci **21**(12): 3310-3320.

Zahrt, J., J. R. Taylor, R. G. Mathew and A. F. Arnsten (1997). "Supranormal stimulation of D1 dopamine receptors in the rodent prefrontal cortex impairs spatial working memory performance." J Neurosci **17**(21): 8528-8535.

Zanassi, P., M. Paolillo, A. Montecucco, E. V. Avvedimento and S. Schinelli (1999). "Pharmacological and molecular evidence for dopamine D(1) receptor expression by striatal astrocytes in culture." J Neurosci Res **58**(4): 544-552.

Zarrindast, M. R., M. Nasehi, M. Pournaghshband and B. G. Yekta (2012). "Dopaminergic system in CA1 modulates MK-801 induced anxiolytic-like responses." Pharmacol Biochem Behav **103**(1): 102-110.

Zechel, S., S. Werner, K. Unsicker and O. von Bohlen und Halbach (2010). "Expression and functions of fibroblast growth factor 2 (FGF-2) in hippocampal formation." Neuroscientist **16**(4): 357-373.

Zhang, X., Z. Zhou, D. Wang, A. Li, Y. Yin, X. Gu, F. Ding, X. Zhen and J. Zhou (2009). "Activation of phosphatidylinositol-linked D1-like receptor modulates FGF-2 expression in astrocytes via IP3-dependent Ca2+ signaling." J Neurosci **29**(24): 7766-7775.

Zhang, Y. X., H. Yamashita, T. Ohshita, N. Sawamoto and S. Nakamura (1995). "ATP increases extracellular dopamine level through stimulation of P2Y purinoceptors in the rat striatum." Brain Res **691**(1-2): 205-212.

Zhang, Z., G. Chen, W. Zhou, A. Song, T. Xu, Q. Luo, W. Wang, X. S. Gu and S. Duan (2007). "Regulated ATP release from astrocytes through lysosome exocytosis." Nat Cell Biol **9**(8): 945-953.

Zhu, Y. and H. K. Kimelberg (2001). "Developmental expression of metabotropic P2Y(1) and P2Y(2) receptors in freshly isolated astrocytes from rat hippocampus." J Neurochem **77**(2): 530-541.

Zimmermann, H. and N. Braun (1996). "Extracellular metabolism of nucleotides in the nervous system." J Auton Pharmacol **16**(6): 397-400.

Zonta, M., M. C. Angulo, S. Gobbo, B. Rosengarten, K. A. Hossmann, T. Pozzan and G. Carmignoto (2003). "Neuron-to-astrocyte signaling is central to the dynamic control of brain microcirculation." Nat Neurosci **6**(1): 43-50.

Zucker, R. S. and W. G. Regehr (2002). "Short-term synaptic plasticity." Annu Rev Physiol **64**: 355-405.